Operational effectiveness of hydrofoils for littoral craft

Investigating the potential of hydrofoils for high-speed daughter craft in amphibious operations

MSc Thesis

R.M. Zwinkels

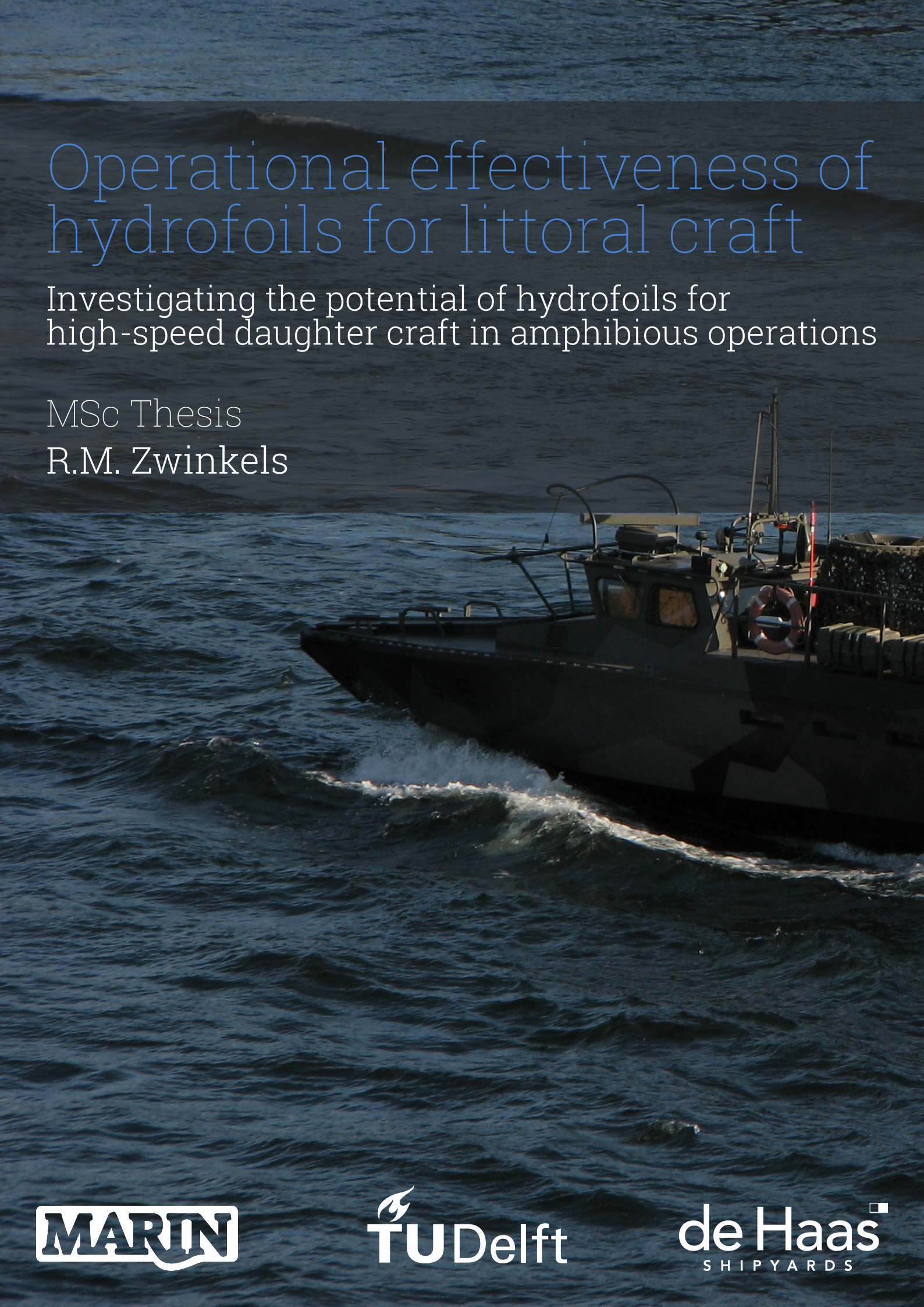

MARIN TU Delft de Haas SHIPYARDS

Thesis for the degree of MSc in Marine Technology in the specialisation of Ship Design

Operational effectiveness of hydrofoils for littoral craft

Investigating the potential of hydrofoils for high-speed daughter craft in amphibious operations

by

R.M. Zwinkels

performed at

De Haas Shipyards

April 23, 2025
Faculty of Mechanical Engineering, Delft University of Technology

Company Supervisors

Ing. R. Kalisvaart	De Haas Shipyards, responsible supervisor
L.F. Minerva, MSc.	MARIN

Thesis Exam Committee

Dr. A.A. Kana	TU Delft, chairperson
Dr.ir. R. Vos	TU Delft
Ir. J.L. Gelling	TU Delft, supervisor
Ing. R. Kalisvaart	De Haas Shipyards, supervisor

Document Information

Author name:	R.M. (Roan) Zwinkels
Thesis number:	MT.24/25.035.M
Student number:	4840380

Cover: CB-90 in Oskar-Fredriksborg by Журавлёв (2018) under CC BY-SA 2.0
An electronic version of this thesis is available at https://repository.tudelft.nl

Acknowledgements

This work is completed as part of the master's thesis of the author in collaboration with De Haas Shipyards and the MAritime Research Institute Netherlands (MARIN). It must therefore be viewed as independent work done for assessment by Delft University of Technology and is not part of any tender procedure.

Declaration of AI-assisted technologies in the writing process

During the preparation of this work, the author used the AI-based language model ChatGPT by OpenAI, in order to improve the spelling, language, and grammar of this thesis. After using these tools/services, the author reviewed and edited the content as needed and takes full responsibility for the content of the publication.

Preface

Dear reader,

With global tensions unfortunately on the rise, military spending feels more relevant than I can ever remember. Therefore, it has been great to focus on a positive topic like hydrofoils. Hydrofoils are a technology that show potential for military use, while also enabling more sustainable transportation due to their energy efficiency. This has led to renewed interest in hydrofoils itself, which have experienced periods of fluctuating relevancy throughout the 20th century. Focusing on hydrofoil integration allowed me to engage with several branches of a "Ship Design Engineer", as the thesis goes into hydrodynamics, propulsion, and general integration. This has been a challenging but rewarding process and I hope that solutions like these can contribute to a more sustainable maritime industry.

I am honoured to have collaborated on this thesis with both De Haas Shipyards and the Maritime Research Institute Netherlands (MARIN). I would like to sincerely thank Ruben Kalisvaart for his daily supervision at De Haas and for making this opportunity possible. Because of Ruben, I was able to connect with industry professionals and the Royal Netherlands Marine Corps. His support was also essential in involving MARIN in the project. Ruben, thank you for your enthusiastic, open-minded and confidence-instilling guidance throughout. I would also like to thank the whole team at De Haas Maassluis for their advise during the project and for being such friendly and supportive colleagues. It was a pleasure to finally experience real shipyard work up close.

I especially want to express my gratitude to all the people of MARIN that helped me during my time there. When I first arrived, I was warmly welcomed by Luigi Minerva, who helped me get settled at the office and enthusiastically provided his experience in hydrofoil design. Luigi, thank you for all your support during our weekly meetings, your advise, and your kindness throughout the project. Furthermore, I had the opportunity to gain experience with several advanced tools available at MARIN, which, in my opinion, significantly elevated the quality of this thesis. In particular, I want to thank Frans van Walree for helping me get familiar with Hydres and the tremendous support in running PanShip. It has been an honour to work with the hydrofoil experts of MARIN at this level. I would also like to thank Alex Grasman for our discussions about advanced propulsion methods.

As my daily TU Delft supervisor, Jaap Gelling was always available for questions or support during the project. During our update meetings I could also count on challenging but constructive feedback. Jaap, thank you for your kind, thoughtful, and inspiring supervision. It was great to have your ship design experience to count on. I would also like to extend my sincere thanks to Austin Kana, as the chair of the thesis committee. I could always count on receiving timely and in-depth feedback, which added to the academic quality of the thesis.

Furthermore, I would like to thank my family and friends for their support throughout my studies. My parents have always been supportive in my studies and interest in all things maritime, whilst not coming from a ship building background themselves. From my friends, I want to thank Daan, Stijn, Mo, and Loet in particular, for reading my work, providing feedback, and for being a generally supporting factor during the thesis. I also want to thank my girlfriend, Sharon, for supporting me and keeping me sane during the project, whilst being in a tumultuous period at the start of her own career.

The completion of this thesis marks the end of my Master's study in Maritime Technology. Looking back, I am grateful for all the new friends, connections and experiences I have made during my time at the Delft University of Technology. I hope that this thesis will spark your interest in hydrofoil design and provides a global understanding of their potential. I would like to leave you with some words of wisdom that my granddad gave me during the thesis:

"Je moet je licht niet onder de korenmaat zetten." - Opa Martin
Meaning: Do not be afraid to show what you are capable of.

Roan Zwinkels
Delft, April 2025

Summary

Landing craft are essential for the rapid deployment of personnel, vehicles, and equipment from ship to shore. These landing craft are launched from mother ships such as the Landing Platform Dock (LPD) and Joint logistic Support Ship (JSS). Due to the current increase in threats from shore however, mother ships will tend to extend their distance from the coast in the future. This implies that their daughter (landing) craft have to traverse a larger distance to the shoreline. Going further offshore shifts risk from the mother ship to the daughter craft, which have to face worse sea conditions as a smaller and more exposed vessel. As a result, even greater emphasis is placed on the seakeeping, speed, and range of new landing craft designs.

To address these challenges the Netherlands Ministry of Defence (NLMOD) introduces a new type of landing craft catered to the new requirements: The Littoral Assault Craft (LAC). Due to the stringent dimensional constraints that are placed on daughter craft however, increasing seakeeping capabilities and range is difficult to achieve with conventional methods. By evaluating different Advanced Marine Vehicle (AMV) concepts it becomes clear that hydrofoils offer the greatest potential in achieving the greater demands of the NLMOD. This is attributed to their transport efficiency, high sustained speed in waves, and ride quality.

This thesis aims to define the operational effectiveness of applying hydrofoils to an LAC design. This is achieved by assessing relevant Measures of Effectiveness (MoEs) based on the identified design drivers: range, speed, and safety. To retrieve these MoEs, a preliminary design methodology is developed for a Hydrofoil Littoral Assault Craft (HLAC) design. The methodology works in two parts:

- Part I represents a parametric iterative model to retrieve the required displacement and main particulars of a HLAC design, based on the top speed resistance. In this model the MARIN Foil Design JIP tool is employed within an approach to retrieve the complete hydrofoil craft resistance.
- Part II evaluates the dynamic equilibrium of the HLAC designs. The dynamic equilibrium requires an equilibrium of all foil- and hullbound forces at each vessel speed. This is evaluated using the program Hydres, also developed by MARIN. As the resulting forces can be derived over the complete speed region, the hump region is assessed as well. The hump region is characterised as the increase in resistance a hydrofoil craft experiences before becoming foilborne, which can be critical for the propulsion system design.

The facilitation of propulsion retraction remains a point of contention and no clear consensus exists for hydrofoil craft. Therefore, two types of transmission are proposed: an inclined shaft system utilising a homokinetic joint (HLAC-HK) and a diesel-electric configuration with an L-drive transmission (HLAC-DE). Both propulsion options require no additional considerations for transitioning through the hump region. Furthermore, using both propulsion systems a range increase of 50% can be realised, extending the range from approximately 300 nm to 450 nm. Further investigation into weight saving measures reveals an exponential relationship between weight reduction and resistance, highlighting the value of weight saving efforts.

To compare seakeeping characteristics of both a planing hull and a hydrofoil craft design, the time-domain method PanShip is used. Using this program, the vertical accelerations of both designs can be evaluated, which define the accumulated fatigue and physical strain of passengers aboard these vessels. At 35 kt in sea state 3 ($H_{1/3}$ = 1.25 m, T_p = 5.75 s), the planing hull can achieve vertical accelerations up to 10 g and waterjet ventilation is an issue due to the vessel jumping between waves. Based on these factors it is deemed unsustainable for a planing vessel to sustain these speeds for the duration that future transits will require. On contrast, for the same conditions the hydrofoil design experiences a maximum of 0.4 g during the simulation time of 450 seconds, which is within safe bounds for long transits.

The improvements in safety, sustained speed, and range show strong potential of hydrofoil systems for future LAC designs. However, significant uncertainties remain. Analysis of the necessary strut length revealed some level of hull-wave interaction may be acceptable, though this depends on hull form and warrants further simulation. Moreover, operational edge cases, such as foil ventilation or broaching must be examined before safe operation with passengers can be commenced.

Contents

List of Figures

List of Tables

Nomenclature

Abbreviations

Abbreviation	Definition
A1/3	Mean value of 33% highest peaks
A1/10	Mean value of 10% highest peaks
ABC	Axe Bow Concept
AC	Alternating Current
ACV	Air Cushion Vehicle
AMV	Advanced Marine Vehicles
AR	Aspect ratio
ATS	Amphibious Transport Ship
BAR	Blade-Area Ratio
CB90	Combat Boat 90
CCM	Combatant Craft Medium
CoG	Centre of Gravity
CZSK	Commandant Zeestrijdkrachten (Commander of the naval forces)
DAF	Design Architectural Framework
DC	Direct Current
DD	Design Driver
DSDS	Delft Systematic Deadrise Series
DWT	Deadweight
EMF	Embarked Military Forces
EPV	Empirical Performance Validity
ESC	Enlarged Ship Concept
ESV	Empirical Structural Validity
EU	European Union
FFI	Future Fast Interceptor
FPP	Front PerPendicular
FLitOC	Future Littoral Operating Concept
FRISC	Fast Raiding Interception and Special Forces Craft
GB	Gearbox
GMDSS	Global Maritime Distress and Safety System
HF REQ	Hydrofoil system requirement
HLAC	Hydrofoil Littoral Assault Craft
HLAC-DE	Hydrofoil Littoral Assault Craft Diesel-Electric design
HLAC-HK	Hydrofoil Littoral Assault Craft HomoKinetic design
HNLMS	His Netherlands Majesty's Ship
IA	Internal Arrangement
ICE	Internal Combustion Engine
IMO	International Maritime Organisation
ISO	International Organisation for Standardisation
IPCC	Intergovernmental Panel on Climate Change
JONSWAP	Joint North Sea Wave Project
JSS	Joint logistic Support Ship
KPI	Key Performance Indicator
LAC	Littoral Assault Craft
LCG	Longitudinal centre of gravity
LCM	Littoral Craft Mobility

Abbreviation	Definition
LCVP	Landing Craft Vehicle Personnel
LCU	Landing Craft Utility
LPD	Landing Platform Dock
LWT	Lightweight
LQ	Literature Question
MARIN	MAritime Research Institute Netherlands
MF	Medium Frequency
MSI	Motion Sickness Incidence
MoE	Measure of Effectiveness
MoP	Measure of Performance
MQ	Main question
NACA	National Advisory Committee of Aeronautics
NATO	North Atlantic Treaty Organisation
NLMOD	Netherlands Ministry of Defence
NR	Newton-Rader
NSS	Naples Systematic Series
OPV	Ocean Patrol Vessel
RAO	Response Amplitude Operator
REQ	Requirement
RHIB	Rigid Hull Inflatable Boat
RNLN	Royal Netherlands Navy
RNMC	Royal Netherlands Marine Corps
RMS	Root Mean Square
RQ	Research question
SES	Surface Effect Ship
SS	Sea State
SWATH	Small Waterplane Area Twin Hull
TRANSFLYTOR	Troop Transportation Flying Vector
TPV	Theoretical Performance Validity
TSV	Theoretical Structural Validity
US	United States
USS	United States Ship
VCG	Vertical Centre of Gravity
VHF	Very High Frequency
WIG	Wing In Ground

Symbols

Symbol	Definition	Unit
-	Range	nm (1852 m)
A	Plan area	m^2
A	Projected area	m^2
A_f	Frontal projected area	m^2
A_p	Projected planing bottom area	m^2
A_E	Expanded blade area	m^2
A_0	Propeller disc area	m^2
AR	Aspect ratio	-
a_z	Heave acceleration	$m\ s^{-2}$
B	Beam	m
B_p	Average chine beam	m
B_{wl}	Waterline beam	m
b	Breadth	m

Symbol	Definition	Unit
C_B	Block coefficient	-
C_F	Frictional coefficient	-
$C_{F,rough}$	Fully rough flow coefficient	-
$C_{F,smooth}$	Hydraulically smooth flow coefficient	-
C_D	Drag coefficient	-
C_{DI}	Induced drag coefficient	-
C_{DV}	Viscous drag coefficient	-
$C_{D,tot}$	Total foil drag coefficient	-
C_L	Lift coefficient	-
C_M	Pitching moment coefficient	-
C_{pu}	Dynamic pressure coefficient	-
c	Chord length	m
$camber$	Camber	-
c_{aft}	Aft foil chord length	m
c_{front}	Front foil chord length	m
c_{mean}	Mean chord length	m
D	Drag	N
D	Propeller diameter	m
D_{max}	Maximum propeller diameter	m
D_{pod}	Pod resistance	N
$D_{roughness}$	Additional roughness drag	N
D_{int}	Intersection drag	N
d	Characteristic diameter	d
E	Elastic modulus	GPa
F_n	Froude number	-
Fn_h	Froude number based on submergence height	-
$Fn_{L_{wl}}$	Froude number based on waterline	-
f	Frequency	Hz
g	Gravitational acceleration	m s^{-2}
$H_{1/3}$	Significant wave height	m
H_p	Pump head	m
h	Head	m
h	Height	m
h_{clear}	Clearance height	m
$h_{ext,strut}$	Strut extension length	m
$h_{submerged}$	Submergence height	m
I	Area moment of inertia	m^4
J	Advance ratio	-
J	Polar moment of inertia	m^4
K_T	Thrust coefficient	-
$K_{T,ship,0}$	Vessel design thrust coefficient	-
K_Q	Torque coefficient	-
k	Wave number	rad m^{-1}
k_e	Number of electrical machines	-
k_s	Equivalent sand roughness	µm
L	Lift	N
L	Hull length	m
LCG	Longitudinal centre of gravity	m
L_f	Length between foils	m
L_{oa}	Length over all	m
L_p	Projected chine length of hull	m
$L_{req,aft}$	Lift requirement aft foils	N
$L_{req,fore}$	Lift requirement fore foil	N
L_{wl}	Length waterline	m

Symbol	Definition	Unit
l	Length	m
l_{hk}	Homokinetic retraction system length	m
l_{strut}	Total strut length	m
$\dot{m}$	Mass flow	kg s^{-1}
m	Mass	kg
m_{aux}	Auxilliary genset mass	kg
m_{axconv}	Axial flux motor conversion mass	kg
m_{buffer}	Buffer system mass	kg
$m_{entrained}$	Waterjet entrained water mass	kg
m_{engine}	Internal combustion engine mass	kg
m_{eprop}	Electrical propulsion motor mass	kg
m_{foils}	Foil structural mass	kg
m_{fuel}	Fuel mass	kg
m_{genset}	Generator set mass	kg
m_{gb}	Gearbox mass	kg
m_{hk}	Single homokinetic retraction system mass	kg
$m_{hk,retract}$	Homokinetic retraction system mass	kg
m_{hull}	Structural hull mass	kg
$m_{outfit.}$	Outfitting mass	kg
$m_{powerelec.}$	Power electronics mass	kg
$m_{waterjet}$	Waterjet mass	kg
m_{lub}	Lubrication oil mass	kg
$m_{payload}$	Payload mass	kg
$m_{propul.}$	Propulsion system mass	kg
$m_{retract.}$	Foil retraction system mass	kg
m_{struts}	Strut structural mass	kg
N	Normal force	N
n	Number	-
n_e	Rotational engine speed	s^{-1} (Hz)
n_{opt}	Optimal propeller speed	s^{-1} (Hz)
OPC	Overall propulsive coefficient	-
P	Power	W
P	Propeller pitch	rad
P_{added}	Added power	W
P_B	Brake power	W
P_{buffer}	Maximum buffer power	W
P_{cruise}	Cruise power	W
$P_{inst.}$	Installed power	W
P_O	Open water propeller power	W
P_{prime}	Prime mover power	W
P_{req}	Requiered power	W
P_T	Thrust power	W
p_a	Atmospheric pressure	Pa
p_v	Vapour pressure	Pa
Q	Torque	Nm
q	Dynamic pressure	Pa
R	Resistance	N
Re	Reynolds number	-
R_{AA}	Air resistance	N
$R_{foilborne}$	Total foilborne resistance	N
R_s	Spray resistance	N
S_{wet}	Wetted surface	m^2
s	Span length	m
s_{aft}	Aft foil span length	m

Symbol	Definition	Unit
s_{front}	Front foil span length	m
sfc	Specific fuel consumption	g/kWh
T	Thrust	N
T	Hull draught	m
T_{foil}	Draught including foils	m
T	Time	s
T_p	Peak period	s
T_1	Mean centroid wave period	s
T_2	Mean zero-crossing wave period	s
t	Thrust deduction factor	-
t	Thickness	m
U	Fluid free-stream velocity	m s^{-1}
V	Volume	m^3
V	Velocity	m s^{-1}
VCG	Vertical centre of gravity	m
v_a	Advance velocity	m s^{-1}
v_{design}	Foil design velocity	m s^{-1}
v_s	Ship speed	m s^{-1}
$v_{takeoff}$	Take-off speed	m s^{-1}
W	Weight	N
w	Wake factor	-
x	Location in x direction	m
z	Heave	m
α	Angle of attack	rad
β	Deadrise angle	rad
δ	Flap angle	rad
Δ	Ship displacement weight	t (10^3 kg)
η_D	Propulsive efficiency	-
$\eta_{dc/ac}$	Electrical converter efficiency	-
η_e	Engine efficiency	-
η_{em}	Electrical machine efficiency	-
η_{gb}	Gearbox efficiency	-
η_{hk}	Homokinetic joint efficiency	-
η_h	Hull efficiency	-
η_o	Open water efficiency	-
η_p	Pump efficiency	-
η_r	Relative rotative efficiency	-
η_s	Shaft efficiency	-
η_{trm}	Transmission efficiency	-
ϵ	Inclination angle	rad
$\epsilon_{payload}$	Payload specific resistance	-
γ	Wave direction	rad
λ	Wave length	m
μ	Peakedness factor	-
∇	Ship displacement volume	m^3
θ	Pitch angle	rad
Ω	Transport efficiency	-
ω_0	Wave frequency	rad s^{-1}
ω_e	Encounter frequency	rad s^{-1}
ρ	Density	kg m^{-3}
ρ_a	Air density	kg m^{-3}
ρ_{sw}	Sea water density	kg m^{-3}
σ_0	Propeller cavitation number	-
τ	Trim angle	rad

Symbol	Definition	Unit
ζ	Resistance factor	-

1 Introduction

This chapter provides an introduction to the master's thesis. The problem definition is introduced in Section 1.1, which is followed by the scope of the project in Section 1.2. This leads into the approach of this study, discussed in Section 1.3. The research questions are posed in section 1.4. Continuing in Section 1.5 the societal and scientific relevance of this research is discussed, and finally, in Section 1.6 the structure of the report is presented.

1.1. Problem definition

1.1.1. Amphibious daughter craft increase their range due to FLitOC requirements

Due to the evolving geopolitical landscape and technological advancements in military technology, changes in strategy for the armed forces are required. Consequently, the Royal Netherlands Navy (RNLN) has to reevaluate their capabilities. In 2019 the Dutch commander of the naval forces (CZSK) introduced the Future Littoral Operating Concept (FLitOC), developed in close collaboration with the United States and the United Kingdom (Strijbosch, 2019). This concept aims to update the doctrine of amphibious operations for 2035 and is of foremost importance to the marine corps. In short, the FLitOC envisions marines operating in smaller, more agile, and autonomous units, positioning them as the "First responders of choice". By enhancing mobility and independence, the CZSK intends to improve the standards of the marine corps and become equipped for future and current threats (de Wit & Thomeer, 2022). This shift in strategy also necessitates updating equipment to support the new operational doctrine. One key implications of the FLitOC is the increased distance of mother ships from shore due to heightened risks of armed opposition. As a result, daughter craft will increase their transit distance from around 10 nm to 40 nm for amphibious operations. Going further offshore places greater emphasis on range, seakeeping, and speed in the design of future daughter craft.

(a) Fast Raiding Interception and Special forces Craft (FRISC) (Dutch Ministry of Defense, 2023b)

(b) Landing Craft Vehicle Personnel (LCVP) (Dutch Ministry of Defense, 2023a)

Figure 1.1: Current amphibious daughter craft fleet of the RNLN

1.1.2. Royal Netherlands Navy introduces the Littoral Assault Craft (LAC)

At the moment of writing, the RNLN amphibious daughter craft fleet consists of RHIB-type crafts for personnel transfer (Fig. 1.1a) and vehicle landing craft (Fig. 1.1b). These craft are less suited to travel long distances. Therefore, the Dutch Ministry of Defence has the intention to replace its entire amphibious fleet of landing craft (Buitendijk, 2023). In alignment with the FLitOC, the craft shall be faster, cover longer distances and be deployable in rough seas. Furthermore, they should offer better protection in bad weather and reduce the physical strain for their crew. A detailed list of requirements is provided in Appendix A. Of these new craft, one type will be dedicated to fast personnel transport: the Littoral Assault Craft (LAC) (Dutch Ministry of Defense, 2023a). The RNLN plans to order 12 new LACs for 2025 (Buitendijk, 2023). These are small (20-30 t) high-speed craft (40-50 kt) and can transport around 20 marines (half a platoon). A potential candidate for this type of craft is the CB90, as shown in Fig. 1.2a. However, current candidates are primarily designed for sheltered shallow water regions such as rivers or fjords (Saab, 2021), which indicates that they may fair less well in open waters.

(a) Swedish Combat Boat 90 (Stridsbåt 90, CB 90) in the port of Gothenburg (Ardon, 2008)

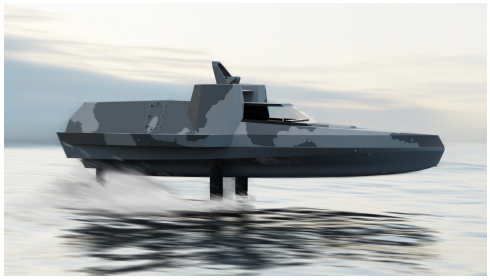

(b) Artistic impression of the EU-funded Transflytor project (SEAir International, 2023)

Figure 1.2: Examples of high-speed craft

1.1.3. Hydrofoils are a potential solution to improve LAC capabilities

Due to the interest in improving speed, range and seakeeping characteristics of a new LAC design, hydrofoils are a potential solution. A hydrofoil craft (Fig. 1.2b) is a watercraft supported on foils immersed in water. As the hull is lifted above the water, the influence of wave incidence and water resistance is reduced. As an example, the decreased resistance of implementing hydrofoils can lower energy consumption by 30 to 50% for high-speed ferries (Godø et al., 2024b). The decision for implementing hydrofoils will be further elaborated in Chapter 2.

1.2. Scope

The thesis will focus on an integrated early design approach of a future hydrofoil LAC and compare its performance to a planing bench. It is furthermore the aim of this study to give an indication of the possible solutions and estimate the operational effectiveness of applying these technologies. The research examines applicable retractable hydrofoil configurations, but does not go into detail of the retractable design. Moreover, it will study how the propulsion system is affected by the implementation of hydrofoils as it is probable that this can change the weight distribution and internal arrangement of the vessel significantly.

1.3. Approach

This study will take a systems engineering approach as described by Kossiakoff et al. (2020). Kossiakoff et al. (2020) identified three principal stages in a system lifecycle as illustrated by the flowchart in Fig. 1.3. This study will focus on the concept development stage as it is the aim of the study to come to a concept design of a hydrofoil LAC.

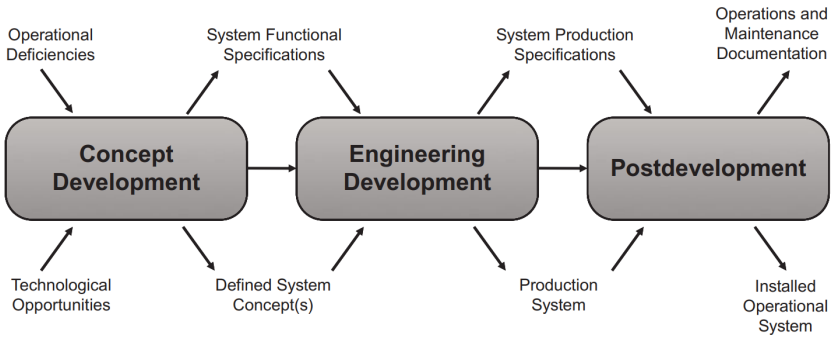

Figure 1.3: Principal stages in a system life cycle identified by Kossiakoff et al. (2020)

The concept development stage can be subdivided into three more stages as is illustrated in Fig. 1.4. The *Needs Analysis* phase defines the need for a new system by asking whether there is a valid need and a practical approach to meet it. This involves assessing if current or future needs can be met through modifying existing systems and if technology can support the desired improvements. Often, a new system emerges from ongoing analysis of operational needs or product innovation, rather than from a clearly defined starting point. The following *Concept Exploration* phase explores system concepts by addressing the required performance to meet the identified need and whether a feasible, cost-effective solution exists. Lastly, the *Concept Definition* phase selects the best system concept by identifying the optimal balance between factors such as capability, operational life, and cost.

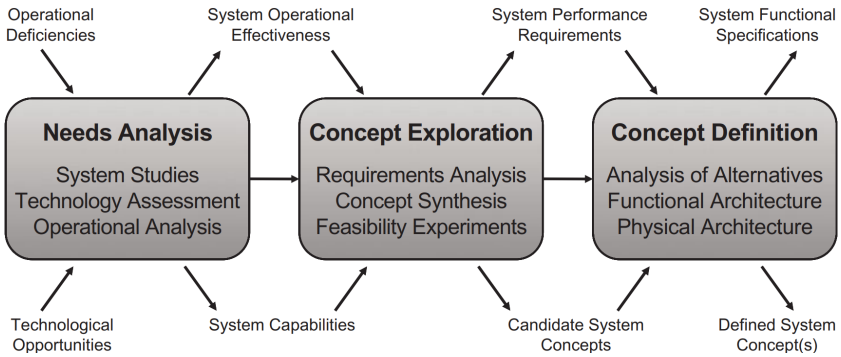

Figure 1.4: Concept development phases in a system life cycle identified by Kossiakoff et al. (2020)

1.4. Research questions

During the thesis the following main research question will be answered:

MQ: What is the operational effectiveness of a high-speed littoral assault craft with a retractable hydrofoil system compared to a planing design when operating in amphibious missions?

To answer this main question, a literature review is conducted first, with the following questions:

- LQ1. What are the design drivers and associated Measures of Effectiveness (MoEs) of a future Littoral Assault Craft (LAC), and what are possible solutions to fulfil these design drivers?
- LQ2. Which types of hydrofoil configurations can be considered for a Littoral Assault Craft (LAC) and what are their applicable propulsion methods?

During the subsequent research the following research sub-questions will be answered:

- RQ1. How do retractable hydrofoil systems influence the weight and resistance of a future Littoral Assault Craft (LAC) design, and what is the range increase potential of this application?
- RQ2. How can hydrofoil systems increase the operational effectiveness of a Littoral Assault Craft (LAC) design in waves, considering speed and safety of the crew?
- RQ3. How can the design methodology for a Hydrofoil Littoral Assault Craft (HLAC) be validated?

1.5. Societal and scientific relevance

There is a growing awareness of the importance of deterrence and defence among NATO member states. Whereas in 2014, 3 out of the 32 member states fulfilled the 2% GPD defence expenditure guideline, in 2024 it is expected that 23 have achieved this target (NATO, 2024). The ongoing conflicts have also highlighted the importance of modern technologically advanced military forces. This study explores an application of a technological advancement that can improve defence capabilities, while also improving the safety of personnel. Moreover, the type of vessels considered in this thesis are also intended for use in humanitarian aid operations.

Furthermore, the resistance reduction potential of hydrofoils enables new possibilities for sustainable high-speed craft designs. Global greenhouse gas emissions continue to increase and have unequivocally caused global warming, with a 1.1°C global surface temperature increase compared to 1850-1900 as a result (IPCC, 2023). The shipping industry contributed to 2.89% of all greenhouse gases in 2018 according to the IMO (2021). Driven by a growing focus on environmental impact, the fast ferry and leisure craft industry already embraces hydrofoil technology. As a result, several companies now offer hydrofoiling boats for the leisure industry (Candela, 2024a; Edorado, 2024; Enata, 2024) or ferry transport (Artemis, 2024; Candela, 2024b). This is also a growing research field (D'Amato et al., 2023; Giallanza et al., 2020; Godø & Steen, 2023; Godø et al., 2024b; Souppez et al., 2019), but research for military hydrofoil applications has largely stagnated after the cold war period. By revitalising the research of hydrofoils for defence applications, it extends the application of current hydrofoils to another type of craft and user. By increasing this user base, innovation of hydrofoil technology can be encouraged. This can also find its uses in other civilian industries that require high-speed passenger transport such as crew transfer vessels, search and rescue boats or daughter craft for wind farm servicing.

Additionally, modern hydrofoil craft designs benefit from advancements in composite materials and control systems. This offers greater potential for transport efficiency compared to earlier designs and can reduce the complexity of their implementation (Godø, 2024).

1.6. Structure

The thesis will follow the structure of the concept development stage described in Section 1.3. First, a *Needs analysis* in Chapter 2 aims to answer LQ1. Next, Chapter 3 explores different hydrofoil systems in the *Concept exploration* stage to address LQ2. The following research falls under the *Concept definition* phase, focusing on developing a defined concept design of a future hydrofoil LAC. Chapter 4 begins this phase by investigating how a hydrofoil system can be integrated into an LAC design to answer RQ1. Subsequently, Chapter 5 then assesses the seakeeping of a hydrofoil design compared to a planing benchmark to address RQ2. This is followed by validation of the design methodology in Chapter 6 to answer RQ3. Finally, Chapter 7 presents the thesis conclusions.

2

Needs analysis

The introduction of the LAC is part of a larger transformation of the amphibious forces of the Netherlands navy. To understand new requirements and design drivers, a greater understanding of current and future operations is required. This chapter will first discuss the current operations of landing craft in Section 2.1, which is followed by the future developments of the amphibious fleet in Section 2.2. Continuing in Section 2.3, the requirements of a LAC are discussed. Section 2.4 shows the state-of-the-art of current designs applicable for the LAC requirements. The following Section 2.5 introduces the main requirements, design drivers and performance indicators of a future LAC design, and Section 2.6 explores different concepts to fulfil these design drivers. Finally, Section 2.7 provides concluding insights to the first literature question:

LQ1: What are the design drivers and associated Measures of Effectiveness (MoEs) of a future Littoral Assault Craft (LAC), and what are possible solutions to fulfil these design drivers?

2.1. Current operational profile

The LAC will foremost be a replacement of the Landing Craft Vehicle Personnel (LCVP). The LCVP, also called a 'Higgins boat', is a moderately fast planing boat for troop transfer over short distances. The typical design of LCVPs has been around since the Second World War and played a crucial role in amphibious landings and logistics. General Dwight D. Eisenhower (1964) stated "If Higgins had not designed and built those LCVPs, we never could have landed over an open beach. The whole strategy of the war would have been different." Since the second world war there have been several iterations of the design but its main characteristics have remained the same: A shallow draft boat with a barge-like hull and a ramp at the bow. Van den Bosch (1970) shows that, although low deadrise designs like the LCVP have relatively low calm water resistance, it is generally accompanied by bad seakeeping performance. The larger version of this craft is called the Landing Craft Utility (LCU), which is intended for heavier equipment or vehicles and their associated personnel. The current model LCVP mkV(c) is shown in Fig. 2.1 with its main parameters in Table 2.1.

Figure 2.1: LCVP mkV(c) (Roeland, 2018)

Table 2.1: Specifications of the LCVP mkV(c) (Netherlands Ministry of Defence, 2023a)

Specification	Value
L_{oa}	15.7 m
B	4.27 m
T	0.65 m
Δ	24 t
P_b	846 kW
Propulsion	Waterjet
v_s (loaded)	25 kt
Operators	3
Embarked forces	35

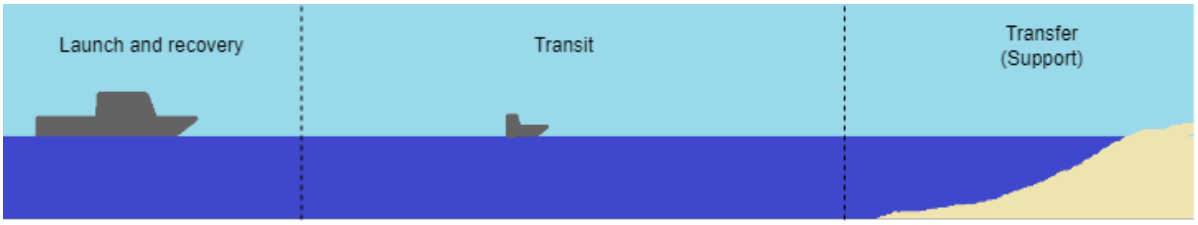

Figure 2.2: Phases during an amphibious landing

As illustrated in Fig. 2.2, the process of an amphibious landing can be divided between three phases: Launch and recovery, transit, and transfer. Similar phases can be identified in daughter craft for the servicing of offshore wind farms (Brans, 2021). Compared to daughter craft in the offshore wind industry, the biggest differences are the launch and recovery vehicle (mother ship) and the transfer to the shore instead of wind turbine. In addition, the landing craft can have a supporting role to the personnel landed on shore with its sensors or armaments.

Table 2.2: Main particulars of mother ships of the RNLN (Netherlands Ministry of Defence, 2024b, 2024c)

Ship	L_{oa} (m)	B (m)	T (m)	Δ (t)	Crew	Troops	P_b (MW)	v_s (kt)	Daughter craft
Rotterdam (LPD)	166	27	6.0	12,750	150	517	14.5	21	3 LCVP (well deck) 2 LCU (well deck)
Johan de Witt (LPD)	176	29	6.0	15,500	146	555	14.5	19	4 LCVP (davits) 2 LCU (well deck)
Karel Doorman (JSS)	205	30	7.6	27,800	129	171	26.0	18	2 LCVP (davits)

2.1.1. Launch and recovery

Table 2.2 lists the ships that can harbour LCVPs currently. Landing Platform Docks (LPDs) are the main mother ships of the RNLN to stage amphibious operations. The Rotterdam (Fig. 2.3a) stores the LCVPs in the well deck, whereas Johan de Witt (Fig. 2.3b) has davits to hoist the craft. The Joint logistic Support Ship (JSS) Karel Doorman, shown in Fig. 2.4, can also carry LCVPs in the davits but is mostly a logistical support ship. The use of davits puts a strict limit on the dimensions of possible designs of daughter craft stored on the ship, whereas a well deck provides more versatility.

(a) HNLMS Rotterdam (Dutch Ministry of Defence, 2020)

(b) HNLMS Johan de Witt with two empty LCVP davits (Bakker, 2009)

Figure 2.3: The two Rotterdam class Landing Platform Docks (LPDs) of the Dutch navy

Figure 2.4: Joint logistic Support Ship (JSS) HNLMS Karel Doorman with one empty LCVP davit (Torn, 2017)

A well deck is a floodable, hangar-like deck located at the ship's aft. By ballasting, the ship can lower its stern to flood the deck. Once the stern gate is lowered, this enables craft to disembark from the mother ship. Extra care must be given to wave generation inside the well deck. Waves inside the well deck are generated by the sloshing of the partially confined volume of fluid inside the ship and external waves propagating into the enclosed space. Wave height in the well deck can be reduced by sailing in head waves or increasing speed of the mother ship. Craft can embark and disembark a well deck safely up to and including sea state 4 (Bass et al., 2004; Hopman et al., 1994).

2.1.2. Transit

There are several reasons why landing craft must transit quickly. First, reducing transit time minimises exposure to threats from shore and sea, enhancing crew safety. Second, high-speed movement limits the ability to detect and respond to a landing, increasing the chances of maintaining the element of surprise (Vasundhara, 2011).

However, high-speed transit currently comes at the cost of the wellbeing of its crew. Most landing craft are small planing boats prone to high slamming forces during bow re-entry in waves (van der Eijk & Wellens, 2020). This results in high vertical accelerations, causing physical strain and increased fatigue for embarked personnel. For instance, measurements aboard the Fast Raiding Interception and Special Forces Craft (FRISC) recorded vertical acceleration peaks of 15 g (Margés, 2018). This leads to a high amount of impact injuries. A study on US Special Operations craft crewmen found that 62% of the crew reported one or more injuries requiring hospitalisation attributed to high-speed craft operations (Peterson et al., 2004).

In addition, high-speed transit is generally accompanied with a high amount of radiated noise and a large wake, which increases the craft's signature. This heightens the risk for early detection and makes the vessel more vulnerable to guided weapons (Kim et al., 2014).

The current doctrine aims to have mother ships near the deployment area, which reduces the transit duration of daughter craft (van der Maat, 2024). As a result, the accumulated fatigue and physical strain of the crew is limited. However, this approach is subject to change, as discussed in Section 2.2.

2.1.3. Transfer and support

Transfer is carried out by beaching the landing craft in low-gradient slopes or by pushing the boat against the shore in high-gradient slopes. A ramp is placed at the bow of the craft for personnel to embark or disembark onto shore. During this process, the embarked forces are the most vulnerable, as the craft reduces speed in the approach and personnel step onto land without cover. Generally, an anchor can be found on the aft of the vessel to help in unbeaching after the transfer (Damen, 2024b). According to the user interview with the Royal Netherlands Marine Corps (RNMC), an operation typically lasts seven days, during which the craft will remain in the region for support tasks before returning to the mother ship (see Appendix E).

2.2. Developments in the amphibious fleet

Increasingly, marines have to take into account armed opposition beginning at sea. Possible adversaries in coastal areas are more often in possession of advanced sensors and weapons with a long range. The new doctrine will have measures for amphibious operations that deal with threats at sea. Table 2.3 provides an overview of the main organisational changes that the changing doctrine will intro-

duce. The emphasis lies on a light, fast, scattered, and stealthy approach of smaller marine units with light logistical support (van der Maat, 2024).

Table 2.3: The main organisational changes of the new amphibious doctrine of the RNLN based on letters to parliament (Kamp, 2021; van der Maat, 2023, 2024)

Current doctrine (2025)	**New doctrine (2035)**
Few large mother ships	More smaller mother ships
Mother ships at small distance of shore ($\approx$ 10 nm)	Mother ships at large distance of shore ($\approx$ 40 nm)
Multiple waves of marines	Simultaneous deployment
Limited deployment areas	Multiple spaced out deployment areas

To realise this new doctrine, serious investments are being made by the Netherlands Ministry of Defence (NLMOD). Fig. 2.5 shows the expected development of the amphibious fleet of the RNLN. Currently, the amphibious daughter craft fleet exists of the LCVP, LCU and the FRISC. Where the LAC will take over most of the personnel transfer of the LCVP, the Littoral Craft Mobility (LCM) is intended to take over the light vehicle transfer. The larger LCU will remain in service at least until early next decade.

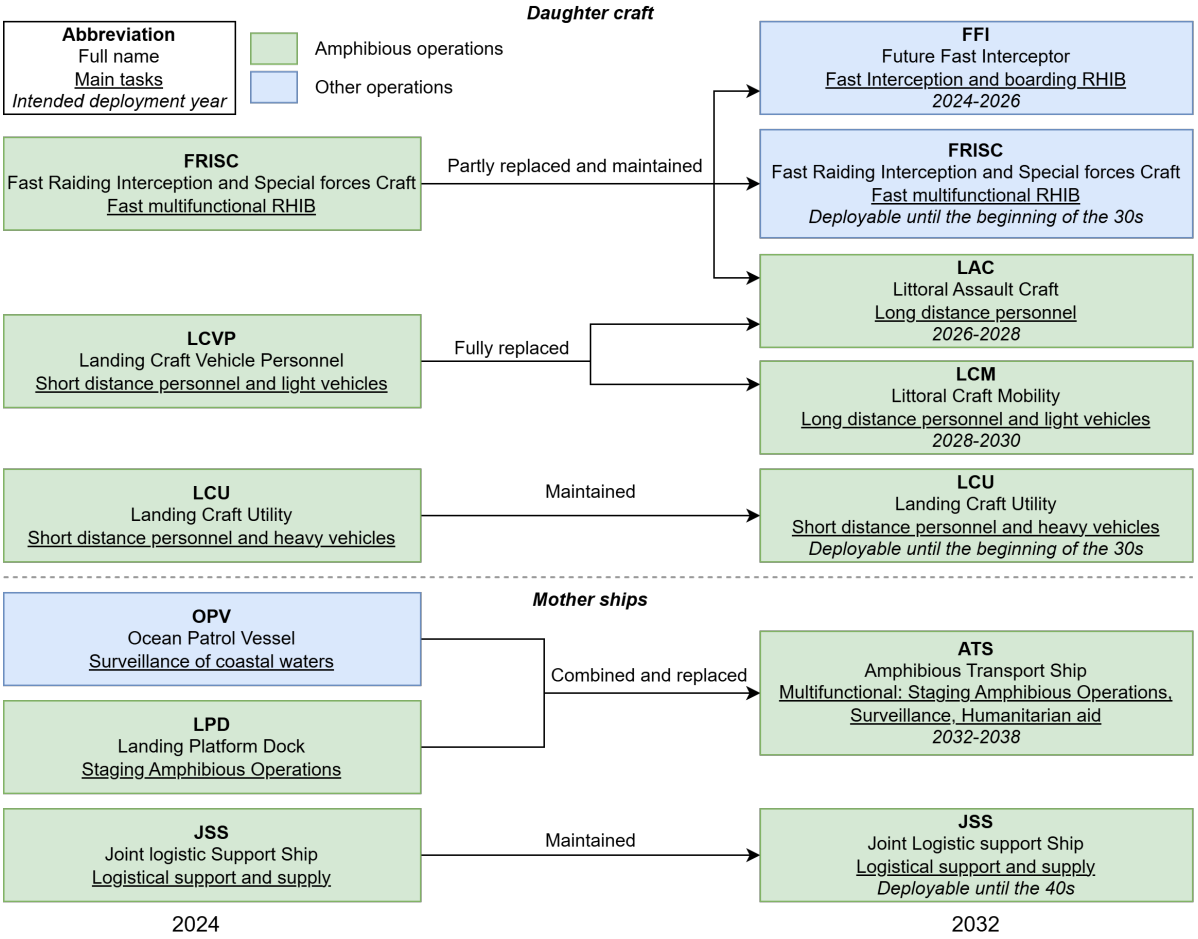

Figure 2.5: Changes in the operational amphibious fleet of 2032 compared to 2024 based on letters to parliament (Kamp, 2021; van der Maat, 2023, 2024)

Although the FRISCs were designed for a multifunctional role in amphibious, interception and boarding operations, they were deemed less ideal for amphibious operations. The FRISC does not provide enough cover for their crew against opposing fire, in a time where the risk of armed opposing forces is ever increasing. The deep V-type hull is less suited for landing on beaches and the relatively high bow

hinders quick (dis)embarking of troops. This high bow is also recognised early by adversaries (Kamp, 2021). The FRISC will partly be replaced with a new design called the Future Fast Interceptor (FFI) and operations of RHIBS will be reduced to interception and boarding. Amphibious tasks will be taken over by a larger order of the new landing craft (LAC/LCM).

Like the amphibious daughter craft fleet, the NLMOD intends to update the mother ship fleet. The two LPDs and four Oceangoing Patrol Vessels (OPVs) will be replaced by six Amphibious Transport Ships (ATSs), also referred to as the LPX (Buitendijk, 2024). The design and builder of this ship is not determined yet, but Damen has already proposed a design, which is shown in Fig. 2.6. As indicated by Table 2.3, the new ATSs will be smaller than the current LPDs due to a smaller detachment of troops (van der Maat, 2024). To deploy the same amount of troops, multiple ATSs will be required in future operations.

Figure 2.6: The Damen Enforcer 12026, a possible design for the new Amphibious Transport Ship (ATS) (Damen, 2023)

2.3. LAC requirements

The requirements posed by the NLMOD for the new LAC are published and available to ship builders. This section will focus on the most important requirements to take into account for a new LAC design, from a naval design perspective. This selection of requirements is also considered to be leading for the continuation of the thesis. The full list of current functional requirements can be found in Appendix A. The requirements are structured as a variant of the MoSCoW method (Wernham, 2012). It uses the following terminology:

- **MUST** is used only to describe mandatory external requirements, e.g. (inter-) national legislation
- **SHALL** indicates a mandatory requirement
- **SHOULD** indicates a desirable requirement

Sizing: According to REQ 9.2 and 9.5 the craft has to fit in the davits and well deck of the current LPDs and the JSS. The bounding boxes can be found in Appendix B. Furthermore, REQ 6.3 prescribes that the wade depth, and therefore draft, of the vessel can not exceed 0.86 meter during (dis)embarking.

REQ 9.2 SHALL fit inside the davit bounding box of HNLMS Johan de Witt and HNLMS Karel Doorman
REQ 9.5 SHALL fit inside the HNLMS Rotterdam and HNLMS Johan de Witt well deck bounding box
REQ 6.3 SHALL cause a maximum wade depth of 0.86 meter for personnel when (dis)embarking at prescribed landing points.

Operability: REQ 3.1 and 3.2 make clear that the LAC will have a broad range of operability across sea states. This is a higher requirement than the safe limit for (dis)embarking, as REQ 9.3 indicates that the LAC shall be launched and recovered from the davits in a sea state not higher than 3. However, safe (dis)embarking with the well deck is possible up to and including sea state 4 (Bass et al., 2004; Hopman et al., 1994).

REQ 3.1 SHALL be fully operational in the following climatological conditions:

- *Sea state: 0 up to but not including 5*
- *Wind speeds: 0-50 km/h (6 bft)*

REQ 3.2 SHALL be reduced operational in the following climatological conditions:
- *Sea state: 5*
- *Wind speeds: 7 bft*

REQ 9.3 SHALL be fully interoperable with the davits of HNLMS Johan de Witt and HNLMS Karel Doorman: LAC can be loaded onboard the mother vessels and safely launched and recovered up to, but not including, seastate 4.

Speed: REQ 9.8 and 9.9 specify the minimum speed of the vessel. Based on these requirements and the fact that the craft should remain "reduced operational" in sea state 5 following REQ 3.2, the plot of Fig. 2.7 can be derived. It is assumed that 10 knots is the minimum speed to remain sufficiently manoeuvrable and in safe operation in sea state 5. This is also the minimum viable speed considered for container transport according to Ng (2022).

REQ 9.8 SHALL be capable of a minimum speed of 40 knots at sea state 0 in fully laden condition
REQ 9.9 SHALL be capable of a minimum speed of 25 knots, at sea state 3 in fully laden condition

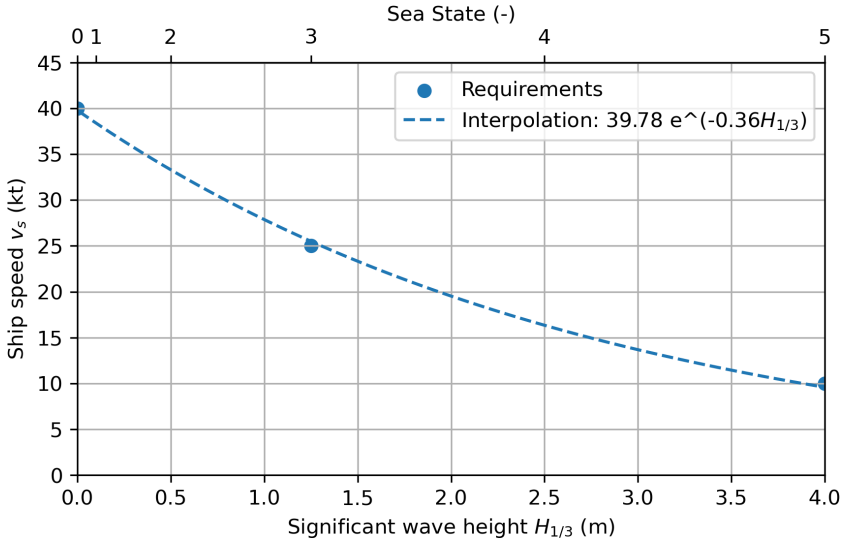

Figure 2.7: Required speed development based on sea environment following an exponential fit

Range: REQ 5.3 states that the craft should at least have a range of 200 nm at a speed of 18 knots. However, the preference of a higher speed of 25 knots indicates the strategical importance of a high-speed design to reduce transit duration.

REQ 5.3 SHALL have an uninterrupted distance of at least 200 nautical miles at a sustained speeds of 18 knots, preferably 25 knots

Operational area: REQ 2.12 and 3.3 prescribe the main operational area of the LAC being the Caribbean, North Sea, North Atlantic and Baltic.

REQ 2.12 SHALL support Humanitarian Aid & Disaster Relief operations in the Caribbean part of the Kingdom of The Netherlands.
REQ 3.3 SHALL have excellent sailing properties in the A1 and A2 areas in North Sea, North Atlantic and the Baltic.

A1 and A2 areas are designated by the Global Maritime Distress and Safety System (GMDSS) to denote different coverage zones for maritime communication and safety. A1 areas are areas that are within radiotelephone coverage of at least one VHF coast station. A2 areas are within range of one MF coast station. In practice, A1 areas are within 20-30 nm from shore and A2 areas are up to 100-150 nm from the coast line (Zhyvotova, 2024). Larger distances are covered by A3 and A4 areas and require other methods of communication with the shore such as satellite. Fig. 2.8 shows the coverage

of different sea areas in northwestern Europe. Although this requirement can imply that the LAC will operate up to 150 nm from shore, this is unrealistic as the previously stated range requirement is 200 nm. A realistic distance from shore currently remains 40 nm, which is within the A2 area (Netherlands Ministry of Defence, 2023b). Due to the increasing range of drones and guided weapons however, the LAC range is prone to increase in the future as well. The United Kingdom, a close partner of the Netherlands in amphibious operations, is already exploring amphibious surface connector concepts capable of operating at a range of 100-150 nautical miles from shore (Navy Lookout, 2024; Scott, 2023).

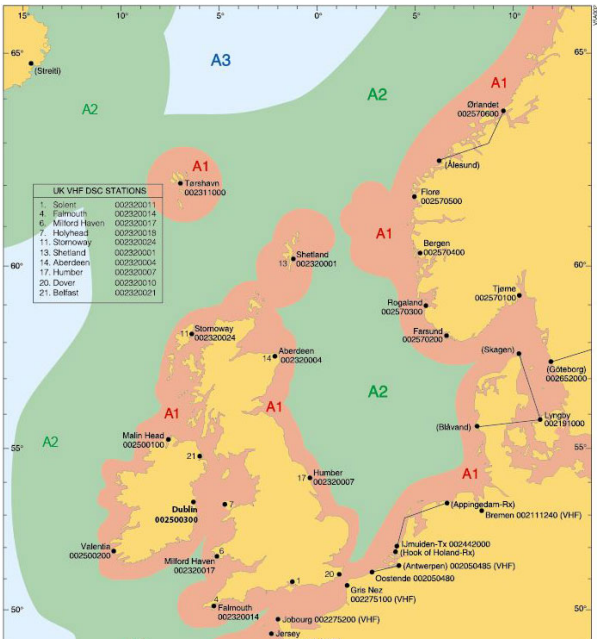

Figure 2.8: GMDSS sea areas in northwestern europe (Her Majesty's Stationary Office and the UK Hydrographic Office, 2015)

As shown in Fig. 2.9, significant wave heights up to 2.5 meters (sea state 4) can become a regular occurrence at the prescribed range, specifically in the North Sea. This is within the operability requirements, but can reduce the speed of the vessel substantially, as is seen in the speed requirements.

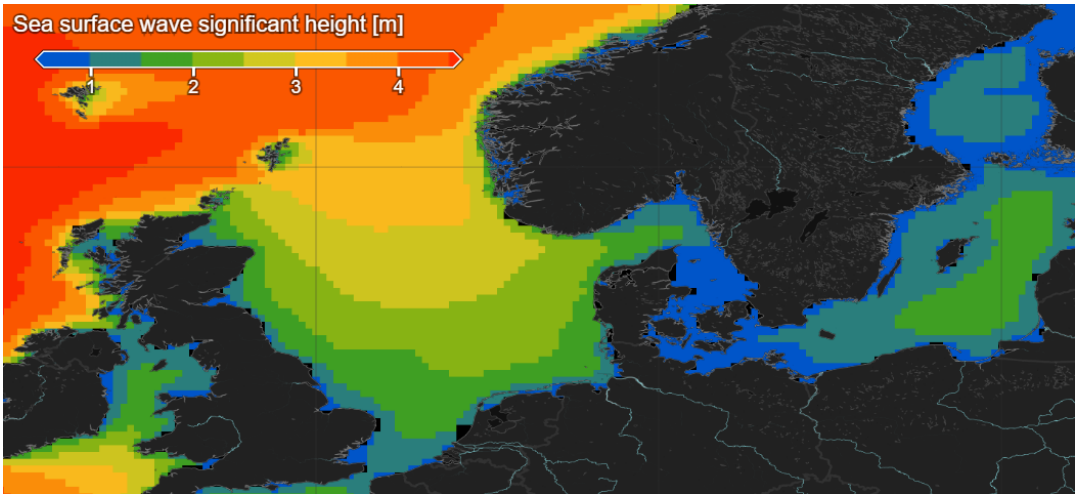

Figure 2.9: Median significant wave height in January (worst yearly condition) for northern Europe (E.U. Copernicus Marine Service Information (CMEMS). Marine Data Store (MDS), 2024)

Fig. 2.10 shows the median significant wave height for the Caribbean Netherlands. In general, the sea conditions are better than in northern Europe, but can still reach significant wave heights up to 2 meters.

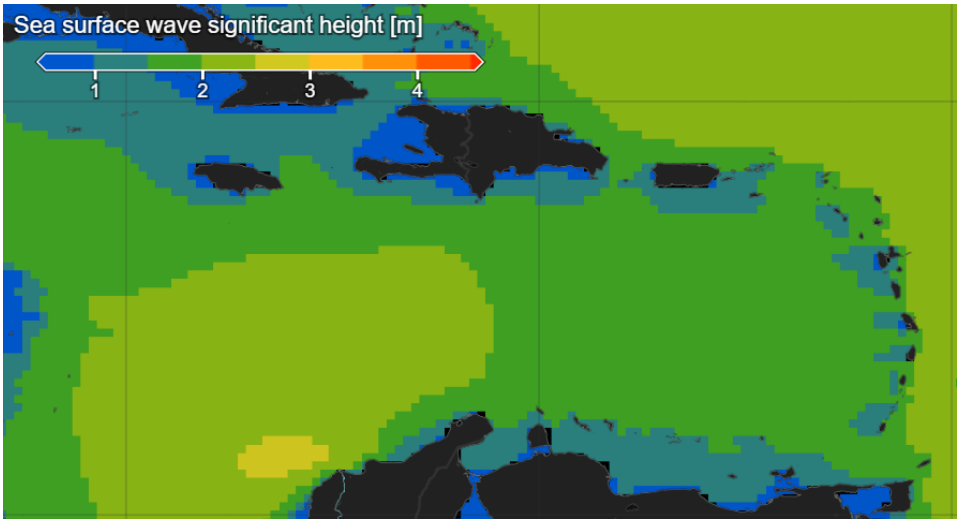

Figure 2.10: Median significant wave height in January (worst yearly condition) for the Caribbean Netherlands (E.U. Copernicus Marine Service Information (CMEMS). Marine Data Store (MDS), 2024)

Passengers: REQ 9.10 states that the craft will have 16 passengers or Embarked Military Forces (EMF). This corresponds to a payload of 4500 kg. Furthermore, it can be concluded from other requirements that the LAC requires a crew of 3 operators to navigate the craft, which makes the total amount of people on board 19.

REQ 9.10 SHALL have an EMF compartment capable of embarking, transporting and disembarking all three of following configurations (full payload 4500kg):

- *6 EMF-personnel + full personal gear + arctic gear, or*
- *12 EMF-personnel + full personal gear, or*
- *16 EMF-personnel without gear*

Safety and comfort: According to REQ 9:13 and 9:15 a defined EMF-compartment is required for the transit of personnel. This compartment is specifically designed to reduce physical strain and fatigue. Although not prescribed in the functional requirements, the NLMOD does have a prescribed maximum vertical acceleration for their vessels. The maximum for the LAC is not yet known, but the prescribed limit of the FFI (replacement of the FRISC) is published. The FFI's vertical acceleration limit is 35 m/s^2 (3.6 g) in sea state 4 for the most forward passenger[1] (Netherlands Ministry of Defence, 2024a). This limit can be taken as a benchmark, but operators will most probably reduce speed earlier, as professional crews will react to acceleration peaks to reduce physical strain and damage to the vessel. A vertical acceleration peak of 1.25 g can already cause professional crews to reduce vessel speed (Keuning, 1997).

REQ 9:13 SHALL be equipped with individual seating for Crew and EMF, compliant with the MoD shock standard as per Annex B.
REQ 9:15 SHALL provide an EMF-compartment with systems minimizing the physical strain (caused by e.g. temperature, vibrations, sound, shock) on the EMF

[1]The mean value of the 10% highest peaks (A1/10)

2.4. State-of-the-art designs

This section will discuss the current state-of-the art in small littoral craft concepts. It will touch on the most recent or most significant designs. A full list of currently operational littoral craft with their main parameters can be found in Appendix C.

2.4.1. Combat Boat 90 (CB90)

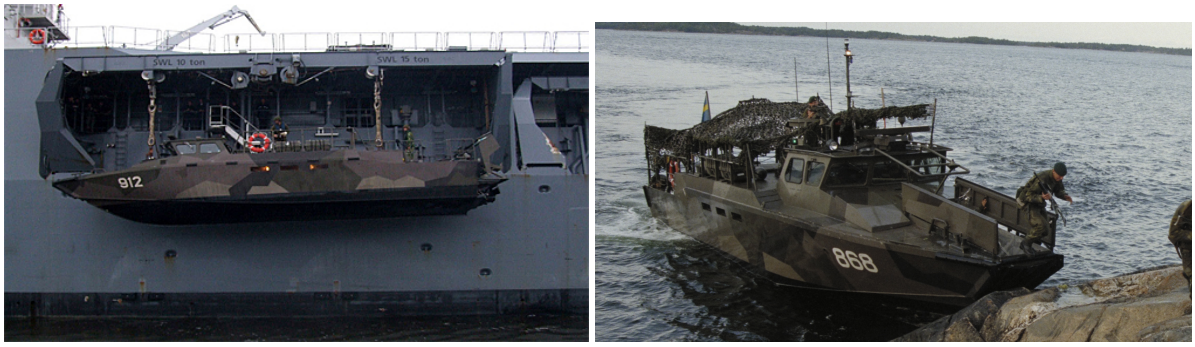

(a) In the davits of LPD Johan de Witt (Karremann, 2015) **(b)** Personnel disembarking from the bow hatch (Dockstavarvet, 2024)

Figure 2.11: CB90s in different operational phases

Although the design of the Combat Boat 90 (CB90) stems from the eighties and nineties, it is by far the most produced littoral craft concept that can be identified as a LAC. Currently, more than 250 CB90s are in operation worldwide and new orders of the craft are still being placed (Naval News, 2024). The design of Saab Dockstavarvet is employed by several navies with their own configurations, such as Sweden, Norway, Greece, Mexico, Malaysia and the United States. Depending on the configuration, the craft can transport around 20 passengers, which does not include 3 operators. The aluminium craft can reach a top speed of 45 knots in calm water. Its shallow draught of 0.9 m and water jet propulsion also allow it to operate in shallow coastal regions. The water jets combined with underwater control surfaces contribute to a good manoeuvring characteristic as well (Naval Technology, 2022). The bow hatch (Fig. 2.11b) and integrated ramp allows personnel to (dis)embark to shore. As shown in Fig. 2.11a, the RNLN have previously tested the CB90 with their own LPDs. In 2010 the RNLN tested its capabilities for a period of six months and they confirmed that the craft can be used as a diving platform (Marineschepen.nl, 2010). In 2015, a detachment of Swedish marines with CB90s were stationed on LPD Johan de Witt to cooperate with an anti-piracy mission (Karremann, 2015).

2.4.2. Jehu (Watercat M18)

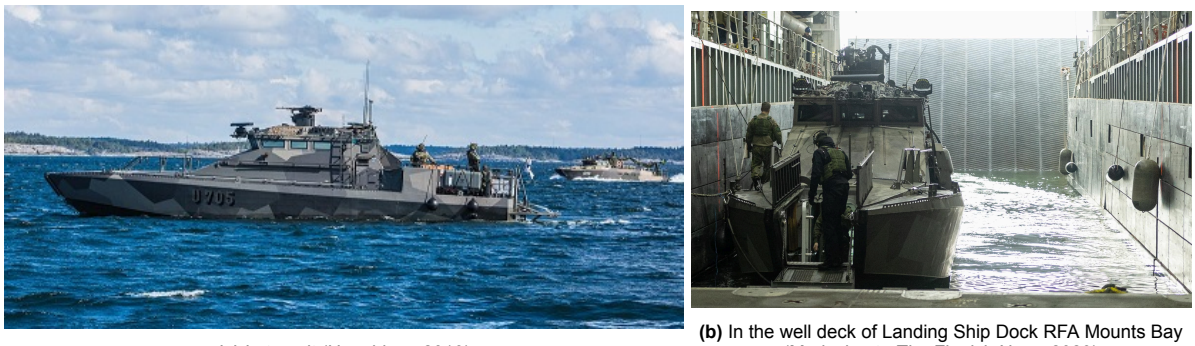

(a) In transit (Häggblom, 2019) **(b)** In the well deck of Landing Ship Dock RFA Mounts Bay (Merivoimat - The Finnish Navy, 2023)

Figure 2.12: Jehu class craft in different operational phases

The Jehu class (Fig. 2.12) is a more recent example of a littoral craft concept and the Finnish answer to the CB90. Until 2014, the Finnish navy only used open or semi-open landing craft with few to no offensive capabilities (the Jurmo class for example). Therefore, for the design of the Jehu class focus was placed on combat ability (Häggblom, 2019). The Jehu can transport up to 31 people (excluding the

crew of 6) or 5.7 t of payload with a maximum speed of 35 kt (Finnish Defence Force, 2024). Although the craft is at the larger end of littoral craft concepts with its 20 meters in length, it can still be loaded onto well decks, as is shown by Fig. 2.12b. Fig. 2.12b also highlights the similar bow hatch and ramp of the Jehu to the CB90.

2.4.3. Combatant Craft Medium (CCM)

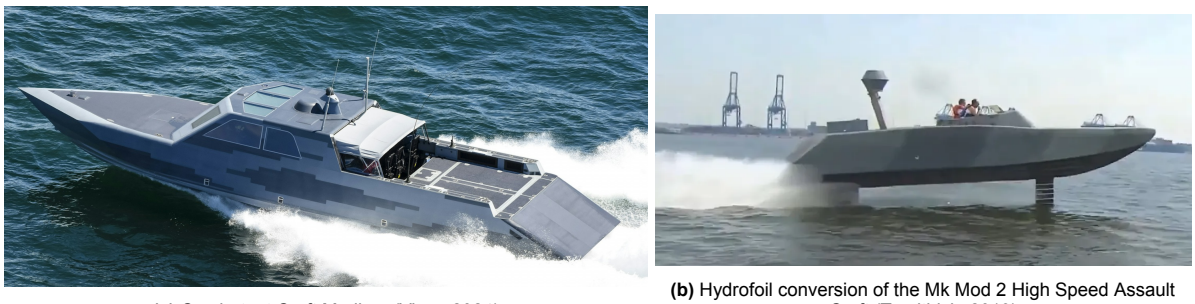

(a) Combatant Craft Medium (Vigor, 2024)

(b) Hydrofoil conversion of the Mk Mod 2 High Speed Assault Craft (Trevithick, 2019)

Figure 2.13: Littoral craft development in the United States of America

Although not defined as a landing craft, the Combatant Craft Medium (CCM) of the United States (US) navy offers similar specifications to the other littoral craft concepts. The craft, shown in Fig. 2.13a, is intended for medium range maritime interdiction or insertion, and extraction of special operation forces. It entered service for the US navy in 2015 but was also recently sold to the navy of Norway (Ozberk, 2023). The manufacturer, Vigor (2024), claims that the craft has a range of 600 nm and can transport 19 passengers with 4 operators. The design incorporates an aluminium hull and an overall length of 18.47 m. The craft is also deployable from the San Antonio class LPD and Wasp class LHD (Lundin, 2023). In 2019, a hydrofoil conversion of an earlier and smaller model from the same family of boats was revealed (Trevithick, 2019). This occurred over 25 years after the US navy retired its six Pegasus-class missile boats, which were the last operational hydrofoils in its fleet. Little information has been revealed about the design (Fig. 2.13b) or its performance, but this indicates the renewed interest of the hydrofoil concept within the US navy.

2.4.4. Troop Transportation Flying Vector (TRANSFLYTOR)

(a) Design overview with conventional propellers (SEAir solutions, 2024)

(b) SEALENCE propulsion set-up (SEALANCE, 2023)

Figure 2.14: Design highlights of the TRANSFLYTOR

In 2021 an EU grant was issued for a joint industrial development programme for research into a Troop Transportation Flying Vector (TRANSFLYTOR). Impressions of the design are shown in Fig. 1.2b and Fig. 2.14. The aim of the project was to “design a high-speed vessel equipped with retractable hydrofoil systems for rapid military interventions at sea” (Directorate-General for Defence Industry and Space, 2021). The craft is designed to use its foils for a high-speed transit in deep sea, and to navigate with retracted hydrofoils in shallow waters or during approach phases. Like other littoral craft concepts, the TRANSFLYTOR will be launched from larger mother ships. SEAir (2022), one of the main contributors

of the project, claims that the hydrofoils can increase stability, reduce the amount of “shocks” up to 50% and decrease fuel consumption with 30% to realise a range of 800 nm. SEAir also claims that the design can achieve a speed of 45 knots and that using hydrofoils makes it more discreet, reducing its signature. In a press release, SEAir stated that the 20 m long (L_{oa}) craft is able to transport 12 embarked forces, with 1 t of tactical payload (a drone for example) (SEAir, 2022). Furthermore, SEAir has expressed its interest in implementing diesel-electric hybrid propulsion to the design. In 2023, the company SEALENCE announced its cooperation with the project, which produces electric water jets (Fig 2.14b). Literature about this type of water jets is difficult to find, but SEALANCE claims a 10-15% efficiency increase compared to current inboard water jets, purely looking at the propulsion method and without considering the engine and transmission efficiencies (SEALENCE, 2020).

2.5. Measuring operational effectiveness

Kossiakoff et al. (2020) describe “In concept development, the analyses that are designed to estimate the degree to which a given system concept may be expected to meet a postulated set of operational requirements is called *operational effectiveness analysis.*” These analyses are based on mathematical models of the operational environment and a candidate system concept that is being analysed. The operational environment is modelled in terms of a set of scenarios. To evaluate the results of effectiveness simulations, criteria are developed that identify the characteristics of the system response to the environment that are crucial to its operational use. These performance indicators are called Measures of Effectiveness (MoEs) or Measures of Performance (MoPs). Kossiakoff et al. (2020) describes MoEs and MoPs as follows:

- “A MoE is a qualitative or quantitative metric of a system’s overall performance that indicates the degree to which it achieves it objectives under specified conditions. A MoE always refers to the system as a whole.”
- “A MoP is a quantitative metric of a system’s characteristics or performance of a particular attribute or subsystem. A MoP typically measures a level of physical performance below that of the system as a whole.”

In the hierarchy of performance indicators, a MoE will always be more important than a MoP. This is due to a MoE evaluating the complete system, whereas a MoP looks at a distinct subsystem.

In the design of naval vessels, the measurement of operational effectiveness is a point of contention (Stam, 2025; Streng et al., 2022). Compared to the commercial shipping sector, measuring the effectiveness of a naval vessel is less straightforward. Effectiveness of a cargo ship is often measured in capacity and speed for example, resulting in efficiency measurements such as transport efficiency or the Energy Efficiency Design Index (EEDI). The effectiveness of a naval vessel is not solely measured based on these efficiencies and is for a greater part measured by its other capabilities. Streng (2022) identified the main capabilities that define the effectiveness of a navel vessel as:

- Offensive capabities - SEnsors Weapons And COmmunication (SEWACO)
- Survivability
  - Susceptibilty
  - Vulnerability
  - Recoverability
- Mobility
  - Top speed
  - Acceleration and deceleration
  - Manoeuvrability
- Range
- Endurance/autonomy

An Overall Measure Of Effectiveness (OMoE) is traditionally deduced from expert opinion and pairwise comparisons on singular aspects of the design (Brown, 2013). Numerical values can then be derived using for example Multi-Attribute Utility Theory (Keeney & Raiffa, 1993) or the Analytical Hierarchy Process (Saaty, 1990). However, also models exist to derive operational effectiveness and automate this process. In these models, vessels are assigned certain reference missions within a set operational situation. As an example, a method to gain numerical values for MoPs and MoEs is the use of a wargaming model (Brown & Salcedo, 2003). This would however require extensive modelling capability. Thus, this thesis aims to provide a qualitative assessment of the operational effectiveness of the application of

hydrofoils by the use of several distinctive MoEs.

The design drivers listed in Table 2.4 are derived through the investigation of the demands from the RNLN and an user interview conducted with the RNMC (Appendix E). For each design driver, a Measure Of Effectiveness (MoE) is assigned to measure performance increases or decreases. In addition, each design driver has a required value and a base value. The required value yields from the current requirements published by the NLMOD, whereas the base value is based on the CB90's performance. Of all LAC concepts, the CB90 is the most established LAC concept. It is the most produced littoral craft and the RNLN has experience in deploying it from their mother ships. Some design specifications of the CB90 are also known to De Haas, therefore this design will be taken as the benchmark of a new hydrofoil LAC design.

As the first performance indicator, the range of the vessel is a measurement that incorporates several factors: resistance, propulsion efficiency and fuel capacity. As mother ships increase their distance from shore, and the LAC starts to include supporting roles to its operational profile, range will become increasingly important. Secondly, the speed in seaway is not only a measurement of how fast the vessel is in itself but also for the development of operability. A plot like shown in Fig. 2.7 gives a more complete image of the operability of the craft. However, this would require a far greater amount of simulations. For an initial indication only one wave condition will be considered. Maximum vertical accelerations are an important factor for safety and the fatigue development of the crew and will be assessed in sea state 3, as this is a representative condition for high-speed transfer of personnel. Values left empty in Table 2.4 will be assessed later in this research.

Table 2.4: Design drivers, performance indicators and requirements for a future LAC design

Design Driver	Criteria to improve compared to base design (MoE)	Required Value	Base value planing hull
Range	Nautical miles in high speed (30 kt) calm water	200 nm	300 nm
Speed	Maximum sustained speed in sea state 3	25 kt	-
Safety	A1/10 positive vertical accelerations in sea state 3 at 35 kt on CoG	35 m/s^2	-

The CB90 and the LCVP are shown to fit in the davits of the mother ships of the RNLN and therefore meets this strict requirement. The future LAC will be based on the design of the CB90 but will retain some freedom in the beam and its internal division. The LCVP has shown that vessels with a bigger beam will fit in the davits of the RNLN and the CB90 is designed for 18 passengers instead of 16. A summary of these additional requirements is listed in Table 2.5. If a design can fulfil the requirements of Table 2.5 and the required values of Table 2.4, it is deemed technically feasible.

Table 2.5: Summary of additional requirements of a future LAC

Parameter	Value	Reasoning
L_{oa}	16 m (max)	L_{oa} of CB90 (Davits)
B	4.27 m (max)	B of LCVP (Davits)
T	0.86 m (max)	Requirement - same as CB90
Payload	16 passengers (4.5 t)	Requirement
Crew	3	Requirement
Bow hatch and ramp	-	Requirement

2.6. Hull concept exploration

An LAC classifies as a high-speed craft. A high-speed craft is defined by hydrodynamicists as having a speed greater than a waterline length Froude number $Fn_{L_{wl}} = v_s/\sqrt{L_{wl} \cdot g} \gtrsim 0.4$ (Faltinsen, 2005). For conventional displacement vessels, this marks the point where the residuary resistance surpasses

the viscous resistance and increases exponentially. After this point, the required engine power of displacement ship types can increase with a third power relation (v_s^3) to fourth power relation (v_s^4) of the forward speed (Keuning & Ligtelijn, 2017). This acts as a bottleneck for achieving higher speeds by displacement vessels, also referred to as the hull speed. In addition, due to the considerable increase of power at higher speeds, a large range is challenging to achieve whilst retaining high speed. To reduce resistance, different types of lift need to be employed next to hydrostatic lift. For example, a planing craft uses hydrodynamic lift of its planing area under water, to lift its hull out of the water and reduce the effect of water.

In addition, due to the stringent dimensional requirements, meeting the seakeeping design drivers of Table 2.4 is challenging. Concepts previously applied to improve seakeeping of high-speed craft, such as the Enlarged Ship Concept (ESC) or Axe Bow Concept (ABC), are build upon the principle of increasing the size of the vessel to reduce maximum vertical accelerations (Gelling & Keuning, 2011). However, this is not a solution for a future LAC design. Increasing the deadrise angle of the vessel can also improve seakeeping performance, but this would introduce difficulties in the landing procedure (Keuning et al., 1992).

Another option is the application of an Advanced Marine Vehicle (AMV) hull form. AMVs embrace a broad range of craft types, but are in most cases applied to attain higher speeds at sea than possible with conventional ship types (McKesson, 2014). The Small Waterplane Area Twin Hull (SWATH) and hovercraft are exceptions as they are used to gain ride quality or amphibious capability, respectively. Table 2.6 shows a comparison of different AMV types. To fulfil the design drivers of Table 2.4, the design has to perform well in seakindliness and speed/power. Hydrofoils and Wing In Ground (WIG) vehicles excel in both seakindliness and speed/power requirements, but a WIG vehicle can not realistically be used as a daughter craft due to its size requirements (aeroplane-like). The Surface Effect Ship (SES) also performs well in these aspects, but Table 2.4 is too simplified to gain insight in its operability. Fig. 2.15 illustrates the speed gains hydrofoil craft can achieve in sea state 3 and above, compared to other AMVs in seaway. It also highlights the speed limitation of hydrofoils, as cavitation limits current hydrofoil craft to a speed of 50 kt (McKesson, 2014). Additionally, it shows the drastic speed reduction in seaway of SESs, caused by the ventilation of the sidewalls and increased added resistance (Keuning, 1997). Furthermore, SESs are prone to cobblestone vibrations, which reduces passenger comfort (Smith, 1995). However, it is important to note that the characteristic curves of Fig. 2.15 are strongly dependent on the size of the vessel and should be viewed as indicative.

Table 2.6: McKesson's (2014) subjective assessment of various AMV hull forms against five performance parameters.

Hull form	Sea-kindliness	Speed[2]/ Power	Comfort & Space	Load Carrying Ability	Economics
Catamaran	2	1	3	2	3
Trimaran	2	2	2	3	3
SWATH	3	1	3	1	2
Hydrofoil	3	3	1	1	1
WIG	3	3	1	1	1
Hovercraft/ACV	1	3	3	2	1
SES	2	3	3	2	1

Next to speed in seaway, there are several other methods of quantifying seakeeping performance, such as ship motions, accelerations, course keeping and sustaining slamming loads (Tan, 1995). High vertical accelerations can reduce operability, whereas lower but frequent accelerations can induce motion sickness. This is therefore an important indicator for personnel transfer. However, hydrofoils are characterised with low vertical accelerations (Faltinsen, 2005). The ship hull operates above the effects of surface waves and the foils that provide lift and control forces operate below the water surface, where wave effects diminish with depth. For this reason, hydrofoil craft are known to offer the smoothest ride available in ferry service (McKesson, 2014).

Although the "load carrying ability" of hydrofoils according to Table 2.6 is relatively low, as payload mass is a critical factor for its ability to become foilborne, hydrofoils have been broadly applied in the ferry industry (Yun & Bliault, 2014). This confirms the feasibility of hydrofoil applications for ferries or personnel transport. Furthermore, the drastic resistance reduction when becoming foilborne makes

[2]Speed addressed as speed in seaway and not only calm water performance

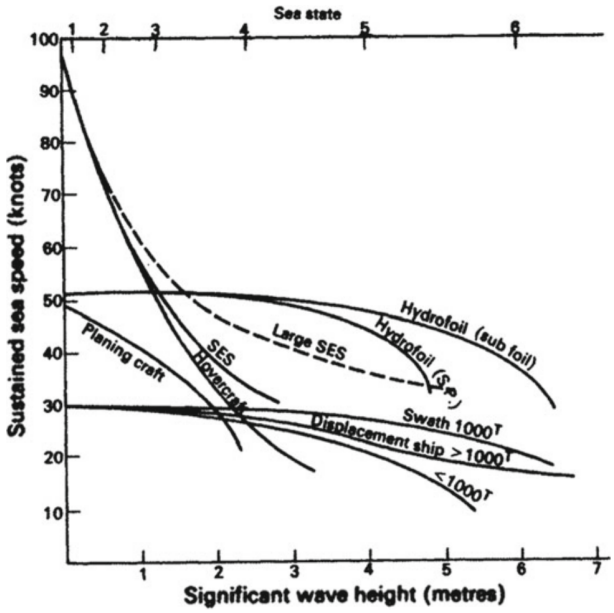

Figure 2.15: A rough comparison of maximum sustained speed in seaway for different AMV types (Rawson & Tupper, 2001)

foiling craft efficient at a high speed. At these speeds, other vessel types become less efficient. This is demonstrated by the transport efficiency. The transport efficiency is defined by Eq. (2.1), where W, V, and P represent the weight, velocity and installed power, respectively (Gabrielli & von Karman, 1950). Fig. 2.16 visualises the transport efficiency of different AMVs, with hydrofoils excelling in the speed range of 35-50 kt. Although the findings of Van Oossanen (1983) are not recent, the same observation is currently made for hydrofoils compared to slender catamarans (Godø, 2024). Battery-electric boat manufacturers employ this characteristic as well, to increase the range of a fast boat that has a relatively small 'fuel' capacity (Artemis, 2024; Candela, 2024a; Edorado, 2024). Doornebos et al. (2023) also demonstrated that hydrofoils can increase the range of a zero-emission 30-40 kt ferry.

$$\Omega = \frac{W \cdot V}{P} \tag{2.1}$$

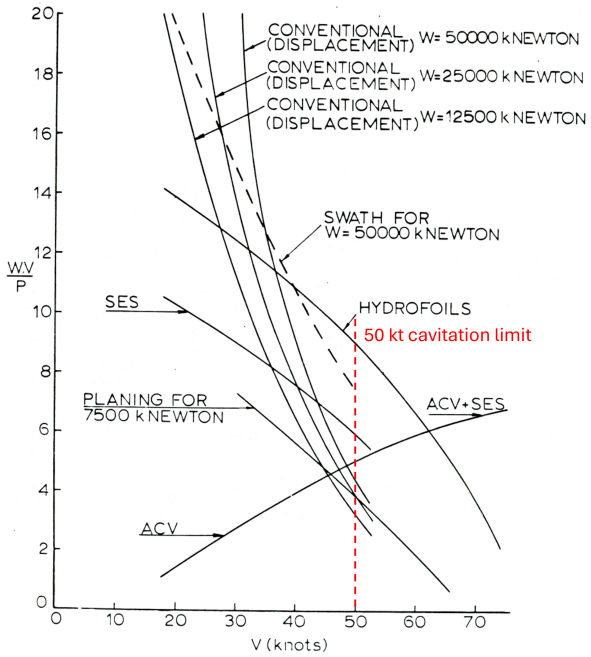

Figure 2.16: Transport efficiency of different AMV types by Van Oossanen (1983) with cavitation limit of current hydrofoils

Hydrofoil craft require a deeper draught compared to an equivalent displacement ship due to their extended foils. Therefore, the dimensional restrictions of Table 2.5 imply that a potential hydrofoil system shall be retractable, meaning that the hydrofoils are lifted to reduce draught. This allows the craft to traverse shallow waters, to beach during the approach phase, and it allows the craft to be stored in the davits. Although this increases the complexity and cost of the system significantly, this has not prevented its application in ferry, leisure and military designs (Yun & Bliault, 2014). A well-known example is the Boeing Jetfoil ferry design, shown in Fig. 2.17. Retraction also facilitates easier maintenance or replacement of the foils and struts (Johnston, 1985). Appendix C contains a database of retractable and non-retractable hydrofoils.

In summary, hydrofoils offer a promising solution for a future LAC design due to:

- the highest transport efficiency at the required speeds of any AMV, which can increase range as a result;
- the high sustained speed through rough seas;
- the low vertical accelerations at high speed to reduce fatigue and physical strain of crew;
- the load carrying ability being sufficient for passenger transport;
- the successful prior application of retraction systems for hydrofoils;
- the reduced importance of economics for the navy, provided sufficient gains in other performance aspects can be realised.

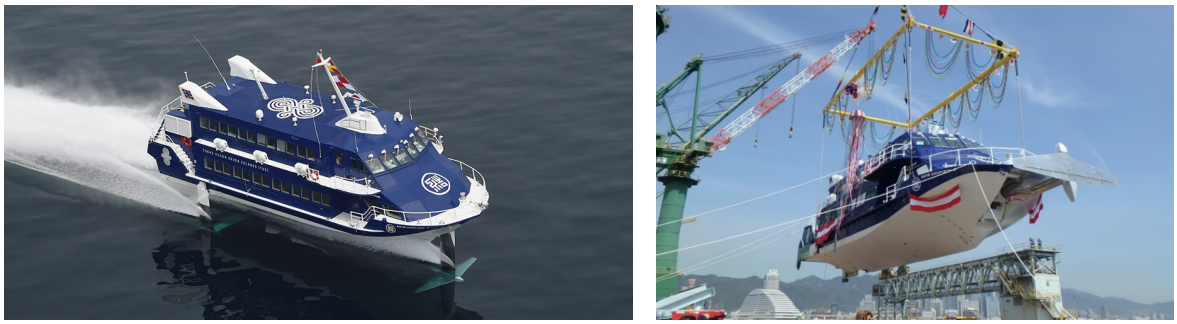

(a) Foiling at high speed with extended hydrofoils (Tokai Kisen, 2024)

(b) Retracted hydrofoils (Baird Maritime, 2020)

Figure 2.17: The Boeing Jetfoil 'Seven Islands Yui' built by Kawasaki and launched in 2020

2.7. Concluding insights

The primary objective of the LAC is to ensure safe and fast transport of personnel between mother ship and shore under a broad range of sea conditions for its size. While several LAC concepts are currently available, the CB90 design is the most established. Design drivers and performance indicators (MoEs) for a future LAC design are identified based on its operational profile and requirements. The design drivers regard range, speed in seaway, and safety. These design drivers are further validated in an user interview with of the RNMC. Furthermore, base requirements are identified to classify a technically feasible design. By comparing hull form concepts to fulfil the design drivers, it is revealed that a retractable hydrofoil system offers the most promising solution. An LAC design equipped with a hydrofoil system will hereafter be referred to as a Hydrofoil Littoral Assault Craft (HLAC).

3

Hydrofoil systems and propulsion concept exploration

This chapter aims to present current applicable hydrofoil configurations for an LAC and to elaborate on their advantages, disadvantages, and possible limitations. First of all, Section 3.1 will provide the background of hydrofoil theory, which is followed by the requirements of a foil system in Section 3.2. Continuing in Section 3.3 the applicable hydrofoil configurations will be discussed. Current methods of retraction and actuation are discussed in Section 3.4. The following sections will elaborate on viable propulsion systems, from the propulsor (3.5) and transmission (3.6) to the prime mover (3.7). Based on the earlier sections, Section 3.8 will then compare possible hydrofoil and propulsion options. Finally, Section 3.9 will provide concluding insights to the second literature question:

LQ2: Which types of hydrofoil configurations can be considered for a Littoral Assault Craft (LAC) and what are their applicable propulsion methods?

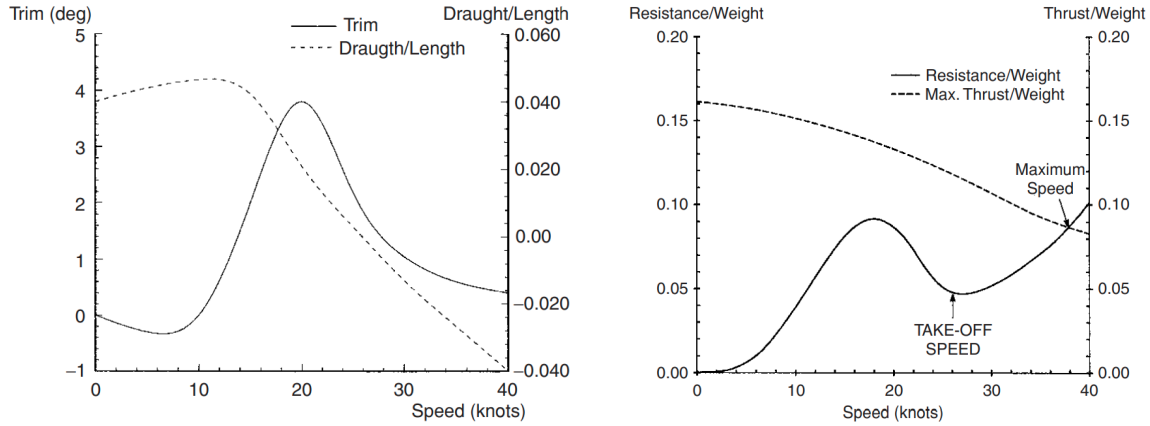

(a) Example of draft (excluding foils) and trim versus speed

(b) Example of resistance and thrust versus speed

Figure 3.1: Typical behaviour of a monohull hydrofoil vessel over speed (Faltinsen, 2005; van Walree, 1999)

3.1. Hydrofoil theory

A hydrofoil craft is a watercraft supported on foils immersed in water. If the vessel gains forward speed, the foils will generate lift. As the speed and generated lift increases, the hull is lifted out of the water and its resistance is reduced significantly. Because the density of water is around 800 times the density of air, a hydrofoil requires less forward speed and a smaller lifting area to generate enough lift for a vessel compared to an aircraft wing. Fig 3.1a shows a typical draft development over speed, where positive

trim corresponds to bow up. This also shows the substantial trim increase when the vessel reaches take-off speed. Compared to a planing hull, the resistance reduction can be as high as 50% at optimal speeds (Clement, 1976; Godø et al., 2024b). A representation of the resistance development over speed is provided by Fig. 3.1b. The drag curve is characterised by a resistance hump and a 'take-off speed', where the lift force of the foils becomes greater than the weight of the vessel. The maximum speed of current hydrofoils is limited by cavitation inception at around 50 kt. Higher speeds can be achieved with supercavitating foils, but this results in a major increase in specific power requirements to get the vessel foilborne (Johnston, 1985). Although recent research indicates that supercavitating hydrofoils can be designed for higher lift efficiencies in the subcavitating regime as well, no commercial application of supercavitating hydrofoils currently exists for fast watercraft (Brizzolara, 2015).

The design of hydrofoil craft is in essence a balancing act between the weight of the vessel and the lift produced by the foils. The lift of the foils is proportional to wing area (squared), whereas the weight is proportional to volume (cubed). Therefore, if the size of the vessel is increased, the foils will outgrow the ship eventually. This is known as the square-cube law and is a fundamental rule in the design of hydrofoil craft (Clark et al., 2004). To date, the biggest hydrofoil vessels built are the USS Plainview with 325 t and the Russian Bobachka with 420 t in displacement (Yun & Bliault, 2014). However, several sources indicate that the real limitation would be around 1000 t displacement (Clark et al., 2004; Johnston, 1985; McKesson, 2014). The 20-30 t displacement of a LAC design fits well within this limit, however, the square-cube law remains relevant. A change in weight and volume can drastically affect the ideal hydrofoil design.

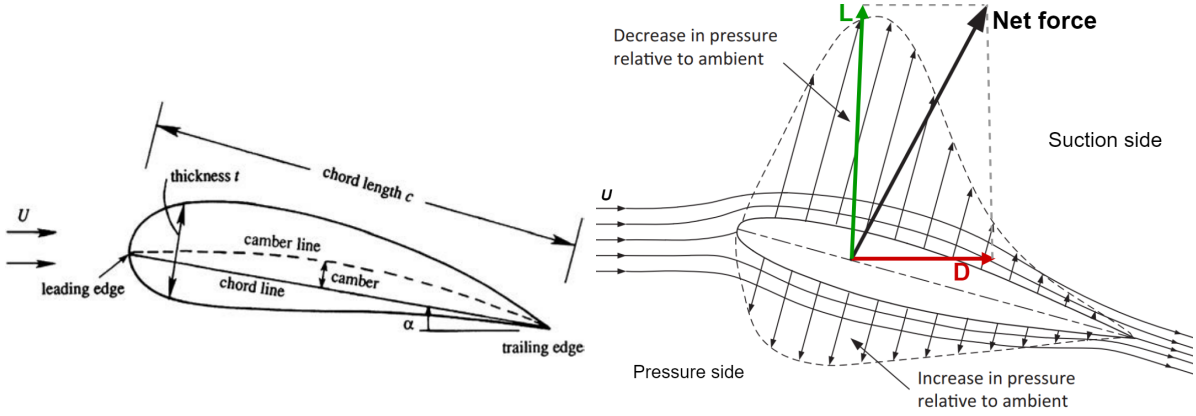

(a) A rounded leading edge and a sharp trailing edge are essential geometrical features of subcavitating foils (Kundu et al., 2015).

(b) Pressure distribution and resulting forces along a foil, adapted from Molland et al. (2021)

Figure 3.2: Foil geometry and resulting forces in a flow

Fig. 3.2a shows the geometrical features of two-dimensional hydrofoil. The span (s), which measures the distance from wingtip to wingtip, and the aspect ratio ($AR = s/c$) are also key defining characteristics for three-dimensional foils. A foil under an angle of attack (α) deflects flow and introduces a difference in average velocity of the flow on the upper and lower side of the foil. This difference in velocity leads to pressure difference following Bernoulli's equation, which can be integrated along the foil surface to gain a net force acting on the foil (Kundu et al., 2015). The net force can be decomposed in the lift (L) and drag (D) force as illustrated by Fig. 3.2b. To compare different foil designs, the nondimensionalised lift (C_L) and drag (C_D) coefficients are important parameters. C_L and C_D can be derived using Eq. (3.1) and (3.2) respectively, where ρ is denotes the fluid density, A the planform area (product of span and mean chord length) and U the fluid free-stream velocity (Newman & Grue, 2018).

$$C_L = \frac{2L}{\rho U^2 A} \tag{3.1}$$

$$C_D = \frac{2D}{\rho U^2 A} \tag{3.2}$$

A designer of hydrofoils aims to maximise the lift-to-drag ratio (C_L/C_D) and the speed for cavitation inception. These are normally in conflict with each other and a trade-off must be made between

the two characteristics. Additionally, the weight of the strut-foil system must be minimised with due consideration of structural strength (Faltinsen, 2005). For subcavitating hydrofoils ($<$ 50 kt) in deep water, hydrofoils have the same fluid-dynamic characteristics (in terms of lift-to-drag ratio, aspect ratio, induced angle of attack) as an airplane wing flying in air (Hoerner, 1965). Therefore, NACA profiles are often used in the design of both hydrofoils and aircraft wings. Abbot and von Doenhoff (1959) have presented comprehensive experimental results for C_L and C_D of two-dimensional NACA profiles. NACA 16 and 64 series without flaps are examples of profiles that fit well for hydrofoils, because they have a relatively flat pressure distribution along the foil (Faltinsen, 2005). This minimises the possibility of local pressure minima, which results in cavitation. Fig. 3.3 shows the characteristic development of lift and drag at varying angles of attack of a two-dimensional foil. C_L increases with a linear relation to the angle of attack. However, as the angle of attack increases further, the streamlined effect of the foil diminishes, eventually leading to separation or stall, which results in a significant reduction in C_L. However, the published results of Abbot and von Doenhoff (1959), like shown in Fig. 3.3, are not directly applicable to a hydrofoil craft design. This is the steady, uniform flow characteristic of a two-dimensional foil, meaning that three-dimensional and interference effects are not taken into account. Moreover, hydrofoils are connected with the hull using struts, which introduces more drag and other viscous effects. The influence of these effects is discussed in Appendix F.

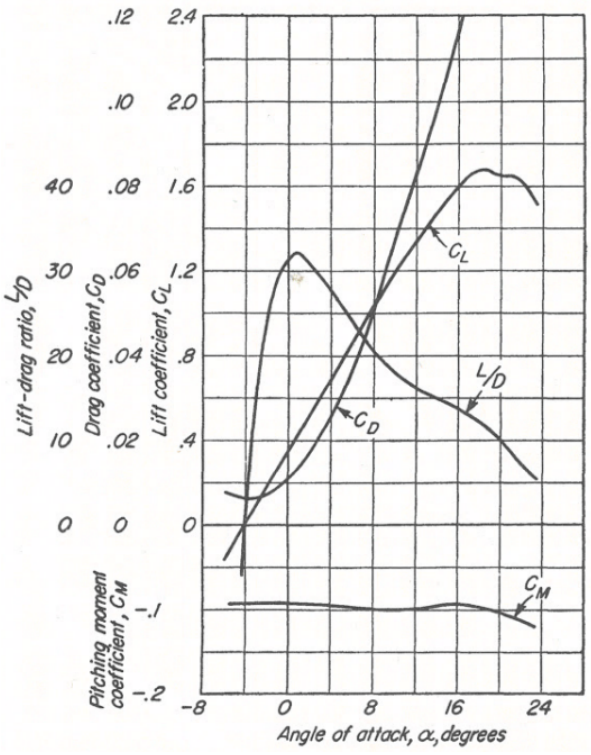

Figure 3.3: Typical lift and drag development over angle of attack (α) for a two-dimensional foil (Abbott & Von Doenhoff, 1959)

3.2. Retractable hydrofoil system functional requirements

Table 3.1 lists the functional requirements of a viable retractable hydrofoil system. The requirements are based on the main concerns of the RNLMC, expressed in the user interview (Appendix E). The small draught requirement (HF REQ 1) yields from the requirement that the craft is beached for personnel transfer. The second requirement (HF REQ 2) expresses the minimum operability of the system demanded by the RNLMC. Other requirements are regarding the redundancy and safety of the system. Section 3.3 and 3.8 will take these requirements in consideration in the selection of a viable retractable hydrofoil system. Although the fifth requirement (HF REQ 5) is deemed out of the scope of this thesis, it is important to note that this is a feature applied in retractable hydrofoil systems (Hosseini, 2024). An additional mitigating system can be a collision-avoidance system, utilising sensors to identify and detect obstacles in advance. Hydrofoil craft manufacturers publicise to have such systems in place, but report little about their effectiveness (Artemis, 2024; Hosseini, 2024).

Table 3.1: Retractable hydrofoil system functional requirements

No.	Requirement
HF REQ 1	The hydrofoil system SHALL not extend further than the maximum draught of the craft (0.86 m) in retracted mode
HF REQ 2	The hydrofoil system SHALL be deployed in conditions up to and including sea state 3 ($H_{1/3} = 1.25$ m)
HF REQ 3	The hydrofoil system SHALL have measures to remain in operation after encountering floating debris
HF REQ 4	The hydrofoil system SHALL have redundancy in its transmission system to remain manoeuvrable after a critical failure of one of the foil systems (per strut)
(HF REQ 5)	The hydrofoil system SHALL have designated shear-off points in the case of collision with a large object or running aground to avoid damage to the hull

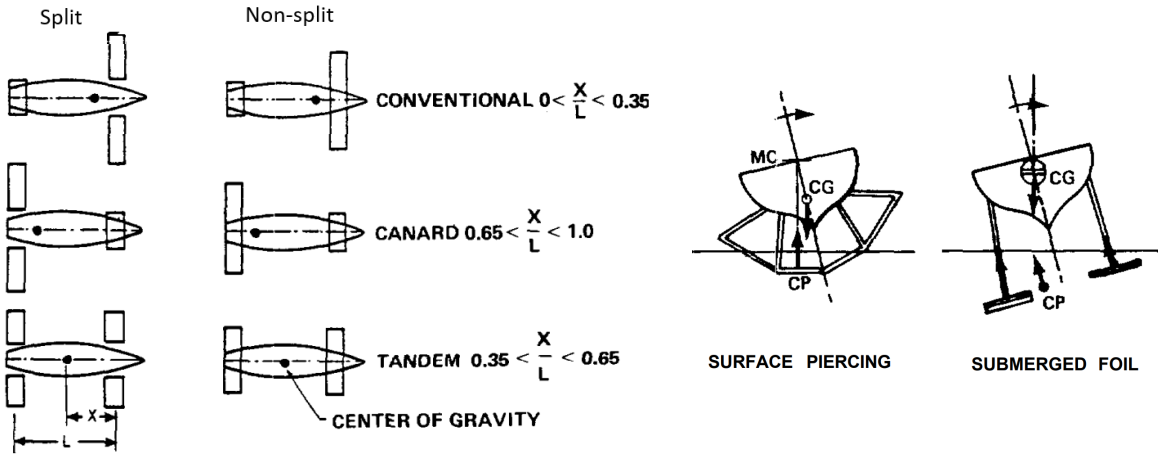

Figure 3.4: Hydrofoil configurations identified by Johnston (1985)

3.3. Hydrofoil configurations

The names of hydrofoil arrangements are derived from aircraft terminology and are divided between conventional (also called airplane), canard, and tandem configuration (Johnston, 1985). This is typically determined by the weight distribution on the foils, illustrated by the center of gravity in Fig. 3.4. In the case of the conventional or canard configuration, it is advantageous to use the smallest foil for pitch control and the bigger foil for roll control due to its larger moment arm. Furthermore, a distinction is made between surface-piercing and fully submerged hydrofoils.

For surface-piercing hydrofoils, portions of the foils extend through the air/water interface. A surface-piercing foil increases its lifting surface as it increases its submergence, and decreases its lifting surface as it descreases its submergence. A properly designed surface-piercing hydrofoil system is therefore

self-stabilising, requiring no active controls for height, roll or pitch. Surface-piercing hydrofoils experience significantly less wave excitation compared to high-speed displacement or planing ships of similar size. On the contrary, the requirement for the foils to balance wave-induced forces, along with the geometric constraints of practical designs, limits the acceptable sea states for high-speed operation (Johnston, 1985). For example, the 28 t surface-piercing hydrofoil Raketa had an operational limit of 0.85 m significant wave height (van Oossanen, 1983). To enhance stability, modern surface-piercing hydrofoils can employ some electrohydraulic control systems as an addition to its passive stabilisation (Yun & Bliault, 2014). This however increases the complexity of its hydrofoil system to the same order as fully submerged foils.

A submerged foil operates fully under water and requires a method of control to remain stable. Due to the lower wave excitation on the hydrofoil, submerged hydrofoils offer superior seakeeping compared to surface-piercing hydrofoils (van Walree, 1999). The United States Navy deemed submerged hydrofoils necessary to attain the required seaway performance for its hydrofoil ships in the past (Johnston, 1985). The limiting sea state for high-speed operation for submerged hydrofoil craft is determined by its strut length. Therefore, their struts are generally longer than the design wave height (Johnston, 1985).

Fig. 3.5 presents the design space of a hydrofoil LAC. It highlights that the design space occupies a middle ground between the traditional focus on hydrofoils for military or ferry use and the recent enthusiasm in hydrofoils, primarily for leisure boating. This suggests that the design of a hydrofoil LAC can blend elements from both the classic and modern approaches. Therefore, Section 3.3.1 to 3.3.6 will discuss retractable hydrofoil systems from both schools of thought.

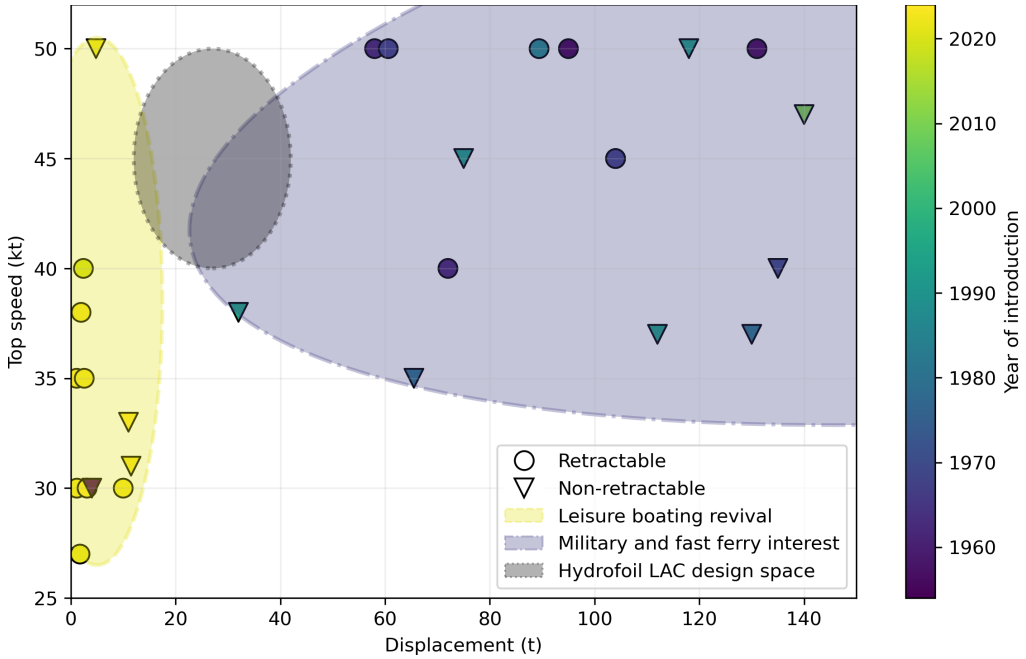

Figure 3.5: Design space of a hydrofoil LAC within existing hydrofoil craft based on the data set provided in Appendix C

3.3.1. Submerged split conventional (airplane)

The conventional configuration positions the larger main hydrofoils near the front of the vessel, while a smaller foil is located at the stern, similar to the layout of a traditional airplane. This design offers practical advantages, as the smaller rear foil can be used for steering or propulsion, with reduced exposure to floating debris in the water. Another benefit is that lift is mostly generated by the front foil, which has no influence of a wake. This increases the lifting efficiency of the hydrofoil system (Mørch, 1992). Furthermore, the split configuration has the advantage that it can be retracted sideways, giving design freedom in the retraction system. This arrangement was applied in the 1960s by the Grumman (currently Northrop Grumman) company out of the United States (Clark et al., 2004), and was utilised in military context until 1991. The craft built by Grumman (USS Plainview, USS Flagstaff and Shimrit class) used propeller propulsion with Z-drive transmission. For foilborne operation, the USS Plainview

housed the propellers in the front foils, whereas the other vessels only used the aft foil to house a propeller.

One disadvantage of the sideways retraction, is the requirement of an additional hullborne propulsion method. The hullborne propulsion systems typically consisted of smaller diesel engines paired with fixed pitch propellers (Johnston, 1985). However, a more exotic solution is the use of a hydraulic transmission. As the ship uses hydraulic power for foil extension, retraction and locking already, the hydraulic pumps can be utilised for propulsion during hullborne operation when the foils are retracted. This method was applied in the Shimrit class, but it doubled the size of the hydraulic system. The two 60 kw hydraulically transmissioned sterndrives can propel the ship with 7 kt (Frauenberger, 1982).

(a) High-speed foiling with extended foils (US Coast Guard, n.d.)

(b) Retracted foils (Mohl, 1971)

Figure 3.6: USS Flagstaff with submerged split conventional foils and Z-drive propeller propulsion

3.3.2. Submerged non-split conventional (airplane)

The submerged non-split conventional configuration is a popular option for upcoming electric leisure boating companies. Instead of folding the hydrofoils to the sides, the entire hydrofoils are retracted vertically. As shown in Fig. 3.7, Candela's C-8 (2024a) uses a stepped hull to stow away the hydrofoils in shallow waters. Similarly, Vessev (2024) employs this configuration with slots in the sidehulls of a catamaran. Because the entire beam of the craft can be utilised for the main foil, this can be an efficient high-aspect ratio foil without extending much outside the hull (Faltinsen, 2005). The vertical retraction also offers the advantage that no secondary propulsion method is necessary when the foils are retracted. In shallow waters the propeller extends as much as a conventional sterndrive. The foil design complexity is increased due to the requirement of the non-split foil to be actuated. As a result, flap actuation is required to act along a greater trailing edge. Shape-adaptive composites can also be used to keep variable incidence control, such as is applied for the Candela hydrofoil boats (Candela, 2024a). To reduce the complexity of the transmission system in the struts, this configuration incorporates either podded propulsion or an L-drive configuration with the electric motor build into the top of the strut. Larger vessel concepts also favour electric propulsion, with Artemis developing a hybrid-electric 20 meter patrol boat, the EF-20H (3.11b), and the TRANSFLYTOR project (2.14) exploring electric propulsion options for a 20 meter littoral craft (Artemis, 2024; SEAir, 2022).

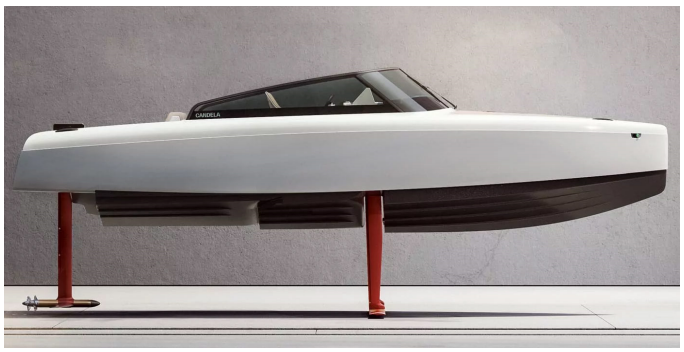

(a) Extended foils (The Green Wave, 2023)

(b) Retracted foils (Candela, 2024a)

Figure 3.7: Candela C-8 with submerged non-split conventional foils and podded propeller propulsion

3.3.3. Surface-piercing split conventional (airplane)

Historically, most surface-piercing hydrofoils have been non-retractable configurations, predominantly used by what was formerly the Soviet Union (Clark et al., 2004). However, the split conventional configuration is a configuration that is applied in surface-piercing retractable designs. The designs, taking inspiration from professional sailing sports designs such as the IMOCA class boats of the ocean race, use L-shaped foils. An example is the Foiler of Enata (2024), shown in Fig. 3.8. This craft uses hydraulically retractable surface-piercing foils, but also uses the hydraulic power for its transmission, similar to the previously discussed Shimrit class (Section 3.3.1). This foil configuration is also viable in combination with lengthened outboard motors as is shown by smaller RHIB designs of SEAir (2024). The surface-piercing hydrofoils do not require a control method and therefore reduce the complexity of the system significantly. However, this comes at a cost. As discussed in Section 3.3, high-speed operation of surface-piercing hydrofoils is limited to lower sea states than submerged hydrofoils. Surface-piercing hydrofoils are less efficient than their submerged counterparts due to the increased water-air interaction and because the foils are located near the free-surface, where the lift of the foils decreases (van Walree, 1999). Furthermore, the craft are less manoeuvrable at high speed due to the lack of active roll control. A submerged hydrofoil can make banked turns, which decreases turn rates and reduces transversal forces on the strut (Faltinsen, 2005).

(a) Extended foils (Enata, 2024) **(b)** Retracted foils (Enata, 2024)

Figure 3.8: Enata foiler with surface-piercing split conventional foils and hydrostatic propeller propulsion

3.3.4. Submerged split canard

In the canard configuration, the smaller hydrofoil (known as the canard) is placed in front of the larger foil. This smaller forward foil can also act as a rudder. This configuration lends itself well for craft with a relatively heavy propulsion system in the aft of the ship because of its lift distribution. The submerged split canard configuration can be integrated with propeller or waterjet propulsion. Military vessels primarily use waterjet propulsion, whereas smaller leisure craft use propellers (Mantaray, 2024; Tyde, 2024). Fig. 3.9 shows an example of this configuration with waterjet inlets in the aft struts.

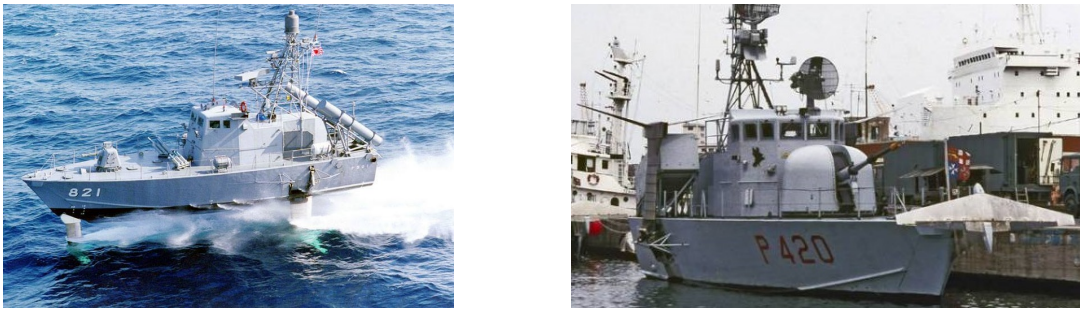

(a) High-speed foiling with extended foils (Asian Military Defense Review, 2013) **(b)** Retracted foils (Military review, 2019)

Figure 3.9: Sparviero class with submerged split canard foils and waterjet propulsion

The canard configuration can offer better seakeeping than other configurations, since the roll control is located at the aft of the ship. While the longitudinal location of roll control is not of a concern when the foils are submerged, broaching may occur in rough seas. In the case of foiling craft, broaching is referred to as the act of a hydrofoil breaking through the water surface or coming close enough to the surface to completely ventilate the upper surface to atmospheric pressure. Operational experience has

shown it is primarily the forward foils which will broach in high seas (Johnston, 1985). In the case of a forward foil broach, the difference between a canard and conventional configuration can be substantial. A canard configuration does not lose its roll stability and simply pitches down until until it recovers its lift in the water. For the conventional foil configuration, the off-centre loss in lift results in a combined roll and downward pitch in the direction of the broached foil. This issue is particularly problematic for split conventional foils, as a complete foil can be broached.

On the other hand, the canard setup yields strong spanwise variations in the inflow to the main lifting hydrofoil (Mørch, 1992), which can potentially reduce the lift-to-drag ratio.

3.3.5. Submerged non-split canard

The non-split canard configuration was developed as an evolution of the split variant and achieved moderate success in both military as ferry markets, as seen in the Pegasus class (Fig. 3.10) and the Boeing Jetfoil (Fig. 2.17), respectively (Yun & Bliault, 2014). Unlike the split configuration, where the aft foils fold to the sides, the non-split design allows the foils to fold entirely to the stern. This necessitates sufficient clearance from the propulsors, such as waterjet buckets. There are also designs, again primarily electric leisure boats, that use vertical retraction of the struts with this configuration (Edorado, 2024; Mantaray, 2024). Like the conventional configuration, the non-split canard configuration can incorporate a high-aspect ratio foil to gain lift efficiency compared to the split configuration.

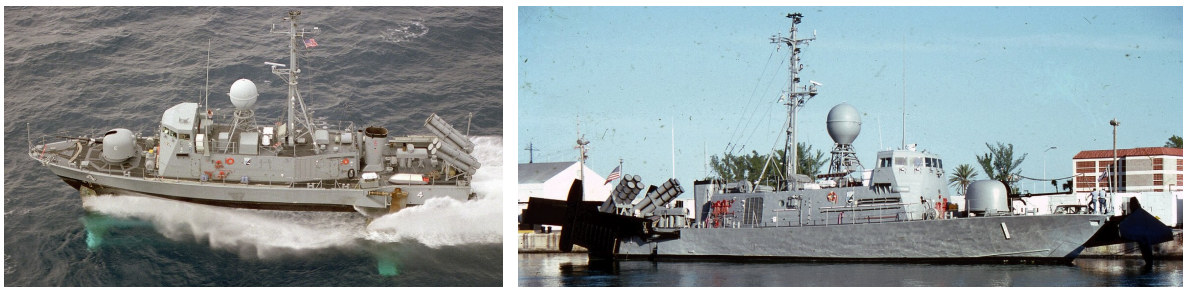

(a) High-speed foiling with extended foils (Taylor, 1986) **(b)** Retracted foils (Blazevic, 1988)

Figure 3.10: Pegasus class with submerged non-split canard foils and waterjet propulsion

3.3.6. Submerged tandem

The submerged tandem configuration distributes the lift evenly between a front and aft foil. Johnston (1985) recognised that bigger hydrofoil ships (larger than have existed today) would prefer this arrangement because of its evenly distributed lift, which enables the use of high-aspect ratio foils in both the front and aft, increasing efficiency. Furthermore, this arrangement can give the vessel better manoeuvrability if both foils are utilised as a rudder. However, this makes the vessel even more complex. Furthermore, tandem hydrofoils mostly use a strut in the middle of the span. This would require vertical retraction through the centreline of the ship, which is often occupied by payload or in board machinery. Due to these difficulties, no retractable tandem hydrofoil craft exist today. Non-retractable submerged tandem hydrofoils are applied in new craft, such as the EF12 work boat of Artemis Technologies, shown in 3.11a. However, Artemis Technologies (2024) preferred a conventional configuration for their first retractable design, which is shown in Fig. 3.11b.

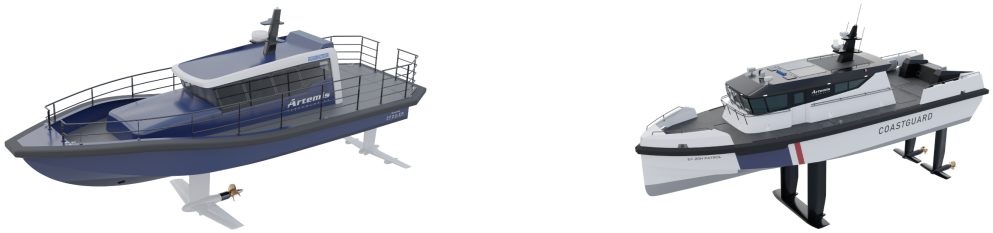

(a) The non-retractable (tandem configuration) work boat EF12 **(b)** The retractable (conventional configuration) patrol boat EF20H

Figure 3.11: Artemis hydrofoil craft (Artemis, 2024)

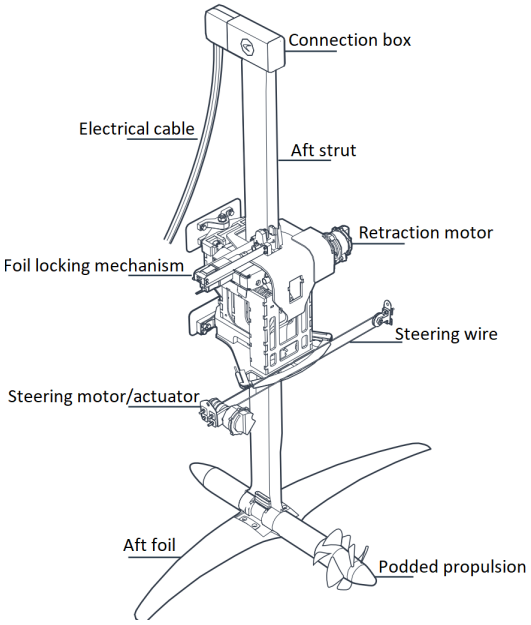

(a) Electromechanical retraction, actuation and steering mechanism of an aft foil with podded propulsion of the Candela C-8 (Fig. 3.7) (Candela, 2023)

(b) Hydraulic retraction mechanism with telescopic cylinders, proposed by Lundin and Eriksson (2021)

Figure 3.12: Hydrofoil retraction mechanisms

3.4. Retraction and actuation systems

Hydrofoil retraction is typically achieved through either electromechanical or hydraulic systems (Johnston, 1985; Yun & Bliault, 2014). Lundin and Eriksson (2021) found that a hydraulic solution has a higher power and weight requirement compared to an electromechanical solution. However, the hydraulic option offers better scalability. If hydraulic lines are already in use for other functions or if multiple foils are involved, a hydraulic retraction system becomes a more feasible solution. Similarly, the choice of retraction and a potential foil actuation mechanisms is interconnected, as these systems complement each other. Adding a hydraulic foil actuation system becomes a more practical option if the vessel already has hydraulic infrastructure in place. Table 3.2 presents main parameters identified by Lundin and Eriksson (2021), indicating that the retraction mechanism alone can constitute as little as 1.8% of the vessel's total weight. Furthermore, Fig. 3.12 shows examples of retraction mechanisms.

Table 3.2: Comparison between electromechanical and hydraulic hydrofoil retraction solution for a 7.5 t battery-electric rescue craft of Lundin and Eriksson (2021)

Parameter	Unit	Electromechanical	Hydraulic
Power	kW	1.15	9.3
Weight	kg	133	> 122
Power/weight-ratio	W/kg	8.6	> 8.6 $\wedge$ < 76.5
Weight fraction	kg/kg	1.8 %	> 1.6%

The total weight fraction of older retractable hydrofoil systems, including the foils and struts, ranged between 10-15%. These systems were constructed from high-strength steel, aluminium or titanium, and did not yet incorporate composite materials (Johnston, 1985). Recent advancements in composite materials allow for a reduced system weight fraction while preserving equivalent strength. A recent study by Godø et al. (2024b) found that the combined weight of carbon composite struts and foils can constitute only 1–5% of the total vessel weight.

In sailing yachts, a different type of retractable propulsion system is applied. The appeal for retractable propulsion in this context lies in the ability to reduce the hydrodynamic resistance when the propeller is retracted and the ship operates under sail. Bieker Boats (2012) and Ship Motion Group (2024) both offer retractable propulsion systems with a homokinetic joint (also called a constant-velocity joint) lifted by a skeg or V-bracket construction. This design enables a simple transmission configuration with minimal energy loss. The systems are available from torques of 0.06 kW/rpm up to 0.9 kW/rpm

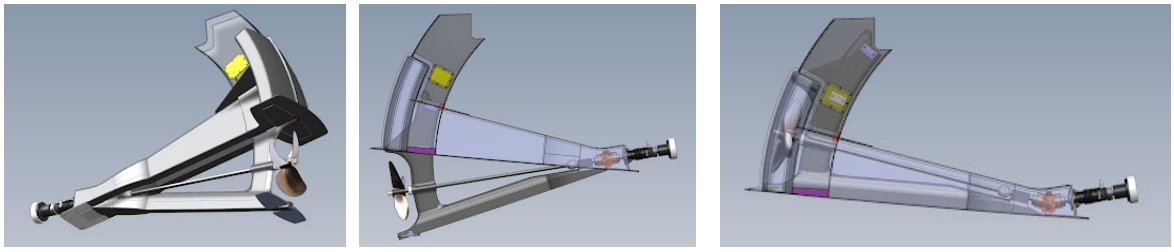

Figure 3.13: A retractable homokinetic transmission system integrated in the skeg (Bieker Boats, 2012)

and can be electromechanically or hydraulically retracted. One of the main challenges of integrating this type of transmission into a hydrofoil craft is the positioning of the prime mover. Putting a propeller at an angle instead of parallel to the waterline will reduce its efficiency due to variable loading of the propeller blades. Furthermore, this variable loading will induce vibrations. Root cavitation can become problematic at shaft angles as low as 8°, which is why larger vessels typically maintain shaft angles below this threshold (Blount & Bartee, 1997). Nonetheless, larger inclination angles have been applied for high-speed craft. An inclination angle of 15° is generally considered the upper limit, beyond which standard engineering precautions can no longer sufficiently mitigate cavitation and vibration risks (Montoya, 2005). To maintain a shaft inclination angle below 15°, the prime mover is moved to the front of the craft. Fig. 3.14 is an example of a hydrofoil with direct drive propulsion that illustrates that the placement of the prime mover is changed. For reference, a 1.5 m height increase with an angle of 15° requires a horizontal shaft length of 5.6 m. The L_{oa} limit of the hydrofoil LAC design is 16.0 m, which indicates that incorporating this method will be a tight fit. This type of transmission can be coupled with a V-drive gearbox to change the prime mover's location more aft for stability considerations.

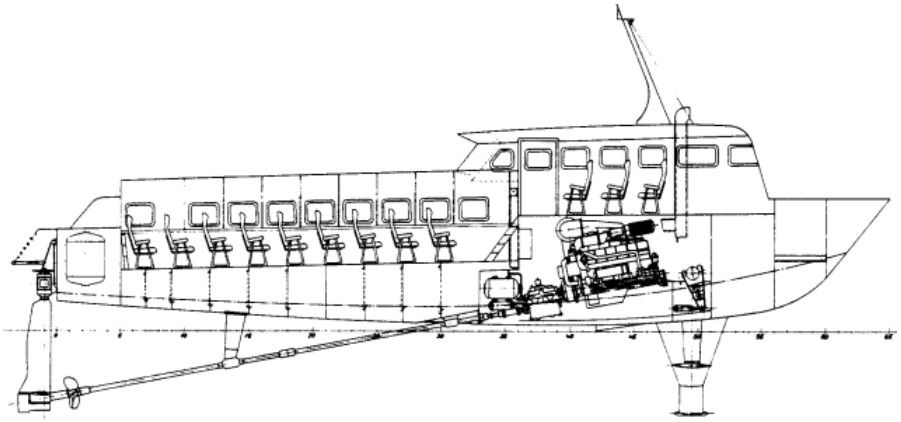

Figure 3.14: A fixed surface-piercing hydrofoil with an angled shaft and diesel engine power (Meyer, 1990)

3.5. Propulsor

For the design of the hydrofoil LAC, the target calm water speed requires to be around 45 kt to match the benchmark speed of the CB90 in calm water conditions. As shown in Fig. 3.15, trans- or supercavitating propellers are the most efficient propulsion method at a range of 40-50 kt for high-speed craft. However, this does not directly imply that these type of propellers are the best suited propulsor for a hydrofoil LAC design. Therefore, this section will discuss the main consideration for a propulsion system of a hydrofoil LAC.

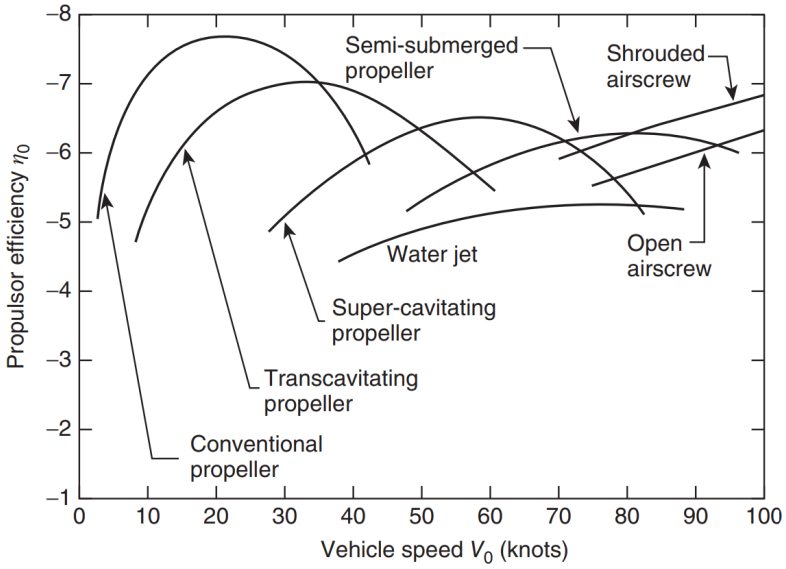

Figure 3.15: Indicative ranges of maximum efficiency of high-speed propulsors by Keuning and Ligtelijn (2017), reproduced from van Oossanen (1983)

3.5.1. Propeller

Above 30 kt of ship speed, cavitation with conventional (subcavitating) propellers becomes a serious issue. Therefore, other types of propellers, which can operate in a cavitating regime, become a more efficient option. A supercavitating propeller operates fully in a cavitating regime, whereas the transcavitating propeller operates in a subcavitating and supercavitating regime. Fig. 3.16 shows examples of these different types of propellers.

Cavitation is the limiting value of pressure on the suction side of the propeller, where the pressure becomes equal to the vapour pressure and water becomes steam. For a conventional propeller, excessive cavitation will reduce the lift generated by the propeller and its efficiency. Furthermore, the collapse of the generated cavitation bubbles causes erosion and vibration-exciting pulses. This is classified as unsteady cavitation. On the contrary, steady cavitation is an acceptable operating regime, which is utilised by the supercavitating propeller (McKesson, 2014).

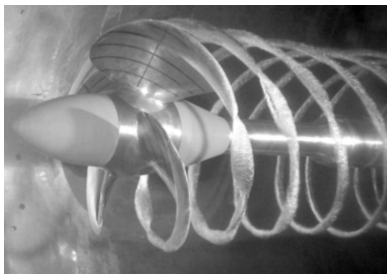

(a) Subcavitating propeller for a high-speed vessel (Faltinsen, 2005)

(b) Transcavitating Newton-Rader series derived propeller (Gaggero & Brizzolara, 2009)

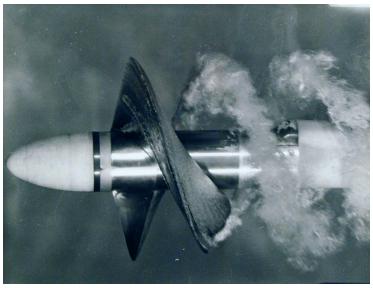

(c) Supercavitating propeller (National Museum of the U.S. Navy, 1958)

Figure 3.16: Different types of high-speed marine propellers

A supercavitating propeller outperforms both the conventional (subcavitating) propeller and the waterjet in terms of propulsive efficiency in specific combinations of propeller loading and cavitation number, as indicated by Fig. 3.15. On the contrary, a supercavitating propeller is less efficient than a conventional propeller when operating at sub- or partly cavitating condition. If supercavitating propellers are used in a hydrofoil design, it must be taken into account that the supercavitating propeller is capable to propel the hull beyond the main resistance hump and therefore beyond its take-off speed (Keuning & Ligtelijn, 2017). In addition, when supercavitating propellers are close to the surface and in variable conditions such as high seas, the cavitation may not stay steady, which causes vibration and localised erosion on the blades. This can also be a problem for the lifting foils (Yun & Bliault, 2014). Supercavitating propellers have been applied previously with success for the hydrofoil craft Denison and Plainview (Johnston, 1985).

In hydrofoil design, both pulling and pushing propellers are conventionally used. A pulling propeller can provide thrust in a uniform wake field, as there is no wake of the attached foil and strut affecting the flow field. This can lead to more efficient propeller designs and delay cavitation inception (Faltinsen, 2005).

The maximum speed range of 40-50 kt of the hydrofoil LAC is between the optimum speeds for efficiency of the subcavitating and supercavitating propeller. For these kind of vessels, a transcavitating propeller can be used. A transcavitating propeller is a combination of a sub- and supercavitating propeller. For transcavitating propellers, blade sections are divided in a supercavitating and a subcavitating domain (Yim et al., 1998). An example of the practical application of transcavitating propellers can be found in the Shimrit-class hydrofoil vessels, which employed a transcavitating propeller achieving a propulsive efficiency (η_D) of 65% at a cruising speed of 40 knots (Frauenberger, 1982).

To obtain initial design characteristics of trans- or supercavitating propellers, the Newton-Rader series of propellers can be used (McKesson, 2014). Fig. 3.18 shows the hydrodynamic characteristics of the Newton-Rader (1961) series parent propeller. These characteristics vary with propeller cavitation number (σ_0), which is the cavitation number at the root of the propeller blade ($r = 0$). The propeller cavitation number can be defined as in Eq. (3.3), where h denotes the submergence depth and v_s the ship speed. Fig. 3.17 shows the development of propeller cavitation number over ship speed. The Newton-Rader propeller series provides data for cavitation numbers until a propeller cavitation number of σ_0 = 0.25, whereas the Gawn and Burrill series stops at σ_0 = 0.4 (Molland et al., 2011). From the plots of Figures 3.18 and 3.17, it can be concluded that open water efficiencies (η_o) between 60% and 70% are a realistic estimate for ship speeds between 40-50 kt. Because propulsor-hull interaction for hydrofoil craft is negligible, it can be assumed that the open water efficiency is the same as the propulsive efficiency (η_D) (Buermann et al., 1953).

$$\sigma_0 = \frac{p_a + \rho g h - p_v}{0.5 \rho v_s^2} \tag{3.3}$$

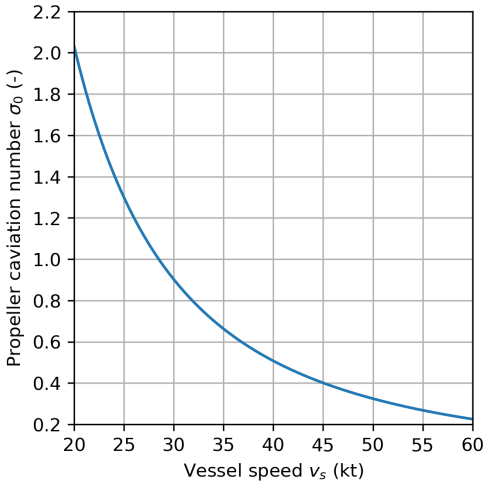

Figure 3.17: Propeller cavitation number σ_0 as a function of vessel speed v_s, ambient pressure based on 1m of propeller submergence

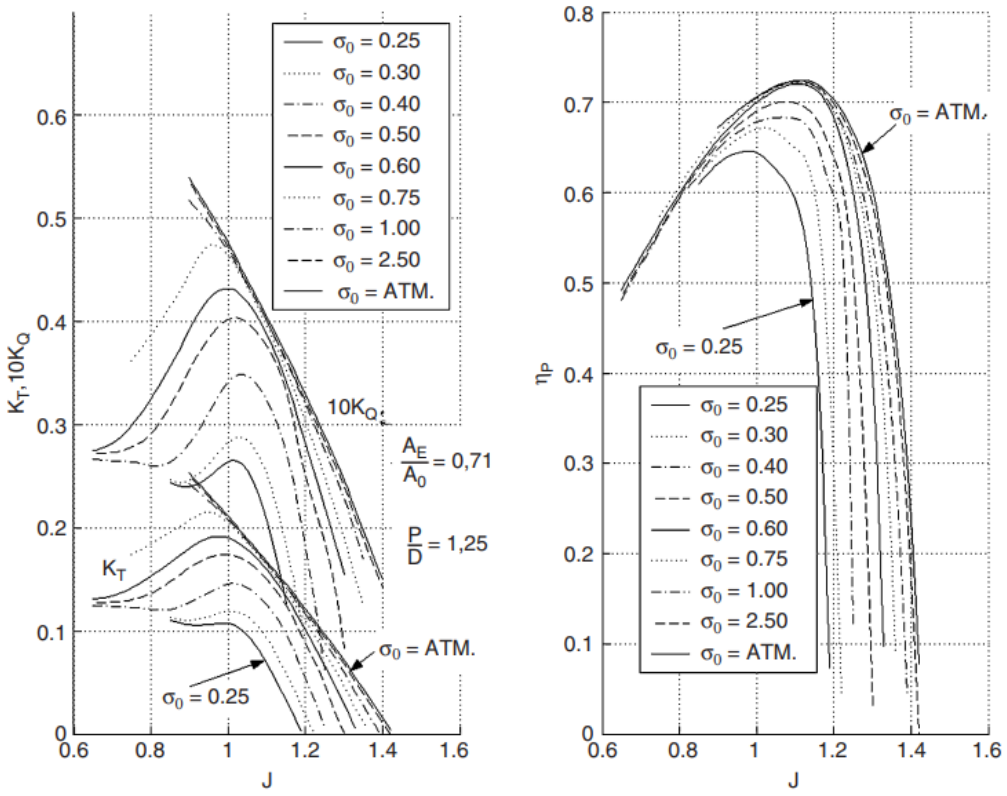

Figure 3.18: Hydrodynamic characteristics of the Newton-Rader series parent propeller by Faltinsen (2005), reproduced from Newton and Rader (1961). J = advance ratio, K_T = thrust coefficient, K_Q = torque coefficient, η_p = open water efficiency, σ_0 = propeller cavitation number, A_E = expanded blade area, A_0 = propeller disc area, P = propeller pitch, D = propeller diameter.

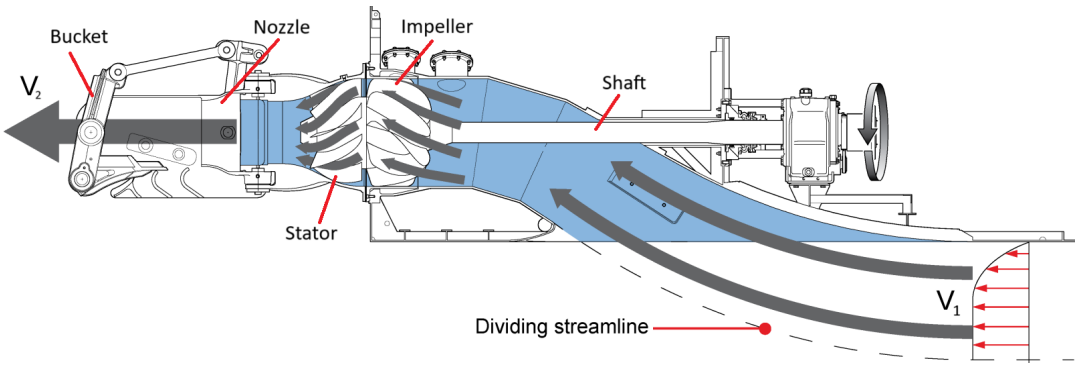

Figure 3.19: Waterjet main characteristics and flow, adapted from Wärtsilä (2015)

3.5.2. Waterjet

Waterjets are propulsors primarily applied in high-speed craft. The benchmark vessel of this thesis, the CB90, also uses two Kamewa waterjets. A waterjet can suppress cavitation due to pressure build up in the waterjet duct, which allows it to operate at high speeds (> 30kt) (Faltinsen, 2005). Fig. 3.19 shows the main characteristics of a conventional waterjet system. The waterjet works due to the conservation of momentum. A waterjet accelerates incoming water from V_1 to V_2, which results in a thrust as defined by Eq. (3.4). Further elaboration of the physics behind waterjets is provided in Appendix D.2.

$$T = \rho A_2 V_2 (V_2 - V_1) \tag{3.4}$$

Reliability issues with the gear transmission systems in early hydrofoil craft led to the interest in waterjet propulsion for hydrofoil designs. In 1968, the hydrofoil craft Flagstaff (Fig. 3.6) and Tucumcari

were built along the same specifications to compare a canard configuration with waterjets (Tucumcari), to a conventional configuration with propellers (Flagstaff). The waterjet propulsion of the Tucumcari proved to be more reliable than the propeller drive of the Flagstaff and served as the foundation for the following Pegasus class hydrofoil ship and the hydrofoil ferry Jetfoil (Clark et al., 2004; Johnston, 1982).

The hydrofoil ferry Jetfoil is an example of waterjet propulsion applied to a hydrofoil craft currently in operation. Its propulsion system is illustrated in Fig. 3.20. An additional strut in the middle of the aft foil acts as an inlet duct for the waterjet. The complete foil system can be retracted hydraulically and the waterjet has an alternative inlet at the hull bottom for slow-speed hullborne manoeuvring (Yun & Bliault, 2014).

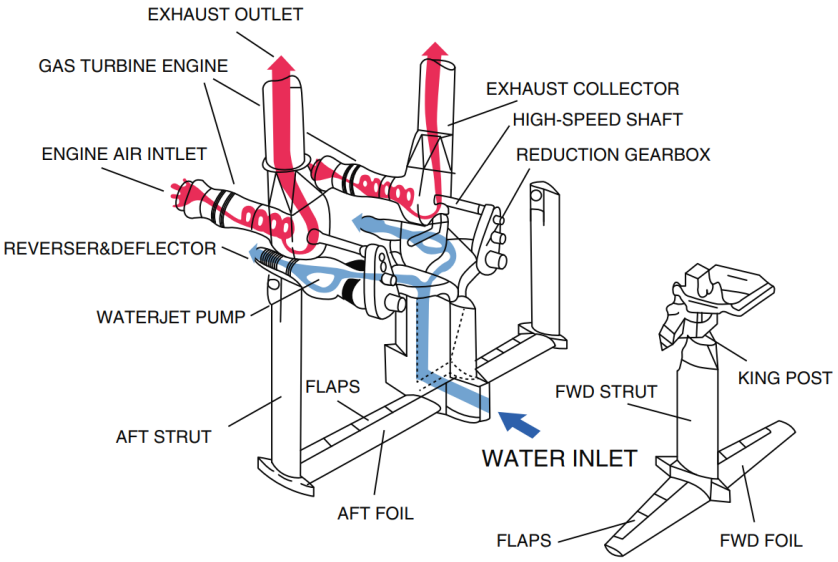

Figure 3.20: The propulsion system of the Boeing Jetfoil 929 (Yun & Bliault, 2014)

With the use of waterjets, heavily-loaded gears and long transmission shafts are eliminated and the number of moving parts is reduced. This simplicity, however, comes with a considerable increase in required power. Johnston (1985) considers an increase of required power compared to propellers of around 20% at 50 kt to approximately 100% at take-off speed (20-30 kt). In addition, Appendix D provides an estimate for the efficiency of current waterjets. The propulsive efficiency (η_D) of a waterjet on a hydrofoil craft is estimated in the order of 0.50 (50%). Meanwhile, a propeller can deliver an η_D between 60% to 70%, as discussed in Section 3.5.1. This is in accordance with earlier findings of Johnston, as shown in Fig. 3.21. In Fig. 3.21 the propulsive coefficient is defined as the product of propulsive efficiency (η_D) and transmission efficiency (η_{trm}). Next to this inherently lower efficiency, waterjets deliver lower thrust at take-off speed, the water column inside the waterjet adds a substantial amount of weight to the vessel and the widened struts that act as inlets will increase resistance.

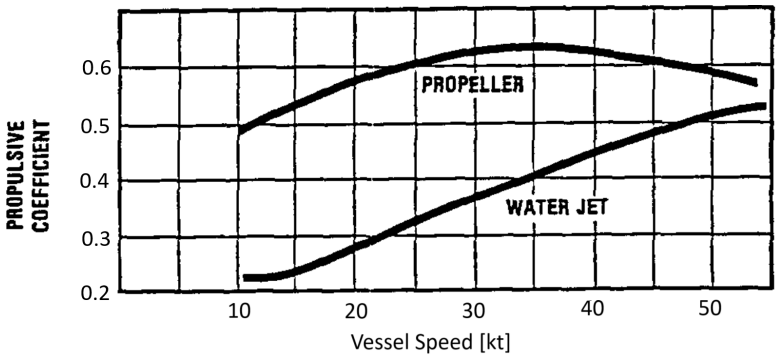

Figure 3.21: Typical hydrofoil propulsor performance from Johnston (1985)

On the contrary, waterjets do offer other benefits. A waterjet will reduce the amount of radiated noise compared to a propeller and can improve manoeuvrability (Carlton, 2019). Waterjets have a relatively high power density up to 8 MW/m^2, where supercavitating propellers have a power density up to 6 MW/m^2 (Keuning & Ligtelijn, 2017). In addition, waterjets require a lower engine margin due to its flat torque characteristic (Grevink, 2022a). Furthermore, if the struts are replaced, only the duct of the waterjet is affected instead of a complete driveline.

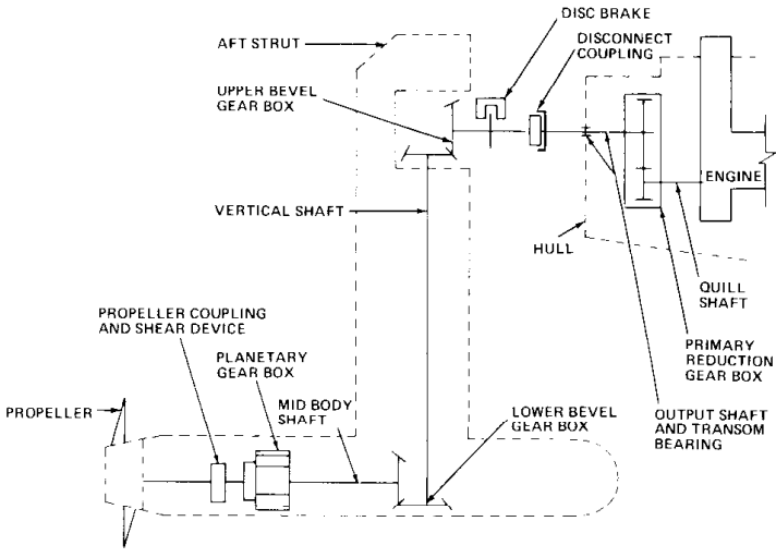

Figure 3.22: Integrated Z-drive transmission system in the aft foil of a Shimrit class vessel (Frauenberger, 1982)

Table 3.3: Transmission performance estimates with the losses per component, the total transmission efficiency (η_{trm}) and number of components n. The geared drive transmission is the benchmark transmission system found in the CB90. Long shafts are shafts that travel through the hydrofoil struts.

Geared drive		**Homokinetic**		**Z-drive**		**Electric L-drive**		**Electric podded**		**Hydrostatic**	
Comp.	Loss	Comp.	Loss	Comp.	Loss	Comp.	Loss	Comp.	Loss	Comp.	Loss
Gearbox	1.0%	Gearbox	1.0%	2 Gearboxes	1.0%	Power elec.	4.0%	Power elec.	4.0%	Hydraulic pump	9.0%
2 Shafts	0.5%	Shaft	0.5%	2 Shafts	0.5%	Electric motor	3.0%	Electric motor	3.0%	Hydraulic motor	6.0%
		Long shaft	1.0%	Long shaft	1.0%	Gearbox	1.0%	(Reduced η_o)[1]	5.0%	Gearbox	1.0%
		Joint	2.0%			Shaft	0.5%			Shaft	0.5%
		(Prop. angle)	3.5%			Long shaft	1.0%				
η_{trm}	98%	96% (92%)		96%[2]		91%		93% (88%)		84%	
n	3	4		5		5		2		4	

3.6. Transmission

Propulsion transmission for hydrofoil craft is typically integrated in the hydrofoil struts, such as shown in Fig. 3.22. Table 3.3 lists the estimated performance of applicable transmission systems for retractable hydrofoil craft derived from literature and supplier data. Shaft and gearbox losses are based on recommendations by Klein Woud and Stapersma (2002). Power electronics losses are the losses incurred by converters, inverters and motor controllers, which for an DC-grid account for around 4% based on supplier data (ABB, 2022). The estimate of electric motor losses of 3% is derived from industrial electric motors of ABB (2023), whereas the estimates for hydraulic systems of the hydrostatic drive are values taken from Dymarski and Skorek (2006). Furthermore, the homokinetic joint losses of 2.0% are based on performance with a 15° angle of Cirelli et al. (2021). The inclined shaft angle also reduces propeller efficiency due to the variable loading and unoptimal thrust-direction. The productive thrust can be derived with Eq. (3.5), where ϵ denotes the inclination angle.

[1] Increased pod drag is taken into account for η_o and accounts for around 5% of power loss (Grevink, 2022b; Mewis, 2002)

[2] The Grumman (currently Northrop Grumman) company claimed an equal efficiency of 96% for the Z-drive transmission of the Shimrit class hydrofoil vessel (Fig. 3.22) (Peek & Bauer, 1981)

$$T_x = T\cos(\epsilon) \tag{3.5}$$

In addition, the number of main components provides an indication of the complexity of the system, but this remains a large simplification. A podded electric motor is for example a complex system on its own, where a bevel gear transmission may be less complex as a whole.

As shown in Table 3.3, making the transmission system suitable for retractable hydrofoils decreases the transmission efficiency (η_{trm}). Compared to a geared drive, the transmission losses are expected to increase between 2% to 14%. In the case of waterjet propulsion, it is assumed that geared drive transmission is applicable. However, waterjets for hydrofoil craft have additional losses, as previously discussed in Section 3.5.2.

3.7. Power density of prime movers

The power density of prime movers is one of the primary concerns for the design of high-speed craft due to their increased weight sensitivity (McKesson, 2014). The prime movers of current hydrofoil craft are primarily high-speed 4-stroke engines and marinised gas turbines, with the exception of battery-electric designs. Table 3.4 shows an example of main performance parameters of these prime movers. The engine characteristics are in accordance with the values found by Klein Woud and Stapersma (2002), but the derived specific mass and volume of marinised gas turbines is lower than expected. Klein Woud and Stapersma identified a specific mass between 1.0-1.4 kg/kW and a specific volume of 2.5-4.5 dm^3/kW for marinised gas turbines. This can be caused due to suppliers not taking into account the same volumes and weight for external features such as the inlet and exhaust duct. In addition, performance parameters of generator sets (gensets) are provided in Table 3.4, as this can be an option for diesel-electric hybrid designs.

Table 3.4: An excerpt of prime mover performance parameters based on supplier data from Appendix G. Volume (V) based on block dimensions. Engine efficiency (η_e) based on MDO with an LHV of 42700 kJ/kg. Specific fuel consumption (sfc) for MCR. The Scania DI16 (marked green) is the engine installed in the CB90.

Marinised gas turbine	P_b (kW)	m (kg)	V (m^3)	Specific m (kg/kW)	Specific V (dm^3/kW)	sfc (g/kWh)	η_e (%)	Source
GE LM500[3]	4570	2779	7.7	0.61	1.68	270	31	(General Electric, 2017)
Honeywell AGT1500[4]	1120	1134	1.3	1.01	1.16	288	29	(Honeywell, 2000)
Rolls Royce Allison 501-KF[5]	3230	1134	5.2	0.35	1.60	306	28	(General Motors, 1986)
High-speed 4-stroke engine	P_b (kW)	m (kg)	V (m^3)	Specific m (kg/kW)	Specific V (dm^3/kW)	sfc (g/kWh)	η_e (%)	Source
CAT C18 (In-line 6)	747	1949	3.0	2.61	4.05	n/a	n/a	(Caterpillar, 2024a)
MAN LE 426 (V8)	735	1780	2.4	2.42	3.22	205	41	(MAN, 2024)
Scania DI16 072M (V8)	662	1670	2.4	2.52	3.56	224	38	(Scania, 2024a)
Yanmar 6AYEM-GT (In-line 6)	749	2418	3.7	3.23	4.99	206	41	(Yanmar, 2024)
Constant speed generator set	P_b[6] (kWe)	m (kg)	V (m^3)	Specific m (kg/kWe)	Specific V (dm^3/kWe)	sfc (g/kWh)	η_e (%)	Source
Boudain 12M26.2	880	6500	9.1	7.39	10.36	207	41	(Boudain, 2024)
CAT C18	565	2961	7.1	7.01	12.50	214	39	(Caterpillar, 2024c)
CAT C32	940	7131	12.9	7.59	13.68	200	42	(Caterpillar, 2024d)
Volvo D16 MG	508	3926	7.1	7.73	14.01	206	41	(Volvo, 2024)

Although gas turbines offer the highest power density of any prime mover considered, they are not necessarily the best option. Gas turbines in this category are mostly of the turboshaft type, which are intended to produce shaft power instead of forward thrust. Gas turbines are typically used for larger output powers than required for a hydrofoil LAC design, with marine applications generally starting around 3 MW. The current installed brake power of the CB90 is approximately 1.3 MW and provided by two Scania DI16 motors. The required propulsion power of a hydrofoil LAC will be even lower due to its resistance reduction (Chapter 4). Additionally, running gas turbines at part load condition can

[3] Used in the Foilcat foiling catamaran
[4] Used in the M1 Abrams tank but can use MDO as a fuel
[5] Used in the Jetfoil foiling monohull
[6] Based on 60Hz AC

lower its efficiency even further compared to diesel engines (Klein Woud & Stapersma, 2002). Despite this, gas turbines within the considered power range can be found in the helicopter industry, such as the Rolls-Royce M250 or RR500, which can deliver power between 200-500 kW (Rolls-Royce, 2024). Prior design studies have shown that although gas turbines can halve the weight fraction of propulsion machinery, this is mostly negated by the increased fuel capacity requirement due to the reduced engine efficiency (η_e), but this depends on the range requirement (Johnston, 1985).

High-speed engines, in particular V-type engines, can still offer a high power density at a higher efficiency compared to gas turbines. Due to its simplicity, maintainability and reliability, it remains the current prime mover of choice for smaller high-speed craft (Yun & Bliault, 2014). The high-speed engines of Table 3.4 are rated for a minimum of 600 hours per year, as is requested by the NLMOD (Appendix A). Ratings differ per engine manufacturer, but this would generally fall within the lightest load factor and the highest available rating. As a result, this is the maximum power that can be delivered by these engine blocks for commercial applications and will be the highest power-to-weight ratio available for combustion engines of this category.

Diesel-electric propulsion can facilitate less complex transmission to foilborne propulsors and offer flexibility in the placement of onboard systems. Unfortunately, employing generator sets as a prime mover in a traditional sense with constant speed generators in an AC-grid will increase the mass of prime movers drastically. Table 3.4 shows increases of specific mass and volume of the prime mover from two to three times compared to using diesel engines. In addition, a complete diesel-electric propulsion system requires more systems not taken into account in Table 3.4, such as power electronics, electric motors and systems to deal with transient loads such as batteries or supercapacitors. This will increase the weight of the propulsion system and in turn the weight of the vessel. As a result, the foil size is required to increase and this will add to resistance significantly. A comparison of the weight development of gas turbines, diesel engines, and constant speed generators is provided by Fig. 3.23.

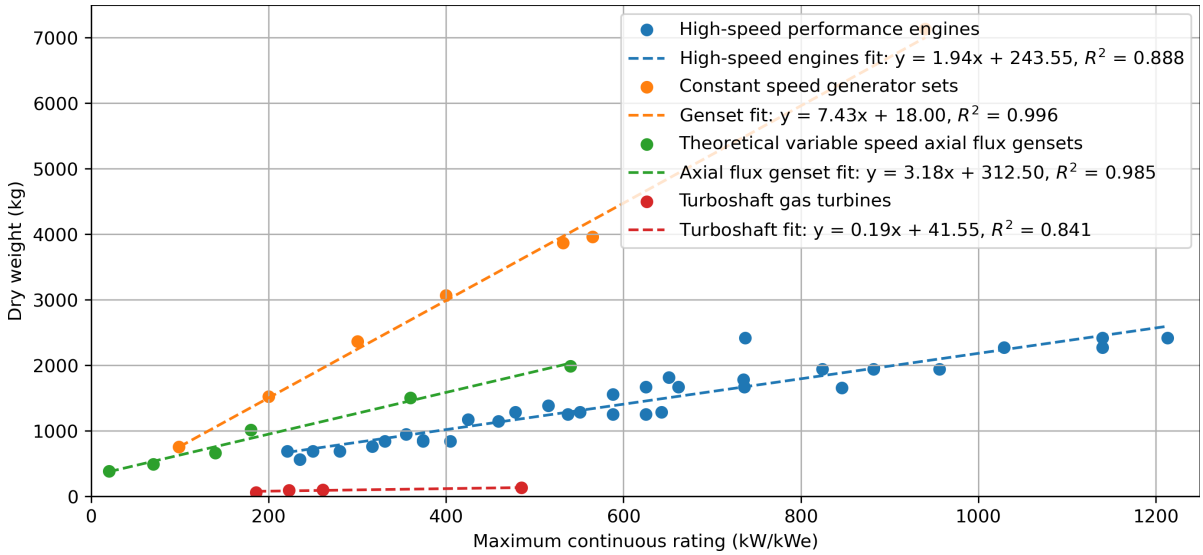

Figure 3.23: Development of prime mover weight over power, based on published manufacturer data of Appendix G

However, the published manufacturer data of generator sets of Table 3.4 shows a skewed image of the potential of a diesel-electric propulsion configuration. Engine manufacturers publish the data of constant speed generator sets for an AC-grid application for continuous operation. Therefore, the generators are optimised for efficiency and durability, and are rated for continuous use, whereas high-speed performance engines can have a low load factor with higher power densities as a result. Additionally, the engine speed is limited by its requirement to produce a stable alternating current. For a 60 Hz AC-grid, this would generally limit the engine speed to 1800 rpm, where high-speed engines can reach rotational speeds of 2300 to 3000 rpm for the considered region of power requirements. To improve the power-to-weight and volume-to-weight ratio, variable speed generator sets in combination with a DC-grid architecture can be used. Variable speed generator sets are currently applied in offshore vessels to match fluctuating load requirements more efficiently (Habermaas & Thurner, 2020), and in smaller diesel-electric vessels as a drop-in solution for DC-architectures that also use other energy

carriers such as batteries (Cronborg, 2022). A variable-speed generator adjusts its speed according to the electrical load that is connected, instead of working at a fixed speed. This makes the generator quieter and more efficient at part-load conditions (Habermaas & Thurner, 2020). Moreover, the combustion engine can operate at higher speeds, which results in a higher delivered brake power for the same engine block. A DC-grid has the same electric stability as an AC distribution system (Kim & Jeon, 2022; Kyunghwa Kim & Chun, 2018); yet, the adoption of DC distribution systems is not widespread. This is partly due to a historical lack of DC protection devices, but these are available for vessels with a power requirement below 10 MW (Chai et al., 2018). All in all, the most power dense diesel-electric propulsion solution can be found by matching a normal high-speed performance diesel engine with a separate electric motor/generator as a variable speed generator in a DC-grid.

(a) Radial flux motor AMXE250 (ABB, 2024) **(b)** Axial flux motor AXM (Beyond Motors, 2025) **(c)** Triple stacked axial flux motors (Beyond Motors, 2025)

Figure 3.24: Different types of electrical traction motors

Diesel-electric propulsion with an even lower required weight can be achieved by applying axial flux generators and motors, instead of its traditional radial flux counterparts. Both types are shown in Fig. 3.24. The difference between these types of electrical machines is the magnetic flux orientation (Nishanth et al., 2023). For axial flux motors, their produced torque increases with the cube of rotor diameter, whereas this is only quadratic for radial flux motors. Therefore, they have a characteristic flat geometry which gained them the nickname “pancake motor”. These types of electrical drives currently find their use in aviation and high-performance automotive industries (Beyond Motors, 2025; Emrax, 2025; Evolito, 2025; Phi-Power, 2025), where power density is a critical issue as well. Axial flux motors are also applied as an in-line propulsion option for power take-off and take-in in motor yachts (Hydrosta, 2024). Fig. 3.25 shows the weight decrease that the application of axial flux motors can realise. With a power density of around 0.5 kg/kW of axial flux motors compared to approximately 1.4 kg/kW of radial flux motors, axial flux motors are 2 to 3 times less heavy. Fig. 3.24 also illustrates that axial flux motors are generally produced for powers lower than 300 kW. However, their flat design allows axial flux motors to be stacked in a modular fashion. As shown in Fig. 3.24c, axial flux motors can be stacked up to three times to achieve a power of around 1 MW.

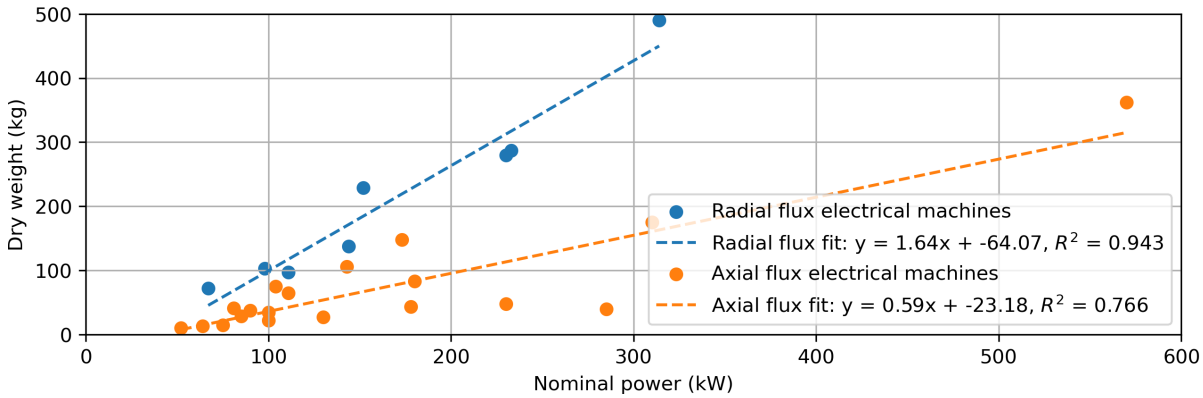

Figure 3.25: Weight development over power of radial flux and axial flux electrical machines, based on published manufacturer data of Appendix G

By adding the weight of an axial flux generator conversion of Hydrosta (2024) to the fitted weight of high-speed engines for their respective power, a theoretical weight of variable speed axial flux gensets is derived. This weight is plotted in Fig. 3.23 as the green line. Although the weight increase is still substantial compared to the high-speed engines alone, the weight decrease compared to constant speed generators is even greater.

3.8. Comparison of foil and propulsion options

From this chapter, it can be concluded that the choice of foil configuration, transmission, propulsor and prime mover can not be taken independently. Their characteristics are strongly dependent on each other and must be considered as a complete system.

Table 3.5 shows a relative decision matrix of hydrofoil systems derived of the findings of this chapter. The decision matrix evaluates different foil configurations based on the Pugh method (Pugh, 1991). The Pugh method is a qualitative method to rank multi-dimensional options of an option set to a reference design. The reference option, in this case, is a planing boat and alternatives can be be better or worse on a scale of -3 to 3, based on the findings of this chapter. Although the list of criteria options and its grading remains arbitrary, this method allows for a direct comparison and an initial selection of design options can be made. The scores in this matrix are not tallied for a total score, as the weighting of each design consideration is inherently subjective. Instead, it provides a qualitative overview of design options, which is further discussed in detail in this section.

Table 3.5: Relative decision matrix for retractable foil configurations using the Pugh method

Configuration of main foil	**Planing**	**Submerged split conventional**	**Submerged non-split conventional**	**Surface-piercing split conventional**	**Submerged split canard**	**Submerged non-split canard**
Lift efficiency	0	2	3	1	2	3
Seakeeping	0	2	2	1	3	3
Manoeuvrability	0	1	1	-2	1	1
Foil complexity	0	-2	-3	-1	-2	-3
Propulsion vulnerability	0	-1	-1	-1	-2	-3
Generally applied transmission	Geared drive Waterjet	Z-drive	Electric L-drive Electric Podded	Electric L-drive Hydrostatic	Electric L-drive Waterjet	Electric L-drive Waterjet
Main foil retraction direction	-	Lateral	Vertical	Lateral	Lateral	Vertical Astern
Maximum propulsion efficiency $\eta_e \cdot \eta_{trm} \cdot \eta_D$	0.28 0.41*0.98*0.70	0.26 0.41*0.96*0.65	0.24 0.40*0.91*0.65	0.24 0.40*0.91*0.65	0.24 0.40*0.91*0.65	0.24 0.40*0.91*0.65

In Table 3.5, the biggest difference between foil configurations can be identified between surface-piercing and fully submerged configurations. The surface-piercing option's decreased complexity comes at the cost of lift efficiency, seakeeping and manoeuvrability. The different submerged retractable hydrofoil configuration have less significant differences. The canard configuration has some increased seakeeping capabilities due to the reduced possibility of foil broaching compared to the conventional configuration. Furthermore, non-split versions have some increased lift efficiency due to a reduction in induced drag. The differentiation between submerged options has a more direct implication for the possible propulsion methods. For example, waterjets are only applied in combination with a canard configuration due to its lift distribution and ability to let struts act as a water inlet. Based on the requirement that the foil system has to remain deployable in sea state 3 (Section 3.2) and that 'lift efficiency' and 'seakeeping' encapsulate the design drivers (Section 2.5), submerged hydrofoils are selected as a foil design for further investigation.

To achieve redundancy in the propulsion system, it must be split into two independent propulsion lines. This configuration positions the propulsors on either side of the vessel rather than placing a single propulsor along the centreline. An added benefit of this arrangement is that the propulsion system can be retracted higher than the vessel's keel, potentially allowing propeller systems to provide thrust even when retracted. This can work similar to a sterndrive propulsion system. Furthermore, using two propulsion lines helps manage torque demands, preventing the excessive torque that a single propulsion line would require in a high-speed vessel. Additionally, this setup enables differential steering capability.

For a non-split canard configuration, the main aft foil is also used to house the propulsion system.

Therefore, in the case of failure of the foil system, the complete propulsion system is at risk. This makes it not a viable option as this does not comply with the hydrofoil requirements (HF REQ 4). The split version of the canard configuration can have redundancy in its transmission, as it will be split over two foil systems. However, these foil systems are still more exposed than the conventional configurations. On contrast, a conventional configuration would first be hit in the forward struts and foils by potential obstacles before it can reach the aft propulsion system. Furthermore, a potential collision avoidance system can be able to detect these objects to react in a mitigating manner.

Considering the propulsion vulnerability of the canard configurations, a conventional configuration is preferred. This also implies that waterjets will be excluded as a propulsion method. As it is the aim of this thesis to show which gains current hydrofoil technology can offer, the non-split version is chosen over the split version for the main front foil for its superior lift efficiency. To house the separate propulsion lines however, the aft foil system does need to be split. An added benefit of this arrangement is that the craft can keep its pitch stability in the case of one foil system failure. The resulting foil configuration is illustrated in Fig. 3.26 and is similar to the Artemis EF-20H patrol boat design, shown in Fig. 3.11b. It is also known as a π fore and split-T aft configuration. To facilitate the retraction of the front foil, a slot in the hull is necessary to make a hydrodynamically efficient hull in a retracted mode. Recent hydrofoil craft designs use a similar approach (Candela, 2024a; Vessev, 2024).

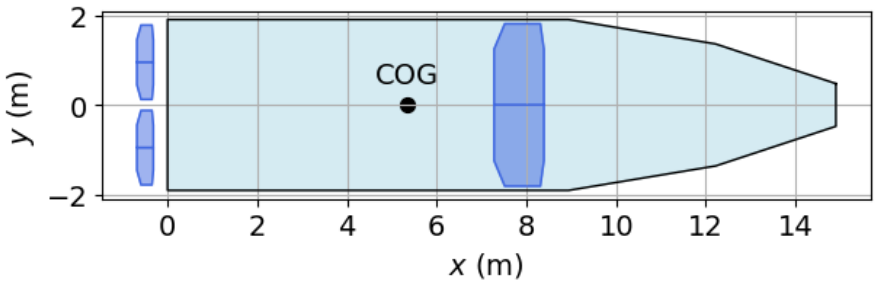

Figure 3.26: Bottom view of an example hull (light blue) and foil design (dark blue) of the conventional foil configuration chosen in this chapter

3.9. Concluding insights

Retractable hydrofoil systems have been applied in a broad range of vessels. Traditionally, this has been applied for military or high-speed ferry purposes. More recently, also leisure craft embrace this technology. A hydrofoil LAC occupies a design space between these vessel types. Between surface-piercing and submerged hydrofoils, a submerged hydrofoil system shows the most potential fulfil the design drivers of Chapter 2 the best.

The transmission for foilborne propulsion remains challenging to implement in a retractable system. Waterjets can be implemented, but decrease propulsion efficiency drastically. By contrast, propeller propulsion can offer high propulsion efficiency, but this requires a complex transmission system. Due to propulsion vulnerability considerations of canard configurations, a conventional configuration is preferred and waterjets are excluded as a propulsion system. However, this means that a complex transmission system is required. Current battery-electric designs are able to capitalise on their electric transmission to reduce the complexity of the retractable design. Using a similar electric transmission for an LAC design will increase the weight of the propulsion system substantially and may reduce the feasibility of the design. All in all, there appears to be no consensus on which type of transmission and retraction system is suited for small high-speed hydrofoil craft. However, recently developed electric propulsion systems with axial flux motors, can be a potential enabler for a diesel-electric design. Furthermore, an inclined shaft retraction system, conventionally applied in sailing yachts, can be an option to apply an inclined shaft propulsion system.

4

Integration of hydrofoil systems

This chapter presents the methodology to develop a preliminary design of a hydrofoil LAC to compare this with an equivalent planing LAC. Section 4.1 will discuss the relevance of resistance estimation of planing and foiling designs. In the following Section 4.2, the design method of hydrofoil craft will be presented. Moreover, Section 4.3 will provide the requirements for the foil design as a starting point and Section 4.4 gives context about an iterative model used as a preliminary design tool. Section 4.5 elaborates on the propulsion systems that can be integrated in the design. To continue, 4.6 will compare the results of several resistance estimation methods to provide insight in their application. Section 4.7 will then assess the weight division of each proposed design. Furthermore, Section 4.8 will elaborates on the dynamic equilibrium of these designs, whereas Section 4.9 will present the designs' range estimates. Section 4.10 adds to the prior sections by investigating the effect of weight saving measures. Finally, Section 4.11 will provide concluding insights on the research question posed in this chapter:

RQ1: How do retractable hydrofoil systems affect the weight, resistance, and range potential of a future Littoral Assault Craft (LAC) design?

4.1. Resistance estimation

To start, the hydrofoil LAC design will be designed to achieve its required top speed with the necessary payload. Next to propulsion system efficiency and fuel capacity, resistance is also a primary factor to consider in determining the range of a vessel. A hydrofoil design primarily requires the evaluation of resistance at two speeds: take-off speed and maximum design speed. Take-off speed resistance refers to the hump in resistance the craft encounters before becoming foilborne, which must be overcome with sufficient margin in thrust. The region before becoming foilborne is therefore also referred to as 'hump region'.

Before take-off the vessel's resistance depends on the interaction of hull, propulsion and foil bound forces, which makes this assessment challenging. Fig. 4.1 provides a simplified illustration of this situation. The submerged hull generates both hydrodynamic and hydrostatic forces (N) while also contributing to resistance (R). Simultaneously, the foils generate a lifting force (L), which is not perfectly aligned with the displacement weight (Δ), thereby adding a component in the negative x-direction. To maintain motion, the total drag must be counteracted by the thrust (T) produced by the propulsor. These force vector directions are defined by the pitch/trim angle (τ), flap or incidence angle (δ/α) and the shaft inclination angle (ϵ). To provide an evaluation of behaviour in this region, it is essential to establish a dynamic force and moment equilibrium (van Walree, 1999). Consequently, the primary factors influencing resistance are:

- Weight of the vessel
- Hull Design
- Foil Design
- Foil actuation system and the maximum angle of attack
- Propulsor inclination angle

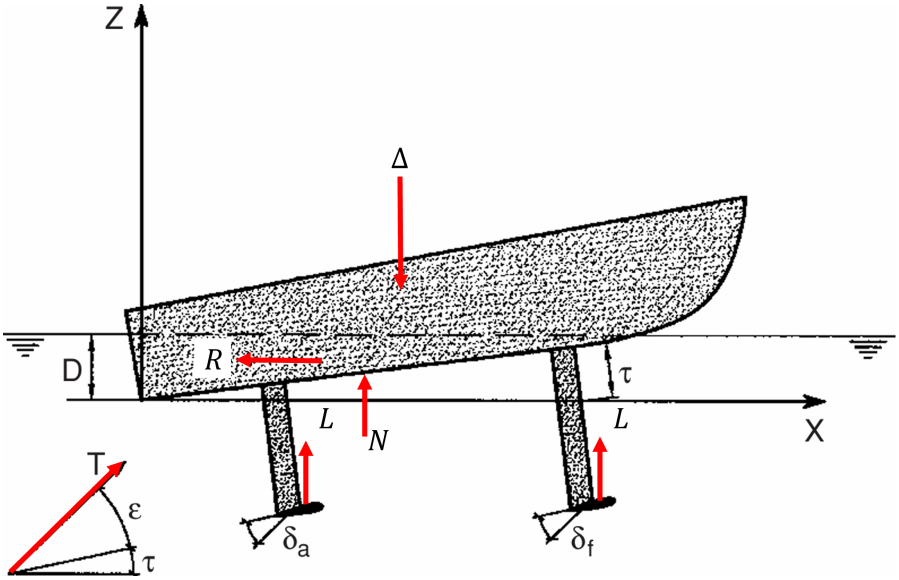

Figure 4.1: Axis system for dynamic equilibrium equations, adapted from Faltinsen (2005) to show force vectors, originally from Van Walree (1999)

For the foilborne design speed, preliminary resistance estimates may be based on the hydrofoil design alone (Doornebos et al., 2023; Francis, 2019). However, a dynamic equilibrium will provide accurate results over the complete speed region of the hydrofoil craft (Faltinsen, 2005).

Planing hull forms have a more pronounced hump in resistance around take-off speeds than multi-hull designs (Faltinsen, 2005). This is because planing hulls experience more wavemaking resistance due to the smaller L/B ratio of the displaced volume and the higher induced trim at these speeds. On contrast, the added trim increases the effective angle of attack of the foils and the underwater planing hull area adds to the lift of the vessel. This can lower the take-off speed necessary for the vessel. Due to the increase in resistance and lower efficiency of high-speed propulsors at low speeds however, the resistance in the hump region can become the determining factor for the required installed power (van Walree, 1999), this is especially a concern for waterjet propulsion designs due to their lower efficiency (Faltinsen, 2005). The consequences of this hump resistance will be further discussed in Section 4.8.

Fig. 4.2 illustrates the difference in resistance development for a bare planing hull compared to a hydrofoil design. Fig. 4.2 also shows the applied resistance estimation methods in their respective domain, which will be further elaborated upon in the following sections.

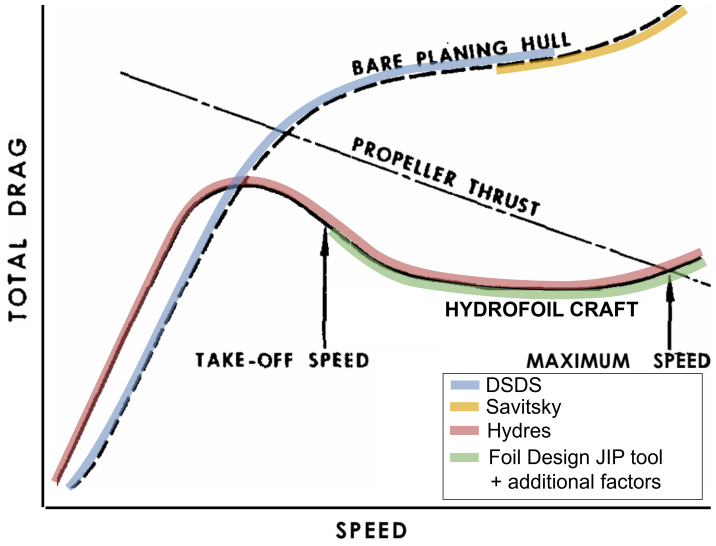

Figure 4.2: Typical calm water thrust-drag curves adapted from Johnston (1985) to indicate resistance estimation methods

4.2. Design method

Fig. 4.3 depicts the design workflow applied to the design of a hydrofoil LAC. Based on an initial lift requirement, the foil design JIP tool is used to explore the design space for the foils' main characteristics. The foil design JIP tool of the Maritime Research Institute Netherlands (MARIN) is a data-driven prediction model of lift and drag of a horizontal foil in a T-foil configuration, excluding the effects of a vertical strut. Whereas this thesis focuses on the application of the tool relevant to the thesis, a more comprehensive description is provided by Minerva et al. (2024). The results of the Foil Design JIP tool only account for the viscous drag, induced drag and wavemaking drag of a hydrofoil. Additional factors need to be taken into account to retrieve the foiling resistance of a complete hydrofoil craft. These additional factors can be derived from a combination of published experimental results such as Abott and Von Doenhoff (1959), and empirical equations such as published by Hoerner (1965). Additionally, this total foiling estimate is used to iteratively evaluate the design's weight estimation and the effect on the foil design. This serves as first displacement estimate for the following step in the design process. During this part, foil interaction effects are neglected as this is a limitation of the Foil Design JIP tool.

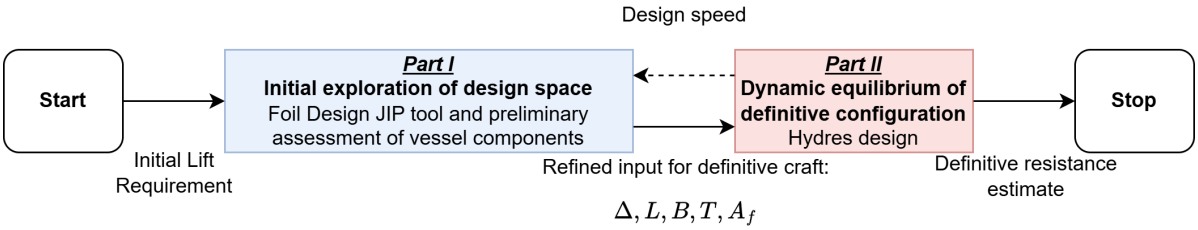

Figure 4.3: Hydrofoil LAC design workflow

After the first part of the design workflow the hydrofoil LAC is modelled in Hydres, another program developed by MARIN (van Walree, 1999). This program is able to calculate the dynamic equilibrium for a hydrofoil craft in steady condition between hull and foil bound forces, based on trim, angle of attack, and height of the vessel. Therefore, Hydres produces an estimate of resistance over the complete speed domain for the subcavitating foil region (< 50 kt). It also includes a design option which that determines a foil system geometry on the basis of global input parameters such as foil system type (canard, tandem, airplane), foil planform type (inverted π, inverted T, double inverted T, surface piercing W), aspect ratio and foil loading. Foil design is based on obtaining the specified foil loading at the design speed with zero flap or foil incidence angles, whereby the craft is foiling under the specified trim and hull clearance.

The mathematical model of Hydres is based on theoretical, empirical and statistical methods. Validation of Hydres, with model and full scale experiments, showed that results for fully submerged hydrofoils were within the experimental uncertainty. Further elaboration on the methodology in Hydres is provided by Van Walree (1999). The main considerations are as follows:

- Hull characteristics are based on the Series 65 model test results
- Foil characteristics are based on Prandtl's lifting line theory
- Fore-aft foil interactions are based on Prandtl's lifting line theory
- Appendage forces are obtained from empirical equations

The Series 65 hull form is a hard chine hull form that is intended for foiling or planing monohulls (Rolling, 1974). During the development of Hydres, this was the hull form where most hydrofoil hull designs were derived from (van Walree, 1999).

The results provided by Hydres are the definitive resistance estimates and the concluding preliminary design of a hydrofoil LAC. Through Hydres, the dynamic equilibrium of the craft can be calculated and the main dimensions of the foils in span, chord, and camber can be defined.

4.3. Dimensional constraints and requirements of foils

Before a preliminary design can be made, the dimensional constraints of the foil system design need to be determined. As discussed in Section 3.9, a non-split conventional submerged hydrofoil system is chosen for a Hydrofoil LAC design. The total lift is distributed by 70% to the front and 30% to the aft foil systems, as this is a generally applied lift division for this foil configuration (Yun & Bliault, 2014).

Together with the retractable hydrofoil system requirements of Table 3.1, the hydrofoil requirements of Table 4.1 can be derived. The assumed maximum trim angle of the vessel is 4°, which is based on the typical behaviour of planing hull form hydrofoil craft, seen in Fig. 3.1 and Appendix H.

The foils will be modelled in such a way that they do not use flaps and are controlled by variable incidence. This reduces the complexity of the foils, but comes at the cost of lift efficiency and precision of control (Wright, 1973). Therefore, the results present a conservative estimate. The maximum angle of attack that can be actuated in this manner is taken as $\pm$ 5 °. Together with a maximum trim angle of 4°, the effective angle of attack can be as high as 9°. Generally, this is within bounds of stalling effects, which develop from around 10° angle of attack depending on the foil section (Abbott & Von Doenhoff, 1959). To provide enough lift, this high effective angle of attack is reached at take-off speed.

For the geometrical constraints of the foils the fore foil's span is bound by the total beam of the vessel. Moreover, the aft foil's span is divided by two and a minimum clearance of 0.25 m between foils is applied. This clearance is around one mean chord length of the aft foils.

Table 4.1: Hydrofoil design requirements

Boundary	**Value**
Vessel trim (τ)	0° to 4°
Actuated foil angle of attack (α)	-5° to 5° (variable incidence)
Span fore foil (s)	< B
Lift requirement fore foil ($L_{req,fore}$)	0.7 $\cdot\Delta \cdot g$
Span aft foils (s)	< $B/2$ - 0.25 m
Lift requirement aft foils ($L_{req,aft}$)	0.15 $\cdot\Delta \cdot g$
Submergence height ($h_{submerged}$)	$\max(0.4$ m$, 0.85 \cdot c_{mean})$[1]
Clearance height (h_{clear})	1.25 m
Thickness to chord ratio (t/c)	0.12
Design speed (v_{design})	38 kt

The submergence height is taken as the maximum between 0.4 m or 0.85 times the mean chord length (c_{mean}). This is considered a good practical operating depth to meet the conflicting requirements of minimising strut drag, while maintaining reasonable foil efficiency and operating depth (van Walree, 1998). Furthermore, the clearance height is taken as 1.25 m, as this is the maximum significant wave height that can be found in sea state 3. The clearance height is defined as the distance between the baseline and the free-surface.

With regards to hydrofoils, the design speed is the speed at which zero angle of attack is required for the foil design to produce the required lift. This is generally achieved by varying the camber and planform area in the foil design (van Walree, 1999). The take-off speed is the speed at which the vessel can produce enough dynamic lift to become foilborne. To investigate which take-off speed and design speed are suitable for a hydrofoil LAC, multiple Hydres runs were performed to give a first indication. Three take-off speeds are analysed. For these take-off speeds, design speeds are reduced until actuated angles of attack within 5° can be achieved for the take-off speed. Fig. 4.4 shows the results of this procedure. A take-off speed of 27 kt results in the lowest resistance at top speed, but results in an extended hump resistance. In contrast, a take-off speed of 23 kt results in a steep increase of top-speed resistance. A take-off speed of 25 kt is posed as the most reasonable option, as the stable foilborne speed region is extended as far as possible without drastic increases in resistance. Subsequently, the design speed is taken as 38 kt and will be taken as a constant for further designs in this thesis.

[1] For optimisation the c_{mean} of the prior iteration is taken, in evaluation and results the c_{mean} of the design itself is used

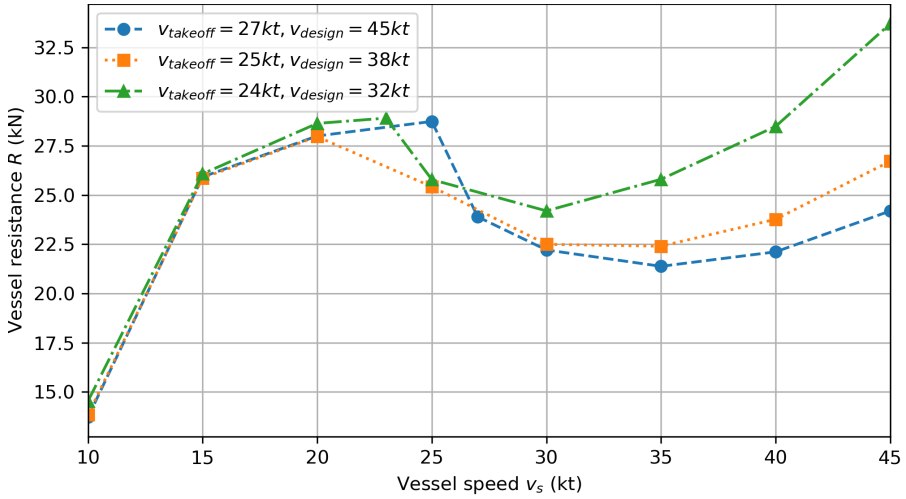

Figure 4.4: Resistance development for different take-off and design speeds from Hydres for a 24.5 t design without appendages (L_p = 13.8 m, B_p = 3.2 m, foil loading = 57500 N/m^2)

4.4. Part I: Initial exploration of the design space

The design method for the iterative model employed in Part I is depicted in Fig. 4.5 and draws inspiration from the methods of Charisi et al. (2022) and King and Devine (1981). The Foil Design JIP tool is employed for designing the T-foils, while a Python-based framework supports the complete design approach. For the design of hydrofoils using the Foil Design JIP tool, two main assumptions are made:

1. Given the constraint on span, it is assumed that the maximum allowed span is optimal for a foil design. This is often the case for designs that have conflicting requirements for vessel beam and resistance (Godø et al., 2024b).
2. A constant foil loading of 57500 N/m^2 is assumed for all foils, as this a reasonable foil loading for the speeds considered within the bounds of cavitation (van Walree, 1999).

Based on these assumptions, the foil chord can be determined for a given displacement weight. Lastly, the required foil camber is derived to provide the target lift at design speed.

Interaction with the Foil Design JIP tool is automated through web scraping, given its web-based interface. To facilitate efficient exploration of design concepts, parametric modelling is applied. Previous studies have employed parametric modelling to provide resistance estimates of hydrofoil configurations (Jansen, 2022; Schachter & Fonteles, 2022; Tannenberg et al., 2023), as well as to assess the feasibility of zero-emission hydrofoil ferry designs (Doornebos, 2022; Francis, 2019). By evaluating multiple design concepts, this thesis aims to achieve a complete assessment of the operational effectiveness of a hydrofoil LAC. As a preliminary design approach, several assumptions are made to simplify calculations. The primary assumptions underlying this methodology are as follows:

1. Results are estimated for a steady calm-water condition.
2. The hydrofoil configurations, including their propulsion systems, can be designed to be retractable to extend no further than the hull form.
3. No rudders are added to the design as it is assumed that the struts can rotate to change the propeller direction or vertical flaps along the strut can be integrated.
4. Loss of lift due to cavitation is not considered, as the design operates in subcavitating conditions.
5. The hull deadrise angle remains a constant 20°.
6. For the results of the Foil Design JIP tool, the requested lift is constant for each foil. This means that the angle of attack can be based on this requested lift. In contrast, the Hydres code varies its angle of attack to attain a dynamic equilibrium.
7. Convergence is based on foil design lift compared to displacement weight and is considered converged for a 1% error.

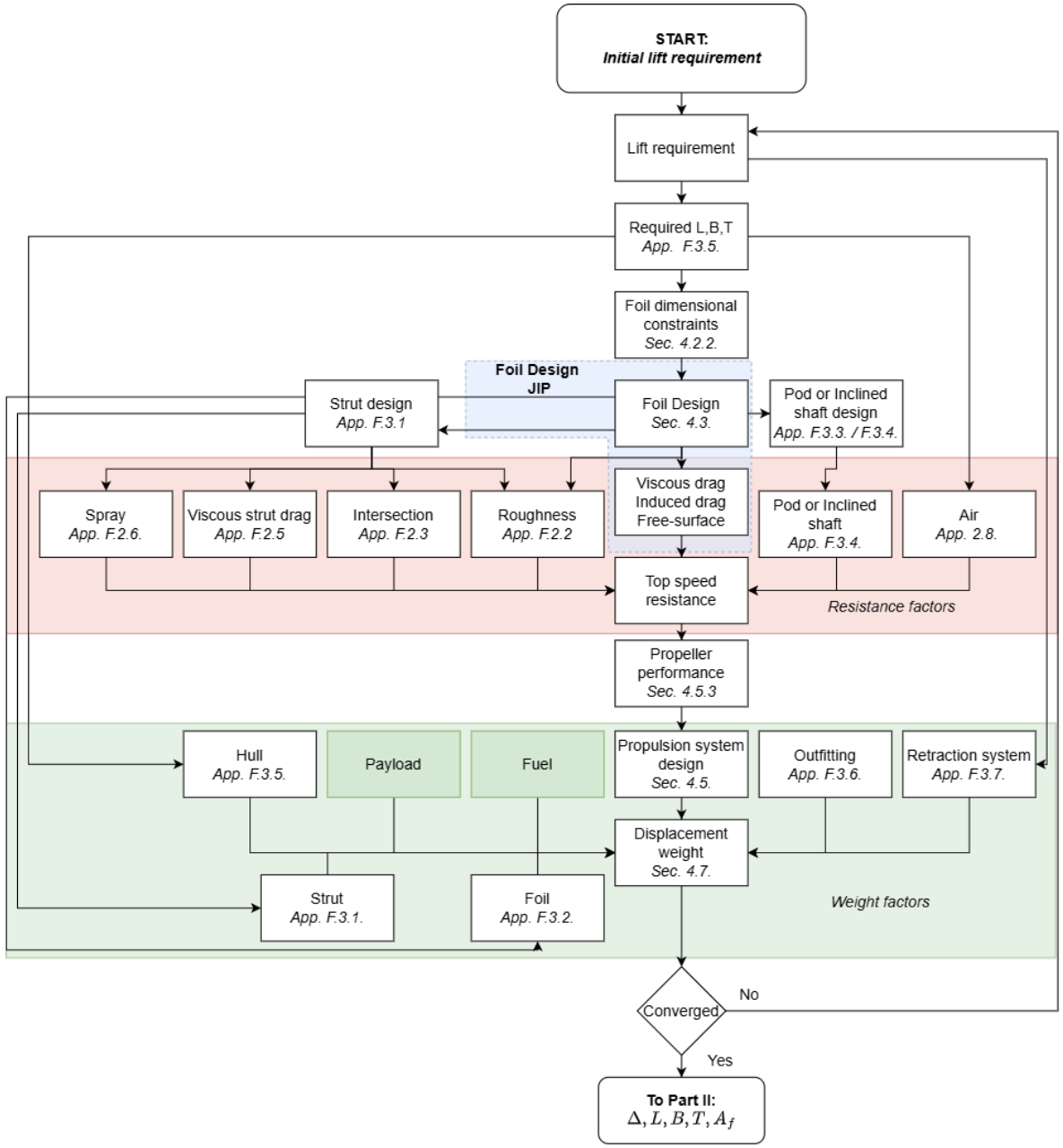

Figure 4.5: Integration of the Foil Design JIP tool in the iterative model of Part I, with the respective appendices and section numbers for further reference

Fig. 4.5 shows the architecture of the iterative model used in Part I. The iteration loop starts by initiating a design with an assumed total lift requirement (or displacement weight). On this initial estimate, the main particulars can be based: total length (L), beam (B) and draught (T). As a function of the hull particulars, dimensional constraints on the foil design are applied. This serves as the input for the foil design. The foil design JIP tool can provide the viscous, induced and free-surface drag, whilst other parameters require to be estimated, based on this foil design. After estimating the complete foiling resistance, the weight of foils and struts can be determined. This also allows for the dimensioning of a propulsion system. The retrieved weight factors are used in the total weight estimation, where payload and fuel are an input to the model. After this step, it is checked if the foil design lift and the estimated displacement correspond. If the error between the foil design lift and displacement is smaller than 1%, it is deemed converged. If not, a new iteration is started with an adjusted displacement. If the design is converged, the concept design can be retrieved with its main particulars in displacement (Δ), length (L), beam (B), draft (T) and projected frontal area (A_f). Based on this design, which will be presented

in Section 4.7, further assessment in Hydres for Part II is conducted from Section 4.8. The iteration loop is generally converged within four iterations, depending on the initial lift requirement given.

As can be seen in Fig. 4.5, the weight of a design is estimated by dividing it into several categories. The displacement is subdivided as denoted in Eq. (4.1). Propulsion weight estimates are based on the sum of required propulsion system weights and will be further discussed in Section 4.5. Further elaboration on each weight factor can be found in Appendix F.

$$\Delta = m_{hull} + m_{propul.} + m_{struts} + m_{foils} + m_{retract.} + m_{outfit.} + m_{payload} + m_{fuel} + m_{lub.} \tag{4.1}$$

4.5. Propulsion systems

To evaluate different propulsion systems for the hydrofoil LAC design, two options are considered: an inclined shaft system and an L-drive system. These solutions were deemed as promising options for the foil configuration as argued in Chapter 3. It also allows for a comparison between a lighter propulsion option, that has increased resistance due to an added appendage, and a heavier option that can be incorporated in a more hydrodynamically streamlined fashion.

The inclined shaft solution takes inspiration from the retractable propeller systems found in sailing yachts, offering a simplified retraction mechanism. It uses a homokinetic joint to lower the driveshaft to the necessary depth. This design will further be referred to as the Hydrofoil Littoral Assault Craft HomoKinetic (HLAC-HK) design.

For a diesel-electric propulsion setup, the L-drive configuration is considered. While podded propulsion is also applied in electric hydrofoil craft, the required power output would necessitate large pod diameters for a hydrofoil LAC replacement. Furthermore, an axial flux motor would not be applicable, due to its larger diameter. Instead, an L-drive system with axial flux motors embedded at the top of the struts is proposed. This can facilitate flexible extension of the struts, where the only tether of the propulsion to the vessel is the cabling and cooling. This design still requires a nacelle at the bottom of the strut, incorporating a right-angle transmission. This type of transmission is also applied in other hydrofoil craft (see Appendix C). The diesel-electric configuration will further be referred to as the Hydrofoil Littoral Assault Craft Diesel-Electric (HLAC-DE) design.

4.5.1. Inclined shaft propulsion architecture

Fig. 4.6 shows the proposed propulsion architecture of a HLAC-HK design. In this block diagram, the only addition to the geared drive with a gearbox (GB), is the homokinetic joint. The propulsion weight of this configuration is modelled as described in Eq. (4.2). In Eq. (4.2) $m_{hk,retract}$ denotes the added weight for the homokinetic retraction mechanism. This weight is derived from a retractable propulsion system intended for sailing yachts. Table 4.2 shows the weight of several retraction systems. To derive the weight required for a hydrofoil vessel, the weight is interpolated for the required power and adjusted to the length of the strut according to a cubic relation, such as stated in Eq. (4.3). In Eq. (4.3) ϵ denotes the inclination angle and l_{hk} the quoted length of Table 4.2. Additionally, the auxilliary genset weight (m_{aux}) is assumed to remain constant and is based on the CB90 genset. Other weight factors are retrieved from system manufacturers and can be found in Appendix G.

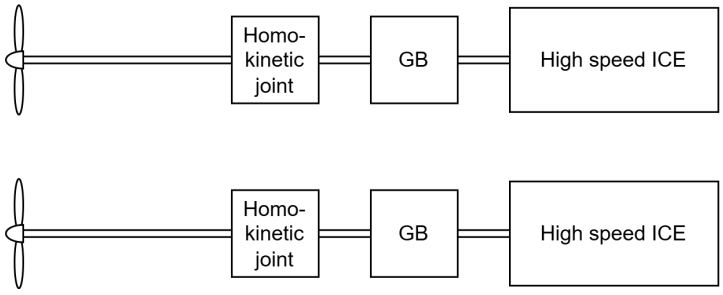

Figure 4.6: Propulsion architecture of a HLAC-HK design, with a retractable inclined shaft

$$m_{propul.} = 2 \cdot (m_{engine} + m_{gb} + m_{hk,retract}) + m_{aux} \tag{4.2}$$

$$m_{hk,retract} = m_{hk} \cdot \left(\frac{l_{strut}/\tan(\epsilon))}{l_{hk}} \right)^{1/3} \tag{4.3}$$

The transmission efficiency of this configuration yields from Eq. (4.4). Gearbox (η_{gb}) and shaft (η_s) efficiencies are in accordance with Klein Woud and Stapersma (2002). As explained in Section 3.6, the power losses of a homokinetic joint are around 2% (η_{hk}), but the propeller is also less efficient due to its inclined orientation. The effect of inclination in propeller design is taken into account for the propeller efficiency of Section 4.5.3 and is not added to the transmission efficiency.

$$\eta_{trm} = \eta_{gb} \cdot \eta_{hk} \cdot \eta_s = 0.98 \cdot 0.98 \cdot 0.99 = 0.95 \tag{4.4}$$

Table 4.2: Homokinetic propulsion retraction system parameters of Ship Motion group (2024)

Model	Power range (kW)	Max. propeller diameter (mm)	Weight estimate (kg)	l (mm)	b (mm)	h (mm)
RPS60C	<350	700	580	4300	1000	1200
RPS70C	<525	900	740	5900	1390	1640
RPS80C	<750	1100	920	7700	1810	2140

4.5.2. L-drive propulsion architecture

Fig. 4.7 illustrates the proposed propulsion architecture of the L-drive configuration. It makes use of axial flux motors for generative and propulsive power. With enough installed power, this system should work with only variable speed generator and no additional energy storage system. However, the question remains if this will work in all dynamic situations. In the case of a take-off, the variable speed generators may lag in their reaction, with overspeed of the generators as a result. Therefore, a 'buffer' is added to the system architecture, which is a battery or supercapacitor pack that can peak-shave in dynamic situations. Eq. (4.5) describes the modelled weight for this propulsion configuration. In Eq. (4.5), m_{genset}, m_{eprop}, $m_{powerelec.}$ and m_{buffer} denote the weight devoted to the gensets, electrical propulsion, power electronics, and the buffer system, respectively. Furthermore, k_e denotes the amount of stacked axial flux motors that are required to produce the propulsive power. It is assumed that the right-angle gearbox weight is negligible, as the displaced volume of the pod will counteract the additional weight and because strut weight is already taken into account. The required weight for power electronics is furthermore doubled to account for the extra weight in integrating the electronic system with switchboards and its housing. The weight of power electronics is defined by Eq. (4.6), in which the amount of stacked propulsive electrical motors (k_e) require an individual motor controller. Lastly, the genset weight is determined by matching a high-speed engine to an axial flux generator conversion, according to Eq. (4.7), in which m_{engine} denotes the engine weight and m_{axconv} is the axial flux generator conversion weight.

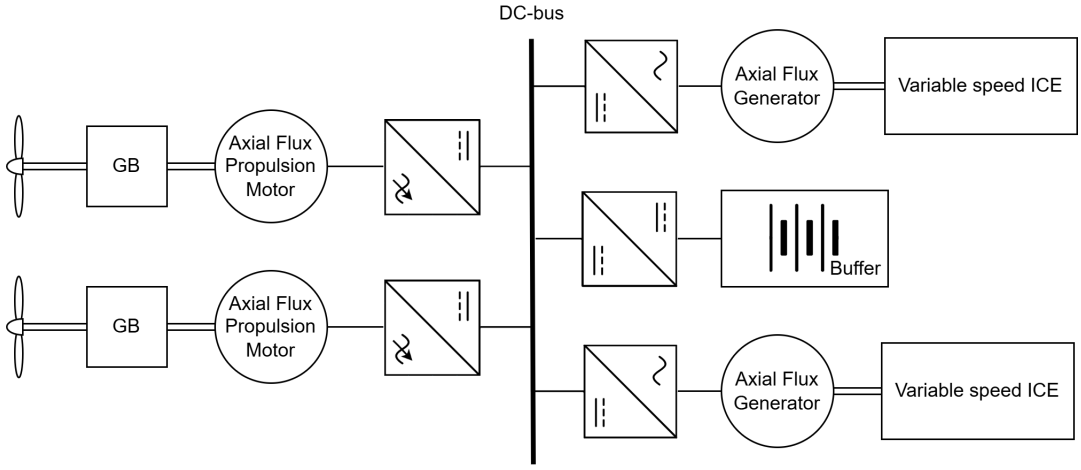

Figure 4.7: Propulsion architecture of the HLAC-DE design, with the L-drive propulsion solution

$$m_{propul.} = 2 \cdot (m_{genset} + k_e \cdot m_{eprop} + 2 \cdot m_{powerelec.}) + m_{buffer} \tag{4.5}$$

$$m_{powerelec.} = (k_e + 1) \cdot m_{inv} \tag{4.6}$$

$$m_{genset} = m_{engine} + m_{axconv} \tag{4.7}$$

The transmission efficiency of this propulsion configuration is derived with Eq. (4.8). In Eq. (4.8) η_{em} and $\eta_{dc/ac}$ denote the electrical machine and inverter efficiency, respectively. Electrical machine and inverter efficiency is based on supplier data (ABB, 2022; Emrax, 2025).

$$\eta_{trm} = \eta_{em} \cdot \eta_{dc/ac} \cdot \eta_{dc/ac} \cdot \eta_{em} \cdot \eta_s \cdot \eta_{gb} = 0.97 \cdot 0.98 \cdot 0.98 \cdot 0.97 \cdot 0.99 \cdot 0.98 = 0.88 \tag{4.8}$$

The buffer system can be dimensioned on the basis of load fluctuations. Based on the experimental results of Appendix H, it can be expected that load fluctuations of around 10% of the total installed power may be encountered. An additional power margin of 30% is taken to prevent the system of pushing at its limits and ensure longevity. The required peak buffer power can therefore be derived with Eq. (4.9). For the buffer system, Lithium-Titanium-Oxide (LTO) batteries and supercapacitors are considered. LTO batteries excel in its safety properties, charge and discharge rate, and total charging cycles compared to other battery types. On contrast, they are the least energy dense option of the conventional marine battery types (Doornebos, 2022). Supercapacitors offer even higher power densities, but lower energy densities (Francis, 2019). Table 4.3 shows an example of the two configurations. Enclosure weight represents 70% of the total module weight, in accordance with the findings of Moreno (2019) and the system is coupled with a converter from ABB (2022). The systems are designed for a minimum release time of 10 seconds, as this can be the response time of a generator to a varying load (Sechilariu & Locment, 2016). The buffer energy capacities do not contribute to the eventual range estimates of Section 4.9. The battery configuration is taken in further consideration as a conservative estimate for a buffer system.

$$P_{buffer} = 0.1 \cdot P_{inst.} \cdot 1.3 \tag{4.9}$$

A buffer system can have additional benefits, such as the option to shortly change to battery propulsion in order to reduce sound signature. In the case of take-off power being the determining factor of the power requirement, these considerations may also serve to create a ‘boost’ system, which can provide additional thrust in difficult take-off conditions (Minerva & Montero, 2021).

Table 4.3: Weight of a 120 kW buffer system (of a 900 kW system), based on manufacturer data (AEP, 2018; Leclanché, 2024), converter weight of ABB (2022)

Design	**LTO batteries**	**Supercapacitors**
Manufacturer	Leclanché	AEP
Model	M2	Cell pack V2
Charge and discharge rate	6C/6C (120 kW)	195 kW (10 sec)
Modules required	8	4[2]
Module weight	50 kg	33 kg
Subtotal	*400 kg*	*132 kg*
Enclosure weight	280 kg	92 kg
Converter	35 kg	35 kg
Total	**715 kg**	**260 kg**
Total capacity	20 kWh	0.44 kWh

[2] 2 rows parallel of 2 modules in series

4.5.3. Propeller model

For the investigation of propeller performance at the vessel speed domain considered for this thesis, the Newton and Rader series (NR-series) of transcavitating propeller data is digitised from the original paper (Newton & Rader, 1961). This propeller series is also discussed in Section 3.5.1. Using this data, an assessment of the potential thrust in the hump region and the efficiency at top speed can be derived.

The propeller design is limited in diameter by the limited submergence. To match a propeller design to the prime mover, the optimal rotational speed is derived for the reduction gearbox to derive the highest open water efficiency (Klein Woud & Stapersma, 2002). The ship resistance is transformed into a thrust coefficient (K_T) as a function of advance ratio (J), following Eq. (4.10). Eq. (4.10) denotes T_0, $v_{a,0}$, D_{max}, and ϵ as the requested thrust, advance velocity, maximum propeller diameter, and inclination angle at the design condition, respectively. Constant c_7 only depends on the design condition and the limiting propeller diameter. Eq. (4.11) yields a curve in the propeller characteristics of Fig. 4.8. To derive the propeller characteristics of Fig. 4.8, linear interpolation is applied for the nearest cavitation numbers (σ_0) at the operational velocity. The intersection of the K_T-curves for propellers and the vessel's requested thrust, provides the values of J and consequently the open water efficiency (η_o). Table 4.4 shows an example of a propeller designed with this approach.

$$\left(\frac{K_T}{J^2}\right)_0 = \frac{T_0}{\rho \cdot v_{a,0}^2 \cdot D_{max}^2 \cdot \cos(\epsilon)} = c_7 \tag{4.10}$$

$$K_{T,ship,0} = c_7 \cdot J_0^2 \tag{4.11}$$

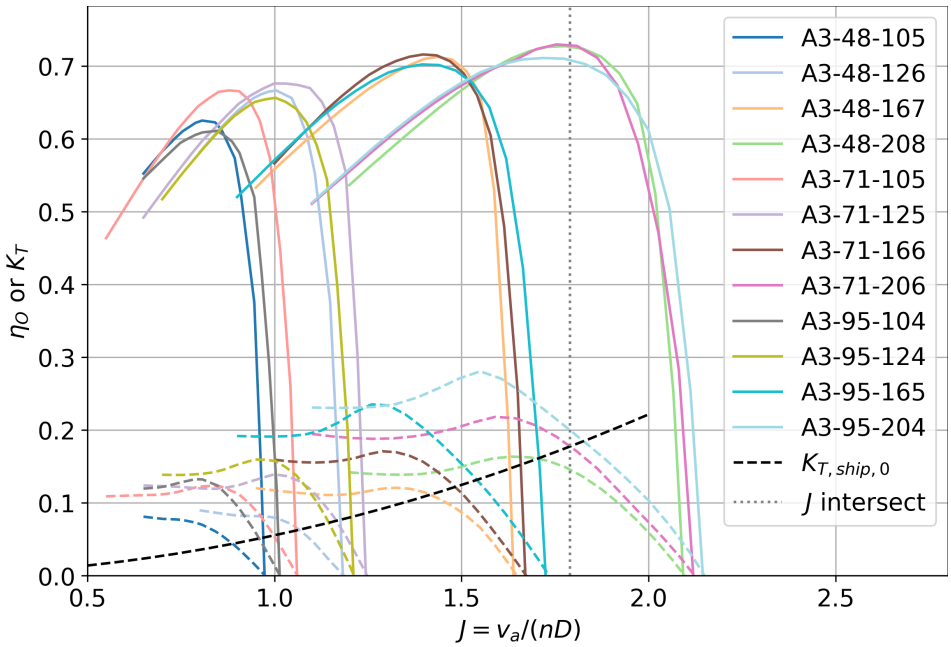

Figure 4.8: Newton and Rader propeller series matching

Table 4.4: NR-Propeller

	Value
$v_{a,0}$	45 kt
σ_0	0.377
D_{max}	0.6 m
ρ_{sw}	1025 kg/m^3
ϵ	0°
h	0.44 m
Propeller	A3-71-206
B.A.R.	0.71
P/D	2.06
J_{opt}	1.79
K_T	0.177
K_Q	0.0695
η_o	0.728
n_{opt}	1293 rpm

As can be seen in Fig. 4.8, the data points for the NR-series propellers is limited. Thus, extrapolation is required to derive the thrust over the complete speed domain of a design. Fig. 4.9 shows the development of the thrust coefficient over speed of the propeller design of Table 4.4. The data is extrapolated linearly for lower advance ratios. The linear method was chosen because of the nonconforming datapoints, to for example quadratic or spline fits.

Until around 25 kt, the NR-series propeller has the same characteristic slope as a sub-cavitating propeller. This is exemplified in Fig. 4.9a. However, from this velocity onwards a distinct angle becomes apparent, as seen in Fig. 4.9b. This is a result of the cavitation that is starting to form (Newton & Rader, 1961). At higher advance velocity, the sharp angle decreases and the thrust coefficient has a flat characteristic at lower advance ratios, illustrated by Fig. 4.9c. Looking at the other propeller data of this series, the sharp decrease in the thrust coefficient for the lowest advance ratios around σ_0 = 1 (such

as Fig. 4.9b), seems to be incorrect. However, at the velocities that such a low cavitation number can be found, the propeller designs are generally within the domain of the dataset provided by Newton and Rader (1961). The extrapolation primarily plays a role for advance velocities lower than 25 kt. It is therefore gathered that these values will provide realistic results.

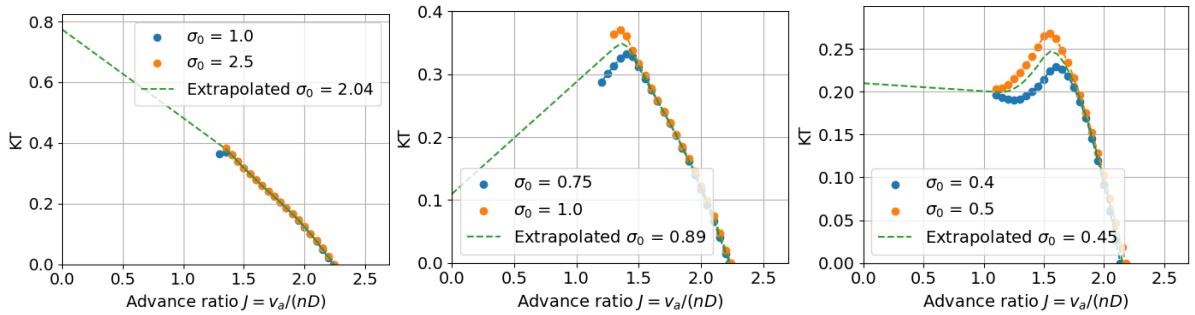

(a) v_a = 20 kt **(b)** v_a = 30 kt **(c)** v_a = 41.5 kt

Figure 4.9: Thrust coefficient datapoints, with the interpolated and extrapolated thrust coefficent curves, for a Newton-Rader A3-71-206 propeller

The same procedure is applied to the torque-coefficient (K_Q) and open water efficiency (η_o). By assessing the maximum thrust that can be gained from a delivered shaft torque, the thrust at each velocity can be derived. This results in the thrust curves of Section 4.8. The maximum propeller diameter is assumed as a constant 0.6 m for further calculations to guarantee propeller submergence.

The interaction effects of the propeller, strut and hull are small and therefore relative rotative and hull interaction losses are neglected (Blount & Bartee, 1997). This results in a hull (η_h) and relative rotative (η_r) efficiency of 100%.

4.6. Comparison of resistance results

Before presenting the results for the different hydrofoil craft designs, this section will provide insight in the application of different resistance estimation methods. Table 4.5 and Fig. 4.10 show an example foil configuration for a 24.5 t design with propulsion in nacelles. This design was evaluated with the calculations of Part I (Foil Design JIP and iterative model) and Part II (Hydres). One reason for the slight variation of span and chord between the designs, is that the Foil Design JIP results require some taper of the foil, whereas the Hydres design is made rectangular without taper. The thickness over chord ratios (t/c) of the struts are derived with the structural strength methodology of App. F.3.1.

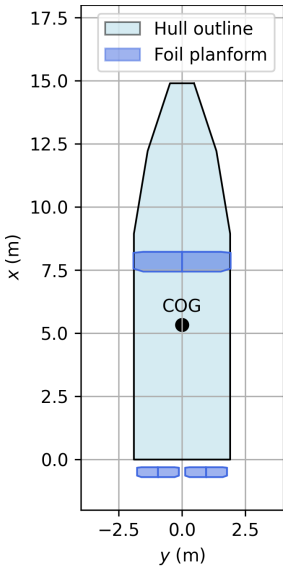

Figure 4.10: Bottom side view of a 24.5 t design

Table 4.5: Main particulars comparison between Part I and II

Parameter	Part I	Part II	Unit
Displacement weight (Δ)	24500		kg
Frontal Projected Area (A_f)	11	11	m^2
c_{front}	0.77	0.76	m
c_{aft}	0.38	0.31	m
s_{front}	3.8	3.8	m
s_{aft}	1.65	1.80	m
t/c foils	0.12	0.12	-
t/c front struts	0.105	0.105	-
t/c aft struts	0.19	0.19	-

Fig. 4.11 compares the resistance derived from Part I of the calculations to Part II. Only the '3D foil viscous resistance' is derived from the Foil Design JIP tool, and this resistance encapsulates viscous profile drag, induced drag and wave-making drag. All other resistance factors of Part I are estimations to derive a complete craft foiling resistance. Both methods work to see that the foils will produce enough lift at the take-off speed of 25 kt. Furthermore, in both results the general trend of a high drag at take-off speed (due to a high amount of induced drag) and top speed (due to mostly viscous drag) is discerned. Overall, the drag of Part I is between 5-15% lower than the results of Hydres. This discrepancy can have several sources. Firstly, the Foil Design JIP tool has some inaccuracy due to its data-driven nature. Secondly, the interaction effects are neglected for the calculations of Part I, whereas Hydres does take this into account. The downwash of the front foil will not vary much in the spanwise direction of the aft foils however, due to the larger span of the front foil. It is therefore presumed that this error will be small. Thirdly, the Foil Design JIP tool uses foil sections derived from the Eppler 817 series, whereas Hydres' foil sections are based on the NACA-66 series. The results of Part I also do not continue for speeds higher than 43 kt, as this is a limitation of the Foil Design JIP tool.

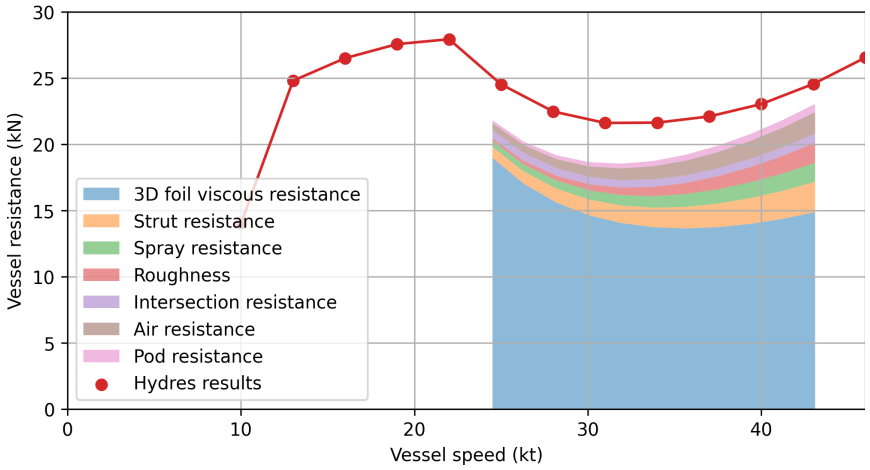

Figure 4.11: Foil Design JIP resistance results compared to Hydres

After testing at multiple displacements the discrepancy stayed consistent. Therefore, a margin of 10% is taken above the resistance at 43 kt of Part I, to gain a realistic estimate for the resistance at 45 kt. Additionally, a comparison with experimental resistance results was performed. This can be found in Appendix H and gave satisfactory results.

Fig. 4.12 shows the required angle of attack at speed for both results. It can be concluded that both results have the same general trend and that the assumption of a constant lift requirement for each foil in Part I is realistic.

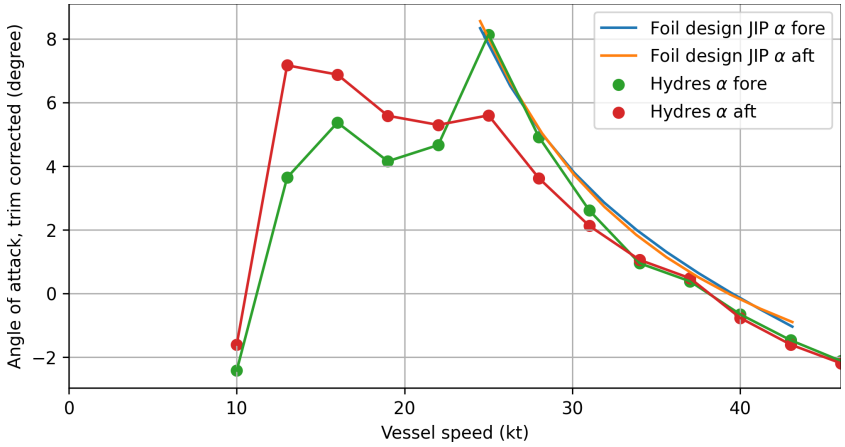

Figure 4.12: Foil Design JIP angle of attack results compared to Hydres

To compare the performance of a hydrofoil design to a planing hull, the planing hull resistance is estimated. To derive the resistance of the planing benchmark vessel multiple methods can be used. Savitsky's (1964) method is particularly suitable for planing vessels at higher speeds, though it does not account for wave-making resistance. Another approach involves using planing hull series, with well-known examples including the Delft Systematic Deadrise Series (DSDS) (Keuning et al., 1992) and the more recent Naples Systematic Series (NSS) (De Luca & Pensa, 2017). Among these methods, the DSDS and NSS are the most accurate for the considered vessels as they include wave-making resistance, which is crucial to compare the hump region of a planing vessel to a hydrofoil vessel. Furthermore, it uses a modern hard-chine hull which is more often found in littoral craft concepts. In this thesis, the DSDS will be used considering that the polynomial data of this series is available. Furthermore, Savitsky's method will be applied for speeds that exceed the polynomials of the DSDS. For designs with differing displacement or deadrise than the published polynomials, linear interpolation is applied as recommended by Keuning and Hillege (2017). Fig. 1.2a shows the resistance estimations following from the DSDS and Savitsky with the parameters listed in Table 4.6.

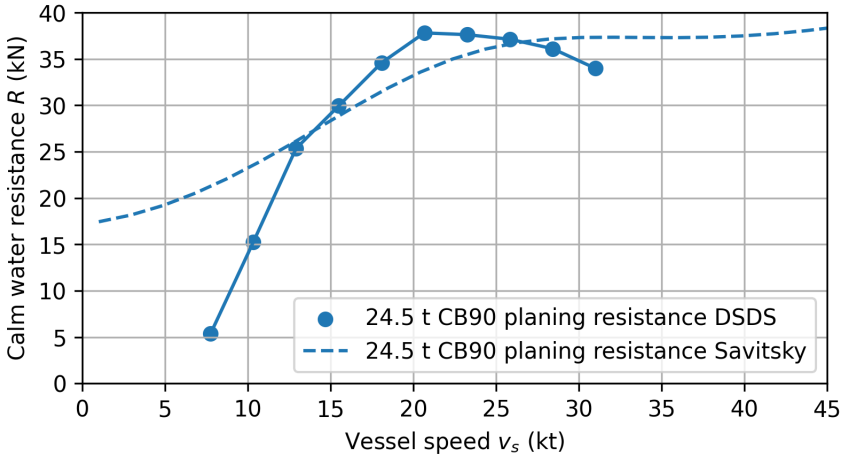

Figure 4.13: Planing resistance estimation following Savitsky (1964) and the DSDS (Keuning & Hillege, 2017) of a 24.5 t CB90

Table 4.6: Derived resistance estimation parameters of the reference CB90 planing hull

Symbol	Definition	Value	Unit
Δ	Displacement mass	24.5	t
β	Deadrise angle with respect to the horizontal plane	20	°
A_f	Frontal projected area	11	m^2
	DSDS		
L_p	Length of projected planing bottom area, length over chines	13.5	m
B_p	Maximum breadth over chines, excluding external spray strips	3.2	m
A_p	Projected planing bottom area, excluding area of external spray strips	38.5	m^2
LCG	Longitudinal Center of Gravity from centroid of planing area (% of L_p)	-3	%
	Savitsky		
LCG	Longitudinal center of gravity measured along the keel from transom (m)	5.33	m
VCG	Vertical center of gravity measured from keel line (m)	0.7	m
a	Distance between the viscous drag component D_f and the center of gravity, measured normal to D_f	0.4	m
b	Beam	3.2	m
f	Distance between the thrust vector and the center of gravity, measured normal to the shaft line	0	m
ϵ	Inclination of thrust line relative to keel line	0	°

By combining the resistance curves of the hydrofoil design (Fig. 4.11) and the planing hull (Fig. 4.13), a comparison can be made in Fig. 4.14. It can be concluded from Fig. 4.14 that the hydrofoil craft

already reduces its resistance drastically in the foil-assisted planing regime (15-25 kt). Moreover, the resistance reduction can be as high as 40% at optimal speeds. However, this is a simplified illustration of the impact of applying hydrofoils to the design. The application of hydrofoils requires other propulsion methods and the hydrofoil system including its retraction imply additional weight. Therefore, section 4.7 will elaborate on the weight impact of these systems.

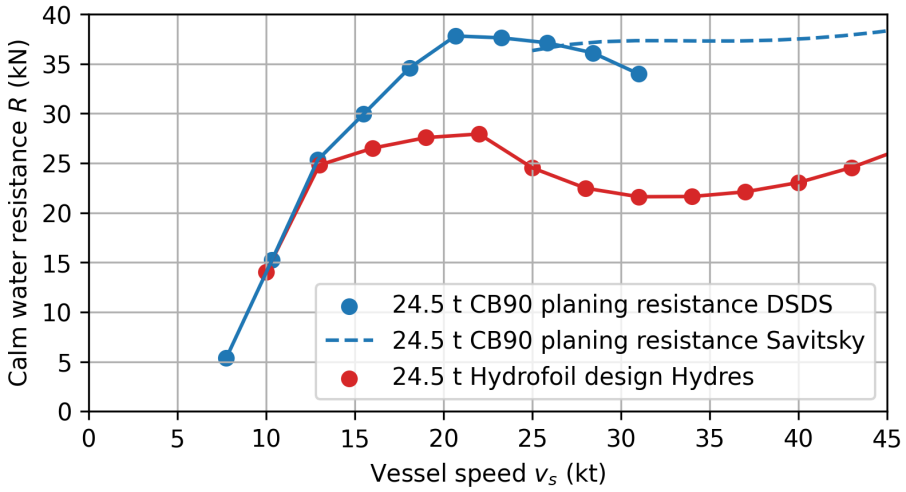

Figure 4.14: The 24.5 t planing hull against a hydrofoil design

4.7. Part I: Resulting weight estimates

The calculations of Part I of the preliminary design result in the first weight estimates. The weight estimates can be compared to a prior design study of Hoerner et al. (1954). Fig. 4.15 visualises the weight distribution of hydrofoil craft based on this study. Although the study is not recent (1954), it can give an indication of how the proposed designs of this thesis compare to other hydrofoil craft, and if the derived weights of the calculations in this thesis are valid. With current technology however, it is reasonable to expect that some weight components are reduced.

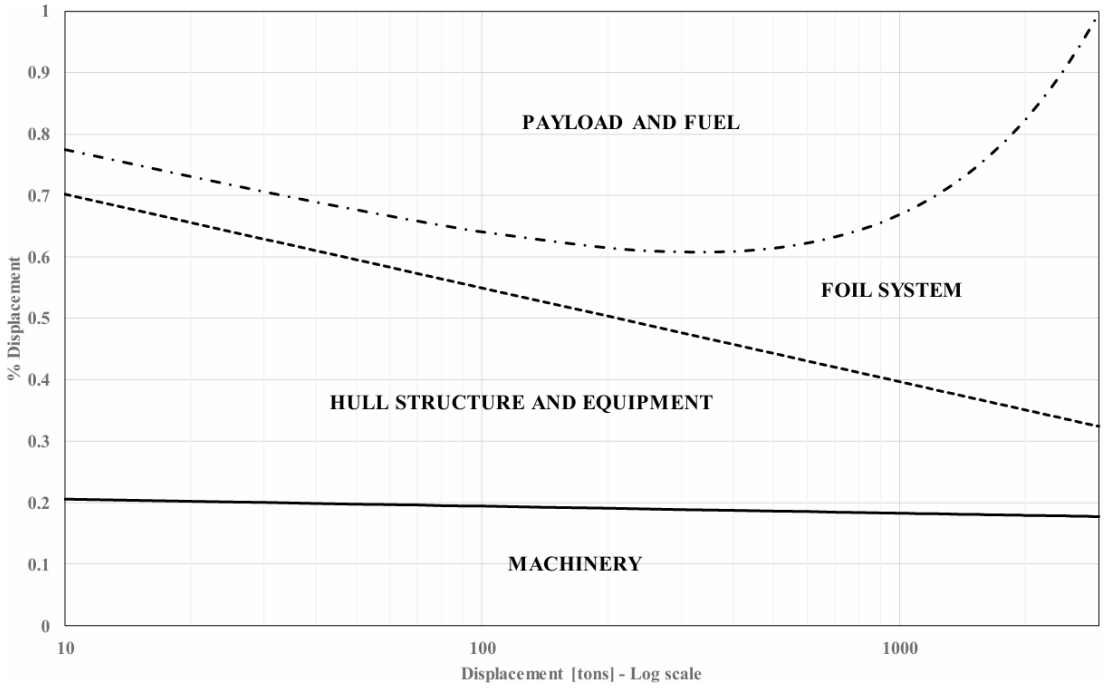

Figure 4.15: Weight development of hydrofoils indicated by Minerva and Montero (2021), derived from Hoerner et al.(1954)

Table 4.7: Weight estimates resulting of Part I of the modelling with the reference masses of Hoerner et al. (1954) in brackets

Design	**CB90**		**HLAC-HK**		**HLAC-DE**	
R @ 45 kt (kN)		38.5		30.4		27.2
η_{trm}		0.97		0.95		0.88
η_o		0.7		0.710		0.725
ϵ (°)		0		15		0
P_{req} (kW)		1320		1090		1030
			DWT			
Payload and fuel (kg)				***(6620)***		***(7030)***
$m_{payload}$		4500		4500		4500
m_{fuel}		1980		1980		1980
m_{lub}		80		80		80
Subtotal		6560		(-1%) 6560		(-7%) 6560
			LWT			
Hull structure and equipment (kg)				***(10790)***		***(11460)***
m_{hull}		4960		4960		5200
$m_{outfit.}$		7280		7280		7280
Subtotal		12240		(+12%) 12240		(+8%) 12480
Foil System (kg)				***(2210)***		***(2340)***
m_{foils}		-		260		300
m_{struts}		-		260		290
$m_{retract.}$		-		650		690
Subtotal		0		(-47%) 1170		(-45%) 1280
Machinery (kg)				***(4900)***		***(5210)***
m_{engine}	2x Scania DI16 077M (662 kW)	3340	2x MAN LE 426 (588 kW)	2500	2x MAN LE 446 (537 kW)	2500
m_{axconv}		-		-	2x HPIL 3 x3	1400
m_{eprop}		-		-	2x3 Emrax 348LV-LC (178 kW)	260
$m_{waterjet}$	2x Kamewa S32	1360		-		-
$m_{entrained}$		350		-		-
m_{buffer}		-		-		840
$m_{powerelec.}$		-		-		790
m_{gb}	2x Twin disc MGX 5126A	480	2x ZF 400	320		-
m_{aux}	Westerbeke (7.5 kW)	180	Westerbeke (7.5 kW)	180		-
$m_{hk,retract}$		-		1620		-
Subtotal (kg)		5710		(-6%) 4620		(+11%) 5800
LWT total (kg)		17950		18030		19480
Displacement Δ (kg)		24500		24590		26140
L (m)		14.9		14.9		15.6
B (m)		3.8		3.8		3.8
T (m)		0.86		0.86		0.86
A_f (m^2)		11		11		11

Table 4.7 lists the weight results of the HLAC-HK and HLAC-DE designs compared to the estimated CB90 benchmark weights. The mass of each factor is rounded to tens of kilograms. For comparison, the weights derived from Fig. 4.15 and the change with respect to the proposed designs is also shown within the brackets. Generally, the weights are in line with the expectations of Hoerner et al. (1954), with weight factors not differing more than 12%. However, a larger change can be seen in the reduction of hydrofoil system weight. This can be explained by older hydrofoil craft using high-strength steel or aluminium for their hydrofoil designs (Johnston, 1985), whereas the modelled weight estimation considers a carbon composite structure. The foil system weight found is comparable to a single portside or starboard foil for the AC75 class foiling sailing yachts (America's cup, 2022), which are between 1200 to 1300 kg. The HLAC-HK design does not require an increase in displacement to facilitate the hydrofoil conversion. In contrast, the HLAC-DE design has a displacement increase compared to the CB90 of 6%, which increases the estimated required total length to 15.6 m. This length reaches the limits of the davits, but is still within reasonable bounds considering there is no other appendage extending the length, such as waterjet buckets.

Although heavier in displacement, the resistance found for the HLAC-DE configuration is lower than the HLAC-HK configuration. This is caused by the added appendage drag of an inclined shaft of the HLAC-HK configuration. For this inclined shaft, an estimated diameter of 50 mm is applied following the calculations of Appendix F.3.3. However, it is unfortunate that the iterative model can not find an

engine with a different weight for the lower power requirement of the HLAC-DE design. As a result, the engine weight of the HLAC-DE and HLAC-HK configuration is the same. In general, the weight and size do not require a drastic increase in order to obtain the same payload and fuel capacity. With weight saving measures it can be expected that a hydrofoil conversion of an LAC design can have the same payload and outfit carrying capacity.

Fig 4.16 and 4.17 provide an illustration of the developed hydrofoil designs, with their main foil particulars in Table 4.8. From the parameters listed in Table 4.8 it can be gathered that the design camber is rather high, as standard foil sections are generally around 2% (Abbott & Von Doenhoff, 1959).

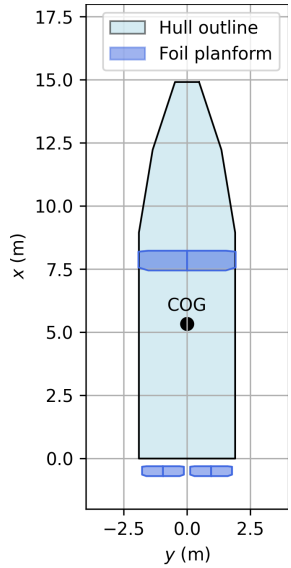

Figure 4.16: HLAC-HK

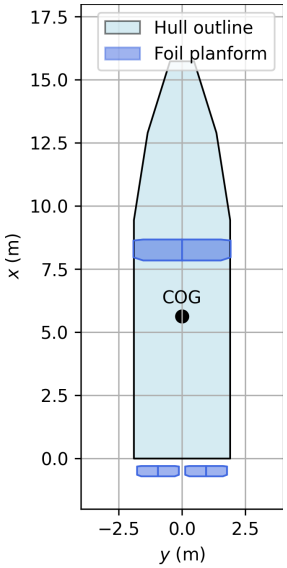

Figure 4.17: HLAC-DE

Table 4.8: Main foil particulars of the HLAC-HK and HLAC-DE designs

Parameter	HLAC-HK	HLAC-DE	Unit
c_{front}	0.78	0.83	m
c_{aft}	0.39	0.41	m
s_{front}	3.8	3.8	m
s_{aft}	1.65	1.65	m
$camber_{front}$	5	5	%
$camber_{aft}$	4.2	4.4	%
t/c foils	0.12	0.12	-
t/c front struts	0.105	0.105	-
t/c aft struts	0.19	0.19	-

4.8. Part II: Dynamic equilibrium of definitive configurations

As the displacement and main particulars of each vessel is determined, these designs can be modelled in Hydres to provide an estimation of the resistance over the complete speed region of the vessel.

Before the results are presented, some considerations require to be stated. Firstle, the series 65 hull form used in Hydres is different from the CB90 hull and therefore the Centre of Gravity (CoG) can not remain at the same position for modelling in Hydres. Using the same CoG placement (x = 5.33 m) would result in a unreasonably high trim at zero speed of around 5°, which increases to even more highly unreasonable trim as velocity increases $>$ 20°. Therefore, the CoG is put at a constant 0.5 times the projected planing bottom area (L_p), which results in a static trim of 0.05 ° with the bow up. However, this means that Hydres will calculate the dynamic equilibrium for another foil position than initially designed. Nevertheless, it is expected that the planing and foil lift will react in a similar manner for this design. The variation of the CoG placement with differing hull forms is left for further research. The complete Hydres input for the designs can be Found in Appendix I.

Hydres can provide the required foil actuation to achieve a dynamic equilibrium for each advance velocity. However, for each velocity, multiple dynamic equilibria can be found with differing trim and draught positions. Therefore, the dynamic equilibrium found with the lowest resistance will be provided. In reality, the craft will naturally tend towards the position with the least resistance as well.

4.8.1. Dynamic equilibrium of an inclined shaft design (HLAC-HK)

Fig. 4.18 shows the resistance curve determined for the dynamic equilibrium using Hydres for the HLAC-HK design. The resistance at 45 kt is a bit lower than initially estimated (29.8 kN vs. 30.4 kN). Nevertheless, this does not change the dimensioning of the propulsion system. Plotting the maximum thrust that can be derived from a NR-series propeller (Section 4.5.3) for a given torque results in the thrust curves of Fig. 4.18. Thrust values that are a result of extrapolation are indicated with the dotted

line. The delivered torque characteristic of a diesel engine is often assumed as a constant (Klein Woud & Stapersma, 2002). However, this assumption paints a bleak picture for the thrust produced in the hump region. It is generally recommended to maintain a thrust margin of 20%-25% in the hump region to ensure take-off under rough sea state (Faltinsen, 2005; Johnston, 1985). Although there is still a significant thrust margin, the thrust curve falls just short of this target and risks to be too low for this design.

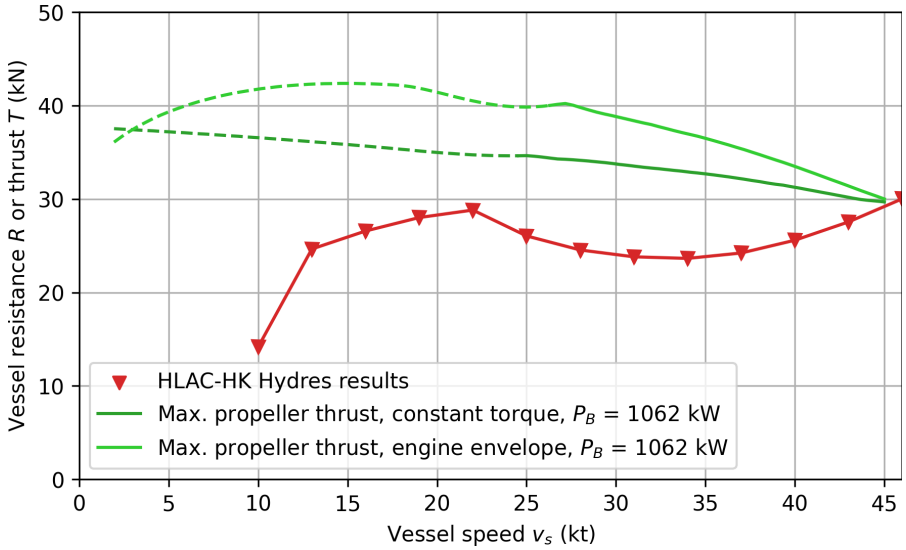

Figure 4.18: Resistance and thrust curves for the HLAC-HK design

Further investigation of the high-speed engine types used in high-speed craft, showed that these engines can provide relatively more torque at a moderate engine speed (Scania, 2025; Volvo Penta, 2025). This is illustrated in the engine envelope of Fig. 4.19, where up to 20% additional torque can be produced at lower engine speed. The torque and power envelope depends on the type and tuning of the engine. To illustrate the difference this can make, an additional thrust characteristic is plotted in Fig. 4.18 based on engine envelope. For each advance velocity, the maximum propeller thrust is assessed by deriving the maximum shaft torque produced by the engine, following the engine envelope of Fig. 4.19. This engine envelope is deemed representative of all engines assessed in this thesis, however additional care should be taken in the definitive choice for an engine installation. With the thrust curve derived from the engine envelope, ample thrust margin is found for the hump region. This is also advantageous for planing craft, as they can utilise more torque in the transition to planing mode.

If the thrust at the hump region would still not suffice, there are other methods to increase thrust. For example, by integrating Controllable Pitch Propellers (CPP) (Martens, 2025) or a two-speed gearbox matched for this torque requirement (McKesson, 2014).

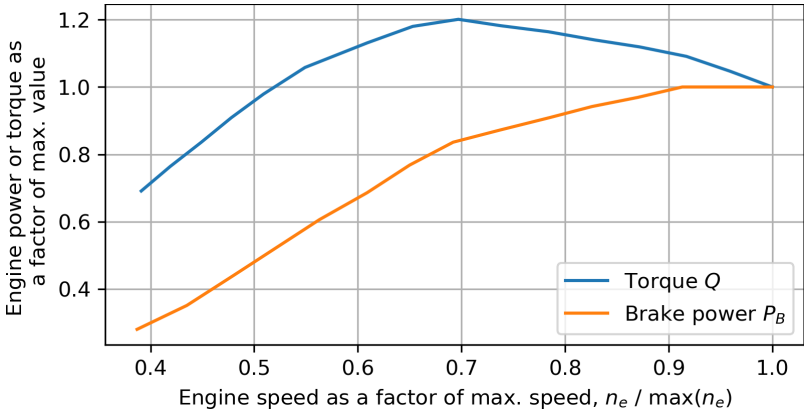

Figure 4.19: Engine envelope of the Scania DI16 076M 900 HP engine, adopted from technical specifications (Scania, 2024a)

4.8.2. Dynamic equilibrium of a diesel-electric design (HLAC-DE)

Fig. 4.20 shows the thrust and resistance curve of the HLAC-DE design. The resistance at 45 kt is somewhat higher than initially estimated (28.4 vs. 27.2 kN), but this does not change the weight estimation. If the propulsive power of this design is dimensioned for the minimum installed generative power, the thrust in the hump region is critically low. This is illustrated with the 'constant torque' assumption in Fig. 4.20. However, electric motors generally have the capability to produce additional 'peak power' for short periods of time. As seen in Appendix G, axial flux motors can produce peak powers higher than two times the nominal power. The period that this peak power can be delivered is short however, and depends on the cooling capacity of the integrated electric motor. Quoted peak power durations are between 10 and 60 seconds (Phi-Power, 2025). Research on boosting methods has shown that, with sufficient thrust margin, a period of 10 seconds is sufficient to provide enough thrust for take-off (Minerva & Montero, 2021).

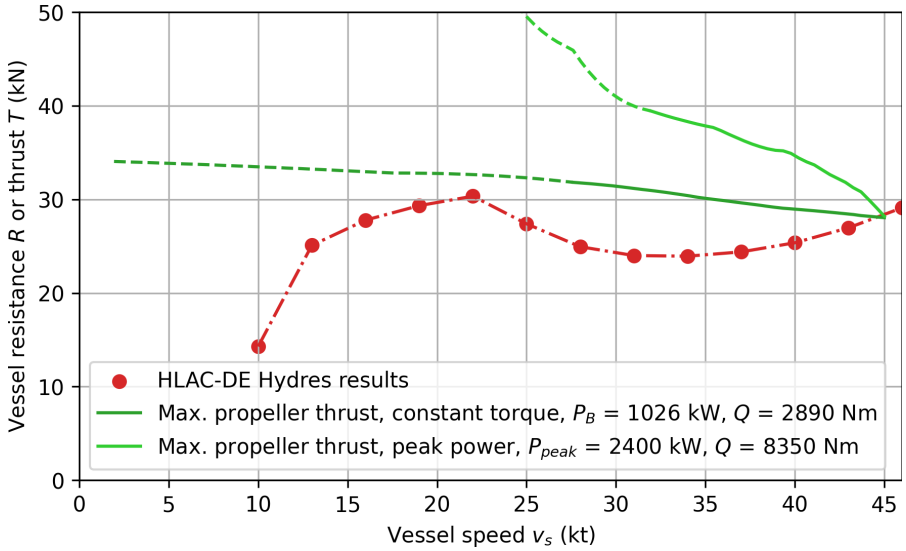

Figure 4.20: Resistance and thrust curves for the HLAC-DE design

The peak power of Fig. 4.20 is based on the specifications of 6 Emrax 348 axial flux motors, which can deliver a combined peak power of 2400 kW. The installed generator power cannot deliver this amount of power of course. However, the determining factor at the hump region is the peak torque, rather than the peak power. As the generator power and propulsion power are decoupled in their shaft revolutions, the maximum power can be provided for each electric motor speed. As a result, the provided maximum thrust can be simplified to Eq. (4.12). With the proposed installed generator power (See Table 4.7), enough power is generated to advance through the hump region up to 54 kN, which vastly exceeds the requirement. Thus, no additional power delivery is required.

$$T = \frac{P_B \cdot \eta_{trm} \cdot \eta_o}{v_s} = \frac{1030 \cdot 0.88 \cdot 0.70}{23 \cdot \frac{1852}{3600}} = 54 \text{ kN} \tag{4.12}$$

4.9. Resistance and range comparison

Fig. 4.21 compares the different designs developed in this chapter on their calm water resistance development. Both hydrofoil designs have a higher resistance curve than was previously seen in Fig. 4.14. For the HLAC-HK this is caused by the added appendage drag of an inclined shaft, whereas the HLAC-DE design increases its resistance due to a heavier propulsion system. These different types of drag increase also result in a differing resistance characteristic: the HLAC-DE resistance has a higher hump region resistance, whereas the HLAC-HK has a higher top speed resistance. For both hydrofoil designs, there is a region from 27 kt to 40 kt where the resistance is substantially lower than the planing benchmark. The planing CB90 has a resistance around 38 kN, whereas the hydrofoil designs have a resistance around 25 kN. This is a drag reduction of approximately 35%.

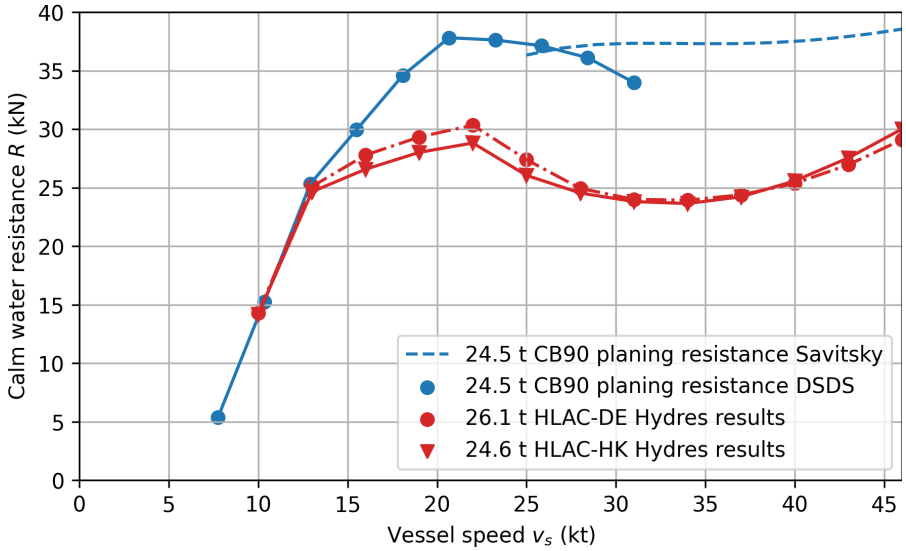

Figure 4.21: Resistance development of different designs

Based on the derived resistance, the Overall Propulsive Coefficient (OPC), and the Specific Fuel Consumption (sfc), the range of each vessel is evaluated. The OPC is the product of transmission and propulsive efficiency, as defined by Eq. (4.13). The conventional range equation is defined by Eq. (4.14), where L and D denote the total lift (weight) and drag of the vessel at a given speed (McKesson, 2014). The factor of $198 \cdot 10^3$ captures the conversion of m/s to kt, g per kg. and the division by gravitational acceleration ($3600/1852 \cdot 1000/9.81 = 198 \cdot 10^3$). However, this formulation assumes constant displacement, meaning that resistance and power remain unchanged even as fuel is consumed during sailing. This assumption can misrepresent the range of long-range advanced marine vehicles. The Breguet formula (Eq. (4.15)) introduces a logarithmic term, to reflect the vessel's weight reduction as fuel is burned. Instead of assuming constant displacement, this equation assumes constant L/D (McKesson, 2014).

To analyse the relation between speed and energy consumption, also the transport efficiency can be evaluated (Trancossi, 2016). First defined by Gabrielli and von Karman (1950), the analysis introduces a physical parameter, named specific resistance (ϵ) of the vehicle. It represents the ratio between the required power divided by the total vehicle weight times its speed. This can also be defined for a payload weight, as in Eq. (4.16). The inverse of specific resistance represents the transport efficiency.

$$OPC = \eta_{trm} \cdot \eta_D \tag{4.13}$$

$$\frac{m_{fuel}}{\Delta} \cdot 198 \cdot 10^3 \cdot OPC \cdot \frac{L}{D} \cdot \frac{1}{sfc} \tag{4.14}$$

$$-\ln\left(1 - \frac{m_{fuel}}{\Delta}\right) \cdot 198 \cdot 10^3 \cdot OPC \cdot \frac{L}{D} \cdot \frac{1}{sfc} \tag{4.15}$$

$$\epsilon_{payload} = \frac{P}{m_{payload} \cdot g \cdot v_s} \tag{4.16}$$

Table 4.9 lists performance characteristics of the designs introduced in this chapter. it is assumed that the sfc is a constant for each design. Both hydrofoil designs can increase the range of the vessel with around 50% in calm water. Furthermore, the difference between Breguet range and a constant displacement estimate is small, with only a 10 to 20 nm gain in range. This can indicate that the vessel is relatively heavy in other aspects than fuel. Additionally, the payload transport efficiency is increased with aproximately 45% for cruising speed and 30% for top speed.

It should be noted that these results are still only considering calm water estimates. As the vessels are intended for use in further offshore areas, operating in waves will start to play a larger role. This can result in the craft experiencing added resistance in waves or having to reduce to less than ideal speed to ensure safe operation. It is expected that the hydrofoil designs will excel in this circumstance,

as added resistance in waves is minimal or even negative (Godø et al., 2024a) for hydrofoil designs. Further elaboration on this aspect is provided in Chapter 5.

Both hydrofoil designs show similar performance characteristics. However, the HLAC-DE design has a higher L/D characteristic. It is therefore expected that, if weight saving measures are applied, the gains in resistance reduction will be larger for the HLAC-DE design. The HLAC-HK will keep approximately the same appendage drag due to the inclined shafts, whereas the HLAC-DE design's nacelle drag will remain relatively small. Additionally, the HLAC-HK design will have worse seakeeping performance due to the inclined shaft's interaction with the waves. Thus, the HLAC-DE design is taken for further investigation.

Table 4.9: Performance characteristics of hydrofoil designs compared to the planing benchmark design

Design	CB90	HLAC-HK	HLAC-DE
Displacement weight Δ (t)	24.5	24.6	26.1
OPC @ 45 kt (-)	0.68	0.66	0.64
OPC @ 30 kt (-)	0.68	0.64	0.62
sfc (g/kWh)	205	205	205
L (kN)	240	241	256
D @ 30 kt (kN)	37.5	24.5	24.5
L/D @ 30 kt (-)	6.4	9.8	10.4
P_{cruise} @ 30 kt (kW)	850	590	610
P_{req} @ 45 kt (kW)	1320	1090	1030
Constant displacement range @ 30 kt (10% fuel reserve) (nm)	295	440	430
Breguet range @ 30 kt (10% fuel reserve) (nm)	310	460	440
1/$\epsilon_{payload}$ @ 30 kt (-)	0.80	1.15	1.12
1/$\epsilon_{payload}$ @ 45 kt (-)	0.77	0.94	0.99

4.10. Weight saving measures

As the design of hydrofoil craft follows the square-cube relationship for its hydrofoil design compared to displacement, it is of interest how a design is affected by applying weight saving measures (McKesson, 2014). Therefore, this section will propose multiple methods to reduce weight of the hydrofoil craft design. It is expected that the required hydrofoil planform area and camber will reduce, which increases the L/D of the complete design. Moreover, the displacement reduction will give rise to the secondary effect of the reducing the propulsion system and hydrofoil system weight.

4.10.1. Composite materials

The weight reduction of marine applications by applying composite materials is of interest in enabling sustainable vessel designs due to the potential for range-extension and energy consumption reduction (Doornebos, 2022; Francis, 2019; Stenius et al., 2011). Composites can also offer advantages in naval applications due to their ballistic protection and signature reducing capabilities (Mouritz et al., 2001). Moreover, depending on the application they can simplify series production (Mathijsen, 2016). A composite consists of two or more distinct materials that, when combined, offer enhanced properties that none of the individual components can achieve on their own (Reddy, 2003). Composite structures in maritime applications are mostly Fibre Reinforced Polymers (FRP), of which the most common types are glass and carbon (Hertzberg, 2009). In addition, aramids are also a known fibre used in ship building (Daniel & Ishai, 2006). Of these three types, Glass Fibre Reinforced Polymer (GFRP) has the lowest specific strength and stiffness, but is generally the lowest costing FRP option (Daniel & Ishai, 2006). Aramid Fibre Reinforced Polymer (AFRP) is the toughest FRP type and has better fatigue resistance, making them ideal for use as ballistic protection such as kevlar. Aramids have a specific strength similar to carbon composites, but a lower stiffness. Lastly, Carbon Fibre Reinforced Polymer (CFRP) has the best specific strength and stiffness, but is also generally the most costly.

In FRPs the fibres are the principal load-carrying member and a matrix material keeps the fibres together in its intended shape. The matrix material acts as a load-transfer medium between the fibres,

and protects fibres from being exposed to the environment (Reddy, 2003). In FRPs the matrix is a polymer, which is typically a type of resin. Moreover, composites are naturally anisotropic materials. Fibre orientation and the stacking of the layers define the strength and stiffness of the material in each direction. To increase the bending stiffness, a sandwich structure with a lightweight core material can be used (Daniel & Ishai, 2006). The load-bearing laminate sheets are then moved from the neutral axis, without a large increase to the weight of the material.

Stenius et al. (2011) assessed the weight reduction of a 24 m monohull patrol craft by converting aluminium hull structure to GFRP and CFRP concepts, the results of which are presented in Table 4.10. The designs use vinylester as the resin and optionally a Divinycell PVC foam core. The CRFP design decreases the hull weight with around 50%, whereas GFRP can realise a reduction of around 20%, when compared to aluminium. A weight reduction of approximately 50% by applying carbon composites is in accordance with other research for monohull applications under 30 meters in length (Oh et al., 2018; Olofsson et al., 2008), and the same reduction can be observed for catamaran designs (Gurit, 2015).

Table 4.10: Structural weights of a 24 m high-speed monohull patrol craft of Stenius et al. (2011)

Material concepts	Structural mass (t)	Structural mass normalised (-)
Sandwich: Carbon/Vinylester/Divinycell	4.4	0.51
Sandwich: E-glass/Vinylester/Divinycell	6.9	0.79
Single-skin: Carbon/Vinylester	4.6	0.53
Single-skin: E-glass/Vinylester	7.7	0.89
Standard marine aluminium: NV-5083	8.7	1.00

Aside from structural weight, the use of composites affects insulation requirements (Hertzberg, 2009). Maritime composites generally require more fire insulation but less acoustic and thermal insulation. For preliminary design considerations, these weight changes tend to balance out to negligible impact (Gurit, 2015).

Applying composites can have some additional benefits. First of all, the underwater magnetic signature of a vessel made of composites is lower than aluminium (Mathijsen, 2016). Due to its lower heat conductivity, it can also lower the infra-red signature (Hertzberg, 2009). Secondly, composites offer higher corrosion resistance and fatigue life which results to less maintenance costs (Gurit, 2015; Olofsson et al., 2008). On the contrary, one drawback of FRP composites is that they are difficult or even impossible to recycle (Burman et al., 2016).

As a weight saving measure, a CFRP hull structure is further investigated. This composite material can offer the biggest weight saving potential, and is already applied in maritime constructions.

4.10.2. Reducing system capabilities

By reducing the system capabilities of a HLAC design, other performance characteristics may be increased. Therefore, some additional options for weight reduction are presented.

Firstly, although increasing the range from around 300 to 450 nm is a significant benefit to hydrofoil craft, it is also of interest to see how the design spiral will converge for the same range requirement. The vessel can be designed for a range of 300 nm, but have a feature to fill an additional fuel tank when this would be required for example.

Secondly, the outfitting weight is a substantial weight fraction of the complete design. For the hydrofoil and planing craft designs, around 30% of the displacement is devoted to the outfitting weight. It is difficult to pinpoint where most of this weight results from as this information is not publicly available. Substantial amounts of weight can be assigned to ballistic protection, sensors, armaments or other onboard systems for example. An arbitrary weight reduction of 30% of this weight factor is taken to give an indication of how the hydrofoil design is affected by reducing outfitting weight.

Thirdly, the payload specified by the NLMOD (see Appendix A) may be overstated. With 4500 kg allocated for 16 EMF and 3 operators, this equates to approximately 240 kg per individual. A more realistic estimate can be 150 kg per person, accounting for body weight and gear. This adjustment reduces the total payload weight with 1650 kg to 2850 kg.

4.10.3. Implementation of weight saving measures

Table 4.11 summarises the weight saving measures that can be implemented for a HLAC-DE design. The outfitting weight is the largest weight fraction of the design where weight can be saved. However, the hull structure can achieve the biggest relative reduction in weight due to applying composite materials.

Table 4.11: Weight saving measures identified for a hydrofoil LAC, based on the HLAC-DE design

Measure	A. CFRP composite hull	B. Constant range (300 nm)	C. Reduced outfitting	D. Reduced payload
Original weight (kg)	5200	1980	7280	4500
Original weight fraction	20%	8%	30%	18%
Weight saving within weight fraction	50%	Design dependent	30%	36%

Table 4.12 lists the different designs with weight saving options taken into account. Each design is given an indicator which stands for the measures taken in the design preceded by "M" for measure. This means that a design M.ABCD has all measures taken into account. The iterative weight modelling is performed again as outlined for Part I (parametric model) of this chapter, while the definitive resistance curves are derived from Part II (Hydres). The discrepancy between the two methods was within 5% of the resistance value, which resulted in minimal adjustment of the propulsion system.

In addition to the direct weight savings that can be gathered from implementing these measures, the indirect weight saving of the propulsion and foil system are presented in Table 4.12. The weight reduction due to the minimisation of the foil system is minimal however, as the weight of the foil system itself is already relatively small. The M.ABCD design realises a weight reduction of the foil system of 590 kg, which is almost half its original weight, but also only around 3% of the total weight.

The weight of the propulsion system is heavily dependent on the weight of the prime mover. As the parametric model chooses the lowest weight option for the power requirement of the dataset of Appendix G, there exists a mismatch between the required power (P_{req}) and the chosen prime mover power (P_{prime}). There appears to be a gap of prime movers between 537 kW and 459 kW, which results in the M.B variant to have the same engine power as the original HLAC-DE design. The same can be seen for the M.AC, M.ABC, and M.ACD variants, which occupy the same 374 kW Volvo D8-510 engines.

By reducing the fuel weight to a range of 300 nm (M.B), the total weight saving already brings the total displacement back to around the CB90's weight of 24.5 t. This also reduces the dimensions of the hull to its original size. The relatively high indirect weight saving is realised by the lower power requirement, which enables a reduction in the amount of stacked axial flux propulsion motors from three to two, for each propulsion line. Overall, the indirect weight saving is within 30% to 40% of the direct weight saving amount.

Table 4.12: Estimated weight fractions for different implementations of weight saving measures on the HLAC-DE design

	HLAC-DE	M.B	M.A	M.AB	M.AC	M.ABC	M.ACD	M.ABCD
$m_{payload}$ (kg)	4,500	4,500	4,500	4,500	4,500	4,500	2,850	2,850
m_{fuel} (kg)	1,980	1,180	1,980	980	1,980	800	1,980	730
m_{lub} (kg)	80	80	80	80	80	80	80	80
m_{hull} (kg)	5,200	4,970	2,480	2,480	2,480	2,480	2,480	2,480
m_{outfit} (kg)	7,280	7,280	7,280	7,280	5,100	5,100	5,100	5,100
$m_{foilsystem}$ (kg)	1,280	1,210	1,080	970	880	830	780	690
$m_{propul.}$ (kg)	5,800	5,550	5,160	4,560	4,540	4,260	4,090	3,930
Δ (kg)	26,140	24,770	22,560	20,850	19,560	18,050	17,360	15,860
Direct weight saving (kg)	0	800	2,720	3,720	4,900	6,080	6,550	7,800
Indirect weight saving (kg)	0	570	860	1,570	1,680	2,010	2,230	2,480
P_{req} (kW)	1,030	960	845	790	730	700	660	610
P_{prime} (kW)	1,074	1,074	918	810	748	748	748	634

The resulting resistance curves of applying weight saving measures are plotted in Fig. 4.22. The hump resistance decreases proportionally to the decrease in foiling resistance, where the foiling top speed resistance has approximately the same magnitude as the maximum hump resistance.

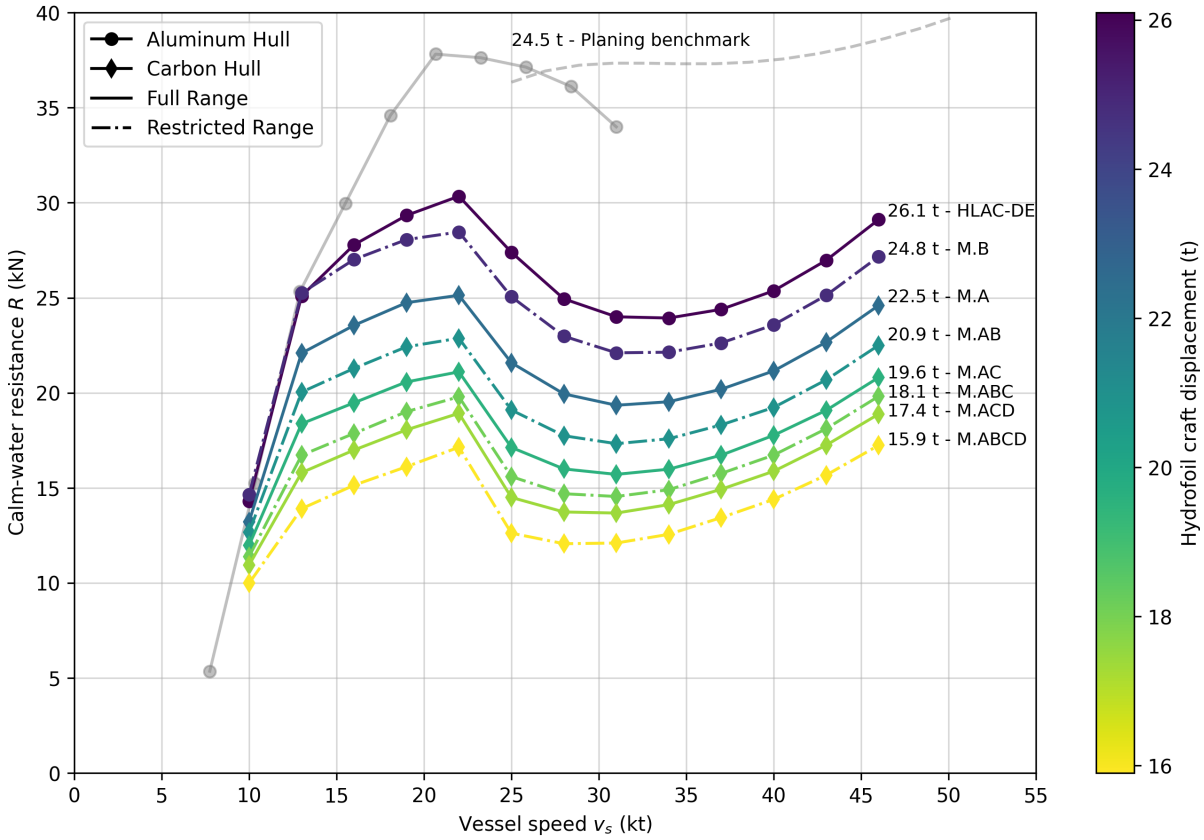

Figure 4.22: Several HLAC-DE designs with weight saving measures

Table 4.13: Development of performance characteristics for different weight saving measures

	HLAC-DE	M.B	M.A	M.AB	M.AC	M.ABC	M.ACD	M.ABCD
L (kN)	256	243	221	205	192	177	170	156
D (kN) @ 30 kt	24.5	22.1	19.4	17.4	15.8	14.6	13.7	12.1
L/D @ 30 kt	10.4	11.0	11.4	11.8	12.1	12.2	12.4	12.9
Breguet range @ 30 kt (10% fuel reserve) (nm)	440	300	560	300	695	300	805	300
$1/\epsilon_{payload}$ @ 45 kt (-)	0.99	1.06	1.21	1.29	1.40	1.46	0.98	1.06

Table 4.13 shows additional performance characteristics for the hydrofoil designs with weight saving measures. By enabling all weight saving measures but maintaining the fuel capacity, the range can be further extended to 800 nm. This far exceeds any requirement of the NLMOD, but exemplifies the energy efficiency of this option. Reducing fuel capacity instead, can also be used to effectively reduce the propulsion system requirements. Overall, the range requirement shows to have a significant effect on the resulting hydrofoil craft design.

As expected, the L/D increases as the weight of the vessels is reduced. This means that the resistance does not reduce linearly for a lower displacement, but has an exponential factor. Therefore, the resistance for different displacements at 30 kt can be illustrated as in Fig. 4.23a, with an exponential fit. Furthermore, this can be reasoned backwards to the direct weight saving that is realised. Fig. 4.23b shows how the direct weight saving of Table 4.12 affects the resistance reduction. This follows an inverse exponential relation, meaning that the largest reductions in resistance can be found for the lowest reductions in weight. As an example, 5% in direct weight reduction already accounts for a 12%

reduction in resistance. However, for the highest weight reduction of 30%, the resistance is reduced with 50%.

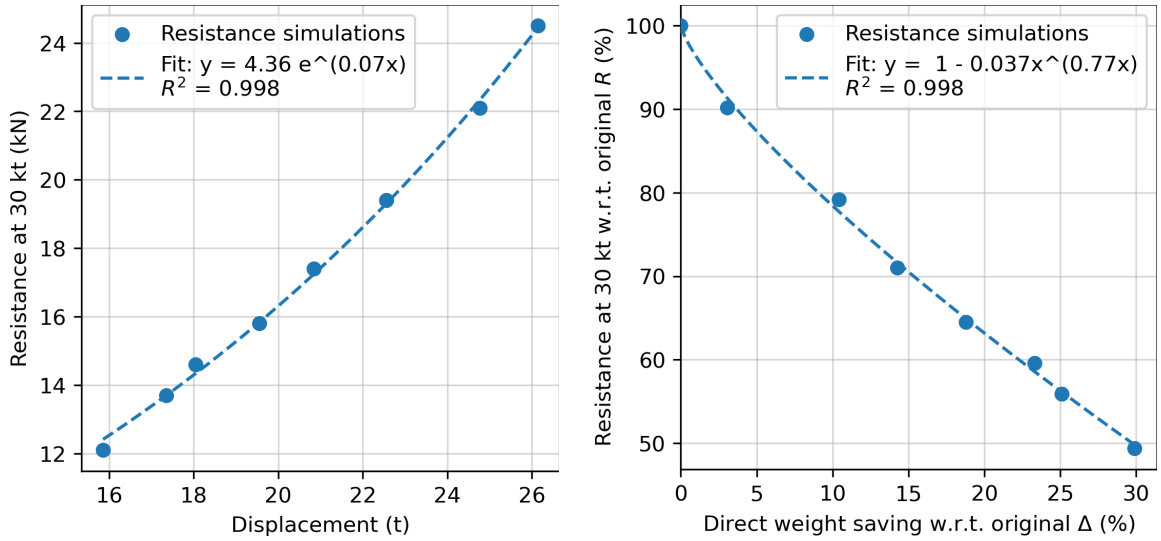

(a) Resistance for different displacements

(b) Direct weight saving effect for the HLAC-DE design

Figure 4.23: Impact of weight saving measures

4.11. Concluding insights

This chapter discussed the design methodology to develop a preliminary design of a hydrofoil LAC, from which the range and other performance indicators can be derived. First, an iterative parametric model is used to provide an initial displacement estimate and their relevant dimensions in length, beam and draught (Part I). For the design of the foils, the Foil Design JIP tool of MARIN is employed. After this first step, the program Hydres can be used to assess the dynamic equilibrium of the design (Part II). Hydres can be used to investigate the hump region in respect to resistance, but also ensures that a dynamic equilibrium can be attained with the designed hydrofoils. During the entire procedure, two types of propulsion systems were evaluated, an inclined shaft system (HLAC-HK) and an L-drive system (HLAC-DE). For propeller characteristics, the transcavitating Newton-Rader series is applied. Both propulsion systems have the capacity to transition through the hump region without additional power requirements. However, both configurations have drawbacks that result in a higher resistance. The HLAC-HK design has additional appendage drag due to the inclined shaft, and the HLAC-DE design has increased resistance due to a heavier propulsion system compared to the HLAC-HK design. Nonetheless, the resistance compared to the planing benchmark vessel, with the same payload carrying capacity, can be up to 35%. This leads to the first MoE of the implementation of hydrofoils, as they can realise a range increase of approximately 50% at 30 kt. This answers the following research question:

RQ1: How do retractable hydrofoil systems affect the weight, resistance, and range potential of a future Littoral Assault Craft (LAC) design?

In addition, the effect of weight saving measures on the hydrofoil craft design was evaluated. The analysis revealed an inversely exponential relationship between weight reduction and resistance, highlighting the value of weight saving efforts.

The assessment also demonstrated that the calculations with the Foil Design JIP tool showed satisfactory results for the complete foiling craft resistance. This conclusion is of particular interest to MARIN and serves as an example of the potential of this tool. Therefore, during the development of this methodology the following additional conclusion was found:

Results of a novel preliminary T-foil design tool can be used to derive a satisfactory complete craft foiling resistance in a preliminary design

5

Seakeeping performance

This chapter presents the seakeeping assessment of a hydrofoil craft compared to a planing craft in a sea state that is relevant to the operations of an LAC. First, Section 5.1 provides theoretical insight regarding seakeeping assessment of high-speed craft. This is followed by Section 5.2, where a sea condition is presented for seakeeping assessment, considering the operational profile of an LAC. To continue, Section 5.3 will elaborate on how the seakeeping assessment was performed using Panship. To conclude, Section 5.4 will provide concluding insights to the research question posed in this chapter:

RQ2: How can hydrofoil systems increase the operational effectiveness of a Littoral Assault Craft (LAC) design in waves, considering speed and safety of the crew?

5.1. Seakeeping theory

In seakeeping assessment of large ships, its motion response is often linearised. This simplifies calculations and allows for a frequency domain methodology to be applied (Journee et al., 2015). In linear theory, vessel responses can be derived using a combination of Response Amplitude Operators (RAO's) and a sea spectrum to gain the response spectrum in irregular waves. Results of these calculations are the standard deviation (also called the Root Mean Square) and the significant value of the accelerations aboard a ship. These averaged statistical measures are used in operability limitation criteria such as NORDFORSK (1987).

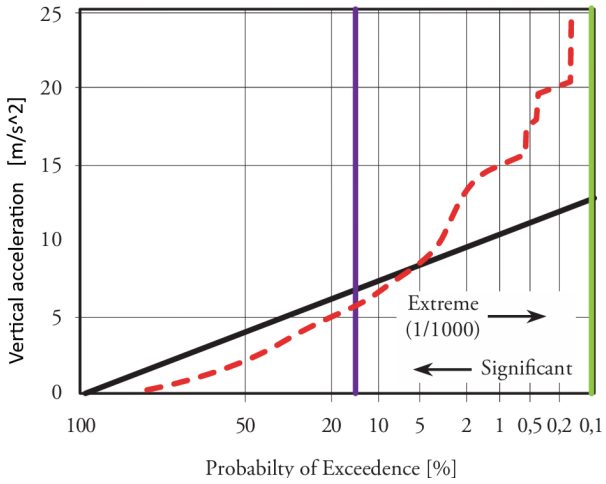

Figure 5.1: Distribution of peaks and throughs of a vertical acceleration signal, adapted from Keuning & Gelling (2011)

However, most high speed craft exhibit non-linear behaviour in waves. This non-linearity originates from various sources and depends on the type of craft under consideration. Typical sources of non-linearity are the change of reference position due to sinkage and trim, the high forward speed and

the large relative motions (Keuning, 1997). When assessing the seakeeping of high-speed design concepts, these non-linearities need to be incorporated to gain accurate estimates. Keuning (1994) identified the peak value of vertical accelerations as the limiting factor of high-speed craft operations, which cannot be drawn out of standard deviations directly. Keuning (1994) also notes that most professional crews respond similarly to acceleration peaks, which are in most instances caused by slamming loads. When experiencing a peak value of approximately 1.25 g (g = 9.81 m/s^2) of vertical acceleration, crews decrease their speed to reduce physical strain and prevent injury. This behaviour is also evident in measurements from pilot boats (Cauwenberghe, 2025) and search and rescue craft (Deyzen, 2013). Van Deyzen (2013) concluded on full scale trial data that the repeated occurrence up to 1 g of vertical acceleration was acceptable for the crew. However, vertical accelerations up to 15 g were recorded for the FRISC (Margés, 2018), though these conditions did not last longer than five minutes. Additionally, vertical accelerations can partly be mitigated by shock-absorbing seats, which decrease the experienced accelerations up to 50% (Marshall & Riley, 2020). Since the transit distance for personnel using a future LAC is 40 nm, leading to a transit duration of over an hour, Keuning's (1997) recommended peak acceleration of 1.25 g is taken as a reference.

To determine these peak acceleration values, the RAO's applied in linear theory do not suffice, necessitating a time domain simulation. As an example, the probability of acceleration exceedance in a time domain simulation can be visualised in a Rayleigh plot, as shown in Fig. 5.1. Since a wave spectrum follows a Rayleigh distribution, deviations of accelerations from the Rayleigh plot (the black line) indicate nonlinear responses to incoming waves. In the case presented here, a distribution according to the Rayleigh distribution may be preferred to the red line to improve operability, even though this would mean a higher significant value for vertical accelerations (Gelling & Keuning, 2011).

Table 5.1: Scatter diagram of sea states at the Gemini wind park (Brans, 2021)

Gemini	Significant wave height (Hs)														
Peak period (Tp)	0.0	0.5	1.0	1.5	2.0	2.5	3.0	3.5	4.0	4.5	5.0	5.5	6.0	6.5	Sum
0.0	35	24													59
0.5	9	26													35
1.0	19	23													42
1.5	11	18													29
2.0	11	58													69
2.5	13	68	1												82
3.0	45	691	20												756
3.5	820	2941	223												3984
4.0	822	4331	3522	18											8693
4.5	465	3061	6000	838											10364
5.0	251	3456	6756	3053	154										13670
5.5	206	3665	5775	5477	866	33									16022
6.0	168	2405	5057	5822	2979	274	4								16709
6.5	97	1650	4262	5305	5120	1224	67								17725
7.0	97	1115	3299	4403	4637	2784	284	8							16627
7.5	76	791	2318	2760	3671	3742	1433	138	1						14930
8.0	155	946	1964	2640	2817	3902	3778	1066	115	2					17385
8.5	105	836	1504	2127	2126	1875	2160	2173	407	24	2				13339
9.0	92	525	786	1009	1044	916	1014	1281	1183	268	17	2			8137
9.5	130	654	1159	1024	1020	930	807	877	834	607	161	15		1	8219
10.0	54	231	597	436	340	279	307	382	425	319	179	64	7		3620
10.5	110	285	832	576	289	256	231	226	249	309	258	196	67	4	3888
11.0	38	112	264	209	140	94	120	78	100	102	116	56	16	8	1453
11.5	98	140	263	376	153	143	83	74	74	94	124	97	43	15	1777
12.0	42	49	85	84	46	49	38	12	20	12	19	13	9	6	484
12.5	36	59	115	125	72	38	40	38	43	26	12	14	12	9	639
13.0	20	18	62	45	51	17	15	25	9	10	11	5	4	7	299
13.5	7	17	34	21	36	16	5	10	13	14	4	8	4	4	193
14.0	11	25	48	24	55	52	2	5	2	6	5	6	7	5	253
14.5	3	9	20	3	4	6		1	5		2				53
15.0	5	6	12	5	9	13	5	5	9	6	2	1	3		81
Sum	4051	28235	44978	36380	25629	16643	10393	6399	3489	1799	912	477	172	59	179616

No data here because waves break due to steepness

5.2. Expected sea conditions

As mentioned in Chapter 2, a potential LAC design will need to extend its distance from shore to 40 nm, with the possibility of further increases in the future. To gain an understanding of sea conditions at this distance, data from the Gemini wind park is utilised. This wind park is situated 45 nm from the coast of the Netherlands (Gemini, 2024). Table 5.1 presents a scatter diagram of the sea states found in the Gemini wind park. Knowing that the LAC has to remain fully operational in sea state 3, the craft must sustain a maximum significant wave height ($H_{1/3}$) of 1.25 m. From Table 5.1, it can be derived that the most probable peak period (T_p) for this wave height is between 6.0 and 5.5 seconds. Based on this finding, the peak period for seakeeping assessment is taken as 5.75 seconds.

The Joint North Sea Wave Project (JONSWAP) wave spectrum provides an accurate statistical representation of the sea states typical in the North Sea (Journee et al., 2015). Using this wave spectrum, the complete sea state is described as in Table 5.2. Furthermore, the wave direction is taken as 180°. This means that the vessel will experience head waves, which is most relevant in assessing vertical accelerations of the planing vessel and for the hydrofoil vessel in its ability to react to incoming waves (Gelling & Keuning, 2011).

Table 5.2: Sea state considered for seakeeping analysis

	Significant wave height	Peak period	Mean centroid wave period	Mean zero-crossing wave period	Peakedness factor	Wave direction	Vessel speed
Symbol	$H_{1/3}$	T_p	T_1	T_2	γ	μ	v_s
Value	1.25 m	5.75 s	4.79 s	4.43 s	3.3	180°	35 kt

5.3. Modelling in PanShip

Panship, a program developed by MARIN, is a method for evaluating high-speed craft motions in a time domain simulation. It employs a time domain panel method based on the transient free surface Green function to incorporate wave-making effects (van Walree, 2015). The free-surface conditions are linearised around the mean free surface, enabling the hydrodynamic problem to be solved using panels only on the ship's surface. As a potential flow method, it assumes the flow to be incompressible, inviscid, and therefore irrotational. Van Walree (2002) provides an extensive description of the numerical methodology. PanShip exists in two versions: a semi-linear (PanShip) and a semi-nonlinear version (PanShipNL). The key distinction between the two lies in the computation of the hydrodynamic solution. PanShip uses the mean wetted body surface at speed for radiation and diffraction forces, while using the instantaneous wetted body surface for the undisturbed wave forces. This approach is numerically efficient as the most computationally demanding tasks are performed only once. In contrast, PanShipNL uses the instantaneous wetted surface for all hydrodynamic forces, providing greater accuracy. This improved accuracy is essential for capturing impulsive wave loads and accelerations, making PanShipNL the preferred method for planing craft. Together, PanShip and PanShipNL are validated for the prediction of resistance, manoeuvring, motions and loads in waves and dynamic stability in stern quartering seas (Turner & van Walree, 2015; van Walree & Carette, 2011).

The simulation in PanShip is conducted with expert support from the software's developer, Frans van Walree, who modelled the two cases within PanShip. This ensures that the study provides accurate results within its time constraints. The input of the planing hull and hydrofoil design, wave conditions, and subsequent analysis are provided by the author.

5.3.1. Hydrofoil and planing hull design

Fig. 5.2a illustrates the planing benchmark hull used for seakeeping assessment. This hull design is based on the CB90 hull form and features a flat bow, representing the bow hatch. Although inspired by the CB90, this design is an independent creation, and no direct conclusions should be drawn about the CB90 itself. The design features a deadrise angle (β) of 20° and a hard chine. Fig. 5.2a also shows the dynamic pressure (C_{pu}) that can occur in waves for this hull in the prescribed sea state of Section 5.2. The substantial dynamic pressure at the bow hatch indicates that this can be a source for slamming forces.

In a test run at full displacement (Δ = 24.5 t), unrealistically high forces were excited on the vessel due to bow diving. Because of this, the displacement is reduced to 21.0 t, which allows the vessel to remain mostly in planing mode in this dynamic condition.

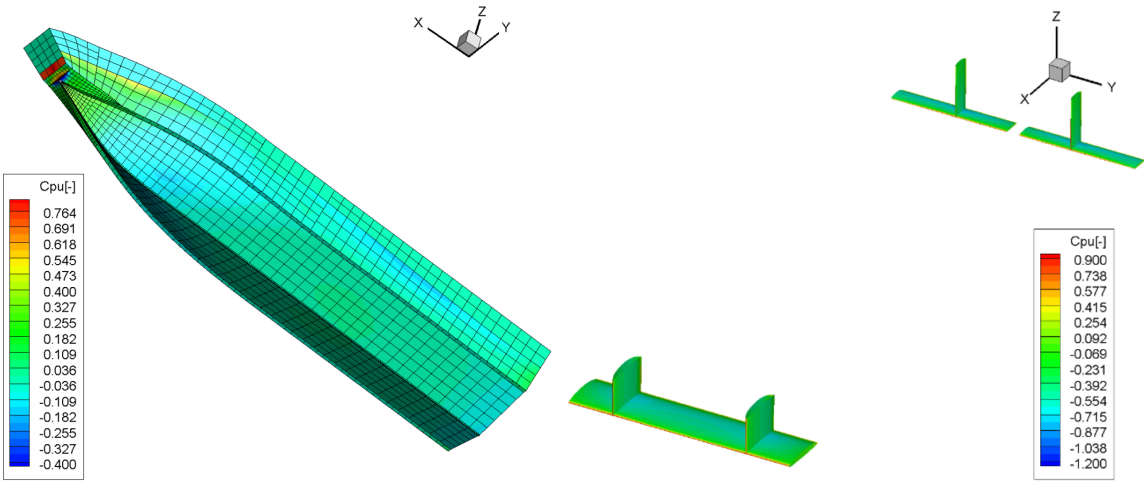

(a) Planing hull (PanShipNL) **(b)** Hydrofoil design (PanShip)

Figure 5.2: Vessels modelled in Panship

Fig. 5.2b visualises how the hydrofoil design is modelled in PanShip. The geometry is based on the Hydres output of the example hydrofoil design of Section 4.6. This is the design for a 24.5 t hydrofoil craft, without additional considerations for added weight of the propulsion or hydrofoil system. Additionally, no nacelles or other appendages are modelled.

The motion control of the vessel is realised by a flap motion control system. It utilises a PID-controller with gains based on experience of van Walree (2025). The vessel remains in platforming mode for this condition, meaning that the vessel sails above the waves, as opposed to riding along the waves in a contouring mode (Faltinsen, 2005). The difference between a contouring and platforming control strategy is illustrated in Fig. 5.3. Contouring is generally employed when the wave encounter frequency is low, whereas a platforming mode is applied for a high wave encounter frequency (Faltinsen, 2005). Active foil control not only stabilises the vessel, but can also effectively reduce heave motions (Saito et al., 1991).

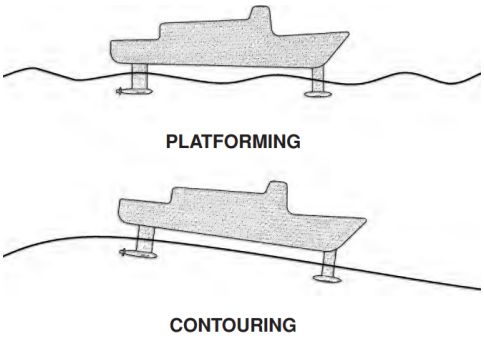

Figure 5.3: Platforming and contouring active foil control modes (Faltinsen, 2005)

Another test simulation indicated that the foil submergence was too low for this design, which resulted in foil ventilation in wave troughs. Therefore, the foil submergence was increased with an additional 0.35 m.

The final simulation is conducted as a run of 15000 time steps of 0.030 s. This results in a total simulation time of 450 s. The planing hull uses the PanShipNL method, whereas the hydrofoil design uses the PanShip version. As the wetted surface-area of the hydrofoil design does not change significantly in waves, the semi-linear PanShip method is considered as an accurate simulation.

5.3.2. Wave induced motions

Fig. 5.4 presents the motions at the Centre of Gravity (CoG) of the planing craft in the sea state described by Section 5.2. The heave (z) presented here is the earth-fixed axis system in reference to an undisturbed water surface, whereas the pitch (θ) is in the ship-fixed frame. It can be concluded from Fig. 5.4 that there are some heavy movements occurring for the planing hull. Pitch can reach values of around 15° and the vessel heaves to values of 4 m above the undisturbed water surface.

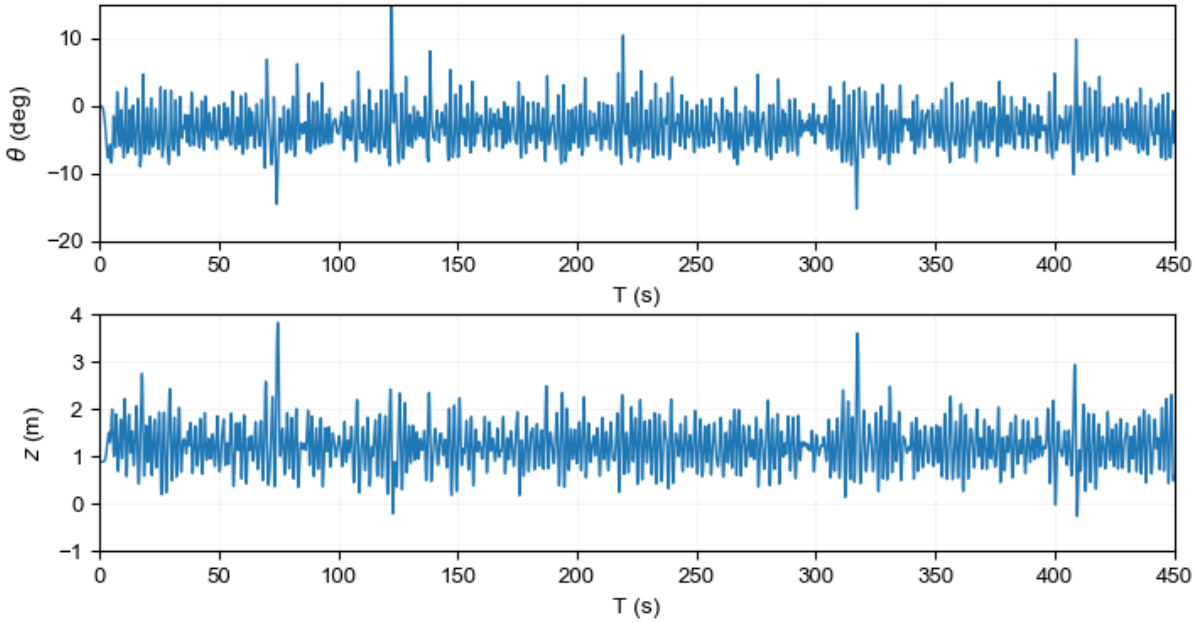

Figure 5.4: Planing hull heave (z) and pitch (θ) with respect to the CoG

Fig. 5.5 similarly visualises the motions of a hydrofoil craft. During the first 50 seconds, larger order oscillations can be observed. This is due to the integrator of the PID-controller requiring some time to turn into affect. As expected, no excessive peaks in heave or pitch are induced by the waves. Moreover, the heave peak magnitude is reduced by approximately 90%, while the remaining pitch variation is around 1% of the planing condition.

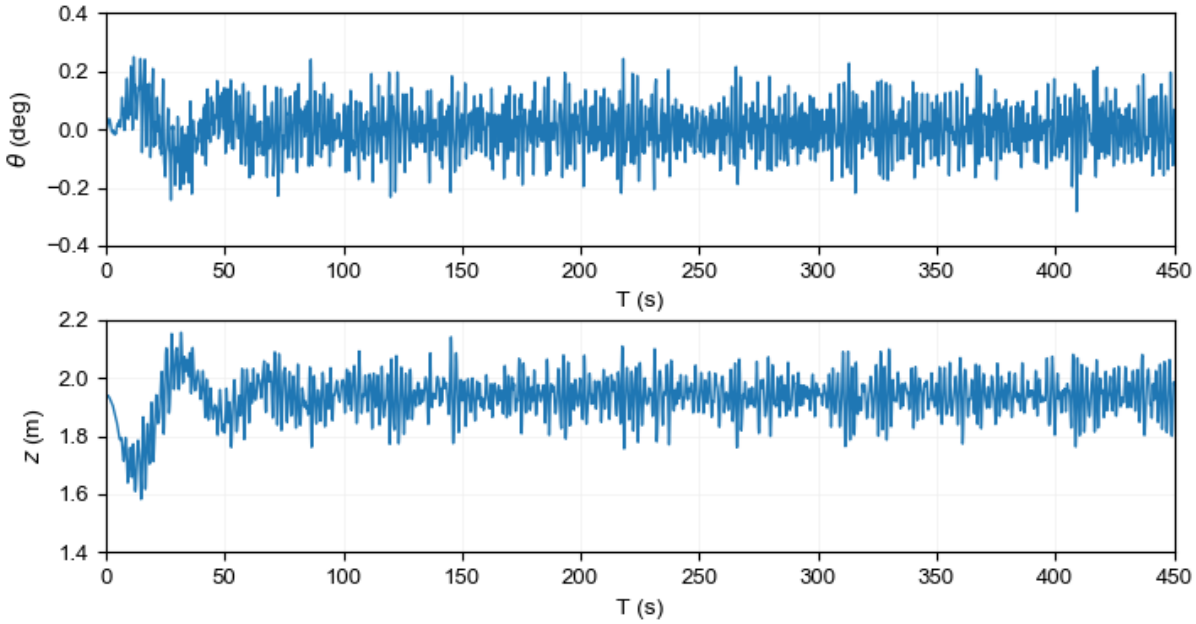

Figure 5.5: Hydrofoil heave (z) and pitch (θ) with respect to the CoG

5.3.3. Maximum vertical accelerations

Fig. 5.6 shows a time trace of the vertical accelerations experienced at the CoG of the planing benchmark hull. The accelerations often touch a value of around -10 m/s^2, similar to the value of gravitational acceleration (g = 9.81 m/s^2). This indicates that the craft is often detached from the water surface and 'flies' between waves, which results in slamming forces. In the total simulation time of 450 s, 160 slams were recorded by PanShipNL. Greater negative peaks occur when the vessel barely touches the water, but a large hydrodynamic force is encountered.

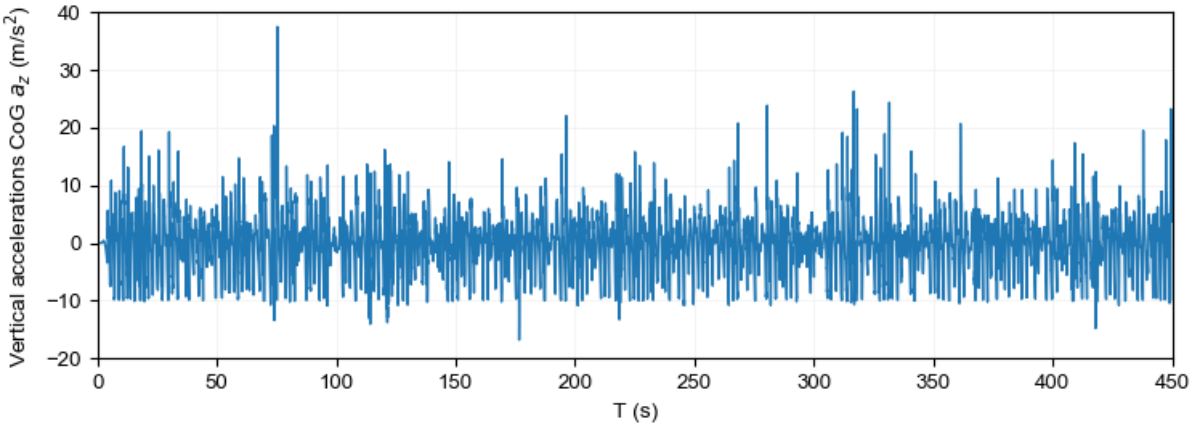

Figure 5.6: Time trace of vertical accelerations at the centre of gravity of the planing hull

Fig. 5.7 visualises the distribution of the accelerations experienced by planing hull. This distribution diverts vastly from a Rayleigh distribution, as the plots are not in a straight line. This indicates the non-linearity of the results, and is even more evident in the results for the stern and bow locations. It is noteworthy that the accelerations at the stern have higher values for the smallest exceedance probabilities compared to other locations. One reason for this occurrence is the high amount of airtime that the vessel achieves at this speed. If the craft hits a wave with its bow, this then increases the probability of nose-diving and broaching. Instead, the craft lands stern-first with high velocity, where the flatter bottom will amplify the acceleration magnitude. Around 15% of the peak vertical accelerations at the CoG are higher than 1.25 g (12.3 m/s^2). Based on the consideration of Keuning (1994) that professional crews will reduce their speed when peak accelerations of 1.25 g are experienced, the vertical acceleration at this speed is considered unsustainable (Deyzen, 2013).

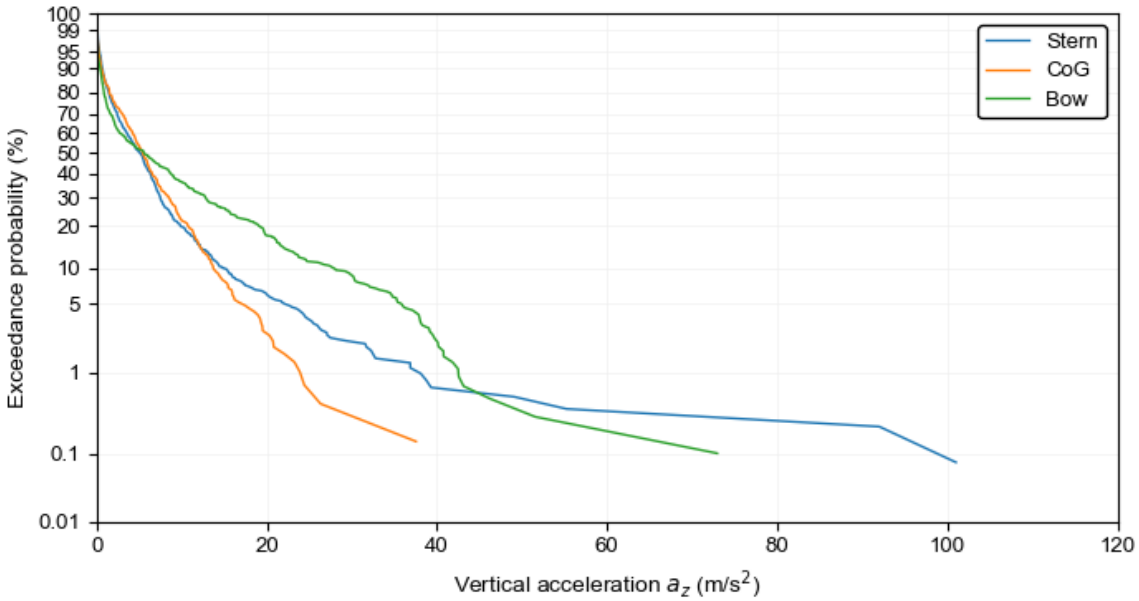

Figure 5.7: Positive acceleration distribution in crests of the planing hull in a Rayleigh plot

Fig. 5.8 presents the vertical accelerations experienced by the foiling craft design. In contrast to the planing hull results, an almost Rayleigh distributed relation is found between exceedance probability and the vertical acceleration. This means that an almost linear motion is experienced by the hydrofoil craft with respect to the incoming waves. Moreover, the 1/1000th vertical accelerations are reduced with approximately 90%, from 38 m/s^2 to 2.8 m/s^2, at the CoG.

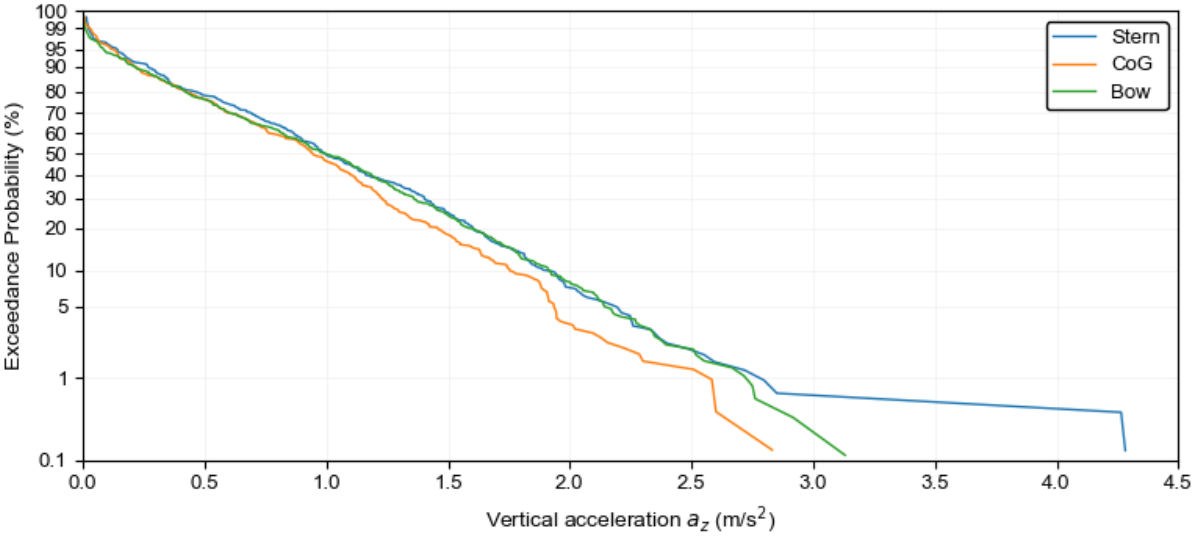

Figure 5.8: Positive acceleration distribution in crests of the hydrofoil craft in a Rayleigh plot

5.3.4. Sustained speed in seaway

To determine the sustained sea speed of a vessel, two factors are considered: 'natural speed reduction' due to added resistance caused by wind and waves, and the 'voluntary speed reduction' by the vessel's crew, to avoid severe motions or their consequences (Journee et al., 2015). However, as Keuning (1997) observed, voluntary speed reduction is not a matter of choice; it can be a necessary limit to prevent excessive physical strain and fatigue among the crew.

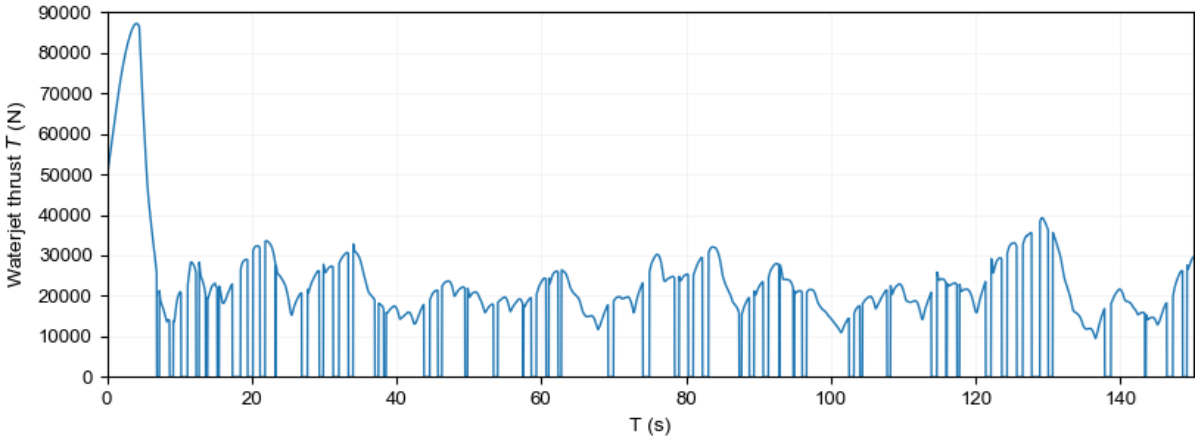

Figure 5.9: Thrust of a single waterjet for the planing craft

Fig. 5.9 shows an excerpt of the modelled waterjet thrust of the planing ship in Panship. To reach the required speed of 35 kt, substantial peaks in thrust are required. As Fig. 5.9 shows the thrust of a single waterjet, double the value is required to yield the required thrust magnitude. The mean total thrust required amounts to 38 kN, which is within the maximum of 40 kN delivered by the waterjets installed in the CB90 (see Appendix D). Nonetheless, the peaks in required thrust can be as high as 80 kN, indicating that this speed cannot be maintained constantly. Moreover, the time trace drops to zero 50 times in a timespan of 150 seconds. This drop in thrust indicates that waterjet inlet is above the

water, with air ingestion as a result. The air ingestion of waterjets due to waves is also known as waterjet ventilation. Ventilation prevents the waterjet from generating thrust, while the resulting pressure fluctuations increase mechanical stress on the propulsion system (Faltinsen, 2005). The fluctuating propulsor performance confirms that, together with the high vertical accelerations and induced motions of the craft, this speed can not be sustained in the currently considered sea state by the planing craft.

For hydrofoil craft operating foilborne, there is generally no natural speed reduction caused by the added resistance in moderate waves. Even more, hydrofoil vessels can demonstrate negative added resistance in waves (Godø & Steen, 2023). The same can be concluded for the Panship results of the hydrofoil design. Fig. 5.10 shows the time trace of the resistance of the foiling LAC design in waves. The mean value of this resistance is 18 kN, which is a significant reduction to the calm water resistance found by Hydres.

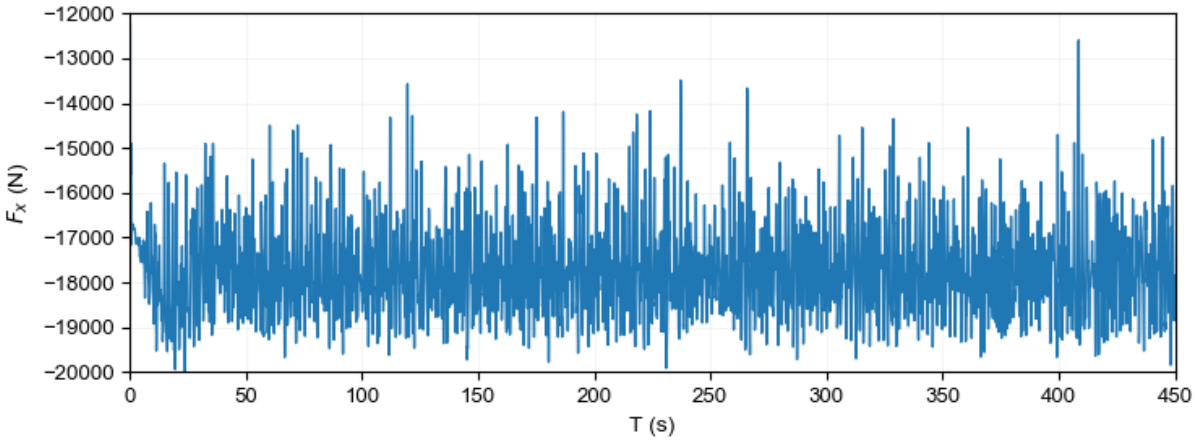

Figure 5.10: Resistance forces for the hydrofoil craft

In Fig. 5.11, the Hydres results for the design modelled in Panship are plotted. At 35 kt, the mean resistance in waves of Panship is approximately 10% lower than the Hydres result. The presented results are for an increased submergence depth and without resistance of nacelles or pods. Furthermore, no surface roughness allowance is applied and air resistance is neglected. Nevertheless, it is likely that Hydres still provides more accurate resistance results. This is due to Panship being aimed at the derivation of large motions in waves, rather than pure hydrofoil resistance. As a panel method, Panship cannot calculate viscosity effects directly, and simplified derivations are made to take these into account (van Walree, 2015).

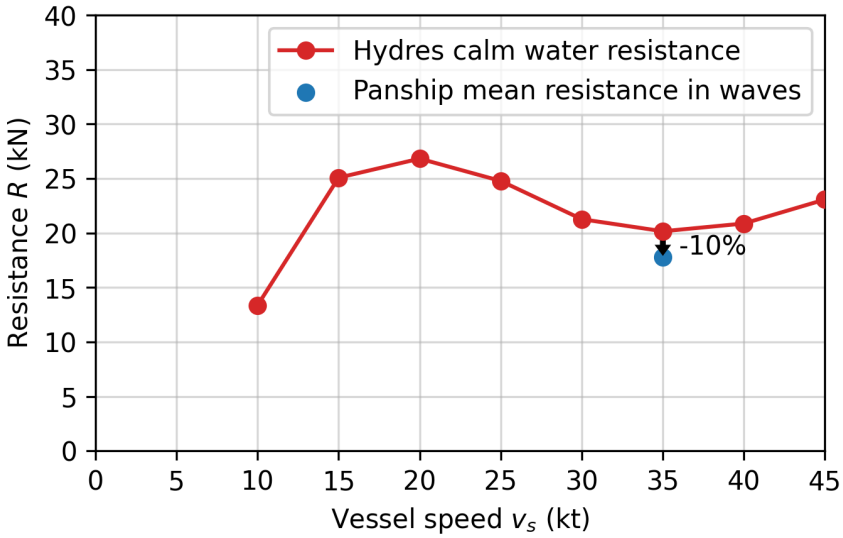

Figure 5.11: Panship resistance in waves compared to the calm water resistance of Hydres

Even though Panship will likely underestimate the resistance of the hydrofoil craft, it is expected that hydrofoils will experience less resistance in waves than in calm water. Unsteady simulations of hydrofoils in waves show that resistance reduction of hydrofoils can be achieved by extracting wave-energy. For an unoptimised control strategy this can account to a reduction of 2% to 3% of the calm-water resistance value (Godø & Steen, 2023). This phenomenon is caused by the orbital velocity of water particles in waves (Godø et al., 2024a), and can be explained using Fig. 5.12.

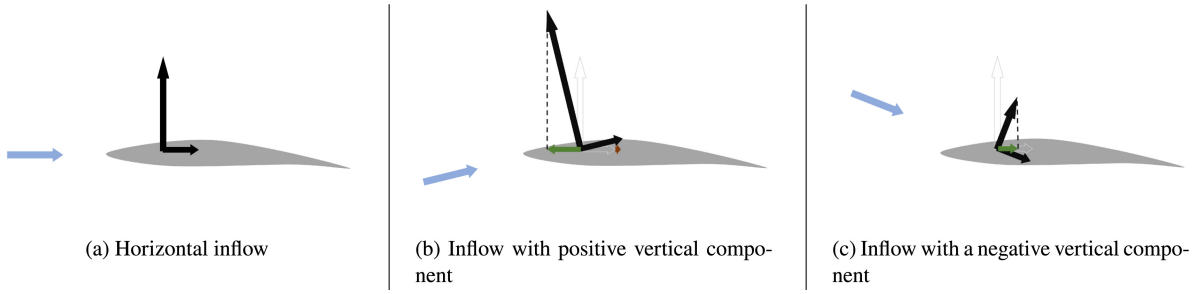

(a) Horizontal inflow

(b) Inflow with positive vertical component

(c) Inflow with a negative vertical component

Figure 5.12: Lift and drag acting on a cambered hydrofoil undergoing three different inflow conditions (Godø et al., 2024a)

Fig. 5.12b illustrates a wave-induced flow field with an upwards direction. This tilts the lift and drag vectors, which remain perpendicular and parallel to the inflow direction, respectively. In addition, the angle of attack is increased, leading to an increased lift and drag magnitude. Based on the assumption that the hydrofoil operates in its ideal angle of attack in undisturbed inflow conditions (Fig. 5.12a), the relative increase of lift will be larger than that of drag. This is a result of the lift-drag characteristic of cambered foils, such as shown in Fig. 3.3, where the lift coefficient has a steeper curve than the drag coefficient at angles of attack near 0°.

When the inflow direction becomes downwards, the lift and drag force vectors rotate clockwise as shown in Fig. 5.12c. The magnitude of these vectors also decrease due to the lower angle of attack. Contrasting the first situation, the lift vector decreases more than the drag vector, again due to the difference in steepness of the lift and drag coefficient. Decomposing the lift vector into horizontal plane of the foil then adds a small increase to drag.

Comparing the conditions in Fig. 5.12, it can be derived that the forward facing contributions of the changes in lift and drag vectors are larger than in backwards direction. Therefore, it can be concluded that a net resistance reduction can be realised if the hydrofoil traverses through moderate waves compared to a calm-water situation. Moreover, applying this theory to ride control algorithms can have a beneficial effect. Development of a neural network-based flight control system trained via reinforcement learning to actively extract wave energy, indicates that energy savings up to 60% can be realised for submerged hydrofoil craft (Godø et al., 2024a). Using this strategy can come at the cost of passenger comfort however, and a trade-off between energy extraction and passenger comfort needs to be made. Still, this application can offer substantial gains for Unmanned Surface Vessels (USVs) for example. These considerations are not factored into the further results of this study but serve as examples of the potential of hydrofoils.

Fig. 5.13 shows historical data of the voluntary speed reduction of submerged hydrofoil craft. This data, accompanied with the low vertical accelerations seen in Section 5.3.3, support the finding that little to no reduction in speed is required as wave heights increases. It should be noted however, that the crafts shown here are larger than intended for the hydrofoil LAC (L_{oa} = 16.0 m), which will reflect in the possible strut length and limits foiling wave height. Therefore, the required strut length is evaluated in Section 5.3.5.

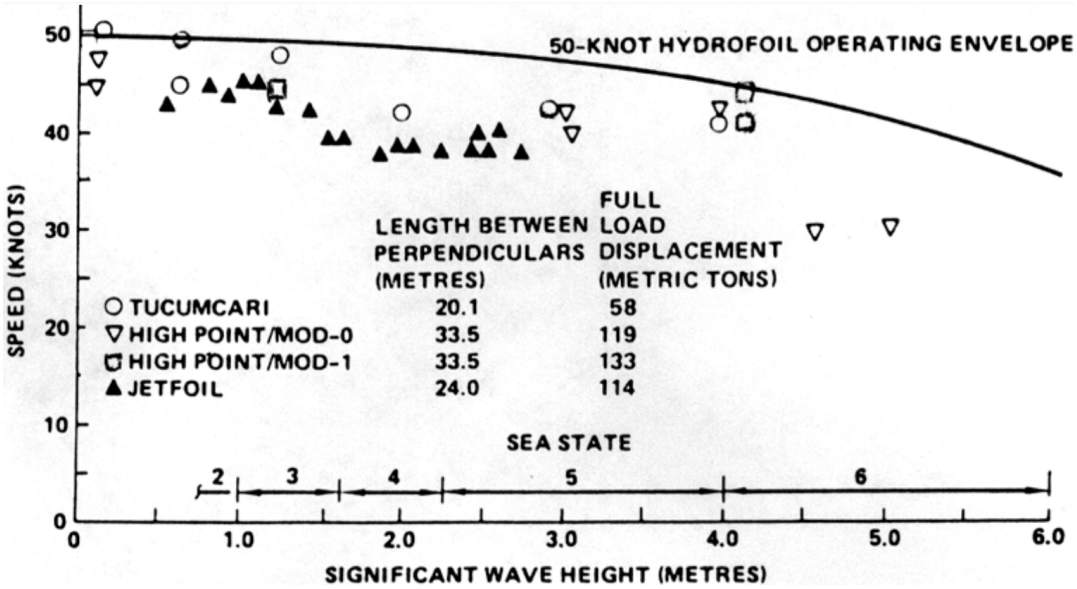

Figure 5.13: Historical data of sustained speed in sea state of submerged hydrofoil craft, identified by Johnston (1985)

5.3.5. Required strut length

To analyse if the designed strut length of the hydrofoil design is sufficient, the relative wave height of the vessel is investigated. The relative wave height is a variable to measure the possibility of foil ventilation, broaching, and slamming (Faltinsen, 2005). Foil broaching is discussed in Chapter 3, but ventilation can also be a limiting factor to operability. Ventilation occurs when there is a connection or air tunnel between the free-surface and the foil (Barden & Binns, 2012). In this case, air is sucked into a cavity at the suction side of the foil, which leads to a severe reduction of the lift generated by the foil. Ventilation arises due to free-surface contact of the foil or cavitation near the free-surface, but can also occur if there is a high relative angle between the undisturbed fluid flow and strut. This situation arises when a strut operates as a rudder for example (Faltinsen, 2005). A lower submergence increases the probability of foil ventilation.

Fig. 5.14 visualises the relative wave height with respect to the Front PerPendicular (FPP) of the hydrofoil vessel. From the time trace, it can be derived that the waves oscillate around the mean value of 1.25 m, which is the design clearance height (h_{clear}). The relative wave height should remain below 0 to prevent waves hitting the hull bottom. If the relative wave height would become higher than 0, it could result in a slamming force that destabilises the vessel. However, the waves do not reach the hull bottom and a margin of 0.25 m is left. Due to having this margin, it is concluded that this hull clearance is over-dimensioned.

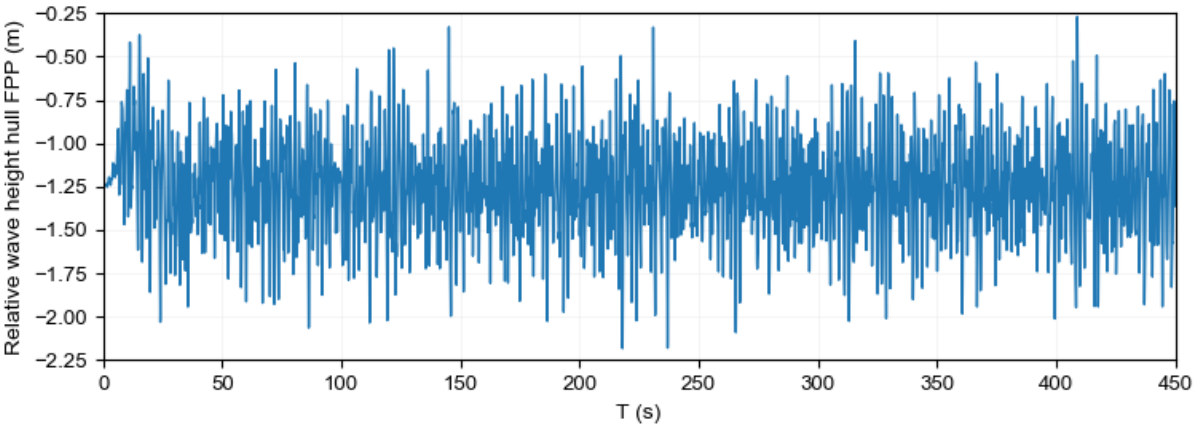

Figure 5.14: Relative wave height from the FPP of the foiling craft

Fig. 5.15 shows the relative wave height with respect to the aft foil. During foiling, the relative wave height should remain above 0 to guarantee no foil ventilation will occur. Although mean submergence is already 0.8 m ($h_{submerged}$), there are still some peaks that exceed the threshold of 0 m relative wave height. This means that the aft foil penetrates the wave-surface and the craft will become unstable. If the aft foil's submergence is increased to around one meter, foil submergence can be guaranteed.

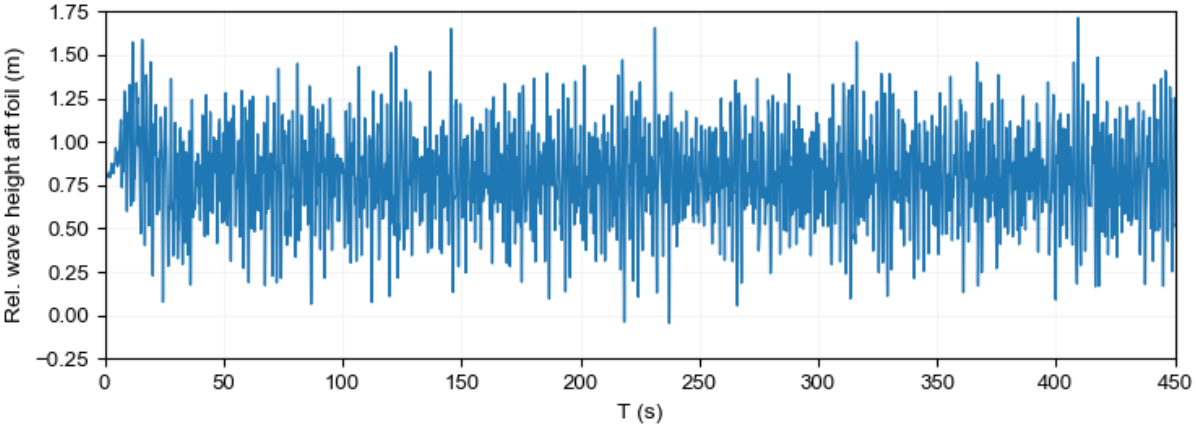

Figure 5.15: Relative wave height from the aft foil of the foiling craft

Lastly, Fig. 5.16 visualises the relative wave height with respect to the front foil. In contrast to the aft foil, the front foil stays submerged during the entire simulation. This is due to the front foil being designed for a deeper foil submergence ($h_{submerged}$) of 1 m. In spite of that, the foil comes close to the free-surface in two instances around 220 and 240 seconds. This can still pose a risk for foil ventilation.

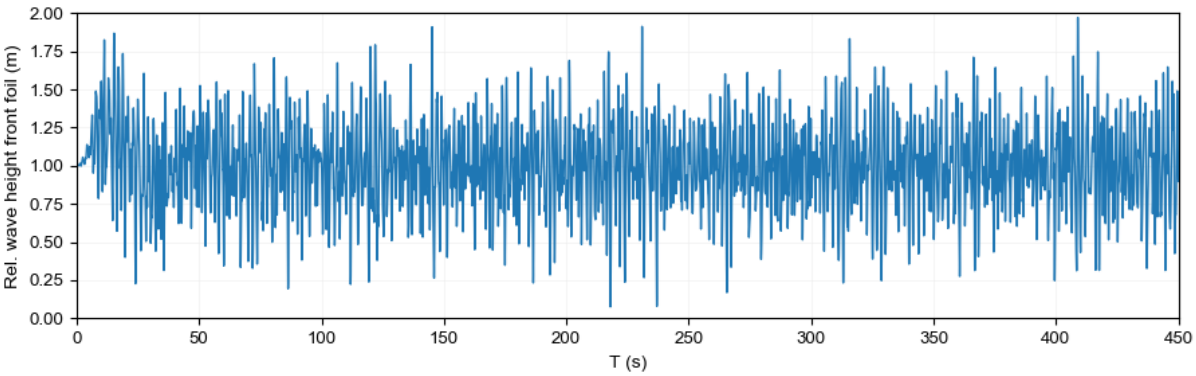

Figure 5.16: Relative wave height from the front foil of the foiling craft

Based on the relative wave motions of the hydrofoil craft, it can be derived that struts extending the hull with two meter (front and aft) guarantees foil submergence and no wave contact with the hull in this sea state. This would require one meter of mean submergence depth, and another meter for mean hull clearance. The length that the strut extends from the hull can then be defined as in Eq (5.1), where $h_{ext,strut}$, T_{foil}, and T denotes strut extension length, draft with foils extended, and hull draft, respectively. The extension height is also referred to as the effective height (van Oossanen, 1983).

$$h_{ext,strut} = T_{foil} - T = h_{clear} + h_{submerged} \tag{5.1}$$

However, investigation of the claims of hydrofoil craft manufacturers indicates that a limited amount of wave contact with the hull can be permitted. For example, Artemis claims that their hydrofoil craft are operational up to a significant wave height of 1.5 m, whereas their strut extension length is only around 1.4 m (Cauwenberghe, 2025). As this is based on significant wave height, defined as the mean wave height (trough to crest) of the highest third of the waves ($H_{1/3}$), higher wave heights than 1.5 m will also be encountered by this vessel (Journee et al., 2015). The strut extension length of several

hydrofoil craft can be plotted as in Fig. 5.17. Although the amount of data points is limited, a linear relation can be derived between strut length and the limiting sea state. It should be noted that sea state is not only dependent on the significant wave height, as described in Section 5.2. Nevertheless, it provides an indication of how hydrofoil craft manufacturers relate their operability limitations to strut design. Generally, the limiting significant wave height is higher than the strut extension depth.

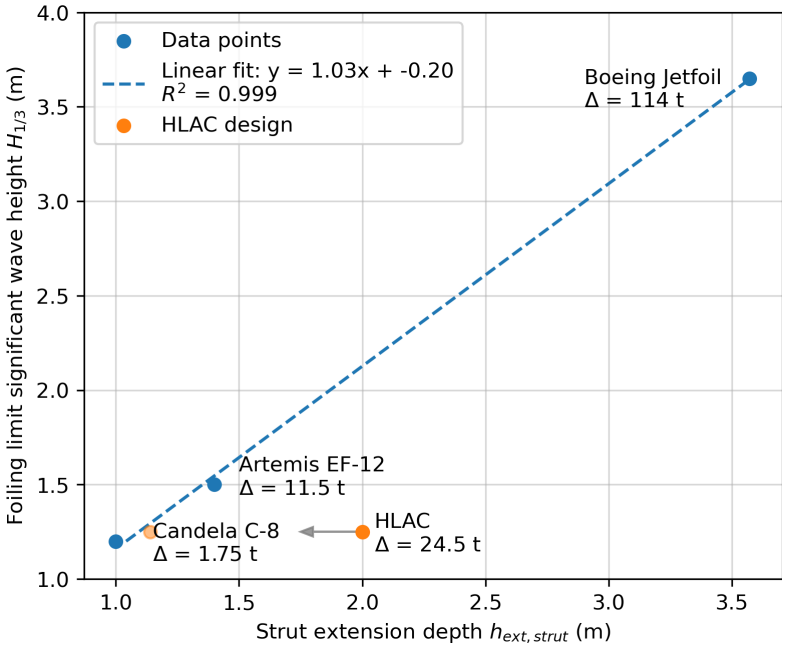

Figure 5.17: Limiting significant wave height for foiling of several monohull submerged hydrofoil designs (Candela, 2024a; Cauwenberghe, 2025; Yun & Bliault, 2014)

If the findings for the Hydrofoil LAC design (HLAC) are plotted in Fig. 5.17, it is derived that a strut extension length of 2 m does not align with other hydrofoil designs for a limiting $H_{1/3}$ of 1.25 m. However, if the hull draft is removed from the hull clearance (T = 0.86 m), the design does align with the other designs. This indicates that wave contact on its own is not necessarily the limitation for foiling, but when wave contact develops up to the hull draft line stability issues will occur.

Although a longer strut length is beneficial for operability, it also makes stabilisation more difficult and requires further strength considerations. Longer struts require stronger strut sections and may increase the required thickness (see Appendix F.3.1), which in part increases resistance. Additionally, the stabilisation of a hydrofoil craft is similar to an inverted pendulum problem, which is naturally unstable (Franklin et al., 2009). Longer struts extend the moment arm, causing small angular deviations in the foil to result in a larger applied torque. This mirrors the behaviour of a taller inverted pendulum, which is also more challenging to stabilise. Appendix J provides more context about this particular problem.

Still, it is likely that the hydrofoil strut length for an LAC design can be larger than for a minimum $H_{1/3}$ of 1.25 m. Van Oossanen (1983) found the relation of Eq. (5.2) based on several submerged hydrofoils. Based on a displacement of 24.5 t, a $h_{ext,strut}$ of 1.75 m can be found. Furthermore, the LAC design will be larger than the Artemis EF-12 and Candela C-8 designs. Hence, it is concluded that a $h_{ext,strut}$ between 1.5 and 2 m is realistic. Based on Fig. 5.17 alone, this would extend the operability in foiling mode far into sea state 4.

$$h_{ext,strut} = 0.61 \cdot \nabla^{\frac{1}{3}} \tag{5.2}$$

5.3.6. Summary of PanShip results

Table 5.3 lists a summary of the seakeaping characteristics assessed with PanShip. As discussed in Section 5.1, no conclusions can be derived from the significant values. Nevertheless, they are provided here for completeness. The A1/3 values presented here is the significant value, which represents the mean value of the 33% highest peaks. The A1/10 values are also presented, which can provide a better representation of peak behaviour of the craft compared to the significant values. The A1/10 value represents the mean of the 10% highest peaks. The double amplitude (2A1/3 and 2A1/10) values are presented for heave, which defines the difference between the crest and through value of the time trace. As the CoG of the hydrofoil design is placed higher than the planing craft, these values can be compared to eachother, whereas the amplitude compared to the water surface can not capture this difference. The best indication of seakeeping performance can be retrieved by looking at the probability of exceedance (Gelling & Keuning, 2011). In Table 5.3, the 1% probability of exceedance is presented, as enough data was retrieved in the simulation to assess this for each parameter. Lower probabilities can be found in Fig. 5.7 and Fig. 5.8.

Table 5.3: Summary of PanShip seakeeping performance at 35 kt in sea state 3

Parameter	Value	Hydrofoil	Planing hull
Heave z (m)	2A1/3	0.237	1.69
	2A1/10	0.292	2.13
	1% Prob. exc. crest[1]	2.13	3.00
Pitch θ (°)	A1/3 Crest	0.153	3.14
	A1/10 Crest	0.193	5.66
	1% Prob. exc. crest	0.240	10.9
a_z (Stern) (m/s^2)	A1/3 Crest	1.82	16.1
	A1/10 Crest	2.34	27.4
	1% Prob. exc. crest	2.78	37.9
a_z (CoG) (m/s^2)	A1/3 Crest	1.61	13.1
	A1/10 Crest	2.05	18.6
	1% Prob. exc. crest	2.57	23.9
a_z (Bow) (m/s^2)	A1/3 Crest	1.78	23.7
	A1/10 Crest	2.26	36.8
	1% Prob. exc. crest	2.72	42.5
Number of slams (-)		0	160

The MoEs of Chapter 2 can be evaluated following the results of the seakeeping assessment. Table 5.4 shows the performance of each design. Both designs are able to satisfy the safety requirement posed in Chapter 2 in this sea state. Although the planing hull (based on the CB90) is able to attain this speed within the safety bounds, it is expected that this speed can not be sustained for the transfer duration. On the contrary, the hydrofoil design (HLAC) is able to sustain this speed, if its additional requirements can be met. It is furthermore expected that a higher speed can be attained by the HLAC design, given the low vertical accelerations.

Table 5.4: Design drivers, performance indicators and requirements related to seakeeping of a future LAC

Design Driver	Criteria to improve compared to base design (MoE)	Current requirement	Base value planing hull	HLAC foiling craft
Speed	Maximum sustained speed in sea state 3	25 kt	< 35 kt	>35 kt
Safety	A1/10 positive vertical accelerations in sea state 3 at 35 kt on CoG	35 m/s^2	20 - 30 m/s^2	2 - 2.3 m/s^2

[1] CoG position from undisturbed water surface

5.4. Concluding insights

To assess the seakeeping performance of a hydrofoil craft compared to a planing vessel, a time-domain simulation is performed. A time-domain simulation that evaluates the motions of high-speed craft can provide the peak vertical accelerations that restrict the operability of these vessels. In this assessment, the simulation method PanShip is used. The considered sea state for this analysis is based on the requirements of the NLMOD and is the worst condition that can be found in sea state 3, 45 nm from the coastline of the Netherlands. This yields the sea state with a $H_{1/3}$ of 1.25 m and a T_p of 5.75 s.

The simulation results show that a speed of 35 kt can not be sustained by the planing hull in this sea state. Professional crews will not be able to sustain peak vertical accelerations above 1.25 g (12.3 m/s ^{2}) for long periods of time, but this value is exceeded by 15% of the acceleration peaks at the CoG. Even higher probabilities are found towards the stern and bow of the craft. Moreover, the fluctuating thrust requirement and waterjet ventilation indicate that operating in this condition will increase the wear and tear of the propulsion system significantly.

The hydrofoil design diminishes the induced wave motions and accelerations significantly. Peak vertical accelerations are reduced with 90% at the CoG. The reduced heave and pitch motions also make the hydrofoil craft a more stable platform. Furthermore, the added resistance in waves is minimal and can even be negative depending on the control strategy. However, these enhancements assume that the hydrofoil design remains in steady flight, with a correctly tuned ride control system. The tuning of the ride control system can affect the wave-induced motions and resistance in waves. In addition, submerged hydrofoil craft have a unique dynamic stability characteristic, which makes rise to edge cases that should also be analysed before safe operation can be commenced. Scenarios such as nose-diving due to foil ventilation or foil broaching severely affect the safe operation of these craft. The probability of these scenarios depends on foil submergence. Analysis of the relative wave height indicates that 2 m of strut extension is required for foil submergence and hull clearance if no hull wave contact is allowed. However, by evaluating the strut height and operability limits of other hydrofoil designs, it is suggested that a degree of hull wave contact can be permitted at speed. A strut extension length between 1.5 and 2 m is proposed as a suitable length. If these requirements can be fulfilled, safe transfer at 35 kt in this sea state can be realised. This provides the answer to the research question posed in this chapter:

RQ2: How can hydrofoil systems increase the operational effectiveness of a Littoral Assault Craft (LAC) design in waves, considering speed and safety of the crew?

6

Validation of the design method

This chapter aims to provide an assessment of the validity of the design methodology of this thesis. Firstly, Section 6.1 introduces a validation methodology intended for design methods. The next sections will provide the evaluation of different types of validity. This starts with the theoretical structural validity (Section 6.2), and the empirical structural validity (Section 6.3), continues with the empirical performance validity (Section 6.4), and ends with the theoretical performance validity (Section 6.5). Finally, Section 6.6 provides concluding insights to the research question posed in this chapter:

RQ3: How can the design methodology for a Hydrofoil Littoral Assault Craft (HLAC) be validated?

6.1. Validation theory

Pedersen et al. (2000) present a framework for validating both the internal consistency and external relevance of a design method. This framework is based on the "validation square", depicted in Fig. 6.1. The primary goal of this validation is to establish confidence in the method's overall usefulness with respect to its purpose. Usefulness is defined by two criteria: whether the method provides solutions "correctly" (effectiveness), and whether it produces the "correct" solutions (efficiency). The validation square assesses both effectiveness and efficiency through qualitative and quantitative measures, respectively. As illustrated in Fig. 6.1, the validation assessment follows a structured sequence. It begins with the Theoretical Structural Validity (TSV), proceeds with the Empirical Structural Validity (ESV), continues with the Empirical Performance Validity (EPV), and concludes with the Theoretical Performance Validity (TPV). Each of these types is discussed in the following sections.

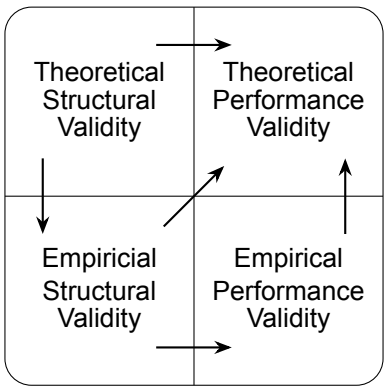

Figure 6.1: The validation square of Pedersen et al. (2000)

6.2. Theoretical Structural Validity (TSV)

The TSV, relies on two key components: The validity of each individual part (construct) within the design method, and the consistency of how each part is integrated in the complete design method.

Pedersen et al. (2000) propose that the main indicator of an individual construct's validity is the quality of the sources supporting its reasoning. Care was taken to ensure that valid sources were provided for each assumption, derivation, and equation. Given the fluctuating relevance of hydrofoil design throughout the 20th century and its recent resurgence, both older and newer sources are cited. When referencing an older source, an effort is made to find current sources that corroborate the information from the earlier reference. Throughout the entire design methodology, tools from other parties are also incorporated alongside the code developed for this thesis. These external tools are validated through their own independent validation studies (Minerva et al., 2024; Turner & van Walree, 2015; van Walree, 1999; van Walree & Carette, 2011).

The internal consistency of the design method is shown through the use of flow-chart representations. Flow-charts in Fig. 4.3 and Fig. 4.5 demonstrated which information is required for each calculation step (construct) and what the eventual output and results are of these steps. By following these flow-charts during the calculations and code development, the internal consistency of the method is ensured.

6.3. Empirical Structural Validity (ESV)

The ESV defines that the individual constructs, that have TSV, are applied within their accepted ranges. Thus, the ESV of a design method can be assessed by comparing the results of example problems, for which the solutions are already known, to the outcomes of the proposed methodology. The largest part of the design method, that does not depend on externally validated tools, is Part I of Chapter 4. Therefore, the resistance and weight calculation of this part is further investigated.

Since there are no current hydrofoil vessels comparable in size to the HLAC design, comparisons must be made with existing craft of different sizes. Additionally, the resistance curves of commercial hydrofoil craft are rarely published. Appendix H provides experimental data from a prototype hydrofoil craft. To assess the ESV of the resistance calculation of Part I in Chapter 4, these calculations are applied to this real-world craft, allowing for a direct comparison of resistance results.

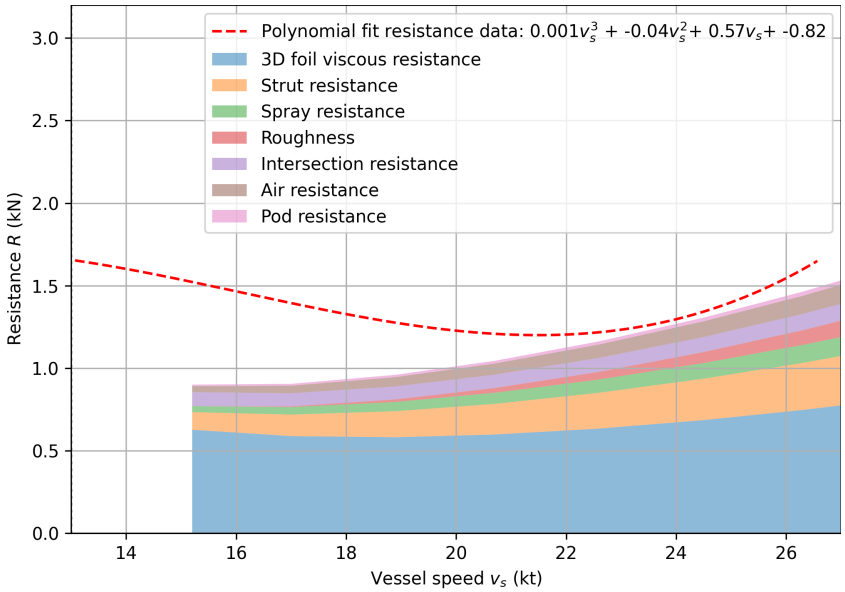

Figure 6.2: Resistance over speed of experimental results compared to estimated results

Fig. 6.2 presents this comparison, showing that the calculations provide a realistic estimate for both top speed and design speed with discrepancies remaining below 5%. However, at lower speeds, the deviations increase. Up to approximately 20 kt, the difference stays within 20%, but at speed as low as 15 kt, the discrepancy exceeds 50%. This significant variation is attributed to how the craft is operated

and data is collected, making the data for vessel speeds below 20 knots unrepresentative. Additional context on this issue is provided in Appendix H. Despite these discrepancies, Fig. 6.2 demonstrates that the resistance calculations from Part I of the design methodology yield realistic estimates for speeds above 20 kt in this case. Additionally, the continuity in the top speed resistance estimates of Part I to Part II (Hydres) demonstrate the viability of this methodology.

The weight model from Part I is compared to a design study by Hoerner et al. (1954) in Section 4.7. Although an older source, the weight factors of the hydrofoil designs were found to align with expectations. The most significant discrepancy is observed in the foil system weight, which showed a reduction of approximately 45%. However, this is anticipated, as Hoerner et al. (1954) used stainless steel for the foil structure, whereas this thesis employs a methodology based on the structural properties of carbon composites. The structural weight of the hydrofoil system is in accordance with the findings of Godø et al. (2024b), which estimated an approximate 3% weight fraction for the structural foil weight, without buoyancy correction, for the design range of an HLAC.

6.4. Empirical Performance Validity (EPV)

EPV is determined by two factors: the usefulness of the method for a specific problem and the usefulness linked to its application (Pedersen et al., 2000). Usefulness is defined as the extent to which an articulated purpose is achieved.

The usefulness linked to its application is evaluated by assessing the contributions of each construct individually on its usefulness (Pedersen et al., 2000). Throughout this thesis, it is demonstrated that the iterative nature of foiling craft design depends strongly on the interaction between vessel resistance and weight. Therefore, a comprehensive evaluation of both is a necessity to achieve a realistic converged design. Furthermore, at the outset of this study, it was uncertain if the hump resistance is a critical factor in determining the propulsion system's requirements. Therefore, investigation of the hump resistance provided valuable insight into whether modifications are necessary to facilitate foiling in all considered sea states. In addition, the seakeeping assessment provided understanding of the improvements in seakeeping that can be made with hydrofoil systems. Each individual part (construct) in the design methodology is useful in the purpose of retrieving the necessary MoEs of the study.

The results of converged hydrofoil craft designs are used to assess MoEs that define the operational effectiveness of an HLAC. Consequently, the outcomes of the design methodology reinforce confidence its usefulness for the specific purpose of investigating the operational effectiveness of an HLAC. Additionally, it supports the broader purpose of the methodology: contributing to advancing scientific knowledge.

6.5. Theoretical Performance Validity (TPV)

The TPV defines if the method is deemed useful beyond some limited instances. Drawing from the previous validity assessments, a level of generality can be attributed to the results. However, the design method is built around fixed dimensional constraints related to the davits of the mother ships. It also incorporates hull particulars of the benchmark vessel (CB90), such as the block coefficient, to calculate vessel displacement. Additionally, the design method only applied one foil configuration and limited itself to propeller propulsion. Nonetheless, with minor modifications, it can be adapted to facilitate vessels of different dimensions and foil configurations. While this study primarily examined the range-extending potential of hydrofoils rather than energy efficiency, the methodology can also be applied to develop more sustainable high-speed craft designs.

6.6. Concluding insights

This chapter evaluated the validity of the design methodology using the validation square method. By examining different forms of validity, on theoretical accuracy and real world data, confidence is instilled for the purpose of the design method: Assessing the operational effectiveness of a HLAC design. This provides the answer to the research question:

RQ3: How can the design methodology for a Hydrofoil Littoral Assault Craft (HLAC) be validated?

7 Conclusion

This chapter presents the key findings of the thesis. First, the limitations of the study are presented in Section 7.1, followed by the conclusions in Section 7.2. The scientific contributions of this research are outlined in Section 7.3, and finally, Section 7.4 provides recommendations for further research.

7.1. Limitations

Several limitations potentially influence the findings of this thesis. Firstly, in Part I of the design method presented in Chapter 4, interaction effects of foils are neglected. This is a limitation of the Foil Design JIP tool and no additional estimation is provided in this thesis. The downwash of the front foil will not vary much in the spanwise direction of the aft foils however, due to the larger span of the front foil. Still, this can affect the required angle of attack of the aft foils, and in turn its resistance. An updated integrated model with the estimation method of Kaplan et al. (1960), can provide more accurate assessment. As Part II (Hydres) took interaction effects into account, it can be concluded that interaction effects are not detrimental to the foil design however.

During part I of the design method, the foil designs are also limited within the design space of the Foil Design JIP tool. Foil designs with rounded tapering instead of straight tapering or foil sections differing from the Eppler-817 section can not be investigated.

The resulting foil designs of Chapter 4 have a relatively high camber, approaching or reaching 5%. While this reduces viscous drag, it increases both induced and profile drag. This significant camber can lead to cavitation at high speeds due to larger localised pressure fluctuations. Reducing the foil loading can decrease the amount of camber necessary.

For the weight calculations of Chapter 4, assumptions are made regarding the weight fractions in outfitting and hull weight. These assumptions are based on the published data of the CB90 and lead to an outfitting weight fraction of approximately 30% of total displacement weight. Although comparison with other hydrofoil designs indicated that this is a realistic estimate, it can misrepresent the payload carrying capacity of the design if a different outfitting is sufficient.

Additionally, the presented structural weight reduction of carbon in Section 4.10 may be optimistic. Although the findings are grounded in literature, contact with industry professionals indicated that generally weight saving of around 25% can be realised with carbon composites compared to a lightweight optimised aluminium hull form, instead of the 50% suggested in this thesis.

Furthermore, the roughness allowance of the hydrofoil designs has a significant effect on the total resistance of a hydrofoil. In the results of this thesis an equivalent sand roughness of 8 µm is applied, but additional care should be taken for comparing these results with other hydrofoils with surfaces of differing roughness.

Lastly, in the seakeeping assessment of Chapter 5, the same Centre of Gravity (CoG) placement is used for the hydrofoil as the planing hull. In reality, the CoG of the planing hull will be further aft than how it is modelled (x = 6.5 m). Based on the placement of the centre of buoyancy, a position of 1 m aft (x = 5.5 m) will be more realistic. Still, the resulting negative trim may have helped in reducing the vertical accelerations of the vessel, as negative trimming is usually done in waves to mitigate vessel motions. Additionally, the real CB90 design has interceptors installed, which can mitigate vertical accelerations.

7.2. Conclusion

The thesis aims to provide an answer to the main research question:

MQ: What is the operational effectiveness of a high-speed littoral assault craft with a retractable hydrofoil system compared to a planing design when operating in amphibious missions?

Throughout the chapters of this thesis, the main research question is answered with several sub-questions. First, the literature review starts with the literature question:

LQ1: What are the design drivers and associated Measures of Effectiveness (MoEs) of a future Littoral Assault Craft (LAC), and what are possible solutions to fulfil these design drivers?

The primary objective of the LAC is to ensure safe and fast transport of personnel between mother ship and shore under a broad range of sea conditions for its size. Therefore, the design drivers regard range, speed in seaway, and safety. By comparing hull form concepts to fulfil the design drivers, it is revealed that a retractable hydrofoil system offers the most promising solution due to:

- The highest payload transport efficiency at the required speeds of any AMV, which can increase range as a result
- The high sustainable speed through rough seas.
- The low vertical accelerations at high speed to reduce fatigue and strain of crew
- The load carrying ability being sufficient for passenger transport
- Retraction systems for hydrofoils being applied before
- Economics playing a lower determining factor for the navy if sufficient gains in other aspects can be realised

The literature review continues with the following literature question:

LQ2: Which types of hydrofoil configurations can be considered for a Littoral Assault Craft (LAC) and what are their applicable propulsion methods?

A future Hydrofoil LAC (HLAC) occupies a design space between the traditional hydrofoil interest of military and ferry purposes, and the more recent interest of the leisure craft industry. Between surface-piercing and submerged hydrofoils, a submerged hydrofoil system appears to fulfil the design drivers the best due to their increased seakeeping cabability and reduced resistance. The transmission for foilborne propulsion remains challenging to implement in a retractable system however. Waterjets can be implemented, but decrease propulsion efficiency drastically. By contrast, propeller propulsion can offer high propulsion efficiency, but this requires a complex transmission system. Due to propulsion vulnerability considerations of canard configurations, a conventional configuration is preferred and waterjets are excluded as a propulsion system. All in all, there appears to be no consensus on which type of transmission and retraction system is suited for small high-speed hydrofoil craft. However, recently developed electric propulsion systems with axial flux motors, can be a potential enabler for a diesel-electric design. Furthermore, an inclined shaft retraction system, conventionally applied in sailing yachts, can be an option to apply an inclined shaft propulsion system.

The literature review is followed by the first research question:

RQ1: How do retractable hydrofoil systems influence the weight and resistance of a future Littoral Assault Craft (LAC) design, and what is the range increase potential of this application?

A design methodology to develop a preliminary design of a HLAC is proposed. First, an iterative parametric model is used to provide an initial displacement estimate and their relevant dimensions in length, beam and draught (Part I). The Foil Design JIP tool of MARIN is employed in the model for the design of the hydrofoils. After this first step, the program Hydres is used to assess the dynamic equilibrium of the design (Part II). During the entire procedure, two types of propulsion systems are evaluated: an inclined shaft system (HLAC-HK) and an L-drive system (HLAC-DE). For propeller characteristics, the transcavitating Newton-Rader series is applied. Both propulsion systems have the capacity to transition through the hump region without additional power requirements. However, both configurations have drawbacks that result in a higher resistance. The HLAC-HK design has additional appendage drag due to the inclined shaft, and the HLAC-DE design has increased resistance due to a heavier propulsion system compared to the HLAC-HK design. Nonetheless, the resistance reduction compared to the planing benchmark vessel, with the same payload carrying capacity, can be up to 35%. This leads to

the first MoE of the implementation of hydrofoils, as they can realise a range increase of approximately 50% at 30 kt. Conversely, maintaining the HLAC-DE's range equivalent to the planing benchmark vessel can realise a similar displacement. In addition, the effect of weight saving measures on the hydrofoil craft design is evaluated. The analysis reveals an inversely exponential relationship between weight reduction and resistance, highlighting the value of weight saving efforts.

Building on these findings, the next research question explores the seakeeping of planing and hydrofoil craft:

RQ2: How can hydrofoil systems increase the operational effectiveness of a Littoral Assault Craft (LAC) design in waves, considering speed and safety of the crew?

To assess the seakeeping performance of a hydrofoil craft compared to a planing vessel, a time-domain simulation is performed. In this assessment, the simulation method PanShip is used. The analysis considers the worst condition in sea state 3 ($H_{1/3}$ = 1.25 m, T_p = 5.75 s) 45 nm of the Netherlands' coast.

Results show that a planing hull cannot sustain 35 kt in these conditions due to excessive vertical accelerations, reaching peak accelerations up to 10 g. Moreover, the fluctuating thrust requirement and waterjet ventilation indicate that operating in this condition will increase the wear and tear of the propulsion system significantly.

In contrast, the hydrofoil design diminishes the induced wave motions and accelerations significantly. Peak vertical accelerations are reduced with 90% at the CoG. The reduced heave and pitch motions also make the hydrofoil craft a more stable platform. Furthermore, the added resistance in waves is minimal and can even be negative depending on the control strategy. However, these enhancements assume that the hydrofoil design remains in steady flight with a correctly tuned ride control system. The tuning of the ride control system can affect the wave-induced motions and resistance in waves.

Further analysis of the relative wave height indicates that 2 m of strut extension is required for foil submergence and hull clearance if no hull wave contact is allowed. However, by evaluating the strut height and operability limits of other hydrofoil designs, it is suggested that a degree of hull wave contact can be permitted at speed. A strut extension length between 1.5 and 2 m is recommended as a suitable length. If these conditions are met, the hydrofoil craft can maintain 35 kt safely in this sea state.

An assessment of the validity of the design methodology of this thesis is provided through the last research question:

RQ3: How can the design methodology for a Hydrofoil Littoral Assault Craft (HLAC) be validated?

The validity of the design methodology is evaluated with the validation square method. By examining different forms of validity, on theoretical accuracy and real world data, confidence is instilled for the purpose of the design method: Assessing the operational effectiveness of a HLAC design.

With the sub-questions individually addressed, the main research question is revisited:

MQ: What is the operational effectiveness of a high-speed littoral assault craft with a retractable hydrofoil system compared to a planing design when operating in amphibious missions?

Table 7.1 lists the results of this thesis by providing a comparison between the planing benchmark vessel (based on the CB90) and the proposed HLAC designs. Although limited in the amount of performance indicators, it provides an indication of the potential of submerged hydrofoil systems through the use of MoEs. Furthermore, the study proposed several methods of integrating hydrofoil and propulsion systems. While the addition of a retractable hydrofoil system introduces considerable design complexity, the results demonstrate the potential of submerged hydrofoil systems to enhance operational performance of a future LAC design.

Table 7.1: Design drivers and Measures of Effectiveness (MoE) of a future LAC

Design Driver	Criteria to improve compared to base design (MoE)	Current requirement	Base value planing hull	HLAC foiling craft
Range	Nautical miles in high speed (30 kt) calm water	200 nm	300 nm	$\approx$ 450 nm (+50%)
Speed	Maximum sustained speed in sea state 3	25 kt	< 35 kt	>35 kt (+)
Safety	A1/10 positive vertical accelerations in sea state 3 at 35 kt on CoG	35 m/s^2	20 - 30 m/s^2	2 - 2.3 m/s^2 (-90%)

7.3. Scientific contributions

This study has resulted in several scientific contributions, which can be summarised as follows:

- **Development of a design method for a high-speed craft with retractable hydrofoils:** The developed design methodology allows for further iteration for a novel vessel design, specifically a HLAC. This approach facilitates early-stage assessment of performance indicators for a complex vessel, where the overall performance is challenging to predict. Furthermore, the design method incorporates multiple advanced tools specific to hydrofoil craft design. By applying these tools in a holistic methodology, this study enhances their utility and contributes to the advancement of hydrofoil craft design. Given the energy-saving potential of hydrofoils, this also adds to the development of sustainable high-speed vessel designs.
- **Investigation of propulsion methods with retraction potential:** The study explores multiple propulsion configurations that incorporate state-of-the-art technology to enable retraction capabilities. While retraction systems do exist, there is limited literature on this topic. Although these applications remain conceptual, the study offers valuable insight into the suitability of these propulsion methods.
- **Seakeeping considerations for a hydrofoil craft and comparison to a planing situation:** The seakeeping assessment provides an initial perspective into the considerations of a HLAC design. This exemplified the vast reduction in vertical accelerations of hydrofoils compared to the planing condition. However, it also indicated the difficulty in assessing the required strut length. This can serve as a foundation for further evaluations, which leads to several recommendations proposed in this thesis.

7.4. Recommendations

The following recommendations are gathered from the research conducted in this thesis. These recommendations concern the design of new hydrofoil craft such as a successor to the LAC, or further research:

- **Weight saving measures:** The results of this thesis substantiate that the gains of weight saving measure can have a large effect on the requirements posed on the propulsion system and the performance of the design. By realising a weight reduction of approximately 5% of the total displacement, already the amount of stacked electric motors for the HLAC-DE design can be reduced from three to two, per propulsion line. This can therefore also reduce the complexity of the complete design, as the amount of systems is reduced. Due to the inversely exponential relationship between weight reduction and resistance, it is recommended to realise a direct weight saving of at least 10% of the total displacement. Together with the indirect weight saving, from reduced propulsion and foil system weight, the total resistance can be reduced with 20%.
- **Critical retrospective of range requirement:** In this study the range requirement of 300 nm has remained a constant within the study, reflecting current expectations of the RNMC. However, as the weight saving measures have indicated, a reduction in fuel weight can offer vast benefits in the hydrofoil craft design with respect to resistance, power, and system requirements. If the concept of operations allows for more frequent refuelling this can be beneficial to the complete vessel design.
- **Edge cases for operability:** Submerged hydrofoil craft have a unique dynamic stability charac-

teristic, which makes rise to edge cases which should also be analysed before safe operation can be commenced. Scenarios such as nose-diving due to foil ventilation or foil broaching severely affect the safe operation of these craft. Testing with USVs can offer a solution to test control strategies at high speeds at (near) full scale, before implementing these for vessels intended for passenger transfer. Furthermore, a worst-case scenario simulation with foil broaching can provide insight in additional safety measures that need to be taken. This can also provide insight in how CoG placement can affect the nose-diving behaviour of the craft.

- **Seakeeping assessment with hull effects:** A comparison of similar monohull hydrofoil craft makes clear that a limited amount of hull-wave interaction is permitted for monohull hydrofoil designs without stability issues. It is therefore of interest to investigate the amount of hull-wave submergence is possible, before the hydrofoil design becomes unstable. The result of this assessment can provide better requirements for the strut length.
- **Seakeeping in following seas:** The seakeeping of the planing and hydrofoil design is assessed in head seas for this thesis. This is due to the fact that generally the highest vertical accelerations are experienced in this wave direction. However, submerged hydrofoils can demonstrate larger relative vertical heave and pitch motions in following seas. This should be taken into account for the development of control systems.
- **Dynamic stability of submerged hydrofoils:** As the strut length increases, so will the roll and pitch motions of the vessel. This is essentially a more complicated inverted pendulum problem as the centre of pressure rotates with the hydrofoil system. Dynamic stability assessment with state-space modelling can offer additional insight in how stability will develop for different hydrofoil and strut configurations.
- **Structural analysis of hydrofoils:** Hydrofoil manufacturers design hydrofoils with designated break points. It is of interest to make an operational analysis of the most probable obstacles that are encountered for a HLAC design to make well-informed decisions on how these break points are implemented.
- **Resistance minimisation with control strategy:** The reduction of resistance with active wave energy extraction through ride control system algorithms can be significant. Additional research in applying this methodology, through deep-learning or other methods, can be a further improvement of the energy efficiency of hydrofoil designs.
- **Signature reducing effects:** The introduction of a hydrofoil design has implications for the signature of the craft. The visual signature is increased due to the increased height, but the wake (reduced resistance), sound (propulsion system), electro-magnetic, and infra-red (propulsion system and other materials) can be decreased. With the limited amount of publicly accessible information it is difficult to make an assessment of this potential. However, it is advised to investigate as it adds to the survivability of the craft.
- **Manoeuvrability:** Submerged hydrofoil craft can offer high manoeuvrability capabilities at high-speed due to the ability of performing banked turns. Manoeuvrability adds to the mobility of the craft and can therefore add to the effectiveness of a hydrofoil craft. Adding this to the operational effectiveness assessment can prove additional potential of this implementation.
- **Additional redundancy for survivability:** The diesel-electric design proposed in this thesis can allow for additional hullborne propulsion to increase redundancy. As the addition of a singular electric propulsion motor is marginal to the complete propulsion system, this can achieve increased survivability at a limited displacement cost.
- **Considerations for a renewed operational concept:** Vertical retraction systems have the added advantage of allowing partial retraction, enabling a foil-assisted planing mode in shallow water. In contrast, lateral and astern retraction do not offer this functionality. Engaging with users of these craft can provide valuable insight into this application's potential, as it involves trade-off between a smooth transition from fully foiling to planing mode or an immediate shift.
- **Potential of waterjet propulsion:** The propulsion assessment of this thesis shows that propeller propulsion has no additional requirements due to the hump region resistance in the proposed designs. However, if waterjets are implemented instead, their lower efficiency at low speed can result in the hump region becoming a critical factor. In such cases, a boost system can become an effective solution.
- **Retraction system design:** For the development of the retraction system, a plethora of linear actuators exist. The weight calculation of the retraction system in this thesis is based on an

electro-mechanical system. However, rapid prototyping of different linear actuation systems can provide insight in the possibilities of other methods of retraction.

- **Shape-adaptive hydrofoils:** The development of shape-adaptive hydrofoils can offer possibilities in the reduction of the complexity of the foil actuation mechanism. For example, by bending the complete hydrofoil no additional flap surfaces are required. Structural assessment can provide insight in the feasibility of such an application.
- **Flexible electrical cabling:** To realise the propulsion system proposed for the HLAC-DE design, the electric cabling for this design must be flexible enough to traverse over the strut retraction length. Extra care should be taken in the facilitation of this flexibility, without reducing the conductivity over time.
- **Cooling system integration:** The cooling system of a hydrofoil craft design is not considered in this study. However, to facilitate the cooling capacity required, also an open-water cooling loop must be integrated within the struts. The strut height and limited inlet diameter add challenges to the cooling system of a hydrofoil design. It is therefore recommended to investigate cooling requirements for a definitive propulsion systems.
- **API development:** In this thesis, webscraping was utilised in combination with the web-based interface of the Foil Design JIP Tool. Developing an Application Programming Interface (API) for this implementation can provide more efficient communication with code developed for further design evaluations and research.

References

ABB. (2022). Product data sheet hes880 traction inverter motor and generator application [retrieved 14-02-2025]. https://search.abb.com/library/Download.aspx?DocumentID=9AKK108467A0006&LanguageCode=en&DocumentPartId=&Action=Launch

ABB. (2023, July). Low voltage water-cooled motors [catalog]. https://search.abb.com/library/Download.aspx?DocumentID=9AKK104379&LanguageCode=en&DocumentPartId=&Action=Launch

ABB. (2024, October). Catalog october 2024 - motors for heavy electric vehicles - amxe series [retrieved 28-1-2025]. https://search.abb.com/library/Download.aspx?DocumentID=9AAU00000000036&LanguageCode=en&DocumentPartId=&Action=Launch

Abbott, I., & Von Doenhoff, A. (1959). *Theory of wing sections, including a summary of airfoil data*. Dover Publications. https://books.google.nl/books?id=DPZYUGNyuboC

AEP. (2018). Cell pack v2 [retrieved 14-02-2025]. https://www.aepint.nl/hybrid-power/products/ultracapacitors-modules/cell-pack/?cn-reloaded=1

Allison, J. (1993). Marine waterjet propulsion. *SNAME Transactions*, *101*, 275–335.

Ambrose, S. E. (1964). Interview with dwight d. eisenhower.

America's cup. (2022, March). Ac75 class rule v2.0. https://www.americascup.com/files/m5498_AC75-Class-Rule-v20.pdf

Ardon, A. (2008). Swedish combat boat 90 (cb 90) in the port of gothenburg stridsbåt 90 [licensed under the Creative Commons Attribution-Share Alike 2.0 Generic license.]. https://commons.wikimedia.org/wiki/File:Stridsb%C3%A5t_90.jpg

Armer, S. (2007). Estimated hull weight. https://www.boatdesign.net/threads/hull-aluminium-weight.15770/

Artemis. (2024). *Ef-24 passenger ferry* [retrieved 11-6-2024]. https://www.artemistechnologies.co.uk/ef-24-passenger-ferry/

Asian Military Defense Review. (2013, December). Sparviero-class patrol boat [retrieved 26-09-2024]. https://www.facebook.com/aseanmildef/posts/sparviero-class-patrol-boatsthe-sparviero-class-are-small-hydrofoil-missile-boat/571788762895502/

Baird Maritime. (2020). Feature: Kawasaki restarts jetfoil production after 25-year halt [retrieved 26-09-2024]. https://www.bairdmaritime.com/passenger/ferry/feature-kawasaki-restarts-jetfoil-production-after-25-year-halt

Bakker, J. J. (2009, July). Hr. ms. johan de witt, amphibious transport ship, (lpd) landing platform dock [licensed under the Creative Commons Attribution 2.0 Generic license.]. https://upload.wikimedia.org/wikipedia/commons/b/b8/HNLMS_Johan_de_Witt_%28L801%29_%281%29.jpg

Barden, T. B., & Binns. (2012). On the road to establishing ventilation probability for moth sailing dinghies. https://api.semanticscholar.org/CorpusID:55552211

Bass, D. W., Molyneux, W., & McTaggart, K. (2004). Simulating wave action in the well deck of landing platform dock ships using computational fluid dynamics. *Warship*. https://nrc-publications.canada.ca/eng/view/object/?id=98b94857-2619-429a-b870-dd1768ec10f1

Beyond Motors. (2025). E-motors [retrieved 28-1-2025]. https://www.beyondmotors.io/e-motors

Bieker Boats. (2012, November). Retracting drive unit [retrieved 13-09-2024]. https://biekerboats.blogspot.com/2012/11/retracting-drive-unit.html

Bikar. (2024). En aw-5083 [retrieved 19-1-2025]. https://www.bikar.com/fileadmin/Unterlagen_BIKAR/Unterlagen_BIKAR_eng/5083-complete-en.pdf

Blazevic, R. L. (1988, February). Phm-1 tied up at trumbo point, key west, fl [retrieved 26-09-2024]. https://www.navsource.org/archives/12/1601.htm

Blount, D., & Bartee, R. (1997). Design of propulsion systems for high-speed craft. *Marine Technology*, *34*, 276–292. https://doi.org/10.5957/mt1.1997.34.4.276

Boudain. (2024). Genset 12m26.2 [retrieved 30-8-2024]. https://baudouin.com/engine_product/12m26-2-2/

Brans, S. (2021). *Applying a needs analysis to promote daughter craft for year-round access to far-offshore wind turbines* [Master's thesis, Delft University of Technology]. http://resolver.tudelft.nl/uuid:c1de0299-b8f5-42a8-9a0e-71549756f57d

Brizzolara, S. (2015). A new family of dual-mode super-cavitating hydrofoils. *SMP 2015*. https://www.marinepropulsors.com/proceedings/2015/MB2-3.pdf

Brogen Motors. (2025). Integrated axle with axial flux motors [retrieved 28-1-2025]. https://brogenmotors.com/product/axial-flux-motor/#4NAKR2d

Brown, A. (2013). Application of operational effectiveness models in naval ship concept exploration and design. *Ciencia y tecnología de buques*, *7*, 9. https://doi.org/10.25043/19098642.80

Brown, A., & Salcedo, J. (2003). Multiple-objective optimization in naval ship design. *Naval Engineers Journal*, *115*(4), 49–62. https://doi.org/https://doi.org/10.1111/j.1559-3584.2003.tb00242.x

Buermann, T. M., Leehey, P., & Stillwell, J. J. (1953). An appraisal of hydrofoil supported craft. *The Society of Naval Architects and Marine Engineers*. https://www.foils.org/wp-content/uploads/2018/01/SNAMEtransactionsVol61-1953.pdf

Buitendijk, M. (2023, March). Dutch navy gets twenty new landing craft: Swz: Maritime. https://swzmaritime.nl/news/2023/03/24/dutch-navy-gets-twenty-new-landing-craft/

Buitendijk, M. (2024, March). Dutch navy gets six new amphibious transport ships. https://swzmaritime.nl/news/2024/03/07/dutch-navy-gets-six-new-amphibious-transport-ships/

Burman, M., Kuttenkeuler, J., Stenius, I., Garme, K., & Rosén, A. (2016). Comparative life cycle assessment of the hull of a high-speed craft. *Proceedings of the Institution of Mechanical Engineers, Part M*, *230*(2), 378–387. https://doi.org/10.1177/1475090215580050

Candela. (2023). C-8 owners manual [Owners manual]. https://help.candela.com/media/manual_c8_en.pdfhttps://help.candela.com/media/manual_c8_en.pdf

Candela. (2024a, May). https://candela.com/

Candela. (2024b, May). https://candela.com/p-12-shuttle/

Carlton, J. S. (2019, January). Chapter 16 - Waterjet Propulsion. In J. S. Carlton (Ed.), *Marine Propellers and Propulsion (Fourth Edition)* (pp. 399–408). Butterworth-Heinemann. https://doi.org/10.1016/B978-0-08-100366-4.00016-X

Caterpillar. (2024a). C18 acert tier 3 [retrieved 30-8-2024]. https://www.cat.com/nl_NL/products/new/power-systems/marine-power-systems/commercial-propulsion-engines/18493267.html

Caterpillar. (2024b). Marine power solutions [Brochure].

Caterpillar. (2024c). Scheepsgeneratorsets c18 (srmp) scheepsaggregaat [retrieved 30-8-2024]. https://www.cat.com/nl_NL/products/new/power-systems/marine-power-systems/marine-generator-sets/1000024700.html

Caterpillar. (2024d). Scheepsgeneratorsets c32 acert imo ii [retrieved 30-8-2024]. https://www.cat.com/nl_NL/products/new/power-systems/marine-power-systems/marine-generator-sets/18495302.html

Cauwenberghe, L. V. (2025). *Developing a new hull design for the tenders of 'het loodswezen' to improve the seakeeping behaviour* [Master's thesis, Delft Universisty of Technology]. https://resolver.tudelft.nl/uuid:680b4a5b-7932-4667-9421-ea551a75c738

Chai, M., Bonthapalle, D. R., Sobrayen, L., Panda, S. K., Wu, D., & Chen, X. (2018). Alternating current and direct current-based electrical systems for marine vessels with electric propulsion drives. *Applied Energy*, *231*, 747–756. https://doi.org/https://doi.org/10.1016/j.apenergy.2018.09.064

Charisi, N. D., Hopman, H., & Kana, A. (2022, June). *Early-Stage Design of Novel Vessels: How can we Take a Step Forward?* https://doi.org/10.5957/IMDC-2022-239

Cirelli, M., Giannini, O., Cera, M., De Simoni, F., Valentini, P., & Pennestrì, E. (2021). The mechanical efficiency of the rzeppa transmission joint. *Mechanism and Machine Theory*, *164*, 104418. https://doi.org/https://doi.org/10.1016/j.mechmachtheory.2021.104418

Clark, D. J., Ellsworth, W. M., & Meyer, J. R. (2004). The quest for speed at sea [retrieved 03-06-2024]. *Technical Digest*. https://archive.foils.org/02_Papers%20dnloads/041115NSWCTD_QuestSpeed.pdf

Clement, E. P. (1976). A lifting surface approach to planing boat design. *International shipbuilding progress*, *23*, 307–312. https://api.semanticscholar.org/CorpusID:108915592

Costa, R. (2021, January). Catch the wind [retrieved 4-10-2024]. https://businessmirror.com.ph/2021/01/23/catch-the-wind/

Cronborg, C. (2022). Volvo penta launches enabler for marine electric propulsion. *Volvo Penta*. https://www.volvopenta.com/about-us/news-page/2022/sep/volvo-penta-launches-enabler-for-marine-electric-propulsion/

D'Amato, E., Notaro, I., Piscopo, V., & Scamardella, A. (2023). Hydrodynamic design of fixed hydrofoils for planing craft. *Journal of Marine Science and Engineering*, *11*(2). https://www.mdpi.com/2077-1312/11/2/246

Damen. (2023). Product sheet lpd enforcer. https://media.damen.com/image/upload/v1694075766/catalogue/defence-and-security/enforcers/enforcer-12026/product-sheet-lpd-enforcer-12026-13226ed.pdf

Damen. (2024a). Fac 1604 - fast assault craft [retrieved 4-10-2024]. https://www.damen.com/vessels/defence-and-security/landing-crafts/fac-1604

Damen. (2024b). Landing craft vehicle personnel (lcvp) [retrieved 1-8-2024]. https://www.damen.com/vessels/defence-and-security/landing-crafts/lcvp-1604

Daniel, I., & Ishai, O. (2006). *Engineering mechanics of composite materials*. Oxford University Press. https://books.google.nl/books?id=x5S_QgAACAAJ

de Wit, R., & Thomeer, E. (2022). Force design - littoral raiding force combat operations from the sea. *Marineblad*, (2). https://www.kvmo.nl/images/Marineblad/2022/Nummer%202/De%20Wit,%20R.%20&%20Thomeer,%20E.,%20'Force%20Design.%20Littoral%20Raiding%20Force,%20Combat%20operations%20from%20the%20sea',%20Marineblad,%20nr.%202,%20jrg.%20132%20(maart%202022)%20p.%204-9.pdf

De Luca, F., & Pensa, C. (2017). The naples warped hard chine hulls systematic series. *Ocean Engineering*, *139*, 205–236. https://doi.org/https://doi.org/10.1016/j.oceaneng.2017.04.038

Deyzen, A. (2013, January). *Improving the operability of planing monohulls sailing in head seas using automated proactive control of the thrust - proof of concept* [Doctoral dissertation, Delft University of Technology].

Directorate-General for Defence Industry and Space. (2021). Transflytor - troop transportation flying vector [retrieved 3-8-2024]. https://defence-industry-space.ec.europa.eu/transflytor_en

Dockstavarvet. (2024). References in sweden [retrieved 2-8-2024]. https://www.dockstavarvet.se/references/sweden/

Doornebos, P. (2022, July). *Design and feasibility of a 30- to 40-knot emission-free ferry* [Master's thesis, Delft University of Technology]. https://repository.tudelft.nl/record/uuid:6973eddc-1bfc-4299-ad19-bfc231c5316b

Doornebos, P., Francis, M., le Poole, J., & Kana, A. (2023). Design and feasibility of a 30- to 40-knot emission-free ferry. *International Shipbuilding Progress*, *70*, 81–114. https://doi.org/10.3233/ISP-230005

Dutch Ministry of Defence. (2020, March). Zr.ms. rotterdam. https://www.defensie.nl/organisatie/marine/eenheden/schepen/zr-ms-rotterdam

Dutch Ministry of Defense. (2023a, March). Nieuwe landingsvaartuigen voor mariniers in alles beter [retrieved 20-6-2024]. https://www.defensie.nl/actueel/nieuws/2023/03/22/nieuwe-landingsvaartuigen-voor-mariniers-in-alles-beter

Dutch Ministry of Defense. (2023b, August). Frisc - motorboot [retrieved 20-6-2024]. https://www.defensie.nl/onderwerpen/materieel/schepen/frisc-motorboot-fast-raiding-interception-and-special-forces-craft

Dymarski, C., & Skorek, G. (2006). A design concept of main propulsion system with hydrostatic transmission gear for inland waterways ship. *Polish Maritime Research*, *2*, 57–61. https://yadda.icm.edu.pl/baztech/element/bwmeta1.element.baztech-article-BWM3-0007-0025

Edorado. (2024, June). https://edorado.com/

Emirates Team New Zealand. (2022, May). Emirates team new zealand take flight in hydrogen powered foiling chase boat [retrieved 4-10-2024]. https://emirates-team-new-zealand.americascup.com/en/news/549_EMIRATES-TEAM-NEW-ZEALAND-TAKE-FLIGHT-IN-HYDROGEN-POWERED-FOILING-CHASE-BOAT.html

Emrax. (2025). Emrax electric motors/generators [retrieved 28-1-2025]. https://emrax.com/e-motors/

Enata. (2024). Marine [retrieved 31-05-2024]. https://enata.com/marine#marineFoiler

E.U. Copernicus Marine Service Information (CMEMS). Marine Data Store (MDS). (2024). Global ocean waves reanalysis [accessed on 05-08-2024]. https://doi.org/https://doi.org/10.48670/moi-00022

E.U. Copernicus Marine Service Information (CMEMS). Marine Data Store (MDS). (2025). Global ocean waves analysis and forecast [accessed on 05-02-2025]. https://doi.org/https://doi.org/10.48670/moi-00017

Evolito. (2025). Axial flux motors [retrieved 28-1-2025]. https://evolito.aero/axial-flux-motors/

Faltinsen, O. M. (2005). *Hydrodynamics of high-speed marine vehicles*. Cambridge university press.

Finnish Defence Force. (2024). Jehu class [retrieved 2-8-2024]. https://puolustusvoimat.fi/en/equipment#/asset/view/id/312

Francis, M. A. J. (2019, August). *Feasibility study of a fast electric passenger ferry* [Master's thesis, Delft University of Technology]. https://repository.tudelft.nl/record/uuid:cf138038-adc9-41b6-a08f-3f2e9359a3fc

Franklin, G. F., Powell, J. D., & Emami-Naeini, A. (2009). *Feedback control of dynamic systems*. Pearson.

Frauenberger, H. C. (1982). Shimrit - mark ii hydrofoil for the israeli navy. *First International Hydrofoil Society Conference*, 157–170. https://foils.org/wp-content/uploads/2017/11/0137-IHS-Nova-Scotia-Conference-Papers-Jul-82.pdf

Gabrielli, G., & von Karman, T. (1950). What price speed? *Mech eng.*, *72*, 775–781.

Gaggero, S., & Brizzolara, S. (2009). A panel method for trans-cavitating marine propellers. *CAV2009*.

Gelling, J., & Keuning, L. J. (2011). Recent developments in the design of fast ships. *Ciencia y tecnología de buques*, *5*, 57. https://doi.org/10.25043/19098642.51

Gemini. (2024). Gemini wind park [retrieved 14-02-2025]. https://www.geminiwindpark.nl/the-wind-park

General Electric. (2017). Lm500 marine gas turbine [retrieved 30-8-2024]. https://www.geaerospace.com/military-defense/engines/lm500

General Motors. (1986). Allison industrial gas turbines 501-k 570-k [retrieved 30-8-2024]. https://intpower.com/wp-content/uploads/1986/10/501-brochure.pdf

German Maritime Museum. (2024). Hydrofoil wss 10 [retrieved 4-10-2024]. https://www.dsm.museum/en/museum/exhibits/hydrofoil-wss-10

Giallanza, A., Marannano, G., Morace, F., & Ruggiero, V. (2020). Numerical and experimental analysis of a high innovative hydrofoil. *International Journal on Interactive Design and Manufacturing (IJIDeM)*, *14*. https://doi.org/10.1007/s12008-019-00616-0

Godø, J. M. K. (2024). *Zero-emission hydrofoil fast ferries: Design, modelling, and performance evaluation* [Doctoral dissertation, Norwegian University of Science and Technology]. https://ntnuopen.ntnu.no/ntnu-xmlui/handle/11250/3172953

Godø, J. M. K., & Steen, S. (2023). An efficient method for unsteady hydrofoil simulations, based on non-linear dynamic lifting line theory. *Ocean Engineering*, *288*, 116001. https://doi.org/https://doi.org/10.1016/j.oceaneng.2023.116001

Godø, J. M. K., Steen, S., Barrett, D., & Triantafyllou, M. S. (2024a). Active wave energy extraction by hydrofoil vessels through deep reinforcement learning-based flight control. *Ocean Engineering*, *312*. https://doi.org/10.1016/j.oceaneng.2024.119236

Godø, J. M. K., Steen, S., & Faltinsen, O. M. (2024b). A resistance model for hydrofoil fast ferries with fully submerged foil systems. *Ocean Engineering*, *301*, 117503. https://doi.org/https://doi.org/10.1016/j.oceaneng.2024.117503

Grevink, J. (2022a). Mt44006: (water/pump)jet propulsion [presentation].

Grevink, J. (2022b). Mt44006: Podded propulsors [presentation].

Gurit. (2015, April). Composite technology for work boats - can composites pay their way? https://www.gurit.com/wp-content/uploads/bsk-pdf-manager/2022/08/gurit-delegate-pack-composite-work-boats-fc.pdf

Habermaas, J., & Thurner, J. (2020). Variable speed generator sets offer advantages for commercial ships. *MTU*. https://www.mtu-solutions.com/cn/en/technical-articles/2020/variable-speed-generator-sets-offer-advantages-for-commercial-sh.html

Häggblom, R. (2019, May). Combat boats and landing crafts [retrieved 2-8-2024]. https://corporalfrisk.com/2019/05/29/combat-boats-and-landing-crafts/

Her Majesty's Stationary Office and the UK Hydrographic Office. (2015, November). British isles and north west europe digital selective calling (dsc) limits of sea areas. https://rnli-lrc.org.uk/sea_areas.html

Hertzberg, T. (2009). *Lass, lightweight construction application at sea*. SP Technical research institute of Sweden. http://e-lass.eu.loopiadns.com/media/2016/08/LASS-SP_Report_2009_13.pdf

Hoerner, S. (1965). *Fluid-dynamic drag: Practical information on aerodynamic drag and hydrodynamic resistance*. Hoerner Fluid Dynamics. https://books.google.nl/books?id=abU8AAAAIAAJ

Hoerner, S., Michel, W., Ward, L. W., & Buermann, T. M. (1954). *Hydrofoil handbook, hydrodynamic characteristics of components*. Bath Iron Works Corporation By Gibbs; Cox. https://www.foils.org/wp-content/uploads/2018/01/HFhdbkVol_II_1954.pdf

Holtrop, J., & Mennen, G. (1982). An approximate power prediction method. *International Shipbuilding Progress*.

Honeywell. (2000, May). Agt1500 turbine technology [retrieved 30-8-2024]. https://web.archive.org/web/20160909103204/http://www51.honeywell.com/aero/common/documents/myaerospacecatalog-documents/SurfaceSystems/AGT1500_Turbine_Technology.pdf

Hopman, H., Kaapsenberg, G. K., & Krikke, E. M. (1994). Design and hydromechanic aspects of the amphibious transport vessel for the royal netherlands navy. *Naval Engineers Journal*, *106*(3), 163–174. https://doi.org/https://doi.org/10.1111/j.1559-3584.1994.tb02849.x

Hosseini, Y. (2024, July). Handling obstacles: Logs and hydrofoil boats [retrieved 25-09-2024]. https://candela.com/handling-obstacles-logs-and-hydrofoil-boats/

Hydrosta. (2024). Hp inline - parallel hybrid propulsion by hydrosta [retrieved 28-1-2025]. https://hydrosta.nl/uploads/documents/FolderHPInLine.pdf

IMO. (2021). *Fourth greenhouse gas study 2020* (tech. rep.). London SE1 7SR. https://www.imo.org/en/OurWork/Environment/Pages/Fourth-IMO-Greenhouse-Gas-Study-2020.aspx

IMOA. (2016). Propelling the boating world [retrieved 19-1-2025]. https://www.imoa.info/download_files/molyreview/excerpts/16-1/Boat_shafts.pdf?utm_source=chatgpt.com

IPCC. (2023). *Climate change 2023: Synthesis report* (tech. rep.). Contribution of Working Groups I, II, III to the Sixth Assessment Report of the Intergovernmental Panel on Climate Change [Core Writing Team, H. Lee, and J. Romero (eds.)]. IPPC, Geneva, Switzerland. https://doi.org/10.59327/IPCC/AR6-9789291691647

ITTC. (1957). Proceedings of the 8th ittc.

ITTC. (2017). *Ittc quality system manual, recommended procedures and guidelines, procedure resistance test: Technical report* (tech. rep.). International Towing Tank Conference. https://www.ittc.info/media/7797/4-resistance-committee.pdf

James, T. (2024, August). Spirit bartech f35 launches with acclaim: 100% electric, 100 nautical miles! https://www.bartechnologies.uk/leisure-boats/spiritbartech35ef-launches-with-acclaim/

Jansen, S. (2022, June). Towards a parametric optimization tool for hydrofoil design. http://essay.utwente.nl/90692/

Johnston, R. J. (1982). History of us involvement in developing the hydrofoil. *First International Hydrofoil Society Conference*, 5–50. https://foils.org/wp-content/uploads/2017/11/0137-IHS-Nova-Scotia-Conference-Papers-Jul-82.pdf

Johnston, R. J. (1985). Hydrofoils. *Naval Engineers Journal*, *97*(2), 142–199. https://foils.org/wp-content/uploads/2017/12/Naval-Engineers-Journal-Modern-Ships-and-Craft-71242.pdf

Journee, J., Massie, W., & Huijsmans, R. (2015). *Offshore hydromechanics* (Vol. Third edition). Delft University of Technology, Faculteit Civiele Techniek en Geowetenschappen.

Kamp, H. (2021, October). Vervanging en instandhouding frisc (fast raiding, interception and special forces craft) [letter to parliament]. https://www.rijksoverheid.nl/documenten/kamerstukken/2021/10/25/kamerbrief-behoeftestelling-vervanging-en-instandhouding-fast-raiding-interception-and-special-forces-craft

Kaplan, P., Breslin, J. P., & Jacobs, W. R. (1960). Evaluation of the theory for the flow pattern of a hydrofoil of finite span. *Journal of Ship Research*, *4*(01), 13–29. https://doi.org/10.5957/jsr.1960.4.1.13

Karremann, J. (2015, January). Zweeds materieel onderweg naar den helder [retrieved 1-8-2024]. https://marineschepen.nl/nieuws/zweeds-materieel-naar-den-helder-090115.html

Keeney, R. L., & Raiffa, H. (1993). *Decisions with multiple objectives: Preferences and value trade-offs*. Cambridge University Press.

Keuning, L. J. A. (1994, September). *Nonlinear behaviour of fast monohulls in head waves* [Doctoral dissertation, Delft University of Technology]. https://api.semanticscholar.org/CorpusID:118221808

Keuning, L. J. A. (1997). Seakeeping of high-speed craft. *25th WEGEMT Graduate school on Small craft technology*, 367–377. https://repository.tudelft.nl/islandora/object/uuid%3Ae4aaa1f4-0c3f-4c98-96dc-daafa1fb71bb

Keuning, L. J., Gerritsma, J., & van Terwisga, P. (1992). *Resistance tests of a series planing hull forms with 30 degrees deadrise angle, and a calculation model based on this and similar systematic series*. Delft University of Technology, Faculty of Mechanical Engineering; Marine Technology. https://books.google.nl/books?id=TE8yAAAACAAJ

Keuning, L. J., & Hillege, L. The results of the delft systematic deadrise series. In: In *Fast2017*. 2017. https://resolver.tudelft.nl/uuid:6ddc5192-107f-47de-8669-38114b9ce16d

Keuning, L. J., & Ligtelijn, D. (2017). High speed craft. *Encyclopedia of Maritime and Offshore Engineering*. https://doi.org/10.1002/9781118476406.emoe540

Kim, D. H., Kim, N., Cho, H., & Kim, S. Y. (2014). A guidance logic development for wake homing guidance system (iccas 2014). *2014 14th International Conference on Control, Automation and Systems (ICCAS 2014)*, 190–194. https://doi.org/10.1109/ICCAS.2014.6987984

Kim, S., & Jeon, H. (2022). Comparative analysis on ac and dc distribution systems for electric propulsion ship. *Journal of Marine Science and Engineering*, *10*(5). https://www.mdpi.com/2077-1312/10/5/559

King, J. H., & Devine, M. D. (1981). Hande - a computer-aided design approach for hydrofoil ships. *Naval Engineers Journal*, *93*(2), 120–130. https://doi.org/https://doi.org/10.1111/j.1559-3584.1981.tb01611.x

Kirkman, K., & Kloetzli, J. (1980). Scaling problems of model appendages. *Proceedings of the 19th American Towing Tank Conference*.

Klein Woud, J., & Stapersma, D. (2002). *Design of propulsion and electric power generation systems*. IMarEST.

Klein Woud, J., & Stapersma, D. (2016). *Selected chapters of design of auxiliary systems, shafting and flexible mounting*. TU Delft.

Kongsberg. (2018). Waterjets aluminium series [retrieved 19-1-2025]. https://www.kongsberg.com/contentassets/8b800421dee947a890f80f746b98b70d/03.waterjet_2p_01.06.18.pdf

Kongsberg. (2020). Kamewa steel series waterjets [retrieved 23-8-2024]. https://www.kongsberg.com/maritime/products/propulsors-and-propulsion-systems/waterjets/steel-waterjets/s-3-ca/

Kossiakoff, A., Biemer, S., Seymour, S., & Flanigan, D. (2020). *Systems engineering principles and practice*. Wiley. https://books.google.nl/books?id=gGzoDwAAQBAJ

Kundu, P., Cohen, I., & Dowling, D. (2015). *Fluid mechanics*. Academic Press. https://doi.org/https://doi.org/10.1016/C2012-0-00611-4

Kyunghwa Kim, G. R., Kido Park, & Chun, K. (2018). Dc-grid system for ships: A study of benefits and technical considerations. *Journal of International Maritime Safety, Environmental Affairs, and Shipping*, *2*(1), 1–12. https://doi.org/10.1080/25725084.2018.1490239

Lastiawan, W.-W. (2019, February). Menguji kmc komando milik tni ad; bisa manuver kecepatan tinggi, kapal anti terbalik [retrieved 4-10-2024]. https://www.prokal.co/advertorial/1773777020/menguji-kmc-komando-milik-tni-ad-bisa-manuver-kecepatan-tinggi-kapal-anti-terbalik

Leclanché. (2024). Power m2 modules [retrieved 14-02-2025]. https://www.leclanche.com/wp-content/uploads/2020/10/LECLANCHE-M2-module-LT34-LTO-34Ah.pdf

Lundin, A., & Eriksson, L. (2021). *Concept development and design of a retractable hydrofoil systems* [Master's thesis, Kungliga Tekniska Högskolan] [Dissertation]. https://urn.kb.se/resolve?urn=urn:nbn:se:kth:diva-305446

Lundin, S. R. (2023). Outsource littoral maneuver to nsw. *U.S. Naval Institute*, *149/6/1,444*. https://www.usni.org/magazines/proceedings/2023/june/outsource-littoral-maneuver-nsw

MAN. (2024). Marine high speed engines for pleasure boats [retrieved 30-8-2024]. https://www.man.eu/engines/en/products/marine/yacht-engines/yacht.html

Man Rollo. (2024). Marine - high speed proulsion engines [Brochure]. https://manrollo.com/wp-content/uploads/Marine_Commercial_220512_web-website.pdf

Mantaray. (2024). Mantaray m25 [retrieved 19-8-2024]. https://www.mantaraycraft.com/m25

Margés, J. (2018). Frisc kent eigen kracht niet. *Alle Hens*, *01*. https://magazines.defensie.nl/allehens/2018/01/00_frisc

Marineschepen.nl. (2010, October). https://marineschepen.nl/nieuws/Zweedse_Combat_Boats_uitgeleend_aan_Nederland_en_UK.html

Marshall, J. T., & Riley, M. R. (2020, February). *A comparison of the mechanical shock mitigation performance of a shock isolation seat subjected to laboratory drop tests and at-sea seakeeping trials* (tech. rep.). Naval Surface Warfare Center. https://apps.dtic.mil/sti/trecms/pdf/AD1110574.pdf

Martens, P. (2025, January 13). Servogear [personal communication].

Mathijsen, D. (2016). Now is the time to make the change from metal to composites in naval shipbuilding. *Reinforced Plastics*, *60*(5), 289–293. https://doi.org/https://doi.org/10.1016/j.repl.2016.08.003

McKesson, C. (2014). *The practical design of advanced marine vehicles*. CreateSpace Independent Publishing Platform. https://books.google.nl/books?id=vb-1oAEACAAJ

Merivoimat - The Finnish Navy. (2023, November). The royal navy's landing ship dock rfa mounts bay participates in exercise freezing winds 23 [retrieved 2-8-2024]. https://www.facebook.com/Merivoimat/?locale=nl_NL

Mewis, F. (2002). The efficiency of pod propulsion. *HADMAR 2001*. https://api.semanticscholar.org/CorpusID:209898546

Meyer, J. R. (1990). *Ships that fly: A story of the modern hydrofoil*. Hydrofoil Technology. https://www.foils.org/wp-content/uploads/2018/01/ShipsThatFly.pdf

Military review. (2019, December). https://en.topwar.ru/165694-italjanskij-urodec-raketnye-katera-tipa-sparviero.html

Minerva, L., & Montero, F. (2021). Experimental investigations on conventional and unconventional boost systems to assist take-off of hydrofoil crafts. *7th High Performance Yacht Design Conference 2021*. https://www.proceedings.com/content/058/058917webtoc.pdf

Minerva, L. F., Odendaal, K., Marelli, G., & Scholcz, T. (2024). Early design of hydrofoils: Foil design jip overview and methods. *28th International HISWA Symposium*. https://hiswasymposium.com/wp-content/uploads/HISWA-2024-Early-Design-of-Hydrofoils_Foil-Design-JIP-overview-and-methods_Minerva-Odendaal-Marelli-Scholcz.pdf

Mohl, M. (1971). Uss flagstaff off the coast of florida [public domain]. https://www.navsource.org/archives/12/1001.htm

Molland, A., & Turnock, S. (2021). *Marine rudders, hydrofoils and control surfaces: Principles, data, design and applications*. Elsevier Science. https://doi.org/https://doi.org/10.1016/C2020-0-01238-7

Molland, A. F., Turnock, S. R., & Hudson, D. A. (2011). *References*. https://app.knovel.com/hotlink/khtml/id:kt00UBHNE3/ship-resistance-propulsion/ship-resis-references-3

Montoya, L. (2005). Shaft angles [retrieved 13-09-2024]. http://www.ricepropulsion.com/cartas/TNL49/Tnl49.htm

Mørch, J. (1992). *Aspect of hydrofoil design with emphasis on hydrofoil interaction in calm water, dr. ing* [Doctoral dissertation, Department of Marine Hydrodynamics, NTNU, Trondheim, Norway].

Mouritz, A., Gellert, E., Burchill, P., & Challis, K. (2001). Review of advanced composite structures for naval ships and submarines. *Composite Structures*, *53*(1), 21–42. https://doi.org/https://doi.org/10.1016/S0263-8223(00)00175-6

National Museum of the U.S. Navy. (1958, September). Super cavitating propeller in the david taylor model basin [Public domain]. https://commons.wikimedia.org/wiki/File:330-ps-9124-usn-710228_15726002325_o.jpg

NATO. (2024). Defence expenditure of nato countries (2014-2024). https://www.nato.int/cps/en/natohq/news_226465.htm

Naval News. (2024, June). Sweden orders new cb90 combat boats from saab. https://www.navalnews.com/naval-news/2024/06/sweden-orders-new-cb90-combat-boats-from-saab/

Naval Technology. (2022, April). https://www.naval-technology.com/projects/combatboat90/?cf-view

Naval Technology. (2023, November). Jurmo-class landing craft (watercat m12), finland [retrieved 4-10-2024]. https://www.naval-technology.com/projects/jurmo-class-landing-craft-finland/?cf-view

Navier. (2024). N30 - the boat of the future [retrieved 19-8-2024]. https://www.navierboat.com/

Navy Lookout. (2024, April). https://www.navylookout.com/ship-to-shore-new-solutions-for-getting-troops-onto-the-beach/

Netherlands Ministry of Defence. (2023a, May). Lcvp-landingsvaartuig (personeel) [retrieved 25-7-2024]. https://www.defensie.nl/onderwerpen/materieel/schepen/lcvp-landingsvaartuig-personeel

Netherlands Ministry of Defence. (2023b, November). European tendering procedure for the delivery of littoral assault craft including associated goods and services.

Netherlands Ministry of Defence. (2024a). *Protocol panship simulation*.
Netherlands Ministry of Defence. (2024b, March). Amfibisch transportschip (lpd) [retrieved 25-7-2024]. https://www.defensie.nl/onderwerpen/materieel/schepen/amfibische-transportschepen
Netherlands Ministry of Defence. (2024c, May). Joint logistic support ship (jss) [retrieved 25-7-2024]. https://www.defensie.nl/onderwerpen/materieel/schepen/joint-logistic-support-ship-jss
Newman, J., & Grue, J. (2018). *Marine hydrodynamics, 40th anniversary edition*. MIT Press. https://books.google.nl/books?id=WptIDwAAQBAJ
Newton, R., & Rader, H. (1961). Performance data of propellers for high-speed craft. *The Royal Institution of Naval Architects*, *103*(2).
Ng, M. (2022). On the feasibility of speed limits in ocean container shipping. *Maritime Transport Research*, *3*, 100067. https://doi.org/https://doi.org/10.1016/j.martra.2022.100067
Nishanth, F., Van Verdeghem, J., & Severson, E. L. (2023). A review of axial flux permanent magnet machine technology. *IEEE Transactions on Industry Applications*, *59*(4), 3920–3933. https://doi.org/10.1109/TIA.2023.3258933
NORDFORSK. (1987). *Assessment of ship performance in a seaway: The nordic co-operative project: "seakeeping performance of ships"*. Marintek. https://books.google.nl/books?id=hdaQOgAACAAJ
Oh, D., Jung, S., & Jeong, S. (2018). Effect of a Lightweight Hull Material and an Electric Propulsion System on Weight Reduction: Application to a 45ft CFRP Electric Yacht. *Journal of the Korean Society of Marine Environment and Safety*, *24*, 818–824. http://www.kosomes.or.kr/journalarticle.php?code=64534
Olofsson, K., Arnestad, G., Lönnö, A., Hedlund-Åström, A., Jansson, T., & Hjortberg, M. (2008). A high-speed craft with composite hull. *Proc. of the 13th European Conference of Composite Materials*.
Ozberk, T. (2023, May). Norway procures 2 ccm special forces boats from the us [retrieved 4-8-2024]. https://www.navalnews.com/naval-news/2023/05/norway-procures-2-ccm-special-forces-boats-from-the-us/
Pedersen, K., Emblemsvåg, J., Bailey, R., Allen, J. K., & Mistree, F. (2000). Validating design methods & research: The validation square. *Proceedings of DETC '00*.
Peek, R., & Bauer, L. (1981). M151 transmission for mark ii hydrofoils. *AIAA 6th Marine Systems Conference*, (81-2084). https://foils.org/m-151-transmission-for-mark-ii-hydrofoils/
Peterson, R., Pierce, E., Price, B., & Bass, C. (2004). Shock mitigation for the human on high speed craft: Development of an impact injury design rule. *RTO-MP-AVT-110*, 14. https://www.sto.nato.int/publications/STO%20Meeting%20Proceedings/RTO-MP-AVT-110/MP-AVT-110-31.pdf
Phi-Power. (2025). Ph-range [retrieved 28-1-2025]. https://www.phi-power.com/en/phi-power-motor-series-2/racing-high-performance/
Pugh, S. (1991). *Total design : Integrated methods for successful product engineering*. Addison-Wesley Pub. Co. http://books.google.com/books?id=RKIQAQAAMAAJ
Puolustusvoimat. (2024). Jehu class [retrieved 4-10-2024]. https://puolustusvoimat.fi/en/equipment#/asset/view/id/312
Rawson, K., & Tupper, E. (2001). 16 - particular ship types. In K. Rawson & E. Tupper (Eds.), *Basic ship theory (fifth edition)* (Fifth Edition, pp. 655–694). Butterworth-Heinemann. https://doi.org/https://doi.org/10.1016/B978-075065398-5/50019-4
Reddy, J. N. (2003). *Mechanics of laminated composite plates and shells*. Taylor & Francis Group. https://doi.org/https://doi.org/10.1201/b12409
Roeland, J. (2018). Lcvp l-9571 in willemstad nl. https://www.vesselfinder.com/nl/ship-photos/388588
Rolling, H. D. (1974, May). *Model resistance data of series 65 hull forms applicable to hydrofoils and planing craft* (tech. rep.). Naval Ship Research and Development Center. Bethesda, Maryland. https://foils.org/wp-content/uploads/2017/11/0139-Model-Resistance-Data-of-Series-65-Hull-Forms.pdf
Rolls-Royce. (2024). M250/rr300 - 2024 first network directory [retrieved 28-1-2025]. https://www.rolls-royce.com/products-and-services/civil-aerospace/helicopters/m250-turboshaft.aspx#section-training
Rose, R. M. (1964). Rough-water performance of the hs denison. *Journal of Aircraft*, *1*(5), 273–279. https://doi.org/10.2514/3.59208

Russian Ships. (2024a). Patrol boats - project 03160 [retrieved 4-10-2024]. https://russianships.info/eng/warfareboats/project_03160.htm

Russian Ships. (2024b). Small anti-submarine ship [retrieved 4-10-2024]. https://russianships.info/eng/warships/project_1141.htm

Saab. (2021). Cb90 next generation at a glance [retrieved 20-6-2024]. https://www.saab.com/contentassets/e40e2f9b6b3b4c1f8e4b86080dc36111/cb90-ng-at-a-glance.pdf

Saaty, T. L. (1990). How to make a decision: The analytic hierarchy process [Desicion making by the analytic hierarchy process: Theory and applications]. *European Journal of Operational Research*, *48*(1), 9–26. https://doi.org/https://doi.org/10.1016/0377-2217(90)90057-I

Saito, Y., Oka, M., Ikebuchi, K., & Asao, M. (1991). Seakeeping of foil catamarans. *FAST'91*, *2*, 1013–1028.

Savitsky, D. (1964). Hydrodynamic Design of Planing Hulls. *Marine Technology and SNAME News*, *1*(04), 71–95. https://doi.org/10.5957/mt1.1964.1.4.71

Scania. (2024a). Di16 077m. 662 kw (900 hp) [retrieved 30-8-2024]. https://www.scania.com/content/dam/scanianoe/market/master/products-and-services/engines/pdf/specs/marine/DI16077M_662kW.pdf

Scania. (2024b). Electric power solutions [retrieved 28-1-2025]. https://www.scania.com/group/en/home/products-and-services/engines/electrified-power-systems.html

Scania. (2025). Specifications of maritime energy systems [retrieved 28-1-2025]. https://www.scania.com/nl/nl/home/products/power-solutions/marine-power-systems/marine-power-systems-specifications.html

Schachter, R., & Fonteles, G. (2022). Preliminary design dimensioning of hydrofoil boats with fully submerged and surface piercing foils. *Mar Syst Ocean Technol*, *17*, 53–69. https://doi.org/https://doi.org/10.1007/s40868-022-00113-2

Schlichting, H. (1979). *Boundary-layer theory*. McGraw-Hill Book Company.

Scott, R. (2023, December). Bae systems lifts veil on littoral strike craft concept. https://www.navalnews.com/naval-news/2023/12/bae-systems-lifts-veil-on-littoral-strike-craft-concept/

SEAir. (2022). Transflytor press release [retrieved 3-8-2024]. https://gican.asso.fr/wp-content/uploads/2023/06/pj_transflytor_press_release_seair_221018.pdf

SEAir International. (2023). Artistic impression of the transflytor project [retrieved 21-6-2024]. https://x.com/SEAirFlyingBoat/status/1663836776769650689/photo/1

SEAir solutions. (2024). https://seair-solutions.com/

SEALANCE. (2023). Transflytor, the latest engineered foiling boat by seair, explores sealence technology [retrieved 3-8-2024]. https://www.linkedin.com/posts/sealence-s-p-a-s-b_technology-maritime-maritimeindustry-activity-7057673514492817408-gIfX/?trk=public_profile_like_view

SEALENCE. (2020). Sealence brochure [retrieved 3-8-2024]. https://www.sealence.it/wp-content/uploads/2020/12/SEALENCE-Pitch-2020-ENG-CFM-.pdf

Sechilariu, M., & Locment, F. (2016). Chapter 3 - backup power resources for microgrid. In M. Sechilariu & F. Locment (Eds.), *Urban dc microgrid* (pp. 93–132). Butterworth-Heinemann. https://doi.org/https://doi.org/10.1016/B978-0-12-803736-2.00003-7

Ship Motion Group. (2024). Retractable propulsion system [Brochure].

Ship motion Group. (2024). Retractable propulsion for racing yachts [retrieved 13-09-2024]. https://shipmotiongroup.com/sailyacht/retractable-propulsion-for-racing-yachts/

Smith, R. (1995). Cobblestoning in surface effect ships its cause and control [3rd IFAC Workshop on Control Applications in Marine Systems, Trondheim, Norway, 10-12 May]. *IFAC Proceedings Volumes*, *28*(2), 158–163. https://doi.org/https://doi.org/10.1016/S1474-6670(17)51666-3

Souppez, J.-B., Dewavrin, J., Gohier, F., & Borba Labi, G. (2019). Hydrofoil configurations for sailing superyachts: Hydrodynamics, stability and performance. *Design & Construction of Super and Mega Yachts 2019*. https://doi.org/10.3940/rina.smy.2019.05

Stam, M. (2025). *Modular naval vessels and the impact on the design and effectiveness* [Master's thesis, Delft University of Technology]. Modular%20naval%20vessels%20and%20the%20impact%20on%20the%20design%20and%20effectiveness

Stenius, I., Rosén, A., & Kuttenkeuler, J. (2011). On structural design of energy efficient small high-speed craft. *Marine Structures*, *24*(1), 43–59. https://doi.org/https://doi.org/10.1016/j.marstruc.2011.01.001

Streng, J., Kana, A., Verbaan, J., Barendregt, I., & Hopman, J. (2022). Alternative energy carriers in naval vessels. *International Naval Engineering Conference*.

Strijbosch, V. (2019). De marine in 2035. *Alle Hens*, (4). https://magazines.defensie.nl/allehens/2019/03/05_doctrine

Tan, S. (1995). Seakeeping considerations in ship design and operations. *Regional Maritime Conference, Indonesia*. https://repository.tudelft.nl/islandora/object/uuid:a7779757-73d0-4721-add6-4f501d20a0ce/datastream/OBJ/download

Tannenberg, R., Turnock, S. R., Hochkirch, K., & Boyd, S. W. (2023). VPP Driven Parametric Design of AC75 Hydrofoils. *Journal of Sailing Technology*, *8*(01), 161–182. https://doi.org/10.5957/jst/2023.8.9.161

Taylor, D. (1986, March). An aerial port beam view of the patrol combatant-missile (hydrofoil) uss aquila (phm-4) underway during high-speed maneuvers in the gulf of mexico. [public domain]. https://commons.wikimedia.org/wiki/File:Aerial_port_beam_view_of_USS_Aquila_(PHM-4)_underway_US_Navy_DN-SC-87-07089.jpg

Technologies, A. (2024). Ef-20h. https://www.artemistechnologies.co.uk/ef-20h-patrol/

The Green Wave. (2023, April). Candela [retrieved 31-05-2024]. https://www.thegreenwave.nl/en/candela/

Tisza, M., & Czinege, I. (2018). Comparative study of the application of steels and aluminium in lightweight production of automotive parts. *International Journal of Lightweight Materials and Manufacture*, *1*(4), 229–238. https://doi.org/https://doi.org/10.1016/j.ijlmm.2018.09.001

Tokai Kisen. (2024). Tokai kisen co., ltd. | travel and tours to the izu islands [retrieved 26-09-2024]. https://www.tokaikisen.co.jp/en/ourship/jetship/

Torn, K. (2017, September). Hnlms karel doorman, ansicht auf die steuerbodseite des schiffes von vorne, in rotterdam. https://upload.wikimedia.org/wikipedia/commons/3/36/HNLMS_Karel_Doorman%2C_Starboard_Bow%2C_04.09.2017.jpg

Trancossi, M. (2016). What price of speed? A critical revision through constructal optimization of transport modes. *International Journal of Energy and Environmental Engineering*, *7*(4), 425–448. https://doi.org/10.1007/s40095-015-0160-6

Trevithick, J. (2019, April). The u.s. navy has unveiled a new hydrofoil, its first in decades [retrieved 4-8-2024]. https://www.twz.com/27350/the-u-s-navy-has-unveiled-a-new-hydrofoil-its-first-in-decades

TU Delft Hydro Motion Team. (2023). Press kit [Picture]. https://hydromotionteam.nl/media/

Turner, K. (2024, June). Bluegame's luca santella on america's cup foiling hydrogen chase cats. https://www.forbes.com/sites/katturner/2024/05/23/bluegames-luca-santella-on-americas-cup-foiling-hydrogen-chase-boats/

Turner, T., & van Walree, F. (2015, January). *Validation studies of the numerical tool panship for predicting the calm water resistance of the armidale class patrol boat* (tech. rep.). Defence Science and Technology Organisation. Fishermans Bend, Victoria 3207, Australia. https://apps.dtic.mil/sti/tr/pdf/ADA625924.pdf

TwinDisc. (2024a). Marine product guide - august 2024 [Brochure]. https://twindisc.com/wp-content/uploads/2210_InteractiveBrochure_MPG.pdf

TwinDisc. (2024b, August). *Marine product guide* [retrieved 19-1-2025]. https://twindisc.com/wp-content/uploads/2210_InteractiveBrochure_MPG.pdf

Tyde. (2024). The icon [retrieved 26-09-2024]. https://tyde.one/the-icon-2

Ukrainian Military. (2018, September). https://www.ukrmilitary.com/2015/09/kentavr.html

US Coast Guard. (n.d.). Uss flagstaff undergoing coast guard evaluations [public domain]. https://www.navsource.org/archives/12/1001.htm

van Oossanen, P. (1983). Geavanceerde scheepstypen (in dutch). *Schip en Werf*, *50*(4), 43–59.

van Walree, F. (1998). *Hydres manual*.

van Walree, F. (1999). *Computational methods for hydrofoil craft in steady and unsteady flow* [Doctoral dissertation, Delft University of Technology]. %7Bhttp://resolver.tudelft.nl/uuid:3bb919b0-7eab-443d-a498-b58c896a7498%7D

van Walree, F. (2002). Development, validation and application of a time domain seakeeping method for high speed craft with a ride control system. *24th Symposium on Naval Hydrodynamics*. https://www.marin.nl/en/publications/development-validation-and-application-of-a-time-domain-seakeeping-method-for-high-speed-craft-with-a-ride-control-system

van Walree, F. (2015, November). *Panship developments for fast ship simulation* (tech. rep.). MARIN. https://www.marin.nl/en/publications/panship-developments-for-fast-ship-simulation

van Walree, F. (2025, February 20).

van den Bosch, J. (1970). *Tests with two planing boat models in waves* (tech. rep.). Delft University of technology. https://repository.tudelft.nl/record/uuid:02d190b3-7646-4228-a5ca-64c93820c1cc

van der Eijk, M., & Wellens, P. (2020). Experimental and numerical assessment of vertical accelerations during bow re-entry of a RIB in irregular waves [Publisher: IOS Press]. *International Shipbuilding Progress*, *67*(2-4), 173–198. https://doi.org/10.3233/ISP-201005

van der Maat, C. (2023, March). Vervanging middelzwaar landingsvaartuig (lcvp) [letter to parliament]. https://www.rijksoverheid.nl/documenten/kamerstukken/2023/03/22/kamerbrief-a-brief-over-project-vervanging-middelzwaar-landingsvaartuig-lcvp

van der Maat, C. (2024, March). Verwerving amfibische transportschepen [letter to parliament]. https://www.rijksoverheid.nl/documenten/kamerstukken/2024/03/07/kamerbrief-a-brief-project-verwerving-amfibische-transportschepen

van Walree, F., & Carette, N. F. (2011). Validation of time domain seakeeping codes for a destroyer hull form operating in steep stern-quartering seas. *International Journal of Naval Architecture and Ocean Engineering*, *3*(1), 9–19. https://doi.org/https://doi.org/10.2478/IJNAOE-2013-0041

Vasundhara. (2011, February). Treading water: The role of amphibious landing craft [retrieved 1-8-2024]. https://www.naval-technology.com/features/feature111085/

Vessev. (2024). Vs-9 [retrieved 13-8-2024]. https://www.vessev.com/

Vigor. (2024). Combaant craft medium (ccm) [retrieved 4-8-2024]. https://vigor.net/projects/combatant-craft-medium-ccm

Volvo. (2024). D16 mg rc marine genset [retrieved 30-8-2024]. https://www.volvopenta.com/marine/all-marine-engines/d16-mg-rc/

Volvo Penta. (2025). All marine engines [retrieved 28-1-2025]. https://www.volvopenta.com/marine/all-marine-engines/

Wärtsilä. (2015). Midsize waterjets product guide [retrieved 26-8-2024]. https://www.wartsila.com/docs/default-source/product-files/gears-propulsors/waterjets/product-guide-o-p-midsize-waterjet.pdf

Wartzack, S. (2021). *Technical pocket guide*. Schaeffler Technologies AG & Co. KG.

Wernham, B. (2012). *Agile project management for government*. Maitland; Strong. https://books.google.nl/books?id=7cZyrdr6CaIC

Westerbeke. (2016). 7.5 mcga low-co. https://www.westerbeke.com/category/7.5MCGAlow-CO/5AF57EA3DCC74045F4705EC8#mainoverview

Wright, H. (1973, April). *Hydrodynamic note a6-18: Flap control of incidence hinge moment and foil cavitation* (tech. rep.). Grumman Aerospace Corporation. https://www.foils.org/wp-content/uploads/2017/11/0133-Flap-Control-of-Incidence-Hinge-Moment-Foil-Cav.pdf?utm_source=chatgpt.com

Yanmar. (2024). 6aye series [retrieved 30-8-2024]. https://www.yanmar.com/global/marinecommercial/products/propulsion_engine-high_speed/6ayeseries/

Yanmar. (2025). Commercial high speed diesel engines [Brochure]. https://www.yanmarmarine.eu/theme/yanmarportal/uploadedFiles/Marine/productDownloads/Commercial-Product-Guide/100x210_Brochure_CHS_Marine_Product_handbook__nieuwlogoLRforweb.pdf

Yim, B.-y., isni Kim, K.-S., Ahn, J.-W., & Lee, J.-T. (1998). Design of trans-cavitating propellers and performance analyses of the test results. *Ship & Ocean Technology*, *2*(1), 13–30.

Yun, L., & Bliault, A. (2014). *High performance marine vessels*. Springer New York. https://books.google.nl/books?id=3wcDzNJpXf0C

ZF. (2025). Product selection guide 2025 - marine propulsion systems [Brochure]. https://www.zf.com/products/media/industrial/marine/brochures_1/Product_Selection_Guide.pdf

Zhyvotova, J. (2024). https://gmdsstesters.com/radio-survey/general/gmdss-equipment-carriage-requirements-for-solas-ships.html

Журавлёв, Е. (2018, April). https://www.flickr.com/photos/142171772@N06/

A

LAC functional requirements

Nr.	Requirements by Ministery Of Defence Netherlands (MODNL)
1	**General**
1.1	LAC (17pcs) and LCM (7pcs) are two types of Assault Craft forming the MOD's future Littoral Assault capability.
1.2	LAC SHALL be transported in davits of NL LPD and NL JSS as specified in Annex C
1.3	LCM SHALL be transported in docks of NL LPDs as specified in Annex D
2	**Operational Tasks**
2.1	LAC & LCM SHALL be a tactical craft for littoral raiding operations from the sea.
2.2	LAC SHALL be used for tactical transportation of personnel over large distances, offshore and in coastal areas.
2.3	LCM SHALL be used for tactical transportation of all terrain vehicles over large distances, offshore and in coastal areas.
2.4	LAC & LCM SHALL be deployed from NL LPD and NL JSS and preferably also from UK RN LPD's and will have to be launched and recovered from these ships
2.5	LAC & LCM SHALL deliver firepower to suppress an adversary on land or at sea during a landing or re-embarkation, both for self-defense and in support of land forces
2.6	LAC & LCM SHALL support casualty evacuation
2.7	LAC & LCM SHALL support logistic supply of goods and personnel, and on the LCM of vehicles.
2.8	LAC & LCM SHALL support tactical diving operations
2.9	LAC & LCM SHALL operate as a forward sensor, collecting and sharing data with adjacent units
2.10	LAC & LCM SHALL deploy EMF (Embarked Military Forces) ashore over large distances
2.11	LAC & LCM SHALL provide fire support to EMF ashore.
2.12	LAC & LCM SHALL support Humanitarian Aid & Disaster Relief operations in the Caribbean part of the Kingdom of The Netherlands.
3	**Operational Environment**
3.1	LAC & LCM SHALL be fully operational in following climatological conditions: - sea state: 0 up to but not including 5 - wind speeds 0 - 50 km/h - air temperature -30 to +45 degrees centigrade - sea water temperature: -2 to +32 degrees centigrade - relative humidity 0 to 100%
3.2	LAC & LCM SHALL be reduced operational in following climatological conditions: - sea state: 5 - wind speeds 7 bft
3.3	LAC & LCM SHALL have excellent sailing properties in the A1 and A2 areas in North Sea, North Atlantic and the Baltic.
3.4	LAC & LCM SHALL be able to operate with reduced speed in "slush ice" occasional ice flows
4	**Rules and Regulations**
4.1	LAC & LCM MUST be compliant with IMO regulations.
4.2	LAC & LCM MUST be compliant with EU legislation.
4.3	LAC & LCM SHALL be compliant with Dutch legislation
4.4	LAC & LCM SHOULD be compliant with the Naval Boat Code
4.5	LAC & LCM SHALL be equipped for operations in Sea Area A2.
4.6	LAC & LCM SHALL be delivered with class approval
4.7	LAC & LCM SHOULD be compliant with IMO Tier III
4.8	LAC & LCM SHOULD be compliant with Stage V
4.9	LAC & LCM SHALL be compliant with the List of Banned and Restricted Substances
4.10	LAC & LCM SHOULD be delivered with a material safety analysis as per for instance MIL 8222E or ISO 12002
4.11	LAC & LCM SHALL be provided with Material Safety Data Sheets for all relevant materials
5	**Properties**
5.1	LAC & LCM SHALL have a minimum lifetime of 15 years without modifications and/or MLU.
5.2	LAC & LCM SHOULD be deployed in a "non-permissive" environment, meaning the craft has adequate weapons for self-defense, for supporting land forces from seaside and sufficient ballistic protection against small arms fire to disengage effectively from a hostile encounter
5.3	LAC & LCM SHALL have an uninterrupted distance of at least 200 nautical miles at a sustained speeds of 18 knots, preferably 25 knots
5.4	LAC & LCM SHALL be equipped with waterjet propulsion
5.5	LAC & LCM SHALL be designed for low susceptibility. Visual, accoustic, thermal and radar signature will be minimised
5.6	LAC & LCM SHALL be equipped with systems for reducing thermal susceptibility (like e.g. watercooling, paintwork or netting).
5.7	LAC & LCM SHALL be equipped with cloaking systems (like e.g. waterspray) to reduce visual susceptibility.
5.8	LAC & LCM SHALL be equipped with a system to disable all its RF transmissions
5.9	LAC & LCM SHALL have camouflage systems and paint systems which can be altered to suit the area of operations.
5.10	LAC & LCM SHALL have robust and technically redundant mission and safety critical systems.
5.11	LAC & LCM SHALL provide working positions for COXSWAIN, BOATCOMMANDER, GUNNER
5.12	LAC & LCM, GUNNER position SHALL provide in: - control of RCWS; - connection to internal communition system;
5.13	LAC&LCM, COXSWAIN position SHALL provide in: - all equipment necessary for save navigation; - common operational picture providing SA - connection to internal communition system;
5.14	LAC & LCM, BOATCOMMANDER position SHALL provide in: - control over the military communications equipment: - common operational picture providing SA - connection to internal communition system; - video display from UxV and RCWS
5.15	LAC & LCM systems SHALL be protected against cyber threats
5.16	LAC & LCM SHALL have intruder protection, intruder detection and connectivity to the shore security guards when in port.
5.17	LAC & LCM SHALL have vesselborne protection for positions of the coxswain and navigator and the machinery space against Chemical, Biological and Radiological threats through the use of an overpressure and filtration system.
5.18	LAC & LCM SHALL have vesselborne flushing system to rinse the vessels after a CBRN attack
5.19	LAC & LCM SHALL be compatible to operate with night vision goggles
5.20	LAC & LCM SHALL provide the systems for Condition Based Monitoring, up to Manufacturer's Standard. Please note that remote monitoring is not allowed
5.21	LAC & LCM SHALL have a platform with a ladder in support of launching divers. No obstructing parts are allowed in the vicinity of the platform.
5.22	LAC & LCM SHALL be equipped with removable seats and stretcher attachment points in the EMF compartment to allow casualty evacuation from the coast to the nearest Role 1 medical facilty.
6	**Landing and (dis)embarking**
6.1	LAC & LCM SHALL be able to embark and disembark both personnel and vehicles on beaches, shores & sandbanks with a gradient up 1:15, with a soil class up to Level 6 (DIN 18300).
6.2	LAC & LCM SHALL be equipped with a reinforced bottom- and keel-plate in support of landing operations.
6.3	LAC & LCM SHALL cause a maximum wade depth of 0.86 meter for personnel and vehicles when (dis)embarking at prescribed landing points.
6.4	LAC & LCM SHALL be equipped with a (heavy) anchor capable of unbeaching the vessels.
6.5	LAC & LCM SHALL have a maximum wading depth of 0.75mtr in accordance with a maximum slope of 23 degrees i.a.w. STANAG 2805. This document includes wading depths for vehicles which can have a direct link to the drafts of the LCM.
7	**Systems**
7.1	LAC & LCM SHALL be equipped with a system measuring acute shock loads to coxswain and navigator, equipped with an emergency signal for possible overload conditions
7.2	LAC & LCM SHALL have vesselborne electro-optical surveillance capability for building up local Situational Awarenes (SA), using IR, thermal and daylight vision and for assisting safe navigation.

7.3	LAC & LCM SHALL provide an internal communication system providing voice connectivity between the crew, with the management of the EMF, to the outside weapon stations, to the maritime communication suite, to the military communications suite.
7.4	LAC & LCM SHALL provide GMDSS maritime communication equipment
7.5	LAC & LCM SHALL be equipped with a High Speed Navigation System
7.6	LAC & LCM SHALL be equipped with at least 18 Units 19 inch rackspace in which military communication equiment can be placed.
7.7	LAC & LCM SHALL be equipped with dedicated antennas for military communication (2x HF, 2x VHF, 2x UHF, 1xTACSAT)
7.8	LAC & LCM SHALL be equipped with a Warship AIS system
7.9	LAC & LCM SHALL support operations in a GPS-denied surrounding with e.g. a Military GPS, Inertial Navigation Systems and an internal clock.
7.10	LAC & LCM SHOULD be equipped with an IFF Transponder Mode 5S
7.11	LAC & LCM SHOULD be equipped with an IFF Interrogator Mode 5S with connection to the Common Operational Picture
7.12	LAC & LCM SHOULD be equipped with a Laser Range Finder supporting safe navigation and target acquisition
8	**Weapon systems**
8.1	LAC & LCM SHALL be equipped with at least three weapon positions ensuring 360 degrees coverage, whereby each direction is covered with al least two weapon positions.
8.2	LAC & LCM SHALL have one weapon position as a Remote Controlled Weapon Station (RCWS) with following requirements: - fully operational in the environmental requirements of LAC&LCM - able to integrate an FN MAG, Browning M2 CQB or a Heckler&Koch 40mm AGW, with munition; - able to engage targets on sea and land; - RCWS can acquire a minimum of 10 targets simultanously and advises the operator - accuracy: with 30kn in SS1, a hitrate of 50% of a burst of 5 will be unsured with the Browing M2 on a target of 1M2 - operated by an underdeck operating station; - manual on-deck emergency operation; - easy HMI and support for initiating tracks; - equipped with a daylight and a thermal imaging camera system; - connection to the Internal Communication System;
8.3	LAC & LCM SHOULD have an RCWS-camera moving independently of the barrel
8.4	LAC & LCM SHOULD be equipped with an RCWS with provision for ATGM (Anti-Tank Guided Missiles)
8.5	LAC & LCM SHOULD have an RCWS able to detect, track and engage airborne targets like - helicopters; - drones;
8.6	LAC & LCM SHALL have manually operated weapon stations to be equipped with: - weapon mount suitable FN MAG, Browning M2 QCB or a Heckler&Koch 40mm AGW, with munitions; - storage for two additional ammunition cases; - storage for spare or hot barrels; - connection to the Internal Communication System; - 24VDC power connection for future additional weapons.
8.7	LAC & LCM SHALL have provisions for two Rheinmetall ROSY Rapid obscuring systems. One facing forward, one facing aft.
9	**Specific Requirements for LAC**
9.1	LAC SHALL be a vessel specifically designed for troop transport and littoral assault: LAC (Littoral Asault Craft)
9.2	LAC SHALL fit inside the davit bounding box of HNLMS Johan de Witt and HNLMS Karel Doorman (see Annex C)
9.3	LAC SHALL be fully interoperable with the davits of HNLMS Johan de Witt and HNLMS Karel Doorman: LAC can be loaded onboard the mothervessels and safely launched and recovered up to, but not including, seastate 4.
9.4	LAC SHALL have a system to guarantee interoperability with the davits.
9.5	LAC SHALL fit inside the HNLMS Rotterdam and HNLMS Johan de Witt welldeck bounding box (see Annex D)
9.6	LAC SHALL be fully interoperable with the welldecks of HNLMS Rotterdam and HNLMS Johan de Witt.
9.7	LAC SHALL be able to embark/disembark vehicles and personnel of the steel beach of HNLMS Karel Doorman. (see Annex D)
9.8	LAC SHALL be capable of a minimum speed of 40 knots at sea state 0 in fully laden condition
9.9	LAC SHALL be capable of a minimum speed of 25 knots, at sea state 3 in fully laden condition
9.10	LAC SHALL have an EMF compartment capable of embarking, transporting and disembarking all three of following configurations (full payload 4500kg): - 6 EMF-personnel + full personal gear + arctic gear, or - 12 EMF-personnel + full personal gear, or - 16 EMF-personnel without gear
9.11	LAC SHOULD have an EMF compartment for 18 EMF including full gear
9.12	LAC SHALL have lashing points in the EMF compartment for securing cargo
9.13	LAC SHALL be equipped with individual seating for Crew and EMF, compliant with the MoD shock standard as per Annex B.
9.14	LAC SHALL be equipped with EMF seating with can be detached, stored or moved to create space, without using any tools.
9.15	LAC SHALL provide an EMF-compartment with systems minimizing the physical strain (caused by e.g. temperature, vibrations, sound, shock) on the EMF
9.16	LAC SHALL be fully operational with a maximum crew of three
9.17	LAC SHALL be operable by a crew of 2 in case of an emergency
9.18	LAC SHALL have battery power for on board systems for up to 8 hours, without the use of the engines/generators
9.19	LAC SHALL have an availability of 85% across all LACs, during the lifespan of the craft
9.20	LAC SHALL be transportable by road transport.
9.21	LAC SHALL be transportable by a Roodberg trailer 30's (RBT30).
9.22	LAC SHOULD be transportable by air transport
9.23	LAC SHOULD be delivered with approved transport and storage cradles
9.24	LAC SHOULD be delivered with an approved trailer for road transport
9.25	LAC SHALL have a lower fuel consumption compared to the MoD's LCVP Mk5, being 107litres/min @ 2500 RPM
9.26	LAC SHALL be equipped with hoisting points and if necessary a hoisting frame in support of on-shore storage of the LAC
9.27	LAC SHOULD be able to come to from full speed to full stop within 3 boatlengths.
10	**Specific Requirements for LCM**
10.1	LCM SHALL be a vessel specifically designed for carrying (all-terrain) vehicles and embarked Forces (LCM: Littoral Craft Mobility).
10.2	LCM SHALL have a capability to sit in the well deck dock of NL LPDs (flat deck) and to get afloat or dry out in a safe methode when the welldeck is filled or emptied.
10.3	LCM SHALL be fully interoperable with the well decks of HNLMS Rotterdam and HNLMS Johan de Witt (Annex D).
10.4	LCM SHALL be able to embark/disembark vehicles and personnel of the steel beach of HNLMS Karel Doorman (Annex D.)
10.5	LCM SHALL be capable of a minimum speed of 25 knots at sea state 0 in fully laden condition
10.6	LCM SHALL be capable of a minimum speed of 18 knots, and preferably 25 knots, at sea state 3, in fully laden condition
10.7	LCM SHALL have the capability to embark, transport and disembark all of the following configurations: - 2 pcs FLATM-BV + 12 EMF-personnel + full personal gear. It is defined as: - tracked vehicle; - maximum full weigth of 15,5 tonnes, maximum curb weight of 9,8 tonnes; - maximum dimentions (LxWxH): 8x2,2x2,55 mtr - 3 pcs FLATM-PV + 12 EMF-personnel + full personnal gear. It is defined as: - tracked vehicle; - maximum full weigth of 3,9 tonnes, maximum curb weight of 2,1 tonnes; - maximum dimentions (LxWxH): 4,6x1,9x2 mtr
10.8	LCM SHALL be fully operational with a maximum crew of four.
10.9	LCM SHALL be operable by a crew of 2 in case of an emergency
10.10	LCM SHALL have a recovery winch on the vehicle deck to support embarking vehicles to the vessel.
10.11	LCM SHALL have vehicle and container lashing points in the vehicledeck for lashing vehicles
10.12	LCM SHALL be equipped with systems for executing multi-day patrols, including setting up a (temporary) amphibious forward patrol base.

10.13	LCM SHALL have a freezer for medical supplies.
10.14	LCM SHALL provide mooring facilities for other landing crafts (FRISC, LCU, LAC)
10.15	LCM SHALL be able to supply electrical power to attached/moored landing crafts
10.16	LCM SHALL be able to supply fuel to LAC and FRISC from its own fuel tanks
10.17	LCM SHOULD be able to store petrol fuel for outboard engines and quads and skidoos in an AFOB setting
10.18	LCM SHALL be able to sustain 17 personnel for three days in "field conditions": place for stretchers, storage for drinking water, cooling for food, a freezer for medical supplies, basic sanitary (no full beds, no shower facilities)
10.19	LCM SHALL be able to provide an FOB package (17 stretchers, water, freezer & fridge for medical supplies)
10.20	LCM SHALL provide a lavatory
10.21	LCM SHALL NOT provide a shower
10.22	LCM SHALL have battery power for on-board systems for up to 8 hours, without the use of the engines/generators
10.23	LCM SHALL have an availability of 85% across all LCMs, during the lifespan of the craft
10.24	LCM SHALL have an EMF compartment capable 12 EMF-personnel + full personal gear;
10.25	LCM SHALL have lashing points in the EMF compartment for securing cargo
10.26	LCM SHALL have individual seating for Crew and EMF, compliant with the MoD shock standard as per Annex B.
10.27	LCM SHALL provide an EMF-compartment with systems minimizing the physical strain (caused by e.g. temperature, vibrations, sound, shock) on the EMF
11	**Documentation**
11.1	LAC & LCM SHALL be delivered with an Integrated Logistic Support package , documentation acoording to based on the Sx-1000i, which can be imported in the MODNL's Product Data Manamgement packages
11.2	LAC & LCM SHALL be delivered with all information and tooling necessary for the MODNL to perform all levels of maintenance and modifications.
12	**Maintenance**
12.1	LAC & LCM SHALL have 600 operation hours for each vessel per year
12.2	LAC & LCM SHALL be able to operate a minimum of two years between large maintenance periodes for each vessel
12.3	LAC & LCM SHALL provide accessible transport routes to replace main components (like an engine) in support of Depot Level Maintenance (DLM).
12.4	LAC & LCM SHALL have easily accessible components for OLM and ILM
13	**Sustainability**
13.1	LAC & LCM SHOULD have lowest carbon emission possible, compliant with Stage V and IMO tier III
13.2	LAC & LCM SHOULD be provided with a material passport (Green) to allow circularity tracing of materials
13.3	LAC & LCM SHALL have an anti fouling system reducing drag and marine pollution

B

Bounding box LPD and JSS

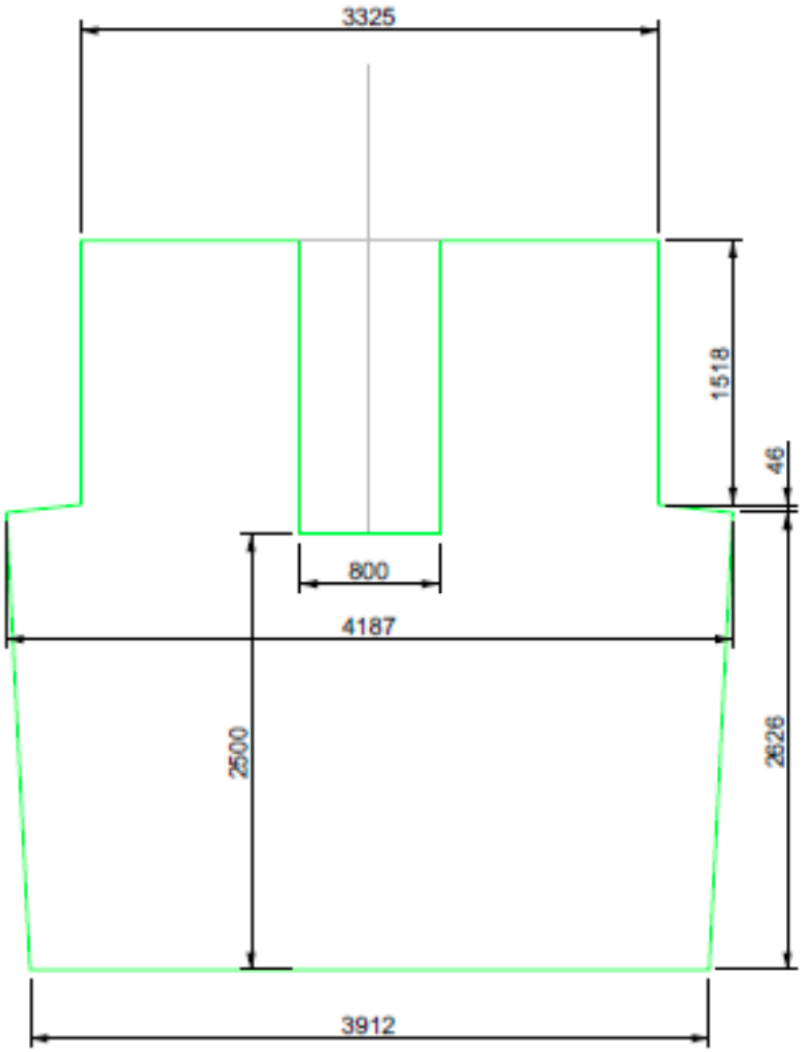

Figure B.1: Section view of the bounding box

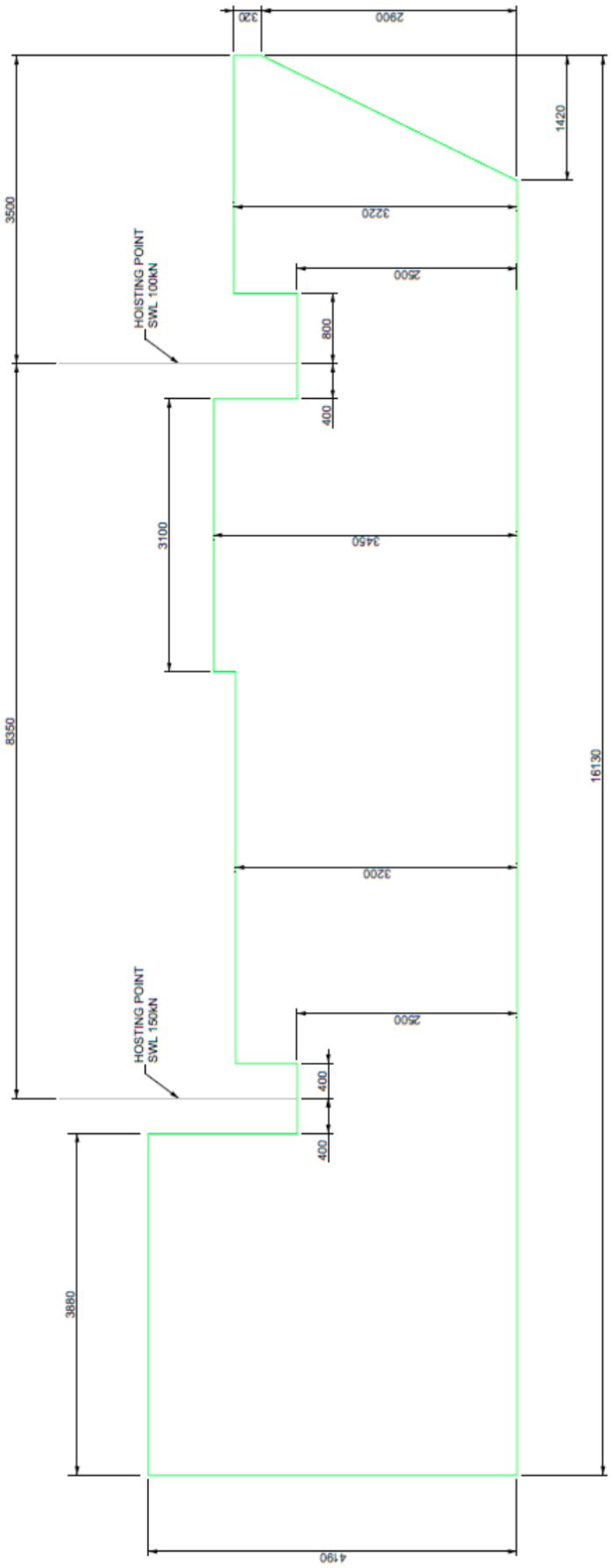

Figure B.2: Side view of the bounding box

C

Vessel parameters

Table C.1: LAC main particulars

Name	Manufacturer	Nationality	Year of intr.	L_{oa} (m)	B (m)	T (m)	Δ (t)	P_B (kW)	v_s (kt)	Range (nm)	Troops (-)	Crew (-)	Compl. (-)	Source
KMC Komando	Tesco Indomaritim	Indonesia	2013	18	4.2	0.7	28	1715	40	250	30	3	13	(Lastiawan, 2019)
Jurmo (Watercat M14)	Marine Alutech	Finland	1990	14.1	3.65	0.7	13.9	662	43	180	20	2	28	(Naval Technology, 2023)
Jehu (Watercat M18)	Marine Alutech	Finland	2012	19.9	4.3	1.1	32	1678	40	200	24	5	12	(Puolustusvoimat, 2024)
CB90	Saab Dockstavarvet	Sweden	1990	16.3	3.85	0.8	24.5	1342	45	300	18	3	275	(Saab, 2021)
Centaur	Kuznya na Rybalskomu	Ukraine	2016	24.3	4.8	1	47		35	500	27	5	2	(Ukrainian Military, 2018)
Raptor	Pella shipyard	Russian	2014	16.9	4.1	0.9	23	1690	48	300	20	3	17	(Russian Ships, 2024a)
Combatant Craft Medium	Vigor Industrial	USA	2014	18.47	4.01	1	27	1864	52	600	19	4	30	(Vigor, 2024)
MPAC mk2	Lung Teh Shipbuilding Co. Ltd	Philippines	2009	17	4.76	0.9	19	1566	45	350	16	5	12	(Costa, 2021)
Fast Assault Craft (FAC)	Damen	Netherlands	Design	15.9	4	0.8			30	200	17	2	0	(Damen, 2024a)
LCVP	Damen	Netherlands	2008	15.7	4.27	0.65	24	846	25		35	3	12	(Damen, 2024b)
TRANSFLYTOR	SEAir International	France	Design	20						800	12		0	(SEAir International, 2023)

Table C.2: Hydrofoil craft main particulars

Name	Manufacturer	Nationality	Market	Year of intr.	L_{oa} (m)	B (m)	B_{oa} (m)	T (Hull) (m)	T (Foil) (m)	v_s (kt)	Δ (t)	Range (nm)	PAX	P_B foil (kW)	P_B hull (kw)	Oper. limit	Hull type	Config.	Foil load (fore/ rear)	Foil type	Split	Retr.	Propulsion	Source
M24	Mantaray	Sweden	Leisure	2023	7.35	2.3	2.3			30	1.15		5	75			Monohull	canard		Submerged	No	Yes	L Drive Propeller	(Mantaray, 2024)
FT80	SEAir	France	Military	2020	7.65	3.15	3.69	1.05	0.83	40	2.4		8	187			Monohull	conventional		Surface Piercing	Yes	Yes	L Drive Propeller	(SEAir solutions, 2024)
M25	Mantaray	Sweden	Leisure	2024	7.7	2.5	2.5			35	1.1	250	6	52			Monohull	canard		Submerged	No	Yes	L Drive Propeller	(Mantaray, 2024)
8S	Edorado	Netherlands	Leisure	2023	8.35	2.5	2.5	1.25		38	1.95	40	5	100			Monohull	canard		Submerged	No	Yes	L Drive Propeller	(Edorado, 2024)
C8	Candela	Sweden	Leisure	2022	8.5	2.5	2.5	1.5		27	1.75	57	8	50		SS3	Monohull	conventional		Submerged	No	Yes	Podded CRP	(Candela, 2024a)
VS-9	Vessev	New Zealand	Ferry/Leisure	2024	8.95	3.1	3.1	1.5		30	3.1	50	11			SS3	Catamaran	conventional		Submerged	No	Yes	L Drive Propeller	(Vessev, 2024)
N30	Navier	USA	Leisure	2023	9.1	2.7	2.7	1.67		35	2.56	75	8	180			Monohull	canard		Submerged	Yes	Yes	L Drive Propeller	(Navier, 2024)
WSS 10	G. C. Jensen Nachf.	Germany	Leisure	1954	9.2	1.95	4.2	2.05	0.65	30	4		8	135			Monohull	conventional		Submerged	Yes	No	2x Z Drive subcavitating propeller	(German Maritime Museum, 2024)
Foiler	Enata	UAE	Leisure	2019	9.8	3.3	7.2	1.9		40	n/a	190	8	552		SS3	Monohull	conventional		Surface Piercing	Yes	Yes	2x Hydrostatic Propeller	(Enata, 2024)
Chase Zero	Emirates Team	New Zealand	Leisure	2022	10	4.5	4.5	2.2		50	4.8	100	6	420			Catamaran	conventional		Submerged	No	No	L Drive Propeller	(Emirates Team New Zealand, 2022)
BGHSV	Blue Game	Italy	Leisure	2024	10.8					50	n/a						Catamaran	conventional		Submerged	No	No	Z Drive Propeller	(Turner, 2024)
P12	Candela	Sweden	Ferry	2023	11.99	4.5	4.5			30	10	40	31	100		SS3	Catamaran	conventional		Submerged	No	Yes	Podded CRP	(Candela, 2024b)
SpiritBARTech35EF	BARTech	UK	Leisure	2023	12.2					30	n/a	100	6				Monohull	conventional		Submerged	No	No	Propeller	(James, 2024)
EF-12	Artemis	UK	Ferry	2023	12.5	4	4	2.2		31	11.5	55	8	250			Monohull	tandem		Submerged	No	No	Podded Propeller	(Artemis, 2024)
The ICON	Tyde	Germany	Leisure	2024	13.15	4.5	4.5	1.9	0.85	33	11	50	8	200			Monohull	canard		Submerged	Yes	No	L Drive Propeller	(Tyde, 2024)
Hayate TSL-F	Kawasaki, Kobe	Japan	Ferry	1994	17.1	6.2	6.36	3.1	1.6	41	n/a	n/a	14	2820		SS5	Monohull	canard		Submerged	No	No	2x Waterjet	(Yun & Bliault, 2014)
PGH-1 Flagstaff	Grumman	USA	Military	1968	22.2		6.5	4.26	1.2	40	72	800	13	2486	150	SS4	Monohull	conventional	70/30	Submerged	Yes	Yes	Z Drive supercavitating propeller	(Yun & Bliault, 2014)
PGH-2 Tucumcari	Boeing	USA	Military	1968	22.7		5.9	4.33	1.5	50	58	800	13	2450	90	SS4	Monohull	canard	70/30	Submerged	Yes	Yes	Waterjet	(Yun & Bliault, 2014)
Sparviero	Rodriquez	Italy	Military	1974	22.95	7.01		1.87	1.45	50	60.6	400	10	3980			Monohull	canard		Submerged	Yes	Yes	Waterjet	(Yun & Bliault, 2014)
MEC-1	Rodriquez	Italy	Ferry	1992	25	6.7	8.4	2.8	0.95	38	n/a	200	146	1680		SS4	Monohull	n/a		Surface Piercing	No	No	Rexroth propeller pod (hydraulic)	(Yun & Bliault, 2014)
Westfoil	Westport shipyard	USA	Ferry	1991	25.6	7.6	8	4.75	1.83	50	89.4	730	149	2500		SS4	Monohull	canard		Submerged	No	Yes	2 x Ducted air propeller	(Yun & Bliault, 2014)
Shimrit	Grumman	United States	Military	1981	25.6	7.3	13	4.75	1.93	45	104	750	15	5400	120		Monohull	conventional	70/30	Submerged	Yes	Yes	Z Drive transcavitating propeller	(Frauenberger, 1982)
Jetfoil 929	Boeing	USA	Ferry	1974	27.4	8.53	8.53	5.4	2	45	104	300	243	4900		SS5	Monohull	canard		Submerged	No	Yes	2x Water jet	(Yun & Bliault, 2014)
RHS 150	Rodriquez	Italy	Ferry	1980	28.7	5.6	11	3.1	1.4	35	65.5	130	150	2054		SS4	Monohull	tandem	60/40	Surface Piercing	No	No	Propeller FPP	(Yun & Bliault, 2014)
North Star	n/a	China	Ferry	1994	29.1	8.6	9.2	4.5	n/a	50	118	100	294	5728		SS4	Monohull	canard	30/70	Submerged	No	No	Waterjet	(Yun & Bliault, 2014)
Foilmaster	Rodriquez	Italy	Ferry	1994	31.2	6.78	13.3	3.89	1.45	37	112	150	242	3100		SS4	Monohull	tandem		Surface Piercing	No	No	Waterjet	(Yun & Bliault, 2014)
Denison	Grumman	United States	Military	1962	31.9		7.01	4.69		50	95			10440			Monohull	conventional		Surface Piercing	Yes	Yes	Z Drive Supercavitating propeller	(Rose, 1964)
Mountain Ge-Lu	n/a	China	Ferry	1996	32	4.8	7.6	2.05	1.1	38	32	216	82	922		SS4	Monohull	tandem	52/49	Surface Piercing	No	No	Propeller FPP	(Yun & Bliault, 2014)
Rainbow SS-400	Mitsubishi, Shimonoseki	Japan	Ferry	1993	33.24	12	13.2	4.5	2.1	45	75	n/a	345	4200		SS4	Catamaran	n/a		Submerged	No	No	2x Waterjet	(Yun & Bliault, 2014)
Foilcat	Fjellstrand	Norway	Ferry	1995	35	12	12	4.7	2.55	45	n/a	300	377	8052		SS4	Catamaran	tandem		Submerged	No	No	2x Waterjet	(Yun & Bliault, 2014)
PCH-1 High Point	Boeing	USA	Military	1963	35.3		9.53	6.04	2.6	50	131	n/a	18	6308	390	SS4-5	Monohull	canard	30/68	Submerged	No	Yes	2 x Z Drive CRP	(Yun & Bliault, 2014)
RHS 200	Rodriquez	Italy	Ferry	1981	35.8	7.6	14.5	4.55	2.05	37	130	200	210	3828		SS4	Monohull	tandem	60/40	Surface Piercing	No	No	Propeller FPP	(Yun & Bliault, 2014)
FSH 38	Rodriquez	Italy	Ferry	2010	37.25	8	8	4.3	n/a	47	140	430	245	4640		SS6	Monohull	canard		Submerged	No	No	2 x FPP or CRP	(Yun & Bliault, 2014)
PHM-1 Pegasus	Boeing	USA	Military	1975	40.5		8.9	7.1	2.7	50	235	600	24	15000	880	SS5	Monohull	canard	31.8/68.2	Submerged	No	Yes	Waterjet	(Yun & Bliault, 2014)
Tayfun	Almaz shipyard	Russia	Ferry	1969	42.55	8.3		4.6	2	40	135	295	250	3800		SS4	Monohull	conventional		Surface Piercing	No	No	Propeller	(Yun & Bliault, 2014)
Sarancha	Almaz shipyard	Russia	Military	1977	45		10	7.3	2.5	58	275	700	40	22260		SS5	Monohull	canard	30/70	Submerged	No	Yes	Z Drive supercavitating propeller	(Yun & Bliault, 2014)
Bras D'Or	DeHavilland	Canada	Military	1968	49.95		6.5	7.16	2.3	63	236	500	25	16325	1090	SS4-5	Monohull	canard	10/90	Surface Piercing	No	No	4x Z Drive supercavitating propeller	(Yun & Bliault, 2014)
Babochka	Gorky shipyard	Russia	Military	1977	50.2	9.76	20	7.2	2.2	52	465	850	40	40267		SS5	Monohull	conventional		Surface Piercing	Yes	No	Propeller	(Russian Ships, 2024b)
AGEH-1 Plainview	Grumman	USA	Military	1965	64.6		12.3	7.6		50	325	500	25	21520	580	SS5	Monohull	conventional	90/10	Submerged	Yes	Yes	2x Z Drive subcavitating propeller	(Yun & Bliault, 2014)

D

Propulsion calculations

D.1. Propulsor-hull interactive factors

Table D.1: Typical propulsor-hull interactive factors for planing high-speed craft $F_{n\nabla}$ >2.5 identified by Blount and Bartee (1997)

Propulsion concept		w	t	η_h	η_r
Propeller on inclined shaft	6°	0 to -0.10	0.03	0.88 to 0.97	0.97 to 1.01
	12°	0.03 to -0.05	0.07 to 0.11	0.84 to 0.96	0.97 to 1.01
Outboard propeller		0.03	0	0.97	0.97 to 1.01
Surface-piercing propeller		0	0	1.00	0.97 to 1.01
Flush inlet waterjet		0.05	-0.02 to -0.07	1.07 to 1.13	0.99
Tractor propeller		0	0 to 0.05	1.05	1.00
Pusher propeller		0.05 to 0.07	0.05	1.00 to 1.02	0.97 to 1.01

D.2. Waterjet theory

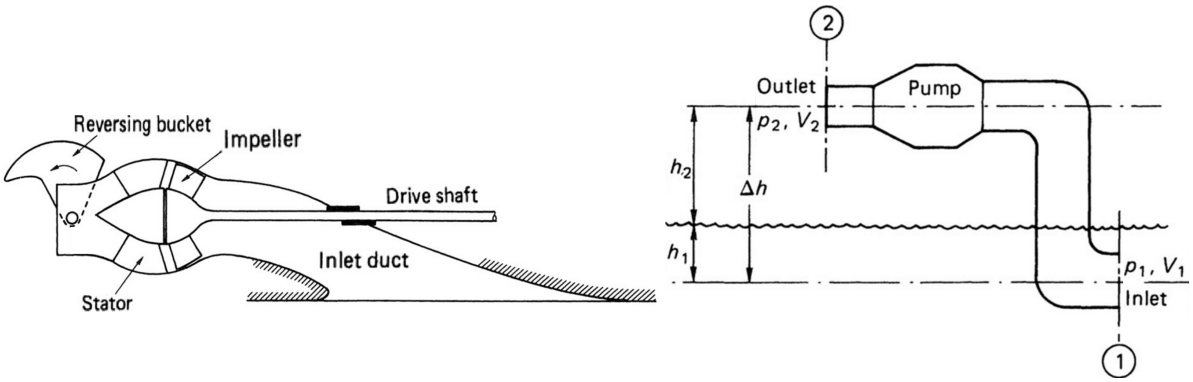

Figure D.1: Typical waterjet general arrangement and its idealised arrangement, adapted from Carlton (2019)

The underlying principles of waterjet propulsion can be explained using the law of momentum conservation (Carlton, 2019). The symbols of Fig. D.1 are used for reference. Following this diagram, water enters the system with velocity V_1 and exits with V_2. The resulting mass flow of the waterjet is given by Eq. (D.1). The increase in rate of change of momentum is then given by $\rho A_2 V_2 (V_2 - V_1)$, which is equal to the thrust produced by the system (Eq. (D.2)). Hence, the thrust power P_T is given by Eq. (D.3), where v_a is the vessel advance velocity.

$$\dot{m} = \rho A_2 V_2 \tag{D.1}$$

$$T = \rho A_2 V_2 (V_2 - V_1) \tag{D.2}$$

$$P_T = Tv_a = \dot{m}v_a(V_2 - V_1) \tag{D.3}$$

The system head of the complete system can be expressed as in Eq. (D.4). H_p is the head generated by the pump, Δh is the difference in static head between the inlet and outlet of the waterjet ($\Delta h = h_1 + h_2$) and h_{loss} is the losses associated with the flow through the system. Eq (D.4) can be rewritten to Eq. (D.5) to get the required pump head, since $p_1 = p_2 + h_1\rho g$.

$$\frac{p_1}{\rho g} + \frac{V_1^2}{2g} + H_p = \frac{p_2}{\rho g} + \frac{V_2^2}{2g} + \Delta h + h_{loss} \tag{D.4}$$

$$H_p = \frac{V_2^2 - V_1^2}{2g} + h_2 + h_{loss} \tag{D.5}$$

The power transferred by the pump can then be expressed as in Eq. (D.6). η_p is defined as the pump efficiency. Combining Eq. (D.2) and Eq. (D.6) yields the equivalent open water efficiency of a water jet as being the ratio between the thrust power and delivered power to the propulsor. This is presented in Eq. (D.7).

$$P_O = \frac{\dot{m}}{\eta_p}\left[\frac{1}{2}(V_2^2 - V_1^2) + g(h_2 + h_{loss})\right] \tag{D.6}$$

$$\eta_o = \frac{P_t}{P_O} = \frac{v_a(V_2 - V_1)}{\frac{1}{\eta_p}\left[\frac{1}{2}(V_2^2 - V_1^2) + g(h_2 + h_{loss})\right]} \tag{D.7}$$

The waterjet equivalent open water efficiency is therefore partly determined by the ratio between the inlet and outlet velocity and the height of the outlet. Fig. D.2 shows the effect of different velocity ratios on waterjet efficiency.

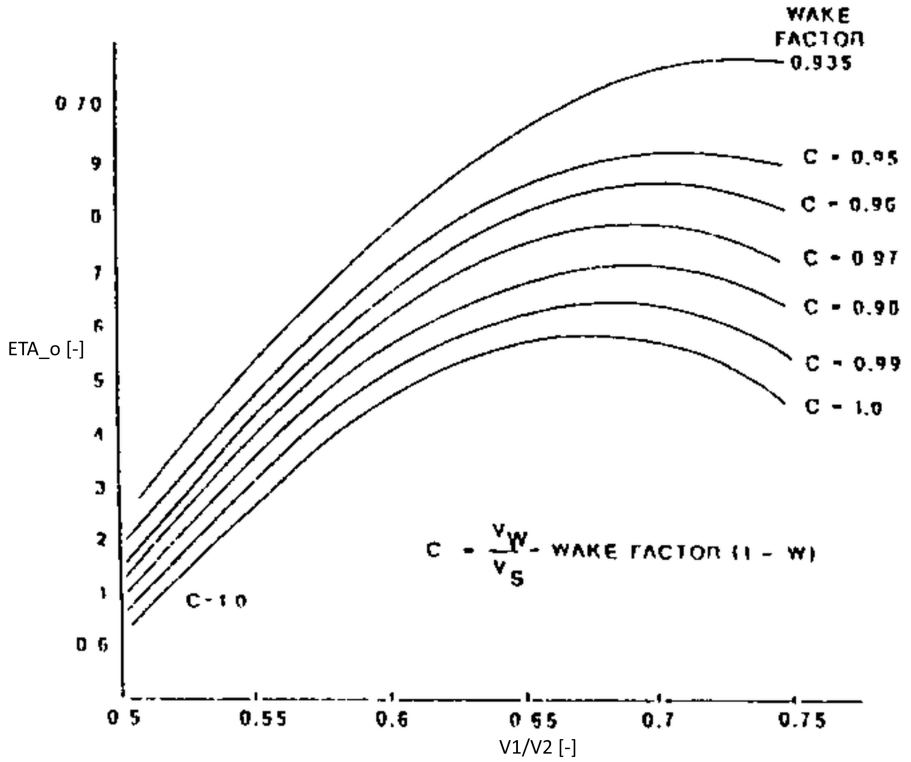

Figure D.2: Typical jet efficiencies over jet velocity ratio (V_1/V_2) and wake ingestion (w), from Allison (1993)

D.3. Open water efficiency CB90 waterjet

The propulsion system of the CB90 compromises of 2 662 kW diesel engines which propel one waterjet each through a reduction gearbox. This makes the total installed engine brake power P_B 1324 kW.

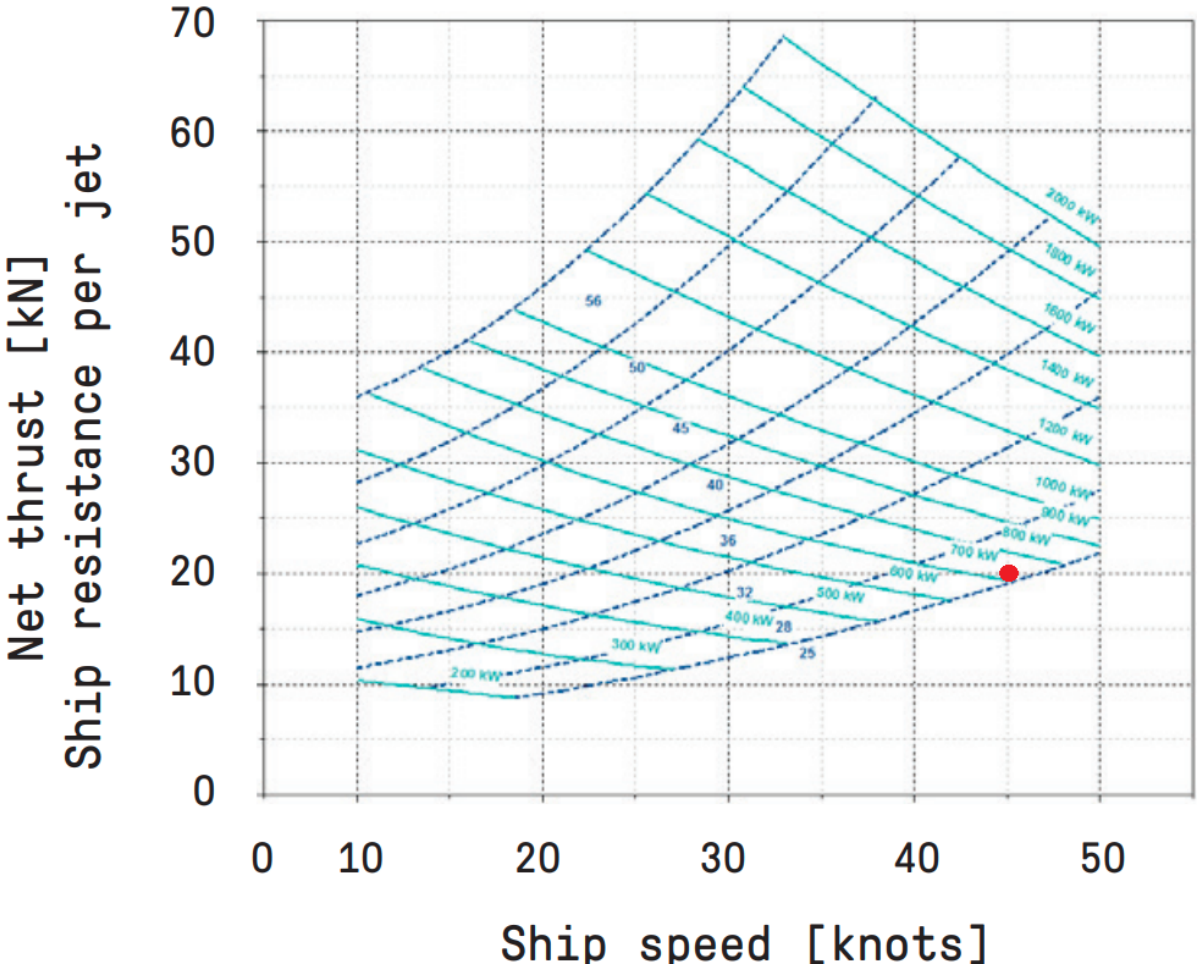

Figure D.3: Kamewa waterjet size 25-56 steel series performance curve of Kongsberg (2020). The working point is indicated by a red dot.

Taking a gearbox efficiency η_{gb} of 0.98 and a total shaft efficiency η_s of 0.99, as recommended by Klein Woud and Stapersma (2002), results in a equivalent 'propeller' power P_P of 1285 kW. This represents 642 kW per waterjet. Based on the published thrust curves of Kongsberg for their steel series water jet, its efficiency can be derived. The CB90 has a top calm water speed of 45 kt. Its working point is indicated in Fig. D.3. This results in a thrust T of approximately 20 kN per waterjet and 40 kN in total. The thrust power can then be derived using Eq. (D.8), where v_a is the advance velocity and w is the wake factor. For high-speed planing craft using waterjets, a typical wake factor is 0.05 according to Blount and Bartee (1997). It is assumed that the relative rotative efficiency η_r is 1, which means that propeller power P_P is the same as open water propeller power P_O. Hence, the open water efficiency can be derived using Eq. D.9.

$$P_T = Tv_a = Tv_s(1-w) \tag{D.8}$$

$$\eta_o = \frac{P_T}{P_O} \tag{D.9}$$

Using Equations (D.8),(D.9) and Fig. D.3, yields that the estimated open water efficiency η_o of a waterjet aboard the CB90 is 0.68 (68%). This is in accordance with other feasibility studies looking into waterjets for high-speed crafts (Doornebos, 2022; Francis, 2019) and literature (Allison, 1993; Klein Woud & Stapersma, 2002; McKesson, 2014).

$$\eta_o = \frac{Tv_s(1-w)}{P_O} = \frac{40[kN]\cdot 45(1852/3600)[m/s]\cdot(1-0.05)}{1,285[kW]} = 0.68$$

D.4. Open water efficiency hydrofoil waterjet

Implementing waterjets into a hydrofoil design adds several factors that will increase the required power for thrust. First of all, the foils lower the waterjet inlet to the bottom of the strut. This difference in head Δh_{strut} is at least 1.25 m, as the struts need to be 1.25 m long to be able to foil in SS3. In SS3 a wave height of 1.25 meter can be encountered often. To remain substantially submerged, 0.25 meter is taken as submergence depth. Secondly, implementing a waterjet in hydrofoils introduces hard bends in the inlet duct. In this case, the inlet duct is assumed to have an additional 90 degree bend. The following added power for each waterjet can then be estimated using Eq. (D.10), where η_p is the pump efficiency. According to Carlton (2019), the pump efficiency of a well designed waterjet is in the order of 0.90.

$$P_{added} = \frac{\dot{m}g}{\eta_p}(h_{bend} + \Delta h_{strut}) \tag{D.10}$$

The inlet diameter of the waterjets of the CB90 is 320 mm. The inlet velocity is assumed to be the same as the vessel speed as wake effects will be reduced when using a inlet in a strut. The mass flow can be estimated using Eq. (D.11). This yields a mass flow of 1,908 kg/s per waterjet, which equals a volume flow of 1.85 m^3/s.

$$\dot{m} = \rho_{sw} A_1 v_s \tag{D.11}$$

$$\dot{m} = \rho_{sw} A_1 v_s = 1,025[kg/m^3] \cdot \pi \cdot \frac{0.320^2}{4}[m^2] \cdot 45(1852/3600)[m/s] = 1,908[kg/s]$$

The losses in head of each added bend can be calculated using Eq. (D.12). The resistance factor ζ of a 90 degree bend is approximately 0.4 (Klein Woud & Stapersma, 2016).

$$h_{bend} = \frac{\zeta v_s^2}{2g} \tag{D.12}$$

$$h_{bend} = \frac{\zeta v_s^2}{2g} = \frac{0.4(45(1852/3600)[m/s])^2}{2 \cdot 9.81[m/s^2]} = 10.9[m]$$

With the head loss in the inlet bend and the strut height being calculated, the added power can be derived. Eq. (D.10) yields an additional 289 kW per waterjet.

$$P_{added} = \frac{1908[kg/s] \cdot 9.81[m/s]}{0.90}(10.9[m] + 1.5[m]) = 286[kW]$$

With Eq. (D.13), the adjusted open water efficiency for the foiling configuration is estimated. The resulting open water efficiency $\eta_{o,foil}$ is 0.48 (48%). Because propulsor-hull interaction for hydrofoil craft is negligible, it is assumed that the open water efficiency is the same as the propulsive efficiency (η_D) (Lundin & Eriksson, 2021).

$$\eta_{o,foil} = \frac{P_T}{P_O + 2 \cdot P_{added}} \tag{D.13}$$

$$\eta_{o,foil} = \frac{880[kW]}{1,285[kW] + 2 \cdot 286[kW]} = 0.48$$

E

User interview: Royal Netherlands Marine Corps

This is an edited transcription of the user interview conducted with the Royal Netherlands Marine Corps. To improve readability and brevity, it is a summarised version of the interview that aims to provide the main conclusions and points of doubt of the conversation. It should be noted that the marine corps currently does not employ LAC yet and that their main points of reference are the LCVP, LCU and FRISC.

Date of interview: | 10-09-2024

Part 1: Operational profile

Amphibious operation consists of the stages: planning, embarkation (troops aboard mothership), rehearsal (drills), movement (with mother ship), route-in (launching landing craft), transit to beach, assault and withdrawal. The most challenging aspect during the operation is the uncertainty of terrain, weather, and adversaries. Due to the reduced speed during the approach and the lack of cover as personnel steps foot on the beach, forces are the most vulnerable in the assault phase. This phase is characterised by the gradient of the beach. In a steep gradient a fast transfer can be achieved as landing craft can be kept at speed for a longer amount of time. In a flat gradient beach, the approach is slower and personnel has more ground to cover which results in a slow transfer of personnel. Other difficulties during the approach are obstacles under the water surface or sudden changes of water depth. Embarked forces can disembark the landing craft at a relatively dry position, but in case of a sandbank or riptide, water depth can increase again before coming to the eventual beach front.

Because of the importance of beach gradient, the draught and trim of the craft are important factors for a landing craft design. These elements determine how far the craft can advance onto the shore to ensure the safety of the embarked forces. In a flat gradient beach the aft of the craft is beached first, whereas in a steep gradient beach the front of the vessel will be beached.

During transit, helmsmen typically do not face significant challenges with high sea states. However, the embarked forces in the passenger compartment often do. They endure shocks, unpleasant odours, and loud noises in a confined space. Although the helmsman aims to ensure a safe and comfortable transit for everyone, this is not always feasible. The worse of a state the personnel is in at the end of the transit, the less effective they become in a combat situation. For instance, roughly one-third of the embarked personnel suffers from seasickness. As the distance from shore for amphibious operations increases, so does the level of fatigue, nausea, and physical strain. Operational limits define when landings can or cannot be performed. Officially a limit of SS4 (Beaufort 6) is applied, while transits back to the mother ship can occur in SS5. However, the final decision is context-dependent and rests with the commander.

Floating debris is encountered often. Primarily in rivers, but this also depends on the region. In riverine conditions such as jungles, big branches can be encountered. In the arctic big pieces of ice

are floating in the sea. Floating debris can cause problems for waterjets. Most of the small branches and thrash can be backflushed, but larger pieces of thrash or rope can not. This requires someone to cut or pull this out of the waterjet. Regarding operability this is considered an issue.

The FLitOC prescribes a distance from shore of 40 nm for mother ships to stage an amphibious operation. The British concepts that look into 100-150 nm from shore is not seen as a feasible goal right now due to the range that current craft provide. The technical limit of range in current landing craft and LAC designs is in the order of 300 nm. The range from shore of 40 nm means that at least 80 nm is already occupied for transit to shore and back to the mother ship. The other 220 nm is divided over the days that forces are operational in the area. For a typical duration of 7 days for example, only around 30 nm per day is left. For the purposes of the marine corps this is really low and therefore, a range of 300 nm is already considered low.

Part 2: Performance indicators

Reducing speed shortly to gain more speed overall (to retract foils for example) is seen as a simple calculation. If the overall transit duration is shortened this is a net win the marine corps. However, this can not be done near the shore (<3 nm) as they would be sitting ducks.

Considering stealth, sound radiation is considered as one of the least important factors. Radar systems or thermal recognition spots landing craft earlier.

To improve seakeeping of current vessels, several factors are considered: hull form, propulsion, seating and the helmsman. The experience of the helmsman is considered the most important factor. Furthermore, the propulsion system can offer better seakeeping in several ways. Firstly, a propulsion system with higher installed power generally offers faster response times, allowing the helmsman to better anticipate waves. Secondly, “trimming” a boat with propeller propulsion can offer advantages. Trimming in this context means changing the propellers shaft angle in relation to the boat. For example, the FRISC comes in two variants: one with waterjet and one with propeller propulsion. The waterjet version cannot be trimmed, whereas the propeller version is often trimmed negatively, meaning that applying throttle pushes the craft deeper into the water. This helps to reduce slamming forces and maintain high speed. On the contrary, waterjets can suffer from ventilation, leading to a complete loss of propulsive power. Thus, a propeller has advantages, but most landing craft use waterjets due to the fact that they have to be beached. This does not mean that propeller propulsion can not be done, earlier LCVP models also used propeller propulsion.

Dampened seats will not be a complete remedy for fatigue, nausea and physical strain. It does mitigate the physical strain on passengers, but due to the increased range and duration of transits this can still become unreasonably high.

Manoeuvrability is an important parameter to consider for survivability. If the craft can outmanoeuvre an adversary or if it helps with a firing position, an increase in complexity to gain manoeuvrability is a choice that can be made, but this should not make it more complicated for the helmsman to navigate.

Part 3: Ship Characteristics

It is not expected to see the dimensions of the LAC increase compared to what is available right now. The limiting factor remains the davits from mother ships. The new mother ships (ATS) will most likely have around the same capacity and the marine corps’s wishes are not leading in that respect. The LCM will be a larger vessel, but this will not be stored in the davits.

The amount of embarked forces will probably not increase, however the amount of mobility that is transported does. Examples of mobility are snow scooters and quads.

As for materials, the marine corps is not bound to using aluminium. Earlier LCVPs used polyester composites for example. The biggest issue considering composites is that this is often a sandwich construction which can fill up with water in case of a leak. The superstructure, such as the wheelhouse, can be made of composites if it still can provide the same amount of protection and armour.

There is no objection for a diesel-electric propulsion system, this is also applied to the LCU in its mid-life update. The biggest foreseeable issue is the weight increase of the vessel it could introduce. This has a direct relation to the draught of the vessel, which is preferred to keep low.

The bow hatch and ramp are a must for a new type of LAC. Without this system it is unrealistic to (dis)embark personnel safely.

Part 4: Concept Exploration

For different foil methods the following conclusions are derived:

- Foil-assisted planing can be seen as a “quick win” to gain speed in waves and increase some comfort. However, this really depends until which sea state this is possible. What is the amount of damping expected in higher sea states?
- Surface-piercing hydrofoils are not a realistic option if the limiting sea-state of using them is low.
- The potential gains of submerged hydrofoils are attractive. However, the main concern of fully submerged foils is the vulnerability that the struts with integrated transmissions introduce. If the strut hits something in the water, is the entire propulsion system lost or can this even damage the hull? Furthermore, during beaching nothing can extend under the hull. If there is a possibility to rest on extended hydrofoils on a beach or welldeck it can be an advantage, as this can help with (dis)embarking or inspection and maintenance.

A retractable cardan-shaft type transmission is seen as a potential transmission option. If a function of trimming the propeller in planing mode is integrated, this can be considered as an additional advantage.

Hydrofoils can also help with weapon systems or other onboard systems. This is due to the fact that it can offer a more stable platform and because the reduced spray keeps optics clear of sight.

Key factors, such as range, speed, remaining payload and reduced physical strain should make the application of hydrofoils worth the increased complexity and possible vulnerability. Reducing physical strain is a more important factor than reducing nausea or motion sickness.

F

Tool Calculations

F.1. Design space of the Foil Design JIP tool

Table F.1 provides a detailed description of the full design space of the Foil Design JIP tool of Minerva el. (2024). The considered parameters are shown as a non-dimensionalised and a dimensionalised value.

Table F.1: Complete range of the foil design space of the Foil Design JIP tool, recreated from Minerva et al. (2024)

Description	Symbol	Units	Minimum	Maximum	Category
		Non-Dimensional			
Froude chord	Fn_c	-	2.016	13.988	Heave, Pitch, Wave
Reynolds chord	Re_c	-	1,010,000	5,990,000	Heave, Pitch, Wave
Aspect ratio	AR	-	0.53	14.982	Heave, Pitch, Wave
Submergence ratio	λ_s	-	1.008	4.995	Heave, Pitch, Wave
Thickness ratio	λ_{th}	-	0.05	0.3	Heave, Pitch, Wave
Camber ratio	λ_{cr}	-	0	0.05	Heave, Pitch, Wave
Taper ratio	λ_{tap}	-	0.501	0.8	Heave, Pitch, Wave
Taper distance ratio	λ_{yk}	-	0.301	0.799	Heave, Pitch, Wave
Reduced frequency	k	-	0.011	0.4	Heave, Pitch
Reduced frequency	k	-	0.001	0.01	Wave
Strouhal number	St	-	0	0.003	Heave
Angle of attack	α	-	0.021	9.99	Pitch
Wave height / Depth ratio	λ_{wa}	-	0.1	0.2	Wave
		Dimensioned			
Mean chord	c_{mean}	m	0.089	0.983	Heave, Pitch, Wave
Root chord	c_{root}	m	0.096	1.181	Heave, Pitch, Wave
Tip chord	c_{tip}	m	0.047	0.651	Heave, Pitch, Wave
Span	b	m	0.082	12.738	Heave, Pitch, Wave
Projected area	A	m^2	0.007	11.616	Heave, Pitch, Wave
Velocity	V	m/s	3.959	22.177	Heave, Pitch, Wave
Depth	d	m	0.16	4.169	Heave, Pitch, Wave
Distance to tapering	y_k	m	0.037	9.204	Heave, Pitch, Wave
Camber	cam	m	0	0.047	Heave, Pitch, Wave
Thickness	t_h	m	0.005	0.245	Heave, Pitch, Wave
Frequency	f	rad/s	0.05	16.565	Heave, Pitch
Frequency	f	rad/s	0.003	0.417	Wave
Heave height (peak-peak)	A_{heave}	m	0	0.423	Heave
Angle of attack	α	°	0.021	9.99	Pitch
Wave height (peak-peak)	A_{wave}	m	0.018	0.745	Wave
Froude depth	Fn_d	-	0.619	17.687	Heave, Pitch, Wave
		Constraints			
Avoid foil emergence	Heave constraint	$(\pi \cdot St)/k < \lambda_s$			
Avoid wave steepness	Wave constraint	$A_{wave}/(T_p^2 \cdot g/(2\pi)) > 1$			
Avoid foil emergence in waves	Wave cons. 2	$2/\lambda_{wh} > 1$			

F.2. Foiling craft resistance estimation based on the Foil Design JIP Tool

This section will discuss the resistance approximation method, which builds upon the results of the MARIN foil design JIP tool. The results of the Foil Design JIP tool only account for the profile drag, induced drag and wavemaking drag. Additional factors need to be taken into account to retrieve the resistance of a complete hydrofoil craft. This section will elaborate on the additional factors implemented in calculations of this thesis. These factors are based on the methods described by van Walree (1999), Faltinsen (2005) and Godø (2024b). Drag factors are often non-dimensionalised using a lift or drag coefficient, prescribed by Eq. (F.1) and (F.2) respectively. These equations denote U as the free-stream velocity and ρ as a medium density. Following equations make a distinction between sea water (ρ_{sw}) and air density (ρ_a). Furthermore, generally a reference area (A) is applied.

$$C_L = \frac{2L}{\rho U^2 A} \tag{F.1}$$

$$C_D = \frac{2D}{\rho U^2 A} \tag{F.2}$$

F.2.1. MARIN Foil Design JIP results

Fig. F.1 shows the results of a selected design at a chosen speed. Although the results here are for quasi-steady conditions, a small hysteresis loop can be seen which causes data points to scatter. This is a result of how the model is trained, as it can also calculate unsteady results. In an unsteady condition with an oscillating hydrofoil, the lift curve slope decreases and a wider hysteresis loop becomes evident (Minerva et al., 2024). The data of these graphs can be downloaded as data points for each speed. In further analysis, quadratic fits are used to get an averaged result of lift and drag curves. This is repeated for each speed point to gain a drag over speed curve.

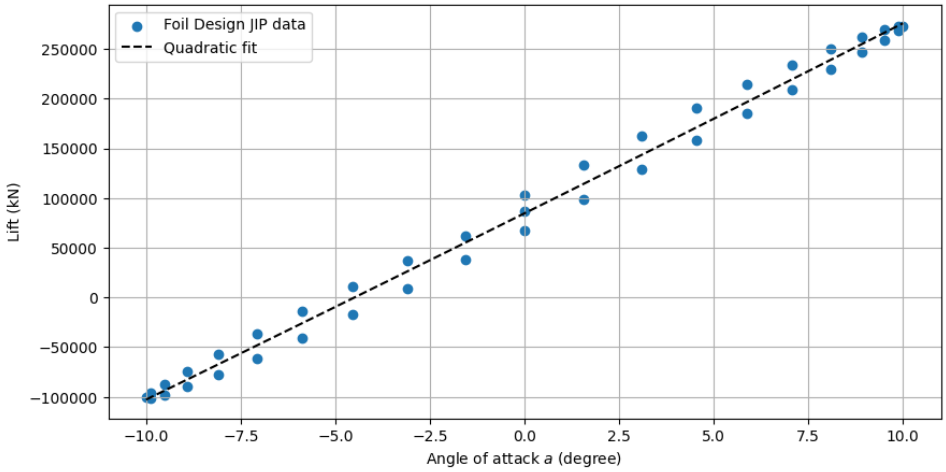

Figure F.1: Quadratic fit of Foil Design JIP tool foil data

F.2.2. Viscous resistance from roughness

Hydrofoils and struts have an amount of surface roughness that introduces additional resistance. To implement this to the resistance estimate, the methodology proposed by Godø (2024b) is applied.

Schlichting (1979) introduces a coefficient for fully rough flow expressed in Eq. (F.3). Here, l represents a characteristic length, taken as the average chord length of the hydrofoil, while k_s signifies the equivalent sand roughness of the surface. Next to the formula for fully rough flow, Schlichting (1979) presents an empirical formula for C_F in hydraulically smooth conditions, presented as Eq. (F.4). The results of the Foil Design JIP tool already account for the viscous forces acting on a smooth surface. Therefore, the difference between the frictional drag in smooth and rough flows is added. The total resistance of a hydrofoil craft is therefore increased with $D_{roughness}$ as prescribed by Eqs. (F.5) and (F.6). A_p, t and c indicate the projected area, thickness and chord length of the hydrofoil, respectively. The projected area is multiplied by a form factor similar to that used for propellers by the ITTC (ITTC, 2017). An equivalent sand roughness k_s of 8 µm is applied, as recommended by Godø (2024b) for modern carbon composite hydrofoils. For the considered hydrofoils in this thesis, this results in a ΔC_F of around 0.0004 at full speed, which is similar to what is considered in Hydres (van Walree, 1999).

$$C_{F,rough} = \left(1.89 + 1.62 \log_{10}\left(\frac{l}{k_s}\right)\right)^{-2.5} \tag{F.3}$$

$$C_{F,smooth} = \frac{0.455}{\log_{10}(Re)^{2.58}} \tag{F.4}$$

$$\Delta C_F = \max(C_{F,rough} - C_{F,smooth}, 0) \tag{F.5}$$

$$D_{roughness} = \frac{1}{2}\rho_{sw} U^2 A_p 2 \left(1 + 2\frac{t}{c}\right) \Delta C_F \tag{F.6}$$

F.2.3. Intersection resistance

Hoerner (1965) derived empirical equations based on experimental data of struts adjoining a wall, which is approximately the condition of a junction between a foil and strut. The effect on resistance from the intersection between the boundary layers of the strut and foils is estimated with Eq. (F.7). In Eq. (F.7), $D_{int,1}$, q,t, and c define the increase in drag, the dynamic pressure, the thickness and chord length of the strut, respectively. Dynamic pressure is defined as $q = 1/2\rho_{sw}U^2$.

$$C_{D,int1} = \frac{D_{int1}}{qt^2} = 0.75\left(\frac{t}{c}\right) - 0.0003\left(\frac{t}{c}\right)^{-2} \tag{F.7}$$

The intersection also affects the pressure gradients on the lifting foil, introducing additional separation and intersection drag effects. Hoerner (1965) presents experimental data, which indicate that the increase in resistance due to circulatory lift in the intersection is proportional to the square of the lift coefficient and approximately linear with the t/c ratio. Based on these considerations, Godø (2024b) derived Eq. (F.8), with the same factors of Eq. (F.7). This equation shows accurate prediction of the experimental drag experiments at higher lift coefficiencts (C_L), but strays from the experimental data for lift coefficients lower than 0.2. The complete intersection resistance can be estimated by adding Eq. (F.7) and (F.8), as in Eq. (F.9).

$$C_{D,int2} = \frac{D_{int2}}{qt^2} = 4.925\frac{t}{c}C_L^2 \tag{F.8}$$

$$D_{int} = qt^2(C_{D,int1} + C_{D,int2}) \tag{F.9}$$

F.2.4. Pod resistance

Streamlined pods, nacelles or fairings are installed in the intersection of foils and struts to house the propeller transmission or foil actuation mechanisms and can also function as waterjet inlet ducts. The pod resistance can be derived using the drag coefficient of streamlined bodies given by Hoerner (1965) in Eq. (F.10) and is also applied in methods of van Walree (1999) and Godø (2024b). This equation denotes the flat-plate frictional coefficient as C_F and the ratio of the diameter over length of the streamlined object with d/l. C_F can be calculated using the friction line formulation of the ITTC (1957), presented in Eq. (F.11). The wetted area of the pod is approximated by Eq. (F.12), where 70% of the pod is assumed to be of cylindrical shape and 30% is a streamlined body. The streamlined body surface area is estimated as the area of a cylinder multiplied by a streamline factor of 0.75. Hoerner (1965) suggests a factor between 0.7 to 0.8 for the wetted surface area of streamlined bodies. As a conservative estimate, no adjustments are applied to the wetted surface area to account for the non-wetted intersection regions with the lifting foils and struts. To conclude, Eq. (F.13) results in the added resistance of a single pod.

$$C_{D,streamlined} = C_F\left(1 + 1.5\left(\frac{d}{l}\right)^{3/2} + 7\left(\frac{d}{l}\right)^{3}\right) \tag{F.10}$$

$$C_F = \frac{0.075}{(\log_{10}(Re) - 2)^2} \tag{F.11}$$

$$S_{wet} = 0.3(0.75\pi dl) + 0.7(\pi dl) \tag{F.12}$$

$$D_{pod} = \frac{1}{2}\rho_{sw}U^2 S_{wet} C_{D,streamlined} \tag{F.13}$$

F.2.5. Viscous strut resistance

The minimum smooth viscous drag of a symmetrical foil can be expressed in basic parameters derived from experimental data such as expressed with Eq. (F.14) by Abbott and Von Doenhoff (1959), where c and t denote the strut chord and thickness, respectively. C_F is the flat-plate frictional coefficient as determined by Eq. (F.11). As a result, Eq. (F.15) yields the strut resistance, where A_p denotes the strut planform area. The additional roughness is estimated as in Eq. (F.6).

$$C_{D,strut} = 2 \cdot C_F\left(1 + 1.2(t/c) + 180(t/c)^4\right) \tag{F.14}$$

$$D_{strut} = \frac{1}{2}\rho_{sw}U^2 A_p C_{D,strut} \tag{F.15}$$

F.2.6. Spray resistance

Struts protrude through the free surface and generate additional resistance, due to the energy spent in generating spray. Hoerner (1965) presents an empirical equation for this effect as in Eq. (F.16), where t denotes the strut thickness.

$$D_{spray} = 0.24\frac{1}{2}\rho_{sw}U^2 t^2 \tag{F.16}$$

F.2.7. Shaft resistance

A simplified version of the calculation proposed of van Walree (1999) is used, where effective angle of attack (α) is simplified to only account for the inclination angle relative to the vessel (ϵ). Therefore, the model does not account for trim, which makes the resistance less accurate in take-off speeds. However, as it is the goal of the model to estimate resistance in fully foiling mode, this does not affect accuracy as much.

According to Kirkman and Kloetzli (1980), the drag coefficient of a two-dimensional cylinder at an inclination angle can be estimated as in Eq. (F.17). In this equation C_F denotes the flat-plate frictional coefficent, estimated by Eq. (F.11). The reference area is the cylinder length l times diameter d.

$$C_{D,cylinder} = 0.60\sin^3(2.25\alpha) + \pi C_F \tag{F.17}$$

All other factors for shafts are derived from Hoerner (1965). For surface piercing shafts, spray drag must also be taken into account. This can be estimated by Eq. (F.18), based on reference area d^2.

$$C_{Ds} = 0.8\sin(\alpha) \tag{F.18}$$

The added drag due to ventilation is estimated with Eq. (F.19), where F_h is the Froude number based on submergence height. The submergence height implied here is that of the shaft's end. The reference area is again l times d.

$$C_{Dv} = F_h^{-2} \tag{F.19}$$

$$F_h = \frac{U}{\sqrt{gh}} \tag{F.20}$$

The wave resistance of surface piercing shafts is given by Eq. (F.21), based on reference area ld.

$$C_{Dw} = \sin(\alpha)F_h^{-2} \tag{F.21}$$

The complete resistance of a surface-piercing inclined shaft can therefore be estimated by Eq. (F.22). Next to resistance, an inclined shaft can also induce some lift. At a speed of 45 knots, this can amount to around 1% for the required lift of the designs considered in this thesis. Therefore, they are assumed as negligible for this resistance model, but they are implemented in the results of Hydres (van Walree, 1999).

$$D_{shaft} = \frac{1}{2}\rho_{sw}U^2\left(\left(C_{D,cylinder} + C_{Dv} + C_{Dw}\right)ld + C_{Ds}d^2\right) \tag{F.22}$$

F.2.8. Air resistance

The frontal projected area of the craft is modelled following Eq. (F.23), where h, B and c_a denote the total height, beam and an area coefficient. The total height of the craft is assumed to be a constant 3.5 m. The area coefficient is a constant 0.827, based on the CB90 design. Air resistance is estimated using Eq. (F.24), with an assumed air drag coefficient $C_{D,air}$ = 0.5 based on the assumptions of Faltinsen (2005) and Godø (2024b) for high-speed craft. In this equation, A_f and ρ_a denote frontal projected area and air density, respectively.

$$A_F = c_a \cdot h \cdot B = 0.827 \cdot 3.5 \cdot B \tag{F.23}$$

$$D_{air} = \frac{1}{2}\rho_a U^2 A_F C_{D,air} \tag{F.24}$$

F.3. Dimensioning with resulting weight and strength estimates

F.3.1. Strut

The submergence height of foils is assumed to be the largest value between a constant 0.4 m or 0.85 times the mean chord length of the foil (c_{mean}). The constant 0.4 m leaves enough distance for a submerged propeller. Likewise, 0.85 c_{mean} is the foil submergence applied in Hydres as this is deemed a practical operating depth to meet the conflicting requirements of minimising strut drag, while maintaining a reasonable foil efficiency with reduced wavemaking drag (van Walree, 1999). Thus, this assumption is also taken in other calculations.

$$h_{submerged} = \max(0.4, 0.85 \cdot c_{mean}) \tag{F.25}$$

The length of the strut required to extend over the deadrise of the craft can be calculated using Eq. (F.26), where β and b denote the deadrise angle and beam from centreline, respectively. The deadrise angle is taken as a constant 20°. This height does not add to the hull clearance height.

$$h_{deadrise} = \sin(\beta) \cdot b \tag{F.26}$$

Eq. (F.27) yields the estimated total length of the strut. $h_{clearance}$ is one of the input design parameters required for a design instance and is strongly dependent on design sea state.

$$l_{strut} = h_{submerged} + h_{deadrise} + h_{clearance} \tag{F.27}$$

The section shape of the struts is simplified to a symmetrical 4-digit NACA foil, as this is described with a simple equation shown in Eq. (F.28) (Abbott & Von Doenhoff, 1959). Eq. (F.28) yields the section thickness (y_t) at an x position of the chord, based on the maximum thickness t. A more accurate section shape for hydrofoil struts would be a NACA 16 series foil (Faltinsen, 2005), but for initial estimations it is assumed that the 4-digit NACA foil shape is sufficient.

$$y_t = 5t(0.2969\sqrt{x} - 0.1260x - 0.3516x^2 + 0.2843x^3 - 0.1015x^4) \tag{F.28}$$

The chord length of the struts is assumed to be the same as the mean chord length of the attached foil, whereas the strut thickness is dimensioned according to Euler Buckling theory as proposed by Godø (2024b). Eq. (F.29) expresses the Euler Buckling theory, where W_E, I, and E denote the buckling load, the cross-sectional area moment of inertia, and the elastic modulus. The equivalent length is assumed as two times the physical length of the lowest attachment point of the struts to the hull to the foils, as described by Eq. (F.27). This approximates the struts as columns fixed at one end and free to translate and rotate at the other end. The dimensioning buckling load is set to three times the steady-state lift, to account for the dynamic forces in waves. Using Eq. (F.28) for the thickness distribution, the cross-sectional area moment of inertia is calculated for a discrete number of spanwise positions according to Eq. (F.30). The strut is modelled as a carbon composite shell (ρ = 1600 kg/m^3) with a foam core (ρ = 250 kg/m^3) as found by Godø (2024b). The core does not add to the strength of the structure. The shell thickness is dimensioned as 29% of the maximum strut thickness, which equates to a cross-sectional area moment of inertia of around 95% of a solid section, for the considered section shapes. Eq. (F.30) utilises the thickness at spanwise position ($t(x')$) and the shell thickness (t_s). The elastic modulus of 135 Gpa of the carbon composite shell is in accordance with Godø (2024b), which found this as a realistic estimate based on best-practice guidelines of hydrofoil designers.

$$W_E = \frac{\pi^2 EI}{2 \cdot l_{strut}^2} \tag{F.29}$$

$$I_{xx} = \frac{2}{3}\int_0^c \left(\left(\frac{t(x')}{2} \right)^3 - \left(\frac{t(x')}{2} - t_s \right)^3 \right) dx' \tag{F.30}$$

Using Eq. (F.28) and (F.27), the area and volume of the carbon composite shell and foam core of the struts can be found. This leads to the weight estimate of the struts. A margin of 50% of the strut weight is also taken into account to accomodate for the necessary structural strengthening at the strut attachment points and internal mechanical systems for foil actuation or propulsion.

F.3.2. Foil

The main foil dimensions are given as an output from the Foil Design JIP tool. However, foil volume is not part of the output and is therefore estimated with Eq. (F.31). The foil is assumed to be a solid structure mad of carbon composites with the same density as the strut shell (ρ = 1600 kg/m^3). Together, this yields the foil weight.

$$\nabla_{foil} = \frac{1}{2} \cdot s \cdot c_{mean} \cdot t \tag{F.31}$$

F.3.3. Propeller shaft

The shear stress of a shaft or pole can be calculated using Eq. (F.32), where T, r, and J denote the torque, radius, and the polar moment of inertia, respectively (Wartzack, 2021). In addition, the polar moment of inertia can be calculated using Eq. (F.33), where d represents the shaft diameter. Merging these equations to Eq. (F.34), yields an equation for the requirement of the shaft diameter. Furthermore, a safety factor (SF) is implemented to ensure safe operation. A typical yield strength for stainless steel marine propeller shafts is around 500 MPa, whereas shear strength of metals is generally half of this value (IMOA, 2016). Therefore, τ_{design} is taken as 250 MPa. Moreover, a safety factor (SF) of 2 is applied.

$$\tau = \frac{T \cdot r}{J} \tag{F.32}$$

$$J = \frac{\pi}{32} d^4 \tag{F.33}$$

$$d = \left(\frac{16 \cdot T \cdot SF}{\pi \cdot \tau_{design}} \right)^{1/3} \tag{F.34}$$

F.3.4. Pods

The pod or nacelle dimensions are taken as a function of the mean chord length of the connecting foil, as recommended by the program Hydres (van Walree, 1998). The pod diameter is retrieved with Eq. (F.35). Moreover, the pod length is taken as 6 times the diameter, which translates to 2.4 times the mean chord length.

$$d_p = 0.4 \cdot c_{mean} \tag{F.35}$$

F.3.5. Hull dimensions and structural weight estimate

Based on the hull form of a CB90, the following displacement calculation can be derived. This calculation is applied to find the required hull dimensions for a given weight. Eq. (F.36) yields the waterline beam (B_{wl}), based on the total beam (B) of the vessel. Similarly, Eq. (F.37) expresses the waterline length (L_{wl}) as part of the total length of the hull (L_{oa}). Based on these expressions, the displacement volume of the vessel is derived with Eq. (F.38), where the block coefficient (C_b) is a constant 0.613.

$$B_{wl} = 0.884 \cdot B \tag{F.36}$$

$$L_{wl} = 0.906 \cdot L_{oa} \tag{F.37}$$

$$\nabla = C_b \cdot T \cdot B_{wl} \cdot L_{wl} \tag{F.38}$$

The structural weight of designs is estimated based on surface area and uses the method proposed by Armer (2007). The hull surface is calculated in Eq. (F.39) as an open frame multiplied by a shape factor, similar to the method of Holtrop and Mennen (1982) to estimate the wetted surface of a hull. In Eq. (F.39), L_{oa}, B and D denote the length over all, beam and depth of the hull until the main deck. The shape factor is derived from the hull surface area of the CB90, which also includes the surface of the main deck. The superstructure area can be calculated with Eq. (F.40), where l, b, and h represent the length width and height of the superstructure. l and b are assumed as constant, whereas b is estimated

Table F.3: Structural weight estimate of the CB90

Part	Area (m^2)	Plate thickness (mm)	Stiffner weight (kg/m^2)	Plate weight (kg/m^2)	Weight (kg) Hull	Superstructure
Hull	145	5	11	24.3	3514	
Keel	3	20	0	53.2	159	
Superstructure	16	4	8.5	19.1		301
Subtotal					3672	301
Margins	Hull bulkheads, girders and tanks			20%	703	
	Superstructure bulkheads, girders			15%		45
	Welding and brackets			5%	219	17
Subtotal					4594	364
Total						**4958**

as $0.7 \cdot B$. Furthermore, keel plating area can be found by applying Eq. (F.41), where h_{keel} is the keel plate height.

$$A_{hull} = 0.81 \cdot L_{oa}(2B + 2D) \tag{F.39}$$

$$A_{ss} = 2 \cdot l \cdot h + 2 \cdot b \cdot h + l \cdot b \tag{F.40}$$

$$A_{keel} = L_{oa} \cdot h_{keel} \tag{F.41}$$

For the density of the aluminium plating, the EN-AW 5083 aluminium type is taken with a density of 2.66 g/cm^3 (Bikar, 2024). Furthermore, additional weight for the stiffeners on the plating is added. Additionally, margins are taken for bulkheads, girders, tanks and welding material. This yields the weight estimates of Table F.3 for the CB90, as an example. This is also the method applied for a hydrofoil LAC design structural weight.

F.3.6. Outfitting weight

The outfitting weight of a LAC is based on the published data of Saab Dockstavervet for the CB90. Table F.4 shows the estimated weight division of the design. Waterjet weight and entrained water weight are based on the Kongsberg FF-series as this data is published. The waterjet weight is corrected to a steel S32 waterjet with a 40% weight increase, based on a study of automotive parts (Tisza & Czinege, 2018). These waterjets are also discussed in Section D.3. The unaccounted weight is taken as the outfitting weight for every hydrofoil LAC design. This is approximately 30% of the total displacement of the CB90.

Table F.4: Weight division estimate of a CB90 design based on published data (Kongsberg, 2018; Saab, 2021; Scania, 2024a; TwinDisc, 2024b; Westerbeke, 2016)

LWT (18000 kg)		Specification	Weight (kg)	DWT (6500 kg)	Specification	Weight (kg)
Propulsion	Engine	2x Scania DI16 077M 900 hp	3340	Fuel oil	2200 L	1980
	Waterjet	2x Kamewa S32	1358	Payload	-	4500
	Gearbox	2x Twin disc MGX 5126A	482	Lub. Oil	96 L	79
	Genset	1x Westerbeke 7.5kW EGTD	175	**Total**		**6559**
	Entrained water	-	349			
Subtotal			**5704**			
Structural weight			4958			
Outfitting			7280			
Total			**17941**			

$$m_{outfit.} = 7280kg \tag{F.42}$$

F.3.7. Foil retraction system weight

The required foil retraction system weight is based on the research of Lundin and Eriksson (2021), which found a weight over lift factor of 1.81 kg per kN foil lift. This is for a vertical retraction system. An additional safety factor of 1.5 is also implemented, to account for the dynamic forces acting on the foil in a rough sea state. The resulting equation is presented by Eq. (F.43).

$$m_{retract.} = \frac{1.81}{1000} \cdot L_{req} \cdot 1.5 \tag{F.43}$$

G

System weight

Table G.1: High-speed engines with a minimum rating of 600 hours per year, with a possible CB90 engine indicated with green (Caterpillar, 2024b; Man Rollo, 2024; Scania, 2025; Volvo Penta, 2025; Yanmar, 2025)

Manufacturer	Type	Name	MCR (kW)	Rating	Speed (RPM)	Dry weight (kg)	Spec. Weight (kg/kW)
Scania	In-line 6	DI13 072M	478	Patrol craft short	2300	1285	2.69
Scania	In-line 6	DI13 077M	551	Patrol craft short	2300	1285	2.33
Scania	In-line 6	DI13 076M	643	Patrol craft short	2300	1285	2.00
Scania	V8	DI16 083M	625	Patrol craft short	2300	1670	2.67
Scania	V8	DI16 072M	662	Patrol craft short	2300	1670	2.52
Scania	V8	DI16 077M	736	Patrol craft short	2300	1670	2.27
Scania	V8	DI16 076M	846	Patrol craft short	2300	1660	1.96
Volvo	In-line 4	D4-230I	235	4	3400	565	2.40
Volvo	in-line 6	D6-300I	221	4	3300	690	3.12
Volvo	in-line 6	D6-340I	250	4	3400	690	2.76
Volvo	in-line 6	D6-380I	280	4	3500	690	2.46
Volvo	in-line 6	D8-450	331	4	3000	840	2.54
Volvo	in-line 6	D8-510	374	4	3000	840	2.25
Volvo	in-line 6	D8-550	405	4	3000	840	2.07
Volvo	in-line 6	D11-625	459	4	2400	1145	2.49
Volvo	in-line 6	D13-800	588	4	2300	1560	2.65
MAN	in-line 6	LE 446	537	Light	2300	1251	2.33
MAN	in-line 6	LE 426	588	Light	2300	1251	2.13
MAN	in-line 6	LE 456	625	Light	2300	1251	2.00
MAN	V8	LE 426	735	Light	2300	1780	2.42
MAN	V8	LE 453	824	Light	2300	1941	2.36
MAN	V8	LE 436	882	Light	2300	1941	2.20
MAN	V8	LE 466	956	Light	2300	1941	2.03
MAN	V12	LE 446	1029	Light	2300	2270	2.21
MAN	V12	LE 426	1140	Light	2300	2270	1.99
MAN	V12	LE 429	1140	Light	2300	2420	2.12
MAN	V12	LE 456	1213	Light	2300	2420	2.00
CAT	in-line 6	C7.1	317	D	2700	760	2.40
CAT	in-line 6	C9.3	355	D	2300	945	2.66
CAT	in-line 6	C12	425	D	2300	1174	2.76
CAT	in-line 6	C18	651	D	2200	1814	2.79
Yanmar	in-line 6	6CXBM-GT	374	S	2700	856	2.29
Yanmar	in-line 6	6HYM-WET	515	S	2200	1385	2.69
Yanmar	in-line 6	6AYEM-GT	737	S	2000	2418	3.28

The maximum power for gearboxes is taken at 2300 rpm as the engine options for a hydrofoil LAC design generally have an engine speed of 2300 rpm or higher. At a higher rpm, the power factor will reduce and put less strain on the gearbox. This makes the maximum power for each gearbox a conservative estimate.

[1] Inverter weight included

Table G.2: Light duty gearboxes (TwinDisc, 2024a; ZF, 2025)

Manufacturer	Model	Ratio min	Ratio max	Max. P @ 2300 rpm (kW)	Power factor	Weight (kg)	Rating
TwinDisc	MG5050	1	2.04	211	0.09	86	Light
TwinDisc	MG5061	1.13	2	265	0.12	98	Light
TwinDisc	MG5065	1.08	2.04	376	0.16	111	Light
TwinDisc	MG5075	1.06	2.05	368	0.16	122	Light
TwinDisc	MG5082	1.06	1.77	460	0.20	135	Light
TwinDisc	MG5091	1.17	2.04	471	0.20	220	Light
TwinDisc	MGX5096A	1.25	2.04	597	0.26	200	Light
TwinDisc	MGX5114	0.93	2.54	629	0.27	215	Light
TwinDisc	MGX5126	1.03	2.04	732	0.32	241	Light
ZF	305-3	0.884	1.968	429	0.19	98	Light
ZF	325-1	1	2.033	538	0.23	130	Light
ZF	400	0.854	2.214	671	0.29	160	Light

Table G.3: Specifications of Radial Flux and Axial Flux electrical machines (ABB, 2024; Beyond Motors, 2025; Brogen Motors, 2025; Emrax, 2025; Evolito, 2025; Phi-Power, 2025; Scania, 2024b)

Manufacturer	Model	Peak Q (Nm)	Peak P (kW)	Peak n (rpm)	Q (Nm)	MCR P (kW)	n (rpm)	U (V)	AC/DC	m (kg)
Radial Flux Electrical Machines										
Scania	Electrical Machine	2000	295	1400	1500	230	2100	650	DC	280[1]
ABB	AMXE132S	389	163	5000	160	67	4000	-	-	72
ABB	AMXE132L	652	273	5000	265	111	4000	-	-	97
ABB	AMXE160S	750	196	5000	376	98	2500	-	-	103
ABB	AMXE160L	1100	288	5000	550	144	2500	-	-	138
ABB	AMXE200S	1205	379	4960	484	152	3000	-	-	229
ABB	AMXE200L	1961	616	5000	741	233	3000	-	-	287
ABB	AMXE250L	3275	686	3500	1500	314	2000	-	-	490
Axial Flux Electrical Machines										
EMRAX	208-HV-LC	150	86	6000	84	52	6000	690	DC	10.3
EMRAX	228 - MV-LC	220	104	4500	112	64	4500	630	DC	13.5
EMRAX	268-MV-LC	500	210	4500	213	100	4500	830	DC	22.3
EMRAX	348 -LV-LC	1100	400	4000	425	178	4000	610	DC	43.9
Beyond	AXM2-MV	180	130	7500	120	75	6000	550	DC	14.5
Beyond	AXM3-MV	525	220	5800	310	130	4000	550	DC	27
Beyond	AXM4-LV	950	430	4500	600	230	3600	550	DC	48
Evolito	D1500 1x3	1450	150	2500	1200	100	800	-	-	35
Evolito	D1500 2x3	1500	285	1800	1400	285	1900	-	-	40
Brogen	Model 7	6000	900	3500	3000	570	1815	620	DC	362
Brogen	Model 6	3000	450	3500	1560	310	1900	620	DC	175
Brogen	Model 5	2400	300	4000	1100	173	1500	630	DC	148
Brogen	Model 4	1200	220	5500	620	143	2200	540	DC	106
Brogen	Model 3	800	188	8000	330	111	3200	540	DC	65
Brogen	Model 2	800	150	6000	450	104	2200	540	DC	75
Brogen	Model 1	420	120	9000	220	81	3500	540	DC	41
Phi Power	Phi301	320	160	3000	190	85	5000	-	-	29
Phi Power	PhE381	640	200	5000	275	90	4000	-	-	38
Phi Power	PhE382	1280	400	5000	550	180	4000	-	-	83

Table G.4: Commercial generator sets for continuous use (Caterpillar, 2024b; Volvo Penta, 2025)

Manufacturer	Type	Name	MCR 60 Hz (kWe)	Speed (rpm)	Dry weight (kg)	Spec. Weight (kg/kW)
Volvo	In-line 6	D13MG	400	1800	3070	7.68
Volvo	In-line 6	D16MG	532	1800	3871	7.28
CAT	In-line 4	C4.4	99	1800	754	7.62
CAT	In-line 6	C7.1	200	1800	1522	7.61
CAT	In-line 6	C9.3	300	1800	2367	7.89
CAT	In-line 6	C18	565	1800	3961	7.01
CAT	V12	C32	940	1800	7131	7.59

Table G.5: Added weight of an axial flux genset conversion of Hydrosta (2024) and the theoretical weight of a complete genset based on high-speed engines

Model	Max. engine power (kW)	Max. output power (kW)	Weight (kg)	Length (m)	Theoretical genset weight (kg)	Spec. weight theoretical genset (kg/kW)
HPIL 1	300	20	105	0.468	387	3.69
HPIL 2	300	70	110	0.468	489	4.45
HPIL 2	300	140	150	0.581	665	4.43
HPIL 3	1200	180	420	0.640	1013	2.41
HPIL 3	1200	360	560	0.800	1502	2.68
HPIL 3	1200	540	700	0.960	1991	2.84

Table G.6: Marinised and other turboshaft gas turbines (General Electric, 2017; General Motors, 1986; Honeywell, 2000; Rolls-Royce, 2024)

Manufacturer	Model	P_b (kW)	m (kg)	V (m3)	Spec. weight (kg/kW)	Specific Volume (dm3/kW)	sfc (g/kWh)	η_e [%]
GE	LM500	4570	2779	7.7	0.61	1.68	270	31
Honeywell	AGT1500	1120	1134	1.3	1.01	1.16	288	29
Rolls-Royce	M250	186	63	1.85	0.34	9.94	424	20
Rolls-Royce	RR300	223	91.6	1.14	0.41	5.12	n/a	n/a
Rolls-Royce	RR500	261	102	1.30	0.39	4.97	418	20
Rolls-Royce	M250 C47E/4	485	131	0.40	0.27	0.83	260	32
Rolls-Royce	Allison 501-KF	3230	1134	5.2	0.35	1.60	306	28

Table G.7: Traction inverter and converters of ABB (ABB, 2022)

Model	I cont. (Arms)	I peak (Arms)	Continuous power (kW)	Peak power (kW)	Dry weight (kg)	Efficiency
HES880-352	214	350	182	297	35	0.98
HES880-602	367	600	311	509	35	0.98
HES880-902	527	900	447	764	45	0.98

H

Experimental data of a hydrofoil craft

Courtesy of the TU Delft Hydro Motion Team (HMT), a dataset of one of their hydrogen-electric hydrofoil craft is provided. The dataset presented here corresponds to their 2023 design. This is a carbon composite monohull, powered by a 44 kW PEM hydrogen fuel cell as its prime mover. It relies on 16 kg of compressed hydrogen stored in 2 tanks as the primary energy carrier. The electric motor is attached in an L-drive configuration, with transmission through the aft strut.

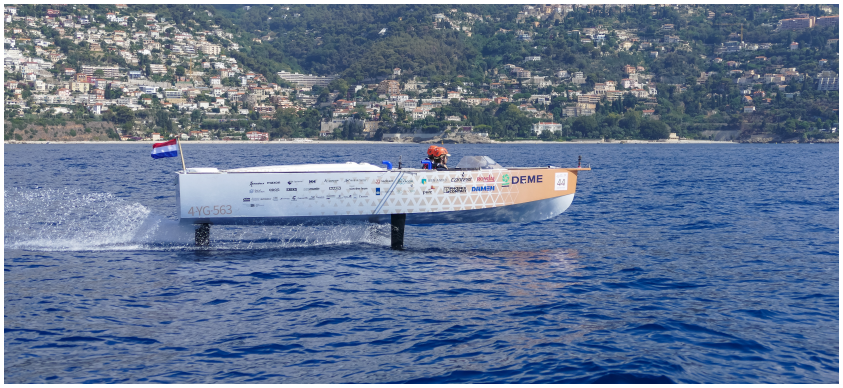

Figure H.1: The HMT23 design sailing in the bay of Monaco (TU Delft Hydro Motion Team, 2023)

Table H.1: Main particulars of the HMT23

Parameter	Value
L_{oa}	7.3 m
B	2.25 m
B (incl. foils)	3.5 m
T	0.3 m
T (incl. foils)	1.4 m
Δ	1.45 t
v_s	25 kt
$P_{installed}$	44 kW

The dataset provided here is of a test run on the fifth of July of 2023. The vessel sailed multiple times back and forth in the bay of Monaco, between the main marina of Monaco (Port Hercule) and Cap Martin. The approximate route is illustrated in Fig. H.2 and the weather conditions are listed in Table H.2.

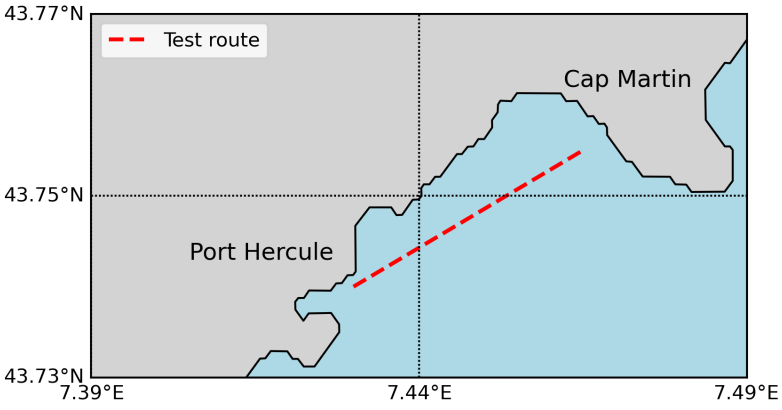

Figure H.2: The test route for this dataset

Table H.2: Weather conditions for the test run at 5-7-2023 9:00 AM (7.466 E, 43.703 N) (E.U. Copernicus Marine Service Information (CMEMS). Marine Data Store (MDS), 2025)

Parameter	Value
$H_{1/3}$	0.41 m
T_p	4.68 s
T_2	3.53 s
Wave direction (μ)	226° SW
Wind velocity	2.24 m/s SE
Sea current	0.295 m/s E

Orientation and position data was collected by a Xsens Inertial Measurement Unit (IMU), positioned at approximately the centre of gravity. The velocity data is gathered by the integrated GNSS receiver in the IMU. Therefore, the speed data provided is a Speed Over Ground (SOG) reading, instead of a Speed Through Water (STW) reading. Height data is gained with the use of a Senix ultrasonic sensor in the bow of the vessel. Furthermore, motor data was collected by the Bamocar D3 motor controller of Unitek. The complete dataset was then stored on a Kvaser CAN logger, which can store the data of the CAN-bus on a SD-card for post-processing.

The sensors of the vessel were configured with different output frequencies, with some sensors sending data every 0.1 second and others every 1.5 seconds. The dataset was matched to the highest frequency to prevent data loss, which resulted in a dataset with a total of around 40000 data points. However, due to the varying frequencies, around 2700 data points are qualitatively distinct.

Fig. H.3 shows the electric propulsion power demand over speed. What is particular, is that the power curve at lower speeds is more clustered than at the highest speeds. From the speeds that the dynamic foil lift becomes to play a role, a larger spread of data points can be observed. This can be caused by several factors:

- The varying wind, wave and current directions play a larger role at higher speeds.
- The orbital velocities of waves playing a larger role for hydrofoil resistance, than planing hull resistance.
- The foil actuation of the craft to achieve dynamic stability varies the drag at the same speed.
- The high sensor output frequency and fast electric motor response can give mismatched readings. For example, the motor can ramp up to accelerate, but the vessel 'lags' behind to gain speed. This is probably the reason for the 'cloud' of high motor power at around 5-8 kt, as this is around the power required where the vessel starts to become foilborne and further accelerates. The same issue holds for deceleration.

To partly remedy this uncertainty of the data points, a polynomial fit is also provided.

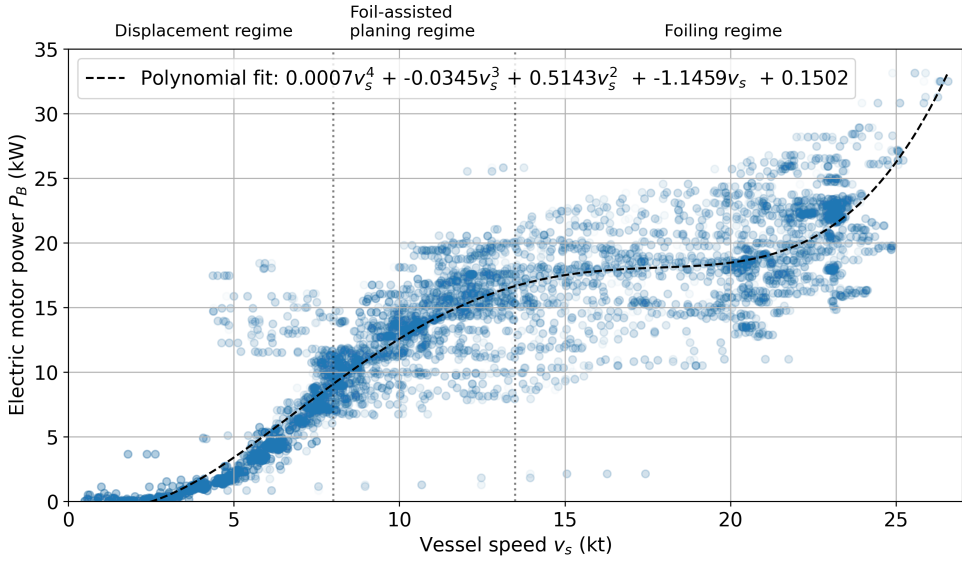

Figure H.3: Electric motor power demand over speed

By assuming a propeller and transmission efficiency of the vessel, a resistance estimate of the vessel can be gathered. For this craft an open water efficiency (η_o) of 0.70 and a transmission efficiency (η_{trm}) of 0.98 is assumed. In addition, relative rotative and hull interaction losses are assumed negligible. This is deemed a realistic estimate as found in accordance with Klein Woud and Stapersma (2002). The resulting resistance curve is presented in Fig. H.4.

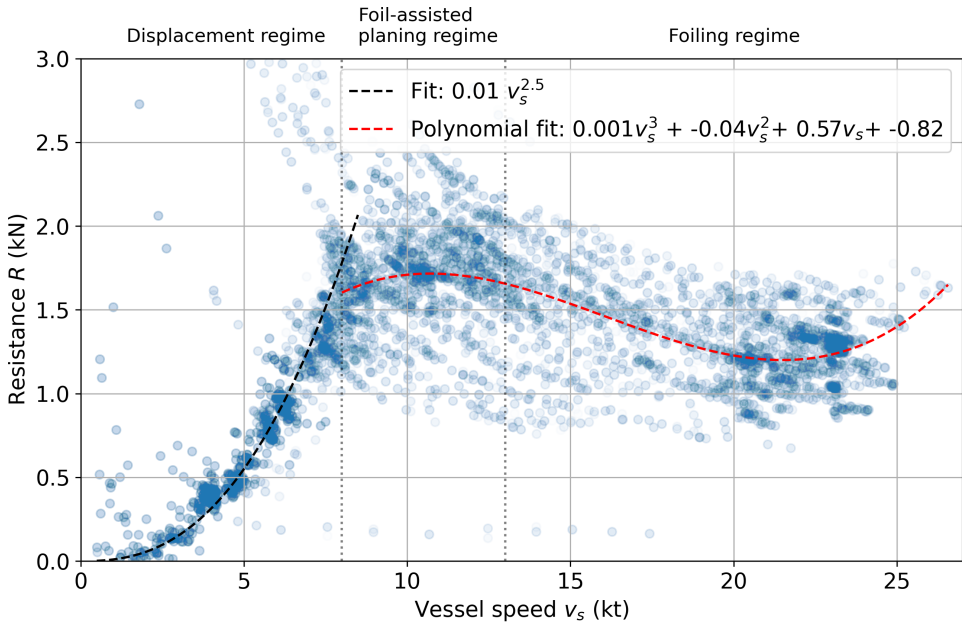

Figure H.4: Resistance estimate based on power curve

The derived resistance curve can be used to provide a validation of the calculations of Part I of Chapter 4. Attention was paid to most closely resemble the real counterpart in its foil design. However, the real foils have a rounded taper and a S8055 foil section, instead of a straight taper and Eppler 817 foil section. This is a limitation of utilising the Foil Design JIP tool in the foil design. Fig. H.5 visualises the modelled design, with the foil design parameters listed in Table H.3.

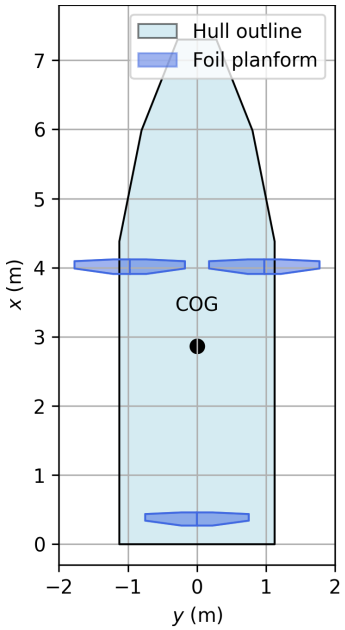

Figure H.5: Validation design

Table H.3: Main foil particulars of the validation design

Parameter	Value	Unit
c_{front}	0.21	m
c_{aft}	0.19	m
s_{front}	1.6	m
s_{aft}	1.5	m
$camber_{front}$	1.6	%
$camber_{aft}$	1.6	%
t/c foils	0.12	-
t/c front struts	0.23	-
t/c aft struts	0.26	-

Fig. H.6 presents a comparison between the calculated results and the experimental data. The calculations provide a realistic estimate for both top speed and design speed with discrepancies remaining below 5%. However, at lower speeds, the deviations increase. Up to approximately 20 kt, the difference stays within 20%, but at speed as low as 15 kt, the discrepancy exceeds 50%. This significant discrepancy can be attributed to how the craft is operated and data is collected. Since no additional power is required between 14 and 20 kt (Fig. H.3), it is likely that the operator selects a power setpoint

and accelerates until the resistance increases enough to necessitate additional power. Due to the high sensor frequency, data is still recorded during this transition. Considering these factors, this method is deemed suitable for estimating resistance at design and top speeds.

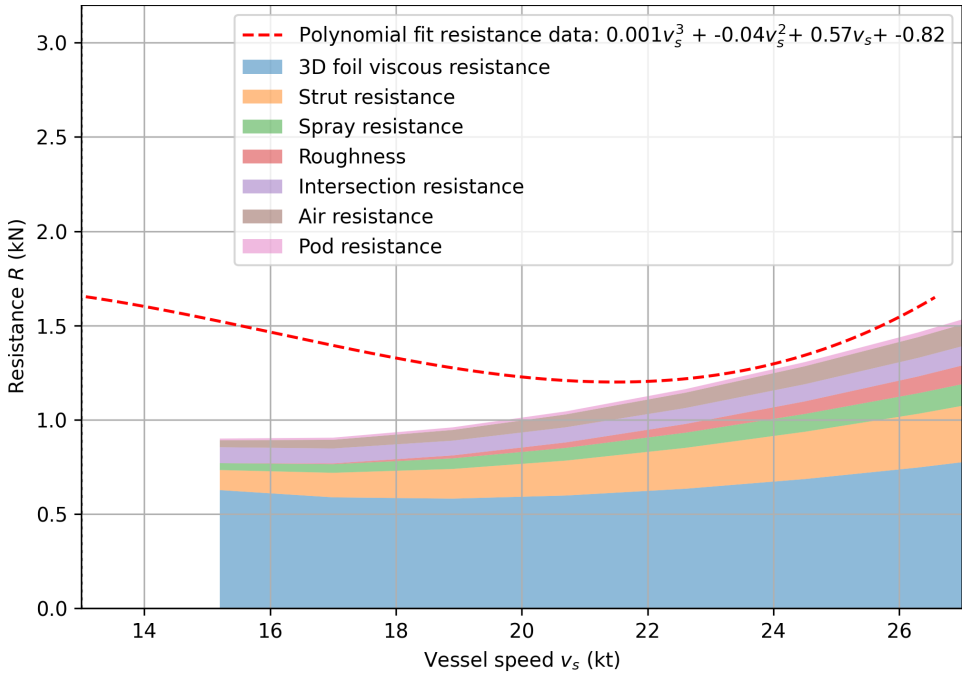

Figure H.6: Resistance over speed of experimental results compared to estimated results

In addition, Fig. H.7 and H.8 show the characteristic attitude of the craft in terms of pitch and height. The derived curves are in accordance with the figures presented by Van Walree (1999), shown in Section 3.1. The clearance height in Fig. H.7 is corrected for the trim of the vessel.

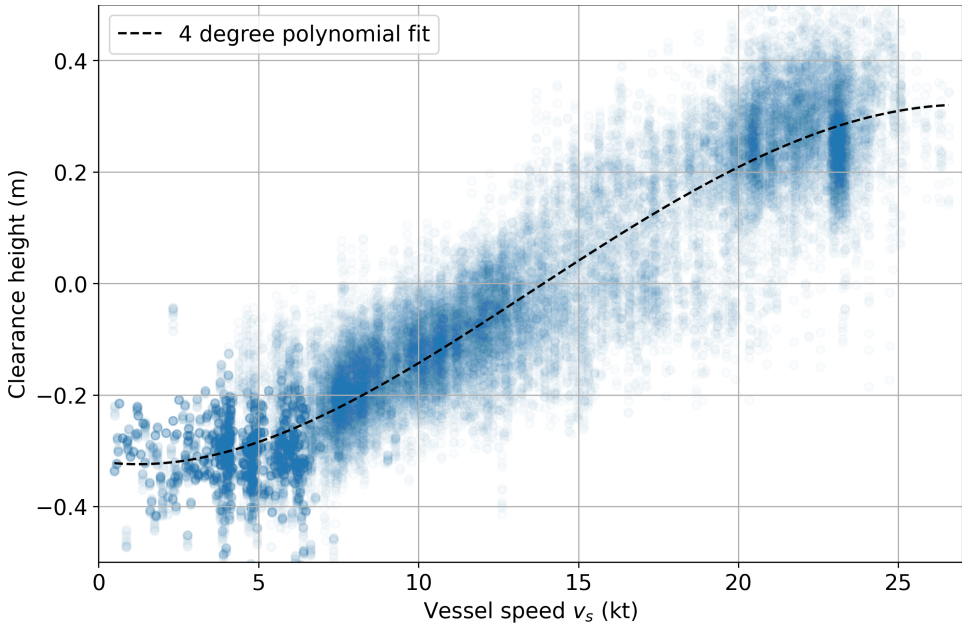

Figure H.7: Vessel height over speed

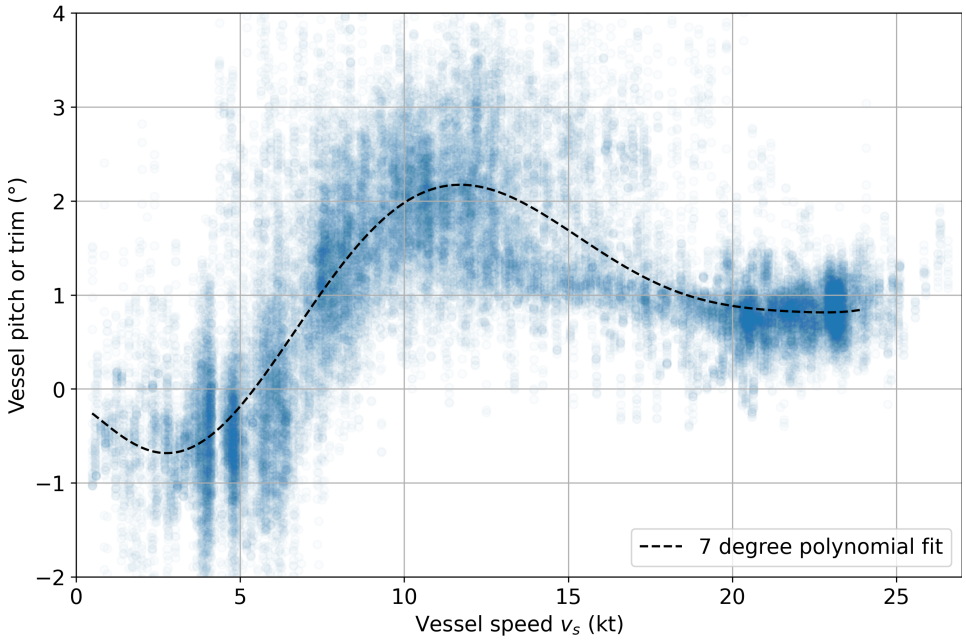

Figure H.8: Vessel trim or pitch over speed

I

Hydres input

HLAC-DE design

```
COMMENT   ########################################################
COMMENT   ############# HYDRES/ example run      ################
COMMENT   ########################################################
OPTIONS   1         0         0         1         1         0         0
GENERAL   3         26100.    .5        .05       1.25      3         2
HULL      14.2      3.2       20.0      0.0       0.0       1
SPEED     38        25        10        46        3
CONST     1025.     15.                 .0004     .0004
PROPUL    3         0         1         0.00      2.00      -2.20     2
PROPELLER 4         1         .6
MATRIX    8         8
STATE     0.50      1.0       0.95      1.25      0         4         .75
AERO      11.       .50       1.25      .5        .15
FOILDES   .3
FOILPAR
FOILGEOM  0.120                         4.6
FOILGEOM  0.120                         6
FLAPS
FLAPS
STRUT     0                             0.105
STRUT     1         1                   0.190
```

HLAC-HK design

```
COMMENT   ########################################################
COMMENT   ############# HYDRES/ example run      ################
COMMENT   ########################################################
OPTIONS   1         0         0         1         1         0         0
GENERAL   3         24600.    .5        .05       1.25      3         2
HULL      13.5      3.2       20.0      0.0       0.0       1
SPEED     38        25        10        46        3
CONST     1025.     15.                 .0004     .0004
PROPUL    1         15.0      1         0.00      2.00      -2.20     2
PROPELLER 4         1         .45
MATRIX    8         8
STATE     0.50      1.0       0.95      1.25      0         4         .75
AERO      11.       .50       1.25      .5        .15
FOILDES   .3
FOILPAR
```

```
FOILGEOM  0.120                       5
FOILGEOM  0.120                       7
FLAPS
FLAPS
STRUT     0                           0.105
STRUT     0         0                 0.190
SHAFT     2         1.218     -1.53   0.05      1.55      15        1
```

J

Hydrofoil transverse stability

The main difference between displacement hull and a submerged hydrofoil´s transverse stability is the direction of the restoring force. A displacement hull will always have a restoring buoyancy force in vertical direction (following Archimedes' principle), whereas the correcting lift of a submerged hydrofoil will remain parallel to the roll angle (Johnston, 1985). A submerged hydrofoil therefore also does not have a metacentre (MC), but rotates around its centre of gravity. This difference is illustrated in Fig. J.1. A wave coming from beam sea, will result in a shift of the centre of buoyancy (CB) of a displacement ship or the centre of pressure (CP) of a surface piercing foil system. On the contrary, no significant force change occurs for a fully submerged hydrofoil. In a straight line a hydrofoil craft will experience minimal roll from waves, due to the hull being detached from the water surface. If a submerged hydrofoil rolls however, the restoring force must be generated by foil actuation. This control action changes the CP of the hydrofoil to create a stabilising moment.

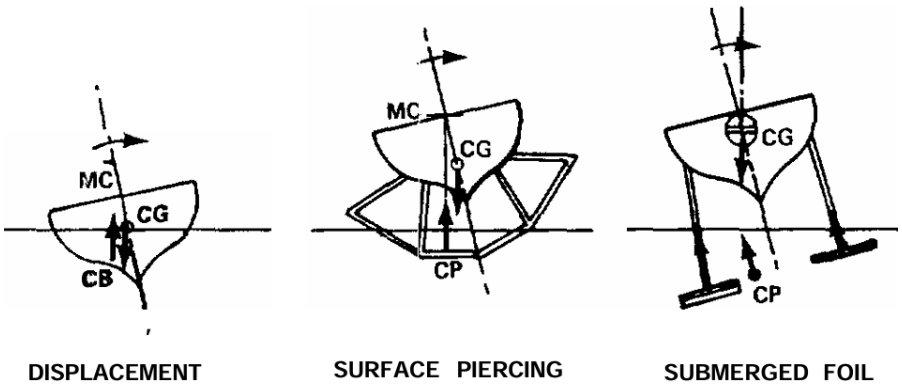

Figure J.1: Roll correction of different hull types (Johnston, 1985)

The roll stability of a submerged hydrofoil can be approached as an inverted pendulum problem as in Fig. J.2. Similar to a self-balancing hoverboard or self-balancing unicycle, the reaction force is in line with the roll angle that is given. However, instead of changing the wheel position to stabilise the system, the centre of pressure is controlled along the spanwise direction. Anhedral foils can increase roll stability even more by increasing the lift in outwards direction. As the moment arm in height is larger than the arm in width, this increases the stabilising roll moment. This comes at the cost of straight-line drag however. A complete roll-stability assessment can be calculated with a state-space representation model (Franklin et al., 2009).

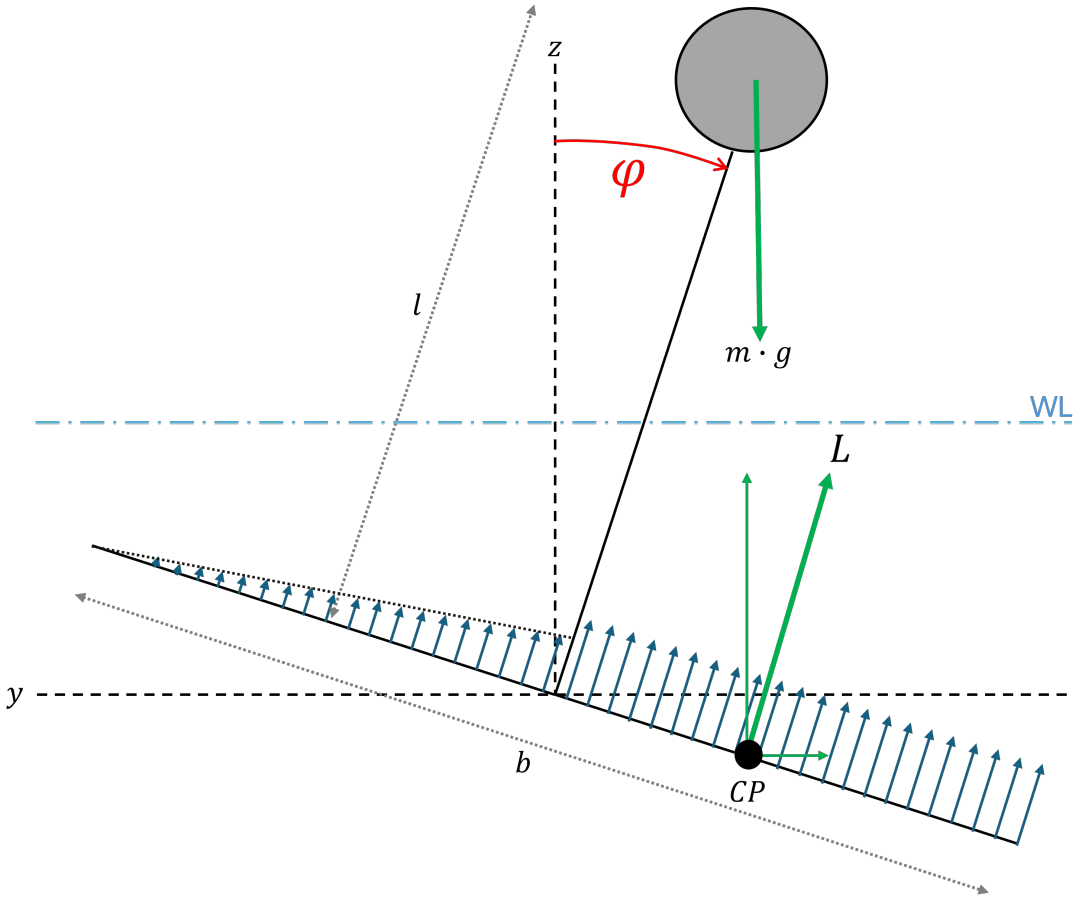

Figure J.2: Simplified free-body diagram of a submerged hydrofoil in a rolling motion